UNIVERSITÀ DEGLI STUDI FIRENZE

DOTTORATO DI RICERCA IN
Scienze Chimiche

CICLO XXVI

COORDINATORE Prof. Andrea Goti

Protein inspired tumor targeted therapy

Settore Scientifico Disciplinare CHIM/06

Dottorando
Dott. *Eleonora Tenori*

Tutore
Prof. *Stefano Menichetti*

Coordinatore
Prof. *Andrea Goti*

Anni 2011/2013

Ai miei nonni

'Il divertimento della ricerca scientifica è anche trovare sempre altre frontiere da superare, costruire mezzi più potenti d'indagine, teorie più complesse, cercare sempre di progredire pur sapendo che probabilmente ci si avvicinerà sempre di più a comprendere la realtà, senza arrivare mai a capirla completamente.'

(Margherita Hack)

Index

1. Protein inspired tumor targeted therapy: the case of Neurotensin

2. Protein inspired tumor targeted therapy: Synthesis of Pt(II) complexes tethered to nuclear targeting peptides

1. Protein inspired tumor targeted therapy: the case of Neurotensin

1.1 Introduction

1.1.1 Introduction to chemotherapy

Chemotherapy (often abbreviated to chemo) is the treatment of cancer with one or more cytotoxic antineoplastic drugs. The term "chemotherapy" has been coined by Paul Ehrlich in the early 1900s to describe a therapeutic approach which implies the use of chemicals to treat infectious diseases.[1] Although now the term "chemotherapy" is currently referred, in its common use, to cancer therapy, it originally indicated the use of drugs to cure diseases which were not caused by an endogenous organ dysfunction, rather induced by allogenous pathogens such as viruses, bacteria, parasites and so on. Cancerous cells, although deriving from sane human cells, are thus considered in the same manner as allogenous pathogens are: a strange sort of "enemy" cells which can be defeated by means of chemical agents, just like a bacterial infection can be eradicated by penicillin. Ehrlich was also the first to envisage a *selective* therapy aimed at eradicating pathogen-caused diseases; a therapy which could take advantage of the many differences existing between a human cell and the cell of the pathogen. He imagined a therapy armed with chemicals (which he inspiredly called "magic bullets") that could specifically interfere with biochemical pathways exclusive to the infective micro-organism.

For instance, *arsphenamine*, marketed under the name of Salvarsan, was introduced at the beginning of the 1910s as the first effective treatment for syphilis. This organoarsenic molecule steamed form Ehrlich's theory that by screening many compounds, a drug could be discovered with antimicrobial activity without killing the human. Thus, it is nowaday consider the first modern chemotherapeutic agent.[2] For sure*, penicillin*, inhibiting DD-transpeptidase, an enzyme which is involved in the synthesis of peptidoglican cell walls, not expressed by human cells, can be the perfect example of a "magic bullet", hitting a bacteria-specific target and avoiding mechanism-of-action related toxicity (Figure 1.1).
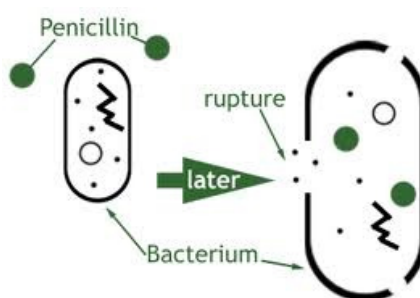
Figure 1.1. Destruction of the peptidoglican cell wall operated by penicillin

Unfortunately, cancer cells, although distorted by a wild mutation process, are human cells and share the majority of biochemical pathways with the latter; as a consequence, a cytotoxic therapy aimed at killing the totality of cancer cells obviously implies a dramatic mechanism-of-action related toxicity. Although chemotherapy still remains one of the most controversial therapeutic approach to cancer,

research has the duty to persevere in its improvement, as it is one of the few approaches which can be adopted in the treatment of metastatic cancer. While surgical interventions are by far the most successful procedures in early cancer cure protocols (although ineffective in the treatment of advanced cancer), chemotherapy (in particular classic chemotherapy, as discussed above) attains satisfactory results in terms of survival and remissions number only in a restricted number of tumors (e.g. chronic myeloid leukemia) and it can often even worsen the clinical situation of the patient.

1.1.2 Classic versus targeted chemotherapeutics

The beginnings of the modern era of chemotherapy can be traced directly to the discovery of nitrogen mustard as an effective treatment for cancer.[3] During World War I *mustard gas* (nitrogen mustard) was used as a chemical warfare agent and was discovered to be a potent suppressor of hematopoiesis (blood production).[4] In 1942, Goodman and Gilman, at Yale University, treated a patient with non Hodgkin's lymphoma with nitrogen mustard, observing a remission, even if only temporary, of the tumorous masses.[5] Later on, in the earliest phases of the development of cancer chemotherapy, emphasis was on cell duplication rate, which constitutes a first discriminating factor between cancer cells and healthy cells. As a matter of fact, cancer cells proliferate several times faster than their "normal cell" homologues as a result of growth-promoting genes activation (oncogenes, such as *ras* genes)[6] and mutation of growth-suppressing genes (oncosuppressors, such as *p53*)[5]. Thus, in the second post war period, every research effort was thus addressed to the development of drugs which could interfere with cells duplication, such as DNA alkylating agents, mitosis inhibitors, antimetabolites and every kind of toxin which could disrupt cellular cycle biochemical pathways, in order to kill high-rate duplication cells in which those processes were statistically more frequent.

Classic Chemotherapeutics. These first chemotherapeutic agents (commonly referred to as *classic chemotherapeutics*) show high toxicity and thus a plethora of side effects, below indicated:

- ✓ Firstly, they act killing cells that divide rapidly, exerting their cytotoxic effect also on healthy cells with a high duplication rate in physiological conditions, such as epithelial, giving rise to a series of often untollerable side effects. In particular, hematopoietic precursors, gastrointestinal epithelial cells and hair follicles are hit, resulting in the typical side effects of chemotherapy: *myelosuppression* (decreased production of blood cells), *mucositis* (inflammation of the lining of the digestive tract) and *alopecia* (hair loss). These side effects lead many already compromised patients to give up therapy, as the latters are often more dangerous than the disease itself. It is, in fact, very difficult to find a compromise between benefits and therapy-associated risk. Among others, frequent, heavy side effects are *emesis* and *neuropathic pain*, which necessarily require dedicated treatment, thus broadening the already wide number of drugs simultaneously administered to the patient, the risk of dangerous pharmacokinetic and pharmacodynamic interactions critically increases. Regarding neuropathic pain, for instance, platinum-based cancer chemotherapies induce a neurotoxicity characterized by a dose-dependent painful sensory neuropathy, presenting with symptoms in distal extremities that forced the patient to suspend the treatment in a early stage of the therapeutic protocol.[7]

- ✓ Secondly, the most threatening risk associated to the use of classic chemotherapeutic agents is the possibility of the development of secondary cancers, provoked by drug-induced DNA damage. This occurs most frequently in patients treated with alkylating agents and recently the

carcinogenicity of platinum complexes such as cisplatin has been anticipated by several studies.[8]

  ✓ Finally, classic cytotoxic agents have often unfavorable pharmacokinetic features which end up in a significant decrease of absorbed drug quantity, not to mention the high biodiversity of CYP 450 and other metabolic enzymes by which many chemotherapeutics are processed in vivo and which would require a personalized therapeutic protocol. Therefore, to reach minimum effective dose in blood stream, the administered drug dose has to be augmented, thus leading to a significant increase of the rise of the previously said side effects, which can be fatal in certain cases.

Targeted chemotherapeutics. In the case of *targeted chemotherapy*, instead, similar toxicological problems have not been observed thanks to the intrinsic specificity of these drugs' mechanism of action. These drugs are indeed designed to attack only tumor-specific targets. During the last decades of the 20th century, consistent research efforts were made in order to develop *targeted drugs* that block the growth and spread of cancer by interfering with *specific* molecules involved in tumor growth and progression. Even though many breakthroughs have undoubtedly been made in this field and although many new, tumor-selective molecules have been successfully developed and tested, it has often been observed that these new drugs, though safer and more tolerable, can lose efficacy in a relatively short period of time due to the arising of specific resistance.[9] The most famous representative of this drug class is certainly *Imatinib* ©, the lead compound in the tumoral kinase inhibitor family. Imatinib has been designed to inhibit BCR-ABL, a kimeric protein deriving only from the Ph+ (Philadelphia gene-positive) cells, which are mutated cells typical in chronic myeloid leukemia and other kind of rare tumors.[10] The inhibition of said kinase is fatal to the cancer cell, while healthy cells are not affected by Imatinib's action. Nevertheless, such a therapeutical approach, which could appear flawless at a first glance, has a significant limit. Because of their extraordinary duplication rate, tumor cells are subjected to develop mutation with a much higher frequency than healthy cells. Targeted drugs such as Imatinib only exert their cytotoxic activity by means of a single, specific mechanism (such as the inhibition of a particular enzyme) and the continuative administration of such treatments can lead, in a relatively short period, to the selection of a resistant generation of cancer cells. Cancer cells acquire this kind of specific resistance, for instance, by alteration of the active site of the target enzyme. Given their absolutely no specific mechanism of action, the activity of classic chemotherapeutic agents is not diminished in the least by this kind of mutation, but targeted chemotherapeutics result completely inactive once specific resistance has risen.

Nonetheless, both classic and target chemotherapy are limited by another kind of tumor cell resistance, namely **multi-drug resistance** (MDR), which can be intrinsic or acquired. If specific resistance to a certain cytotoxic molecule is attained by tumor cells by modification of the molecule's target, multi-drug resistance is a condition enabling the tumor cells to resist distinct drugs or chemicals of a wide variety. Cancer cells explicate multi-drug resistance through various mechanisms:

  • Enzymatic deactivation of the anti-cancer drug;

  • Decreased cell wall permeability to cytotoxic drugs;

  • Altered active sites also in less specific enzymatic targets;

  • Increased mutation rate as a stress response;

- Efflux mechanisms to remove drugs, such as glycoprotein P overexpression.[11]

For all of these reasons, it is evidently necessary to maximize drug dose in proximity of the target, in order to increase the efficacy of the treatment and to minimize chemotherapy's side effects. Therefore, the selective targeting of tumor cells is the goal of modern cancer therapy, aimed at overcoming this non-specific toxicity. This ambitious aim may be achieved by means of a *targeted drug delivery* system-involving therapy. Instead of focusing on a targeted pharmacodynamic activity, which may increase the probability of the development of specific resistance to targeted drugs, emphasis should be put on both selective pharmacodynamic and *pharmacokinetic* activity. This novel kind of therapeutic approach is very promising, for it may overcome the classical limits of chemotherapy, as reported in § 1.1.3.

1.1.3 Targeted drug delivery systems: the new frontier of chemotherapy

A targeted-drug delivery system strategy is aimed at conveying a bioactive molecule to its action site as specifically as possible, thus maximizing the in situ drug quantity without increasing administration dose and minimizing the side effects. The main target of all sophisticated drug delivery systems is to deploy medications intact to specifically targeted parts of the body through a medium that can control the therapy's administration (a process which is also known as *drug vectorization*) by means of either a physiological or chemical trigger. As a matter of fact, instead of exploiting tumor-specific pharmacodynamic targets, such as enzymes, in targeted drug delivery the specificity of action is ensured by interaction between the therapeutic agent and a tumor-specific *pharmacokinetic* target so that the distribution of the drug *in vivo* regards only the cancerous lesion. A similar pharmacokinetic target may be represented, for instance, by a receptor which is overexpressed by the tumor cell. The interaction with the specific target is not cytotoxic in itself (as it was in targeted chemotherapy, see § 1.1.2) but the bond between the targeted drug delivery system and the receptor is exploited as a Trojan horse in order to allow a highly focused distribution of the drug into the tumor cell. Drug delivery is often approached via a drug's chemical formulation, but it may also involve medical devices or drug-device combination products. The most common approach in the development of targeted drug delivery systems consists in conjugating the chemotherapeutic agent, which constitutes the cytotoxic portion of the system, to a *carrier* of various nature (Figure 1.2).
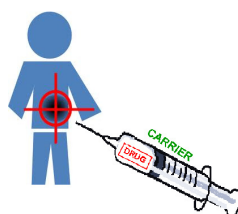
Figure 1.2. Drug delivery system approach

The carrier is the portion of the system which is expected to target the tumor cell, establishing a preferential interaction with the latter. Although the carrier may have an intrinsic cytotoxic activity (as shown in studies on metallic nanoparticles carriers) [12], it usually only works as a vehicle delivering the drug into the cancerous cell. It is thus evident that targeted drug delivery systems present numerous advantages:

- ✓ specific delivery of cytotoxic agents to tumor overexpressed receptors and subsequently a more selective killing of cancer cells. Moreover, the sparing of normal tissues from the harmful side effects of systemic therapy, allows to lower the administered dose in cure protocols. Such a decrease of the initial administered drug dose brings a series of major benefits, as a lowering in the incidence of chemotherapy side effects, not to mention the fact that this would postpone the necessity of dose escalation indicated whenever intrinsic resistance of some tumors to chemotherapeutic agents rises;

- ✓ recycling of those classic, very cytotoxic chemotherapeutic agents which have been eliminated from cure protocols because of their critical toxicological profile. In fact, minimizing drug tissue distribution, dangerous but efficacious cytotoxins may be used (or re-used) in therapy and this could represent a certain benefit both from the therapeutic and the economical point of view. An highly representative example of such a strategy is Inotuzumab-Ozogamicin, which has recently completed phase 2 trials for the treatment of non-Hodgkin lymphoma. [13] It allows the clinical use of ozogamicin, a calicheamicin which, despite being one of the most potent antitumor known,[14] could never be administered in classical formulations for its extremely unfavorable toxicological profile;

- ✓ very versatile entity which offers many modifiable sites on which the researcher can operate to improve the technological performance of the delivery system and the chemical stability of the conjugated pharmaceutical agent. A suitably modified carrier, in fact, may not function only as a mere drug vehicle, but (as in the case of liposomes, for instance) it could constitute a shield for a highly instable drug, protecting it e.g. from chemical or enzymatic hydrolysis in vivo or from degradation and aging during its shelf life.

It is for all these reasons that a rising interest on targeted drug delivery systems has been growing during the last three decades and nowadays, given the recent, impressive breakthroughs of nanomedicine, the possibilities offered by drug vectorization seem to be endless. This is also due to the very broad range of carriers which have been developed since the 1980s. In general, three main generations of vectors can be identified:

1) **First generation carriers**: these first vectors are constituted by organic polymer *microcapsules* or *microspheres,* which are injected intra arterially in the proximity of solid, primary tumors. Besides conveying the drugs directly to the tumoral tissue, they also have a *chemoembolization* effect, which consists in plugging tumoral arteries, causing a vascular disruption and the starving of the tumor, which undergoes ischemical necrosis. [15] The obstruction in tumor-lining blood vessels also prevents the drug from distributing in the systemic blood flow. This therapeutic strategy is not being applied in a very great number of cases; however, transarterial chemoembolization (TACE) has become standard treatment in selected patients affected by hepatocellular carcinoma. [16]

2) **Second generation carriers**: carriers such as *liposomes*[17] and *nanoparticles*[18] belong to this generation of vectors. They normally have colloidal dimensions (<1 µm) and are characterized by better intracellular permeation compared to first generation carriers. Liposomes are artificially-prepared vesicles composed of a lipid bilayer in which a drug may be encapsulated. Their surface offers many modifiable sites that can be functionalized with tumor receptor ligands (e.g. peptides, glycopeptides or even antibodies) to enhance the selectivity of its distribution. Besides working as specific carriers, they can protect the drug from *in vivo* degradation and slow drug metabolism and elimination down. For what concerns nanoparticles, a detailed analysis will be presented in § 1.2.3

3) **Third generation carriers**: *antibodies*,[19] especially monoclonal human or humanized antibodies (mAbs) against tumor antigens, are the most famous representatives of this generation of vectors, as they are undoubtedly the mainly used carriers of conjugated moieties for targeted tumor therapy or diagnosis.

In the1970s, the B-cell cancer myeloma was known, and it was understood that these cancerous B-cells all produce a single type of antibody. This was used to study the structure of antibodies, but it was not possible to produce identical antibodies specific to a given antigen. The process of producing monoclonal antibodies was invented by Georges Köhler and César Milstein in 1975; they shared the Nobel Prize in Physiology or Medicine in 1984 for such discovery.[20] Many antibodies-based pharmaceutical specialties have recently been approved by FDA, such as Herceptin (1998) for breast cancer, Erbitux (2004) and Avastin (2004) for metastatic colorectal cancer, with a subsequent revolution in chemotherapy, which for the first time is concretely stepping towards personalized medicine.[21,22] One possible treatment for cancer involves monoclonal antibodies that bind only to cancer cells specific antigens and induce immunological response on the target cancer cell (*naked antibodies*). Although unmodified mAbs may show some therapeutic potency, their effect tend to be various and ultimately not curative when not used in combination with classical chemotherapy. These antibodies would need to be administered to patients in massive doses to be effective, thus leading to serious side effects. As a result, mAbs have been armed with drugs, toxins, cytokines or radionuclides opening the door to the clinical use of targeted tumor therapy (Figure 1.3).[23]
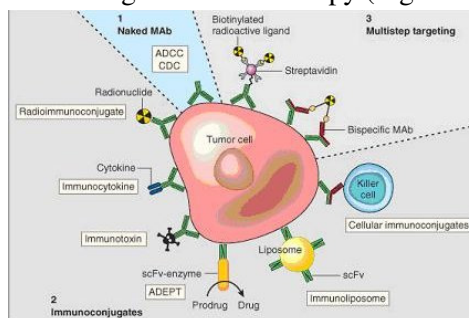

Figure 1.3. Monoclonal antibodies for cancer. ADEPT, antibody directed enzyme prodrug therapy; ADCC, antibody dependent cell-mediated cytotoxicity; CDC, complement dependent cytotoxicity; MAb, monoclonal antibody; scFv, single-chain Fv fragment.

Antibodies-based drug delivery systems employ several mechanism to damage the cancer cell:

- Making the cancer cell more visible to the immune system. The antibody marks the cancer cell as physiological B-cell produced antibodies normally mark pathogen cell during infections; as sometimes cancer cells are not recognized as enemies by the immune system, the antibody-mediated marking induces an immunological response addressed to the cancer cell;

- Blocking growth signals. Certain cancer cells overexpress growth factor receptors, whose interaction with their ligand makes them grow faster than healthy cells. Antibodies can also have an *intrinsic antitumoral activity*, by binding to growth factor receptors, as in the case of trastuzumab (Herceptin ©) or to growth factors themselves, thus inactivating them, as in the case of bevacizumab (Avastin ©). This synergic combination of specific vectorization of pharmaceuticals to the cancer cell and selective cytotoxic activity particularly increases the potency of this pharmaceutical specialties;

- Delivering radiation to cancer cells. By combining a radioactive particle with a monoclonal antibody, radiation can be delivered directly to the cancer cell;

- Delivering powerful drugs into cancer cells. Powerful anti-cancer drugs or toxins can be attached to monoclonal antibodies. Drugs remain inactive until they penetrate the target cells, lowering the chance of harming other cells.

This kind of drug delivery systems has raised great expectations among oncologists, so that ten new antibodies-based targeted therapies have been approved by U.S. Food and Drug Administration (FDA) since 2010. Nonetheless, the use of immunoglobulines as targeting moieties has some backdraws, such as the high costs of production, the difficulty in obtaining specific antibodies for every tumor type and, finally, toxicological issues. In fact, although antibodies can be disguised as human to evade the immune response, the delivery systems are xenobiotic substances and are soon recognized as such. This means there is only a short time when antibody therapy can be used before it becomes ineffective, not to mention the fact that the xenobiotic moiety may trigger an abnormal immunologic response, which could give rise to severe side effects. More fundamentally, the number of tumor cells in patients with terminal disease overwhelms the therapy. Some cells express too little antigen to be targeted and cells in a large mass may escape attention altogether. Antibody therapy is most likely to be useful in the context of minimal, but disseminated disease; in fact just the situation that often occurs after conventional chemo-radiotherapy. Moreover, antibodies conjugates are characterized by suboptimal pharmacokinetics and biodistribution, as well as non-specific uptake by the liver and reticuloendotelial system which may result in a systemic diffusion of the drug, losing the targeting effect.[24] To overcome the limits of antibody-based therapeutic approach, another strategy has been recently developed, in which the targeting moiety of the drug delivery conjugate is a peptide (as discussed in § 1.1.4).

1.1.4 Drug-peptide conjugates as an evolution of antibodies-based drug delivery systems: the case of Neurotensin

The discovery that receptors for different endogenous regulatory peptides are overexpressed in several primary and metastatic human tumors led to their use as tumor antigens; this opened the door to peptide-based therapeutic and diagnostic approaches in oncology.[25] These receptors can be used as molecular targets by which radiolabeled peptides can localize cancers in vivo, a strategy which can be exploited both for therapeutic and diagnostic purposes. As tumor targeting agents, peptides have several advantages over antibodies,[26] including:

- better organ or tumor penetration and more efficient cellular internalization, because the antibody molecules are relatively large and might not reach the tumor easily;

- greater stability (long storage at room temperature);

- lower manufacturing costs (recombinant production takes approximately twice as much, in terms of time and costs than chemical synthesis) and more reproducible production performances;

- batch-to-batch production parameters, due to the advances in solid-phase peptide synthesis;

- fewer and less expensive regulatory requirements (chemical synthesis versus recombinant production) and easier and quicker authority approval.

Peptides can serve as carriers for the local delivery of cytotoxic agents to the tumors, as demonstrated by the successful clinical use of radiolabeled somatostatin analog 'Octreoscan' for the detection and treatment of some somatostatin receptor-positive tumors.[27] Thus, in recent years a series of cytotoxic peptide hormone conjugates were developed.

Moreover, an increasing number of tumors may be addressed by 'peptide-bullet' strategy: peptides can be conjugated with cytotoxic moieties or radionuclides and, provided that the receptor-ligand complex is internalized on binding, the functional moiety can be specifically delivered into the tumor cell.[28]

An excellent candidate for a drug-peptide conjugate therapy is, among many others, *neurotensin*, a regulatory peptide whose receptors are over-expressed by many types of tumors and on which our work has been focused.

Neurotensin

Neurotensin (NT) was first isolated in 1973 from extracts of bovine hypothalamus based on its ability to cause a visible vasodilatation in the exposed cutaneous regions of anesthetized rats.[29] NT is a 13-amino acids regulatory peptide, sharing significant similarity in its C-terminal portion of amino acids with several other neuropeptides (Figure 1.4). This region is responsible for the biological activity as neurotransmitter while the N-terminal portion has a modulator function.
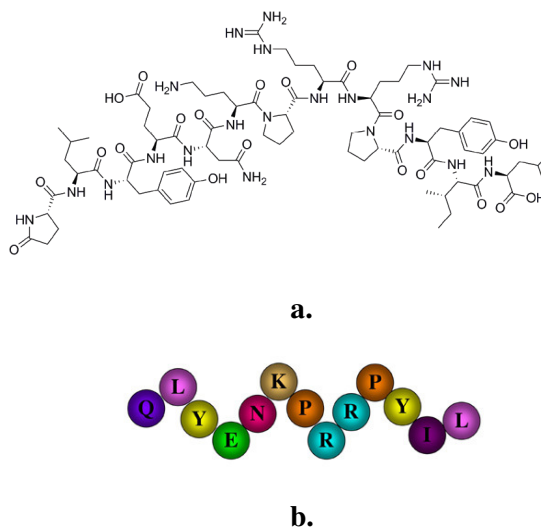
a.

b.

Figure 1.4. a. Neurotensin (NT), **b**. QLYENKPRRPYIL, schematic representation

NT is distributed in discrete regions of the CNS of mammals, where this peptide likely plays an important role as a neurotransmitter or neuromodulator in neuronal signaling. It has also been shown to be present in the hypotalami of a variety of species including rat, mouse, rabbit and man. In 1988, the rat NT gene was isolated and sequenced, finding out that the amino acids 8-13 of NT are essential for biologic activity.[30]

As many other neuropeptides, neurotensin both works as a neurotransmitter in the central nervous system (CNS) and as a local hormone in the peripheral tissues. In mammals, NT is widely distributed throughout the CNS (with highest levels in the *hypothalamus*, *amygdala* and *nucleus accumbens*) and

digestive tract (enteroendocrine cells of the small intestine), where it acts as a growth factor on a variety of normal or cancer cells.[31]

Neurotensin has various physiological functions; firstly it works as a vasodilation and hypotension inducer. In fact, it has been observed that central administration of neurotensin produces a marked dose-related decrease in body temperature of mice and rats at an ambient temperature of 25 °C. Other effects observed after central administration of neurotensin are decreases in locomotion and sedation. The effect is observed in both rats and mice, but only after central administration, neurotensin is, in fact, inactive after peripheral administration. This suggests that the tridecapeptide is not able to cross the blood-brain barrier in sufficient quantities to exert direct brain effects and also that the central nervous system locus of action of this compound lies within the confines of the blood-brain barrier. Thus, although neurotensin has been reported to induce several endocrine (increases in plasma concentrations of gonadotropins, ACTH, growth hormone, prolactin, corticosteroids, and glucagon) and hemodynamic (hypotension, vasodilatation, and cyanosis) changes after i.v. administration, it appears that the brain effects of this peptide are not mediated by such peripheral processes.[32] Major peripheral functions of neurotensin include the stimulation of pancreatic exocrine secretion, inhibition of gastric acid secretion, and inhibition of gastroduodenal motility. Fat ingestion induces a dose-related increase in neurotensin plasma concentrations, whereas glucose and amino acids produce only minor or no effect.[33]

The actions of NT are mediated by the stimulation of several specific receptors, called NTR. Three specific membrane receptors have been described so far. NTR1 shows a high affinity for NT, whereas NTR2 exhibits a low affinity (Figure 1.5).
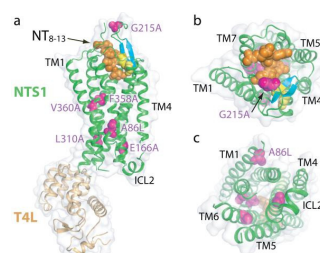

Figure 1.5. Overview of agonist-bound NTR1[34]

NTR1 and NTR2 belong to the family of G protein-coupled receptors (GPCRs). NTR3, also named Sortilin (Sort1) is an entirely new type of neuropeptide receptor with a single transmembrane domain[31] and it has been recently described as having an important role in pancreatic ductal adenocarcinoma cell migration. As previously reported, NT receptors are overexpressed by certain tumor type. Reubi *et al.* found receptors expressed on many tumor cells, such as meningiomas, pancreatic, prostatic, lung and colon carcinomas, in particular the high affinity NTR1.[35] Over 75% of all ductal pancreatic carcinomas were reported to overexpress neurotensin receptors, whereas normal pancreas tissue, pancreatitis, and endocrine pancreas do not.[36] Neurotensin receptors are observed more often in differentiated than in poorly differentiated tumors: indeed, as many as 83% of the differentiated adenocarcinomas are receptor positive; in particular, tumors with tubular differentiation are more often positive than solid tumors. Recently, it has been observed by *Gui et al.*[37] that NTR1 is commonly expressed in breast carcinomas; what is most interesting is that this overexpression is independent of ER/PR/Her2 profile, so a neurotensin based adjuvant therapy may be a breakthrough in the cure of "triple negative" breast carcinomas who cannot be treated with Herceptin and derivatives. Further and

up-to-date elucidations about possible interactions between neurotensin and receptors or other membrane proteins are reported in § 1.4.

For all these reasons neurotensin is considered an excellent lead compound for the design of a drug delivery system targeting moiety and, in particular, it seems to be the best possible candidate for peptide based therapy of exocrine pancreatic carcinomas, due to the high incidence and density of neurotensin receptors in these tumors, and of the whole gastrointestinal tract cancers in general. Unfortunately, the bottleneck for development of peptides as drugs has always been their extremely short half-life, due to physiological degradation by peptidases and proteases. High affinity ligands are also necessary, since unlike antibodies, monomeric peptides do not have the advantage of multimeric binding. To overcome this problem, various neurotensin analogues have been synthesized, including linear peptides, cyclic peptides, and nonpeptide molecules (inserting D-amino acids, or pseudo amino acids),[38] but chemical modification of the native peptide may radically modify receptor affinity and specificity.

Prof. *Luisa Bracci*'s group at the University of Siena, previously reported that synthesis in branched form increased the biostability of certain peptides, including neurotensin, obtaining promising results *in vitro* and *in vivo* both for diagnostic and therapeutic purposes.[39] The synthesis of bioactive peptides in Multiple Antigen Peptide (MAP) dendrimeric form turns out to be useful, leading to acquired resistance to protease and peptidase activity (Figure 1.6).
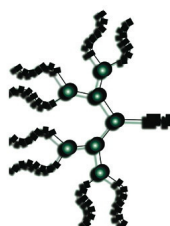

Figure 1.6. Schematic MAP representation

MAPs (Multiple Antigenic Peptides) are a novel, promising tool for generating anti-peptide antibodies, so that they are also currently used in immunization protocols.[40] They provide more *in vivo* stability compared to monomeric peptides, thanks to the greater complexity of their structure which ensure better resistance to proteases and peptidases. The MAP system utilizes a peptidyl core of three or seven radially branched lysine residues, on to which the antigen sequences of interest (in this case a peptide) can be built using standard solid-phase chemistry (Figure 1.7).
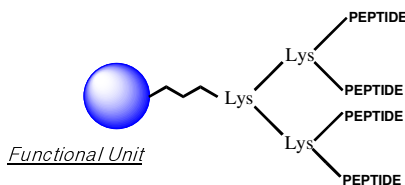

Figure 1.7. Peptide tetramer with three-lysine branched core

14

Thanks to this lysine core, the MAP can bear four or eight copies of the peptide epitope (resulting in high molar ratio), depending on the inner core that generally accounts for less than 10% of total molecular weight. Moreover, the MAP system does not require a carrier protein for conjugation. Besides enhancing the binding capacity, the high molar ratio and dense packing of multiple copies of the antigenic epitope in a MAP has been shown to produce strong immunogenic response; as a matter of fact they exhibit superior immunoreactivity and binding capacity in comparison with both antibodies and monomeric peptides.[41]

Synthetically, the use of MAPs shows some advantages:

- Increased coating efficiency on solid surface;

- Enhanced detection sensitivity for solid phase immunoassay;

- Independence from the use of a carrier protein to elicit antibody response.

Moreover, MAPs can be more efficient than monomeric peptides in diagnostic applications and also have the possibility to be conjugated to various Functional Units such as fluorophores, photosensitizes, cytotoxic groups or chelators for radioisotopes. As said before, the *in vitro* and *in vivo* efficiency of dendrimeric peptides like MAPs is generally ascribed to their multimeric nature, which enables polyvalent interactions.

In order to demonstrate the longer half-life of MAPs derivate, Professor Luisa Bracci's research group (also thanks to AIRC funding) compared the stability monomeric and tetrabranched neurotensine. Bioactivity of monomeric and MAP peptides was checked by testing the inhibition of nM [^{3}H]neurotensin-specific binding to membranes prepared from the human colon adenocarcinoma cell line HT 29.[42] Experiments were performed in the presence of protease inhibitors. MAP NT efficiently inhibited nM [^{3}H]neurotensin-specific binding, and its IC$_{50}$ value was analogous to that of monomeric NT. The resistance to protease activity in human plasma and serum was tested for the two peptides. Monomeric and tetrabranched peptides were incubated with human plasma or serum for 2 or 24 h, and the mixture was analyzed by HPLC and mass spectrometry to follow the presence of uncleaved monomeric and MAP peptides. As a general rule, peptides that are cleaved in plasma in 2h are also cleaved in serum at the same time. Those resistant in serum after 24h are also resistant in plasma It was found that the MAP form was more resistant than the monomeric form (Table 1.1).

Peptide	Plasma (2h)	Plasma (24h)	Serum (2h)	Serum (24h)
NT	+	-	+	-
MAP-NT	+	+	+	+

Table 1.1. The absence (-) or presence (+) of peptide after the incubation times refers to the unproteolyzed peptide sequence as detected by HPLC and MS.

Moreover, in order to test the possible influence of peptide length, number of peptide copies, and steric hindrance on branched peptide stability to peptidases, the monomeric, two branched and tetra-branched forms of NT were synthesized and their stability, after incubation with human plasma and

serum was compared. Prof. Bracci found that the tetra-branched form of neurotensin and was stable in both human plasma and serum for 24h, whereas the two-branched for 5h and and the monomeric analogue was degraded in roughly 5h (Table 1.2).[28]

Peptide	Plasma (2h)	Plasma (5h)	Plasma (24)	Serum (2h)	Serum (5h)	Serum (24h)
Monomeric NT	+	-	-	+	-	-
Two branched NT	+	+	-	+	+	-
Tetrabranched NT	+	+	+	+	+	+

Table 1.2. Stability of the three peptide in plasma and serum

Protease-resistance of tetrabranched neurotensin has been then studied in regard to NT-cleaving enzymes structure.

Neurolysin and *TOP* (thimet oligopeptidase) cleave most bioactive peptides at the same site or sites, but they recognize different positions on some naturally occurring and synthetic peptides. Notably, they cleave at distinct sites on the 13-residue bioactive peptide neurotensin, for which they are the primary metabolizing enzymes. Neurolysin cleaves the peptide between Pro-10 and Tyr-11, and TOP cleaves between Arg-8 and Arg-9 (Figure 1.8).[43]
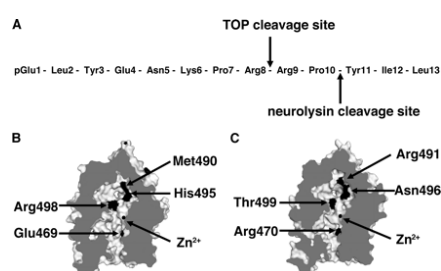

Figure 1.8. NT cleavage sites and key residue differences in the substrate binding channels of TOP and neurolysin. **A.** The sequence of the peptide neurotensin is shown, and the primary hydrolysis sites for the enzymes TOP and neurolysin are indicated. **B.** Cut away molecular surface view of the TOP substrate-binding channel with residues likely to mediate differences with neurolysin in neurotensin cleavage site. **C.** Same view of the neurolysin substrate-binding channel with corresponding residues indicated.

Peptidases acting on small endogenous peptides are mainly Zn metallopeptidases like neurolysin. Neurolysin adopts an overall prolate ellipsoid shape with a dramatic deep cleft or channel running the length of the molecule. The channel extends for about 60 Å and plunges to almost 40 Å below the top of the molecule at its deepest point. It effectively divides the enzyme into two large domains (labeled domain I and domain II) that are connected only at the floor of the cleft by a small number of secondary structural elements. The active site of the enzyme lies at the base of domain II near the bottom of the channel and about midway along its length. the catalytic centre of which is located in a deep channel, to which only small peptides have access (Figure 1.9).[44]
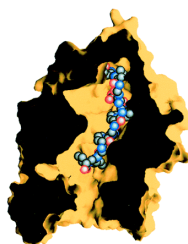

Figure 1.9. Molecular surface representation of neurolysin sectioned to show the large cavity at the bottom of the active-site channel is shown with the 13-residue substrate neurotensin. The N terminus of neurotensin is at the top.

Although binding of the peptide in the catalytic pocket may still be possible, the cleavage site may be geometrically unreachable by catalytic residues, especially in tetrabranched peptides that, unlike two-branched ones, cannot achieve an extended conformation. As a result, steric hindrance may limit their access to the cleavage site of these peptidases, increasing the peptide half-life, with obvious advantages for their use as drugs. The possibility to form supramolecular aggregates is another feature of branched peptides probably accounting for their increased stability. Tetrabranched peptides may arrange their four arms in parallel structures stabilized by intramolecular H-bonding of the backbone. This structure would resemble that of self-assembling β-sheet peptides. Prof. Bracci's results indicate that synthesis in dendrimeric form may be a general method to increase *in vivo* stability of bioactive peptides and so a step forward on the direction of the finding of new specifically targeted cytotoxic drugs.

1.1.5 Towards the synthesis of a MAP-NT based drug delivery system

MAP-NT does not present binding sites for bioactive molecules; therefore, in order to functionalize the dendrimer with the drug moiety, the synthesis of a non-peptidic linker able to bind the theranostic moiety to the lysine core has been necessary. The C-terminal lysine side chain was functionalized with the chemotherapeutic agents spaced by an amino-terminal PEG (polyethylenglycol) moiety, chosen in consideration of synthetic and biological issues. Spacing is necessary, as the hindrance of the branched peptide might impair the access of the activated chemotherapeutic and therefore give poor reaction yields. Moreover the drug moiety, if closely linked to the branched peptide, might impair receptor recognition and, for slow realizing compounds, the closeness of branched peptide might compromise drug-target interaction inside the cell. A special care in choosing the suitable linker to insert between the functional unit and the tetrabranched peptide was taken, considering that in the case of cytotoxic molecules the link has to be broken preferably upon internalization into the tumor cell. In this sense the complex should be considered as a 'pro-drug', defined as a precursor of a drug that has to undergo

chemical conversion by metabolic processes before becoming an active pharmacological agent. The final structure is then a lysine-core NT tetramer functionalized with an amino-terminal linker, which could constitute the binding sites for the therapeutic unit (Figure 1.10). Further details about solid phase synthesis of MAP-NT will be discussed § 1.2.1
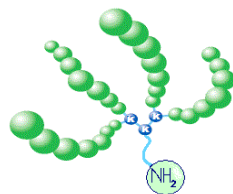

Figure 1.10. Schematic representation of the amino-terminal linker functionalized MAP-NT

It is evident that this kind of protein inspired chemotherapeutics are pro-drugs. The rationale for the development of pro-drugs relies upon delivery of higher concentrations of a drug to target cells compared to administration of the drug itself. In the last decades, numerous pro-drugs that are enzymatically activated into anticancer agents have been developed. Pro-drugs are often divided into two groups: 1) pro-drugs designed to increase the bioavailability to improve the pharmacokinetics of antitumor agents and 2) pro-drugs designed to locally deliver antitumor agents. In this last approach pro-drugs are designed to achieve a high local concentration of antitumor drugs and to decrease unwanted side effects. The activation step makes use of some unique physiological, metabolic or genetic differences between tumor and normal cells, such as different oxygen, ligands and enzymes concentrations.[45] By this concept, referred to as targeting, organ-specific and tumor-specific prodrug activation can be achieved. To specifically activate prodrugs into a certain organ, the enzyme involved in the prodrug activation must be selectively present in the target organ.[46]

The preparation of selected conjugated pro-drugs, drugs and diagnostic tools have been the main challenge of this project. Thanks to AIRC funding, we have synthesized in our laboratory suitable derivatives of some of the most used chemotherapeuticals, such as 5-Fluorouridin or Gemcitabine, so that they could be linked to the amino-terminal MAP-NT moiety (Figure 1.11).
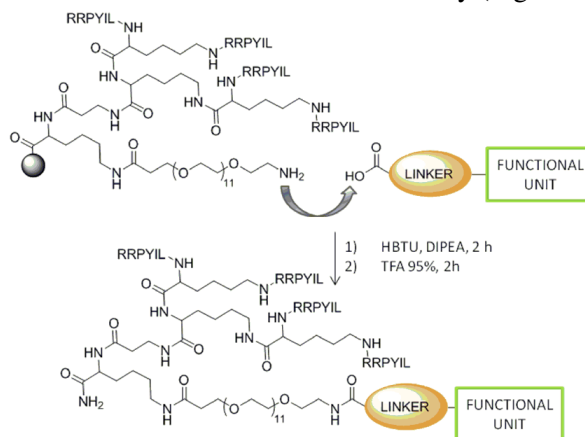

Figure 1.11. Conjugation procedure

Said drugs have been coupled with alifatic α-ω diacids. Such carboxylate-decorated drugs can be then coupled through an amidic bond with the amino-terminal MAP-NT moiety. The advantage of this final coupling on solid phase is that the drug derivatives can be treated as an amino-acid and linked to the

peptide exploiting the same procedure used for building up the primary sequence of MAP-NT on resin. We decide to use ester linkage as covalent bonds suitable for safety delivering the drug inside the cell where the releasing of the anticancer agent occurs by hydrolysis (mediated by ubiquitous esterases). As it will be described in the following sections, we have synthesized a variety of carboxylic derivatives decorating the most common anticancer drugs such as 5-Fluoro-2'-deoxyuridine (5-FdUrd), Gemcitabine, Paclitaxel, Cisplatin, Estradiol, 2-methoxyestradiol, Combretastatin A4 and Camptotechin.

As for the achievement of the targeted drug delivery system, Bracci's group in Siena has set up a general method allowing conjugation by standard solid-phase peptide synthesis (Figure 1.11). In this way we have successfully synthesized drug conjugates with a higher or comparable toxicity to the one of the unreleated drug (for pharmacological results see § 1.3) *in vitro*. Among others, MAP-NT-gemcitabine particularly showed a high toxicological profile in multiple human cell lines, such as T24, HT-1376 (human bladder carcinoma), PANC-1 (human pancreatic carcinoma) and PC3 (human prostate cancer), while in some cases, resistance of certain cell lines, such as HT-29 for combretastatin A4 was observed.

Unfortunately this strategy couldn't be applied to all the chemically modified anticancer drug prepared. Indeed, as described in § 1.2.1, in the last step of Bracci's protocol, peptide-functional unit conjugates are cleaved from the resin by treatment with trifluoroacetic acid (TFA). The drastic acid condition of the cleavage could, in some cases, partially of fully destroy the chemical scaffold of drugs, leading to an irreversible damage to the conjugate. To overcome this problem, we envisaged a 'post-cleavage coupling' strategy in which the peptide is cleaved from the resin prior to the coupling with the therapeutic unit, that thus is led in liquid phase. This allow the conjugate not to undergo acid environment and preserve it from degradation.
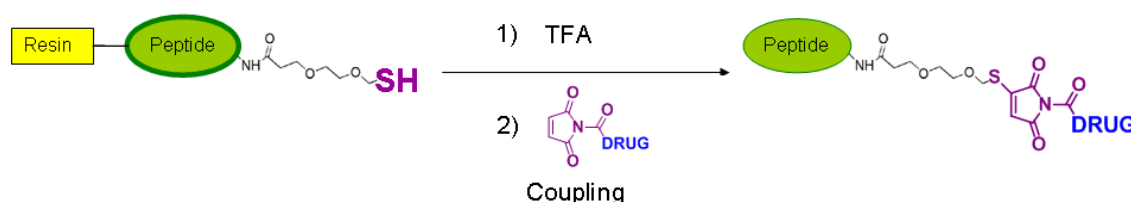

Figure 1.12. Click chemistry protocol for 'post-cleavage coupling' strategy. Step 1) is the simultaneous cleavage from the resin and deprotection of protecting groups on later chain of the aminoacid. Step 2) is coupling through a Michael reaction

To achieve this aim, we exploited a 'click chemistry' strategy to properly decorate either the peptide and the drug. Among other strategies, we chose to insert a thiol group on MAP-NT, through a terminal cysteine residue, that could react with a maleimido group bound on the anticancer agent (Figure 1.12). This Michael reaction is highly selective and does not involve free groups on later chain of the aminoacids that were deprotected with TFA during the cleavage of the peptide from the resin, allowing to lead it in solution phase without formation of side-products. In order to demonstrate the feseability of the method, a MAP-NT-fluorophore (Alexa Fluor [®]750) tagged complex has been synthesized exploiting thiol-maleimide coupling protocol and tested in xenografted mice with HT29 (colon adenocarcinoma). In injected mice the conjugate primarily localized in proximity of the tumor mass, showing and the effective (and specific) targeting of the conjugate to cancer cells. Encouraged by these promising results, we extended the strategy to drugs. Indeed, Paclitaxel, a mitotic inhibitor agent, is the perfect example of successful 'post-cleavage coupling' strategy, as discussed in § 1.2.2.

19

1.1.6 Metallic functionalized nanoparticles: an improvement of MAP-NT strategy

The previously described targeted drug delivery system, composed by a targeting moiety (MAP-NT), an amidic (or thiolic) linker and a functional unit certainly represents an evolution of traditional targeted drug delivery systems, such as mAbs-drug conjugates. As already suggested, peptides in such a dendrimeric form are particularly suitable for *in vivo* use because they acquire a notable resistance to degradation by proteolytic enzymes, though maintaining or even increasing their natural biological activity. Moreover, neurotensin, synthesized as tetramers, even offers accessible linking units for coupling of functional moieties.

Nevertheless, neither this complicatedly engineered delivery system succeeds in solving one of the problems intrinsic to the peptide-drug conjugate strategy. As already highlighted in § 1.1.4, one of the greatest drawbacks of peptide-based targeted therapy is the fact that multimeric drug binding is not possible, whereas, in the case of mAbs, each immunoglobulin is able to carry two (IgG) or five (IgM) ligands. This represents a great limit for this strategy, as the bulky, highly expensive (in terms of cost of production) MAP-NT molecule just delivers one drug molecule to the tumor cell. Moreover, many factors have to be considered, such as the likelihood of premature hydrolysis of the drug-linker bond by means of plasmatic esterases or possible drug release problems, which would even decrease the quantity of drug per carrier molecule which would effectively reach the tumor cell. In order to maximize the poor drug/carrier molar ratio of MAP-NT- drug conjugates, then, our research group has oriented its synthetic efforts on the development of an even more complex drug delivery systems which could match the advantages of MAP-NT strategy with an higher drug-binding capacity.

Therefore, we have chosen to develop a peptide-nanoparticle-drug conjugate (Figure 1.13).
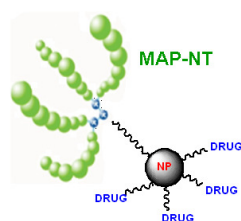

Figure 1.13. Schematic representation of the MAP-NT / nanoparticle (NP) / drug conjugate

Bearing many functional groups, nanoparticles can be linked to a greater number of molecules simultaneously, thus overcoming the stoichiometric problem by which the mere MAP-NT delivery system was characterized. Nanoparticles are revolutionizing almost every science field, from information technology to medicine, thanks to their utmost versatility and their potential contribution to chemotherapy has not to be ignored.[47]

Nanoparticles

There is no official definition of nanoparticles (NPs), although, in nanotechnology, they are commonly defined as small objects that behave as a whole unit with respect to its transport and properties, and whose diameter does not exceed 100 nm. Although, in general, nanoparticles are considered a discovery of modern science, they actually have a very long history.[48] Nanoparticles were used by

artisans as far back as the 9th century in Mesopotamia for generating a glittering effect on the surface of pots. The properties of nanoparticles were proved in 1857 in Faraday's famous paper "Experimental relations of gold (and other metals) to light".[49] In recent years, nanoparticles have increasingly found practical application in several science fields. Growing interest towards NPs is raised by their unique physico-chemical properties, different from those of the bulk material, which develop at a critical length scale of under 100 nm.[50] This may also occur because of their large surface area to volume ratio, which is responsible for their high biological activity.[51] In particular, metallic nanoscale particles have attracted much attention due to their electronic, optical and magnetic properties, which have earned them a very relevant role in modern biomedicine and which renders them truly *theranostic*, term that refers to their capacity to be at once therapeutic and diagnostic (Figure 1.13). Currently, the only clinically approved metallic nanoparticles are employed in diagnosis rather than in therapy; as a matter of fact, superparamagnetic iron oxide nanoparticles (SPIONs) have definitively replaced gadolinium-based contrast agents in magnetic resonance imaging for their slower renal clearance and higher relaxation values.[52] However, metallic nanoparticles have also great therapeutic potential, as it is proved by the wide number of preclinical trials in which they are involved.[53] Modern oncology is increasingly relying on the possibility to use these devices in order to enhance efficacy and selectivity in cancer therapy (Figure 1.14).
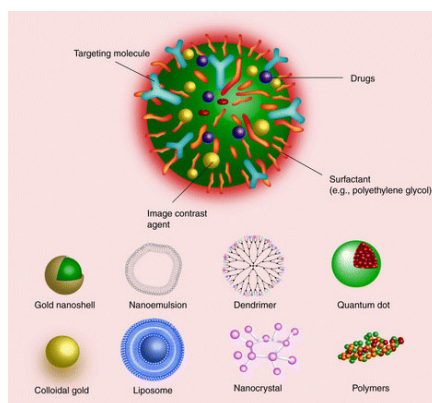

Figure 1.14. General overview of NPs and their functionalization

Drug-loaded nanoparticles thus amount to a relevant breakthrough in targeted oncological therapy, as they can convey chemotherapeutics right to the cancer cell by a series of different, specific mechanisms, as well as having, in certain cases, an intrinsic cytotoxic activity.[54] Nanoparticles can perform their targeting and therapeutic activity through a wide variety of mechanisms, depending on whether they have paramagnetic properties or not. This versatility is therefore very advantageous, since it allows researchers to design a multi-armed therapeutic device in which these several mechanisms of action converge synergically. As previously said, a first discrimination between paramagnetic and non-paramagnetic NPs has to be made. Nevertheless, there are some features that both NP categories present:

✓ They both constitute a second-generation (see § 1.1.3) vector for targeted drug delivery when merely functionalized with drugs (excluding a targeting moiety). In fact, they share an intrinsic tumoritropic *enhanced permeability and retention effect* (EPR effect) which ensures the targeting activity by a *passive* mechanism (Figure 1.15). As a matter of fact, colloidal size objects (such as liposomes, nanoparticles, macromolecules) tend to be accumulated

21

preferentially by tumor tissue rather than normal tissue,[55] presumably because of the accentuated permeability of newly formed tumor blood vessels. However, although NPs have the capacity to be passively delivered to tumor cells, it may be profitable to further increase the targeting capacity of the drug delivery system. This can be achieved by switching from the above said passive vectorization mechanism to an *active* targeting mechanism. This targeting mechanism is characteristic of antibody or peptide-drug-NP conjugates, as they are not simply accumulated by the tumor cell; they rather *actively* "track" the cancer cell by means of their targeting moieties and locally release the massive quantity of drug they are loaded with (usually greater than in the case of simple peptide or mAb-drug conjugates, as said in §1.1.4).
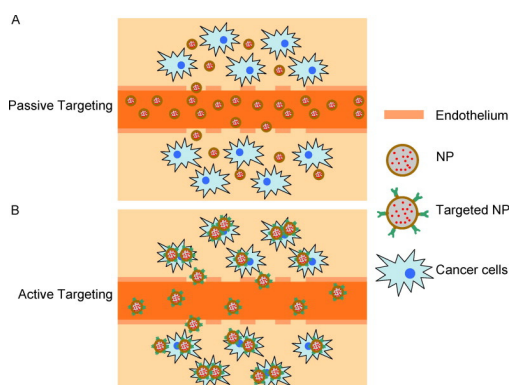

Figure 1.15. Schematic representation of passive (A) and active (B) targeting of NPs

✓ Their capacity to protect unstable drugs from *in vivo* degradation. This may be achieved by the application of a polymer coating on the drug-loaded nanoparticles, which acts as a shield towards the pharmaceutical agent.[56]

✓ Possible use in *tumor-focused hyperthermia*, which may be induced photothermally (in the case of non-paramagnetic nanoparticles, such as gold NPs) or magnetically (in the case of paramagnetic NPs, such as SPIONs).[57] NPs can conduct heat massively and focusedly to the tumor cell in which they have been accumulated, causing tumor tissue shrinking and necrosis. This approach is currently undergoing clinical trials, but could represent a useful adjuvant strategy in oncological multi-mechanism therapy.[58]

At any rate, there are some peculiarities exclusive to *paramagnetic nanoparticles* (and superparamagnetic ones) which may offer some further weapons against cancer. The most evident one is the possibility to enhance the action selectivity of the drug delivery system by performing a *magnetic field assisted targeted therapy*. From the physical point of view, magnetic targeting is derived from the magnetic force exerted on nanoparticles by a magnetic field gradient. The process of drug localization is based on the competition between the hydrodynamic forces exerted on the particles by the blood compartment and the magnetic forces generated from the applied magnetic field (usually neodymium-iron-boron permanent magnets, fixed outside the body over the target site). The NP-based drug delivery system is injected intra arterially in the circulatory system and once the magnetic forces exceed the linear blood flow rates in arteries and capillaries, the magnetic particles are retained at the target site,[56] hence the additional targeting ability of this category of NPs. The advantages of magnetic field assisted targeted therapy are particularly evident when the nanoparticles are loaded with radioisotopes (by means of the suitable radionuclide chelators). Thanks to magnetic

targeting, a high concentration of the cytotoxic radionuclide is reached in proximity of the tumor tissue, thus sparing healthy tissues in which such dangerous radiations could definitely increase the chance of a second malignancy in the future.

Moreover, many magnetic nanoparticles (such as SPIONs) have an intrinsic cytotoxicity[12] (presumably mediated by oxidative stress) which could be exploited synergistically in a targeted oncological therapy: obviously this could raise some toxicological questions, but the multi-approach tumoritropic vectorisation of the drug delivery system should contain the systemic toxicity. It is evident how the use of nanoparticles may guarantee a maximization of the concentration of the chemotherapeutical agent in the tumor tissue, thanks both to their variety of targeting mechanisms (schematized in Figure 1.16) and high drug/carrier ratio.
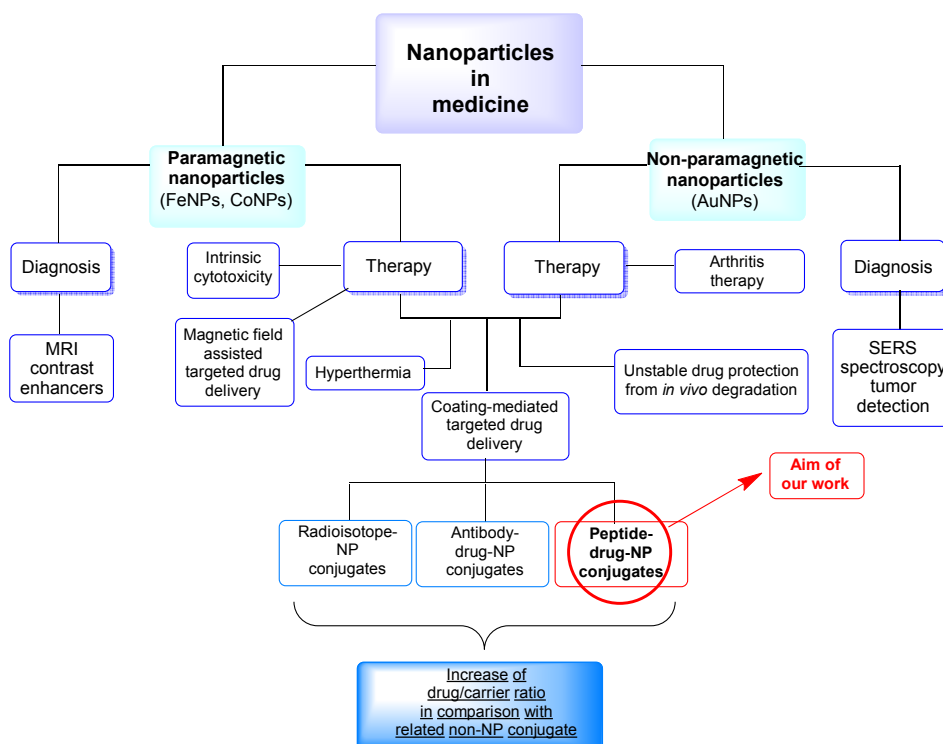

Figure 1.16. An outline of nanoparticles' targeting and therapeutical mechanisms

One of the main aim of my thesis project was to incorporate the nanoparticle unit to the previously developed MAP-NT-drug conjugate. However, before ever conceiving such a complex three-units system, a deep and detailed study on the mere functionalization of the nanoparticle with the chemotherapeutical agent was necessary; it is for this reason that my research efforts have been focused on the development of chemotherapeutical agent-loaded nanoparticles. As a matter of fact, a first, thorough study on the physico-chemical and pharmacological properties of the drug-nanoparticle conjugate was indispensable, in order to anticipate the effective feasibility of the whole, long-term project, so that in the future this system may be further expanded with the addition of the targeting unit (MAP-NT).

As part of my PhD thesis, I had the opportunity to work on the development of three different chemotherapeutic-loaded nanosystems. My work was aimed at conjugating combretastatin, a very promising anti-tumor agent, to three different kinds of nanoparticles, namely:

- Superparamagnetic iron oxide nanoparticles (**SPIONs**);

- Cobalt *TurboBeads* © (**CoNPs**): cobalt nanoparticles coated with an amide or azide-functionalized polymer, which allows derivatization by means of amidation or alkyne-azide click reactions;

- Gold nanoparticles (**AuNPs**).

This three kinds of nanoparticles have been chosen by virtue of their therapeutic and diagnostic potential, which they explicate through different mechanisms, being reciprocally heterogeneous for what concerns magnetical, optical and chemical properties. The synthetic results, as well as the anti-tumor activity, of these first nanosystems (schematized in Figure 1.17) will be reported in this thesis.
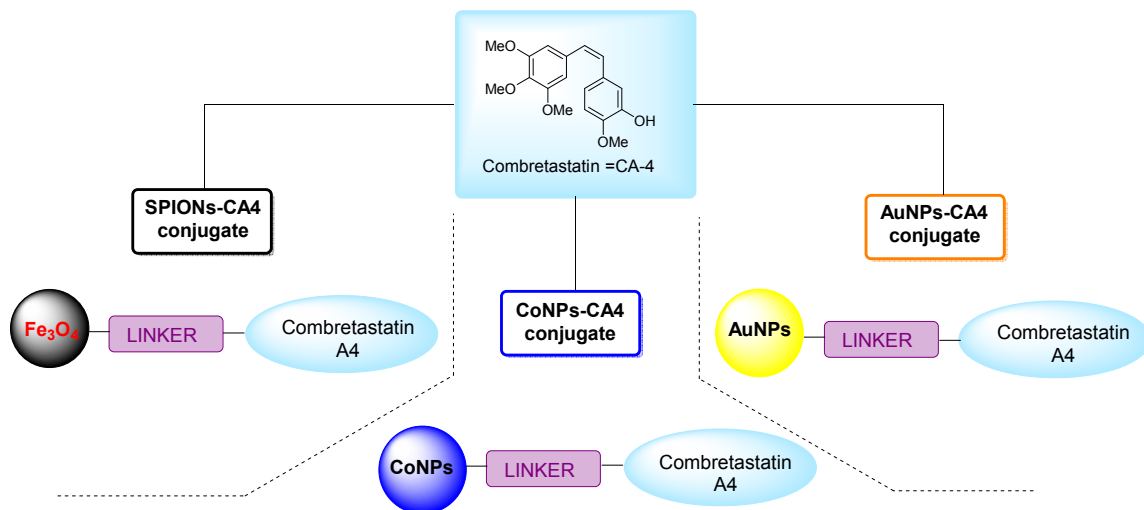

Figure 1.17. Nanosystems developed in our laboratory

1.2 Results and Discussion

Cytotoxin

A *cytotoxin* is any substance which has a toxic effect on cells. The term'*cyto*'is of Greek origin, and refers to 'a hollow container'. Some common examples of cytotoxins include chemical agents and certain snake venoms. Cytotoxins typically attack only a specific type of cell or organ, rather than an entire body. Cells that have been affected by a cytotoxin can perish in several different ways. One is *necrosis*, in this form of cell death, the cells lose integrity in their membrane wall and collapse. Another type of possible cell death is *apoptosis*; this type of death is pre-programmed into the cell itself before the cytotoxin arrives.[59]

Among chemical agent, a large category is represented by *cytotoxic medicines,* commonly used in chemotherapy to treat cancerous deseases. Cytotoxic medicines are toxic (poisonous) to cancer cells. They kill cancer cells or stop them from multiplying. Different cytotoxic medicines do this in different

ways. However, they all tend to work by interfering with some aspect of how the cells divide and multiply. The drawback that all shared is that these drugs often produce toxic side effects due to their poor selectivity between target (e.g., cancer cells) and normal cells.

Use of citotoxic medicin in cancer chemotherapy emerged in the 1940s from toxicological studies of nitrogen mustard-based war gas,forefathers of drug like carmustin and cyclophosphamide (as discussed in 1.1.2). The anticancer activity of nitrogen mustard is due to DNA alkylation, and many other cancer drugs were developed on the basis of this general concept that irreversible modification of DNA impair accurate cellular replication and then optimized on the basis of cytotoxicity in growth proliferation models.[60] Mechanism-based approaches have also been explored for several decades. Antimetabolite drugs (for example, methotrexate and mercaptopurine) were developed on the basis of a scientific understanding of key enzyme steps in nucleotide biosynthesis and the sensitivity of tumor cells to alterations in these pathways. Newer agents in this class, such as gemcitabine (Gemzar),[61] continue to show promise in the management of some cancers. Over the last 30 years, there has been a fundamental shift in the way target identification in cancer is approached. Advances in molecular biology now allow us to identify genes that go awry in cancer, and offer the opportunity to dissect the molecular mechanisms underlying the disease.

Today there is a large variety of cytotoxins alone or in combined pharmacological treatment of malignant tumors. We decided to work on that ones that are chemically most suitable to be synthetically modified and then conjugated to the targerting dendrimer. This implies the presence of an hydrolxyilic group on the scaffold of the molecule as starting point to insert the appropriate linker, through an ester bond.

The chemical nature of the linker and the terminal moiety on MAP-NT was selected on the based of the stability of the anticancer drugs to TFA. In case the drug was stable, a carboxylic acid terminal linker and a free amine moiety on the peptide were chosen. Thus, drug-peptide coupling was directly performed on solid phase (pre-cleavage coupling), as discussed in § 1.2.1.

On the other hand, in some case we experimentally observed the absence of the expected ESI-MS peak, after cleavage from resin. The unsuccess of the procedure was attributetd to the instability of the complex to TFA and an alternative strategy for coupling has to be investigated. We, thus, envisaged a post-cleavage coupling in which the anchorage of the therapeutic unit with the peptide was led in liquid solution after removal of MAP from resin. This entailed a different chemical decoration of both the unit; an amidation coupling was no more conceivable, since treatment with TFA removes the protecting groups on later chains of neurotensin, that could compete with the terminal NH_2 for coupling with the drug. We decide to exploit a 'click chemistry' strategy that resulted useful even for functionalization of nanoparticles.

After a screening in literature, we found out that many different classes of anticancer drugs have requirements we were looking for, such as: A) *antimetabolites*, B) *bioreductive drugs,* C) *estrogens,* D) *mitosis inhibitors* and E) *DNA topoisomerase I inhibitors.* The chemical modification operated and the related experimental procedures are described below.

1.2.1 Cytotoxin: pre-cleavage coupling

A. Antimetabolites

Antimetabolites are substances that closely resemble an essential metabolite and therefore interfere with physiological reactions involving it.[62] Because their structures resemble the endogen metabolite, they are taken up by the cell, but they does no react in the same way with the enzyme that acts on the usual compound. They may inhibit the enzyme or be converted into an aberrant chemical, anyway prevent the cells from carrying out vital functions and the cells are unable to grow and survive.

The scientific understanding of key enzyme steps in nucleotide biosynthesis and the sensitivity of tumor cells to alterations in these pathways led to the developing of antimetabolites drugs. Antimetabolite drugs were among the first effective chemotherapeutic agents discovered and are folic acid, pyrimidine or purine analogues. They are characterized by low molecular weights and have similar structures as naturally occurring molecules used in nucleic acid (DNA and RNA) synthesis. Generally, they induce cell death during the S phase of cell growth when incorporated into RNA and DNA or inhibit enzymes needed for nucleic acid production. These agents are used for a variety of cancer therapies including leukemia, breast, ovarian and gastro-intestinal cancers.[63]

The clinical applications are not limited by the low selectivity, on a hand, because cancer cells spend more time dividing than other cells, inhibiting cell division harms tumor cells more than other cells. On the other hand it often generates serious back side effects like nausea, vomit and loss of hair.

We decided to concentrate our attention on two pyrimidine analogues: 5-Fluoro-2'-deoxyuridine (**1**) and Gemcitabine (**2**).

5-Fluoro-2'-deoxyuridine (5-FdUrd)

5-Fluoro-2'-deoxyuridine (5-FdUrd, **1**) was synthesized for the first time in 1979 by Cook *et al*.[64] Chemotherapy using fluoropyrimidines, like 5-fluorouracil (5-FU) or5-fluoro-2-deoxyuridine (FUdR), often in combination with modulators such as leucovorin, methotrexate or interferon is most often used in particular in patients with colorectal cancer.[65] 5-FdUrd is commonly called doxifluridine or Furtulon® and has a molecular structure consisting of a molecule of 5-Fluorouracil (5-FU) to which a pseudopentose is bound in position 1 (Figure 1.18).
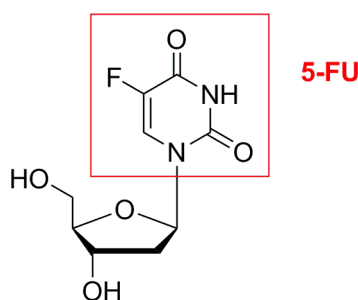

Figure 1.18. 5-FdUrd (**1**)

Regarding its mechanism of action, it is an anti-metabolites masquerade as a pyrimidine, which become the building blocks of DNA. Specifically, 5-Fluoro-2'-deoxyuridine inhibits thymidylate synthase (TS). The inhibition of TS causes an imbalance of intracellular deoxyribonucleoside triphosphate (dNTP) pools which subsequently induced cell death.[66] It prevents the endogenous substances becoming incorporated in to DNA during the S phase (of the cell cycle), stopping normal development and division. Before the incorporation in nucleic acids 5-FdUrd have to be metabolically

transformed in 5-FU and then phosphorylated into FdUMP. This process needs the enzyme Thymidine Phosphorylase (TP), a tumor-associated angiogenesis factor, to occur. It is primarily expressed by cancer cells, stromal cells and tumour-associated macrophages in many human malignancies[67] at higher level than normal proliferating tissues, giving an enhanced selectivity of FdUrd. However, very high activity of TP is found in normal human liver, thus the liver toxicity.

5-FdUrd (**1**) has a relevant role in the treatment of metastatic cancers, either by exerting an appropriate antitumor activity via blocking thymidylate synthase to inhibit DNA synthesis or by incorporation of its metabolite (5-Fluorouracyl) into DNA or RNA.[68] A downstream event of thymidylate synthase inhibition involves the induction of a self-defeating base excision repair process. With the depletion of TP pools, there is also an increase in dUMP. Metabolism of dUMP to the triphosphate dUTP results in elevated pools of this atypical precursor for DNA synthesis. Under these conditions, there is a destructive cycle of dUMP incorporation into DNA, removal of uracil by the base excision repair enzyme uracil-DNA glycosylase (UDG), and reincorporation of dUMP during the synthesis phase of DNA repair. The end point is DNA strand breaks and loss of DNA integrity, which contributes to cell death. UDG is an additional determinant in FdUrd-mediated cytotoxicity and bolster the notion that the self-defeating base excision repair pathway, instigated by elevated FdUTP pools, contributes to the cytotoxic consequences of 5-FU chemotherapy.[69]

Despite of the extended use of 5-FdUrd as anti cancer drug, it exhibits various side effects as a result of its action on highly mitotic tissues such as decreasing in the number of white blood cells (white and red cells, platelets). Moreover, 5-FU shows incomplete and unpredictable oral absorption.[68] One direction vigorously pursued in the last years is the development of orally administered fluoropyrimidines that maintain or improve upon the effectiveness of intravenous 5-FU. There are several potential advantages to oral administration, including patient convenience and reduced costs associated with drug preparation and administration.[70] We chose to insert a succinate linker on the 5-FdUrd structure, as a suitable covalent bond able of a safety release of thecytotoxic molecule 5-FU by both enzymatic and non-enzymatic hydrolysis, considering that previous studies demonstrated that ester derivatives of 5-FdUrd undergo hydrolysis to effectively release the antimetabolite under physiologic conditions.[65]

On this basis, 5-FdUrd appeared to be an ideal candidate for our studies. Synthesis started by protecting the primary alcohol with 4,4'dimethoxytriphenylmethylchloride (DMTrCl) (1.5 equiv.), to overcome possible side reactions in the next coupling with succinic anhydride. DMAP (1.5 equiv.) and succinic anhydride (4.0 equiv.) were then added to a solution of (**2**) in dry DCM. The desired acid was obtained as the unique product in 90% yield, by simple series of basic and acid extractions to remove impurities (Scheme 1.1).[71]
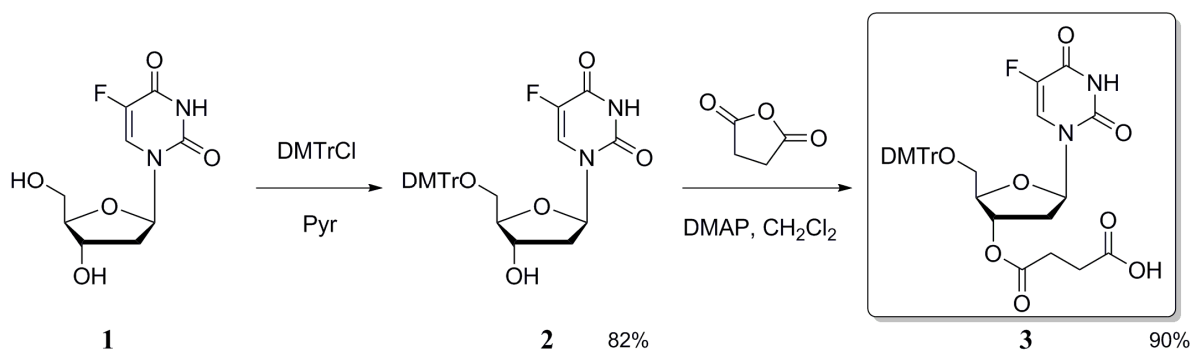
Scheme 1.1.

The ether deprotection of alcoholic groups was not necessary for **3** because it occured while cleaving the conjugated peptide from the solid support at the end of the process.

Gemcitabine

Gemcitabine **4** (dFdC) is a new anticancer nucleoside that is a deoxycytidine analog in which the hydrogen atoms on the 2' carbon of deoxycytidine are replaced by fluorine atoms. It is marketed as Gemzar (Figure 1.19).
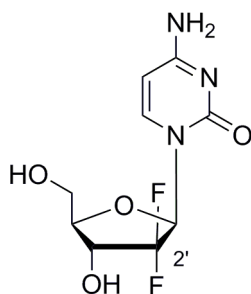

Figure 1.19. Gemcitabine, **4**

5-Fluorouracil has long been the only available drug that offered some promise in the palliative treatment of advanced pancreatic cancer, but its moderate activity has led to unsatisfactory results reported for fluorouracil-containing adjuvant regimens in patients undergoing pancreatectomy. In 1997, *Burris et al.* reported[72] the first results of a phase III study that demonstrated significant improvements both in survival and clinical benefit (pain relief, improved performance status, or both) with single agent gemcitabine compared with fluorouracil as first-line chemotherapy for advanced pancreatic cancer.[73] Postoperative gemcitabine significantly delayed the development of recurrent disease after complete resection of pancreatic cancer. These results support the use of gemcitabine as adjuvant chemotherapy in resectable carcinoma of the pancreas.[74] Now gemcitabine is a drug also used to treat certain types of breast, pancreatic, ovarian, and lung cancer and is being studied in the treatment of other types of cancer. One of the main advantages of the use of this drug is the fact that it has a good safety profile with a low incidence of toxicities (diarrhea, weakness, hair loss, mouth sores, difficulty sleeping, shortness of breath) occurs in 10-29% in patients receiving it.

Gemcitabine is a pro-drug and, once transported into the cell, must be phosphorylated by deoxycytidine kinase to an active form. Both gemcitabine diphosphate (dFdCTP) and gemcitabine triphosphate (dFdCTP) inhibit processes required for DNA synthesis. Incorporation of dFdCTP into DNA is most likely the major mechanism by which gemcitabine causes cell death. After incorporation of gemcitabine nucleotide on the end of the elongating DNA strand, one more deoxynucleotide is added and thereafter, the DNA polymerases are unable to proceed. This action ("masked termination") apparently locks the drug into DNA as the proofreading enzymes are unable to remove gemcitabine from this position. Furthermore, the unique actions that gemcitabine metabolites exert on cellular regulatory processes serve to enhance the overall inhibitory activities on cell growth. This interaction is termed "self-potentiation" and is evidenced in very few other anticancer drugs.[75] The use of gamcitabine is really up-to-date, since in recent time, it is present in numerous therapeutical protocols for cancerous deaseases in combination with other anti-cancer drugs. Combination with cisplatin, for

instance, is a first line treatement for biliary tract cancer[76] and non-small-cell lung cancer[77] and combination with bevacizumab for pancreatic cancer.[78]

The mechanism of action as well as the structure of gemcitabine and 5-fluoro-2'-deoxyuridine are very similar one to each other, so we decided to use the same strategy adopted before. The primary alcohol of **4** was protected with DMTrCl (1.5 equiv.), affecting also primary amine group and then the secondary alcohol of **5** was coupled with succinic anhydride to obtain the desired acid **6** as the unique product in 83 % yield, which was ready to be conjugated to the targeting carrier (Scheme 1.2).
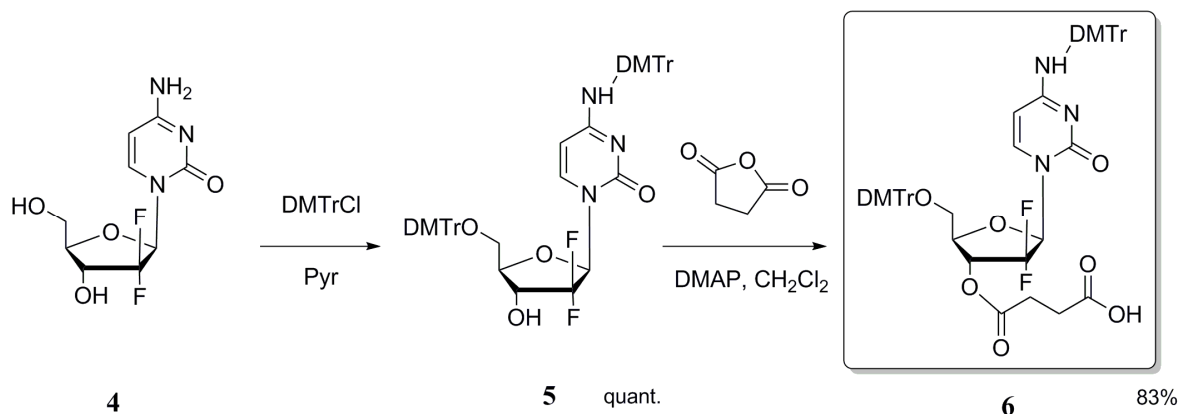
Scheme 1.2.

As well as for derivative **3**, the ether and the amino deprotections were not necessary for **6** because it will occur while cleaving the conjugated peptide from the solid support at the end of the process.

Compound **6** was successfully attached to NT peptide using a pre-cleavage coupling strategy and the cytotoxycity of the resulting complexed was *in vitro* tested, showing a promising activity in different cancer cell lines (as reported in § 1.3).

B. Bioreductive drugs

Hypoxia specific cytotoxins, also known as bioreductive drugs, are compounds that undergo reductive metabolism under low oxygen conditions to produce toxic products.[79] A key strategy in cancer treatment is to try to exploit some intrinsic difference between normal and malignant tissues. One such difference is that a large proportion of solid tumours contain cells at lower levels of oxygenation than in normal tissues. The lower oxygenation level of many solid tumours compared to normal tissues has only recently been seen as therapeutically exploitable. Indeed, because of the resistance of hypoxic cells to killing by ionising radiation, their presence in tumors would be expected to adversely affect cure rates in radiotherapy, and there is considerable evidence that this is the case for several types of malignancies.[80] The hypoxic condition, occuring as a result of poor blood supply due to the faster development of the highly proliferating mass of tumour cells than the vasculature, increases the levels of reductive enzymes and nucleophyles, such as GSH that promote the prodrugs activation. Key criteria for an ideal bioreductive drug should include poor activity against aerobic cells, activation over a broad range of oxygen tensions and, penetration through the aerobic fraction of cells. In addition, the active drug should be capable of killing non-proliferating cells.[81]
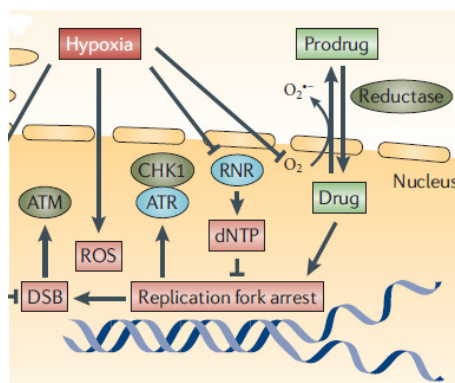
Figure 1.20. Damage of the replication fork pathway

A common feature of all bioreductive prodrugs currently in development is that their active metabolites are DNA-reactive cytotoxins that damage the replication fork (Figure 1.20). Although the DNA replication fork can be considered the most successful chemotherapy target to date,[82] toxicity to proliferating normal tissues is an inescapable consequence. Existing chemotherapy and chemoradiation protocols are already titrated to maximal myelotoxicity, which limits the opportunities to add the current generation of bioreductive prodrugs to standard therapies. This makes it attractive to consider adapting bioreductive prodrug design to release a broader range of active metabolites, including non-genotoxic inhibitors of molecular targets.[83]

Given its central role in tumour progression and resistance to therapy, tumour hypoxia might well be considered the best validated target that has yet to be exploited in oncology. There is an increasing interest in developing bioreductive prodrugs which selectively attack chemo- and radio-resistant hypoxic tumor cells. Despite an explosion of information on hypoxia, there are still major questions to be addressed if the long-standing goal of exploiting tumour hypoxia is to be realized. We selected among others, β-Lapachone (**8**) and cisplatin (**10**).

β-Hydroxy Lapachone

Red Lapacho (*Tabebuia impetiginosa*,), a canopy tree indigenous to the Amazonian rainforest and other parts of South America, has been acclaimed to be one of the "miraculous" cures for cancer and tumours (Figure 18). For the first time, during the 1960s, it attracted considerable attention in Brazil and Argentina as a 'wonder drug'. Traditionally, the botanical drug is widely used in local and traditional phytomedicine, usually ingested as a decoction prepared from the inner bark of the tree to treat numerous conditions like bacterial and fungal infections or fever.[84]
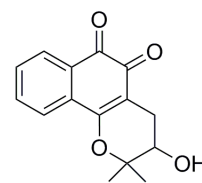
As early as 1873, biomedical uses of Red Lapacho were reported. In 1967 after reports in the Brazilian press it came back to the light of clinicians. Natural sciences interest in the plant also began in the 1960s when the United States National Cancer Institute (NCI) systematically began researching plant extracts all over the world looking for active compounds against cancer and looked at *Tabebuia impetiginosa* in considerable detail. NCI identified the quinone moiety as an important pharmacophoric element for cytotoxic activity. In fact, the two main bioactive components isolated from *Tabebuia impetiginosa*, lapachol and β- Lapachone, have this kind of structure (Figure 1.21).[85] Thus, according to the American Cancer Society, "available evidence from well-designed, controlled studies does not support this substance as an effective treatment for cancer in humans".[86]
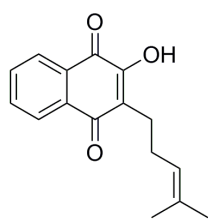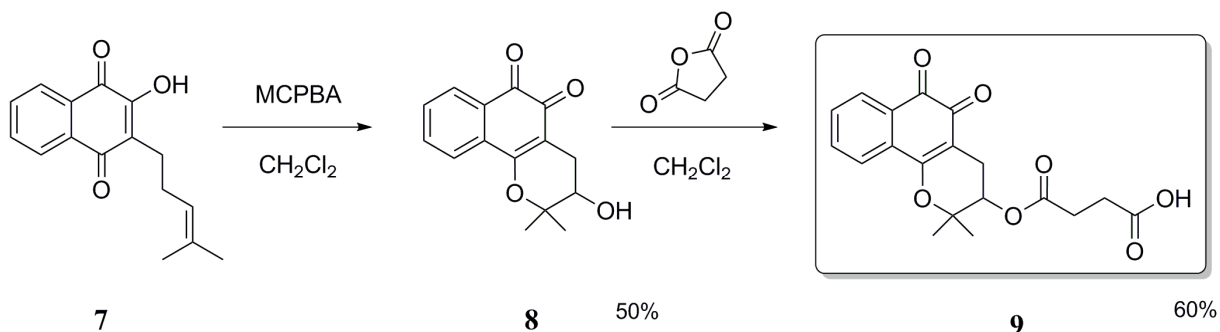
Lapachol, **7** Red Lapacho β-Lapachone,**8**

Figure 1.21.

Lapachol (**7**), 2-hydroxy-3-(3-methyl-2-butenyl)-1,4-naphthoquinone, also occurs in the wood of several species of the family Bignoniaceae and is presently commercialized in Brazil as an antitumor drug. Experimentally, lapachol is active against two types of solid tumors: Walker 256 carcinosarcoma and Murphy-Sturm lymphosarcoma. It is interesting that before Walker 256 was introduced as an experimental tumor, lapachol was considered inactive.[87] β-Lapachone (**8**) is considered to be the main anti-tumour compound, and pro-apoptotic effects were observed *in vitro*. This drug exerts its anti-tumor effect by indirect actions of inducing p53-independent apoptosis and cell cycle arrest mediated through altered activities of cell cycle control regulatory proteins, including down-regulating retinoblastoma protein (pRB), a transcriptional repressor target at transcription factor E2F-1, as well as induces expression of cyclin dependent kinase inhibitor 1A (CDKN1A or p21).[88] Both E2F-1 and p21 are required for G1/S-phase transition during cell cycle. This agent also inhibits DNA topoisomerase I by a mechanism distinct from that of camptothecin[89] and thereby blocks the formation of a cleavable complex leading to enzyme inhibition and prevent DNA repair. Furthermore, β-lapachone could induce reactive oxygen species in vivo, and result in cytotoxicity acting as a bioreductive drug. The most recent view is that β-Lap, which is a quinone compound, undergoes two-electron reduction to hydroquinone form utilizing NAD(P)H or NADH as electron source. This two-electron reduction of β-Lap is mediated by NAD(P)H:quinone oxidoreductase (NQO1), which is known to mediate the reduction of many quinone compounds. The hydroquinone forms of β-Lap then spontaneously oxidizes back to the original oxidized β-Lap, creating futile cycling between the oxidized and reduced forms of β-Lap. It is proposed that the futile recycling between oxidized and reduced forms of β-Lap leads to two distinct cell death pathways. The most important one is that the two-electron reduced β-Lap is converted first to one-electron reduced β-Lap, i.e., semiquinone β-Lap (SQ)·,causing production of reactive oxygen species (ROS), which then causes apoptotic cell death.[90]

The drug appears to be generally safe and one of the most important interactions of *Tabebuia impetiginosa* has been associated with interference in the biological cycle of Vitamin K in the body.[84]

Scheme 1.3.

For the prodrug synthesis, we exploited the presence of hydroxyl group on the naphtoquinone of β-hydroxy lapachone (**8**) to form an ester using succinic anhydride. We started the procedure from the commercially available lapachol **7** which was treated with MCPBA (2.1 equiv.) in DCM for a day and then was purified by flash chromatography (eluent EtP:AcOEt 4:1 followed by EtP:AcOEt 3:1 after first spot came out) to give (**8**) in 50% yield. In this step, first the MCPBA oxidized the double bond to epoxide, then it underwent an intramolecular nucleophilic attack that created the ring. The next coupling with succinic anhydride (2.7 equiv.) gave prodrug (**9**) without further purification (Scheme 1.3).

Cisplatin

Cisplatin (**10**) (Figure 1.22), unlike many cancer drugs, which are organic molecules with complex structures, is an inorganic molecule with a simple structure. Cisplatin (CDDP) is frequently defined the "*penicillin of cancer drugs*" because it has been one of the first and effective treatment for many cancer diagnoses.
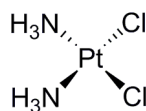

Figure 1.22. Cisplatin (**10**)

Although the mechanism has not fully been elucidated yet, cisplatin is generally believed to kill cancer cells by binding to DNA and interfering with the cell's repair mechanism, which eventually leads to cell death. Inside a cell, cisplatin undergoes hydrolysis, producing the highly reactive charged platinum complex $[Pt(NH_3)_2ClH_2O]^+$. This complex coordinates to DNA through the N7 atom of either a guanine or adenine base. Further hydrolysis displaces the remaining chloride ligand, and the platinum can bind to a second nucleotide base. Consequently, interstrand or intrastrand croos-links where formed in the double strand DNA. The sequence of events extending from the formation of DNA adducts to the completion of the cytotoxic process, namely apoptosis, has been deeply investigated in the 90's. *Bellon* and *Lippard*[91] purposed that this sequence is likely initiated or facilitated following the recognition of DNA damage by over 20 individual candidate proteins, which bind to physical distortions in the DNA that are induced by the intrastrand platinum adducts. These damage recognition proteins include, among others: the hMSH2 or hMutSa component of the mismatch repair (MMR) complex, the nonhistone chromosomalhigh-mobility group 1 and 2 (HMG1 and HMG2) proteins, the human RNA polymerase I transcription 'upstream binding factor' (hUBF), and the transcriptionalfactor 'TATA binding protein' (TBP),[92,93] as depicted in figure 1.23.
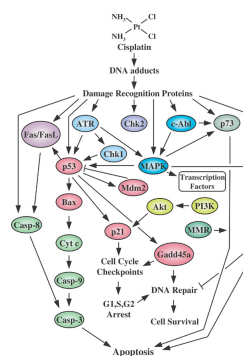
Figure 1.23. Different pathways of cisplatin-induced apoptosis

In particular, the cisplatin-DNA adduct is recognized by the high mobility group (HMG)-domain protein, among other DNA repair protein, which binds tightly to the complex. The adduct causes destacking of the nucleotide bases, resulting in the DNA helix becoming kinked. This action of HMG1 is supported by the finding that overexpression of this recognition protein by pre-exposure to estrogen sensitizes breast tumor cells to cisplatin.[94] In conclusion, many pro-apoptotic signals are activated simultaneously, following cisplatin exposure, and the relative intensity and/or duration of each is integrated downstream to determine the final fate of the cells.[95] In a recent review,[96] it has been purposed that cisplatin damages tumors via induction of apoptosis, mediated by the activation of various signal transduction pathways, including calcium signaling,[97] death receptor signaling,[98] and the activation of mitochondrial pathways.[99] Although there is only little information available on how cisplatin interacts with mitochanodria, an interesting study by *Lippard* has recently undelined the important implication that cisplatin-mitochondria interaction has in its cytotoxicity.[100]

The discovery of CDDP as an anti-cancer drug in the 1960s opened a new era in cancer treatment. More than 100 years earlier, in 1845, it was synthetized for the first time by Michel Peyrone and in 1893 Alfred Werner deduced the structure of CDDP.[101] In the 1960s, Rosenberg and colleagues discovered that electrolysis of a platinum electrode results in generating cisplatin. Later the same group successfully tested the effects of several platinum complexes on rat sarcomas.[102] In 1971, CDDP was applied to a cancer patient[103] for the first time. It became available for clinical practice in 1978, as Platinol® (Bristol-Myers Squibb). CDDP showed a high level and broad spectrum of antitumor activity and, therefore, extensive research developed in the area of drug design to find novel non-platinum-containing metal species with superior anti-cancer activity and low side effects.[104]

Even though it is an "old" drug as chemotherapy agents (having been used for decades), it is most widely prescribed for testicular, ovarian, bladder, lung, and stomach cancers. Nowadays, combination therapies to treat cancer are quite common. CDDP is frequently used in combination with one, two, three, or even four other drugs, with positive results. The hope is that the drugs will work together, producing synergistic or at least additive effects in killing cancer cells, while producing no additional side effects. Among others, the more up-to date combinations in theraphy are with: *gemcitabine* for biliar tract cancer,[105] *docetaxel* for metastatic gastric cancer,[106] *irinotecan* for gynecological cancer,[107] the monoclonal antibody *Erbitux* (cetuximab) given with cisplatin is effective in patients with head and neck cancers.[108] While a combination-chemotherapy with cisplatin is a cornerstone for the treatment of multiple cancers, the challenge is that cancer cells could become cisplatin-resistant. Platinum complexes remain the mainstay of a number of chemotherapy strategies. Despite their

potency and widespread clinical use, there are a number of pitfalls or limitations to platinum complex-based chemotherapy. These limitations are caused by resistance pathways, toxicological profiles and pharmacokinetic considerations.[96] Resistance manifests in a number of forms including reduced cellular accumulation, inactivation from thiol containing reductants (e.g. glutathione)[109] and increased gene specific DNA repair pathways. The intracellular reactivity of cisplatin with membrane phospholipids, proteins, cytoskeletal microfilaments and RNA will also reduce the amount of compound available to react with the intended target DNA.[110] Side effects of platinum therapy include general cell-damaging effects, such as nausea and vomiting, decreased blood cell and platelet production in bone marrow (myelosuppresion) and decreased response to infection (immunosuppression). More specific side effects include damage to the kidney (nephrotoxicity), damage of neurons (neurotoxicity) and hearing loss.[111] Low bioavailability, poor cellular uptake and high reactivity towards macromolecules in biological solutions limit platinum-based chemotherapy by affecting the pharmacokinetic parameters.

Attempts to devise platinum drugs that surpass the anticancer properties of cisplatin have produced many compounds that display biological activity, but only a handful of these have shown any real promise in clinical trials. This loss of activity in the body can be associated with poor circulation and delivery to the tumor as well as deactivation mechanisms that irreversibly alter the chemistry of these molecules, particularly those of platinum(II), rendering them ineffective. We tried to circumvent many pathways that deactivate platinum(II) drug candidates by substitutionally synthesizing more inert platinum(IV) compounds as prodrugs. Pt(IV) complexes provide an attractive alternative to Pt(II) compounds because their inertness results in fewer side effects.[112] These complexes are reduced in the intracellular milieu to yield the citotoxic Pt(II) species through reductive elimination of axial ligands (functional groups above and below the plane of the ''equatorial'' leaving groups Cl in cisplatin).[113] The presence of reducing agents such as glutathione, ascorbate and protein sulfhydryls allows the intracellular reduction and so increase the reactivity of Pt(IV)-complexes with DNA. We, thus, envisaged the synthesis of a Pt(IV) derivative, inserting the free carboxylic moiety in axial position.

We started the synthetic procedure oxidizing cisplatin (**10**) with of H_2O_2 (1.5 equiv.) in 24 mL of H_2O at 65°C for 2 h. After the allotted time we kept the mixture at 4°C to allowed a yellow powder to precipitate. After crystallising it at reflux in water the suspension was cooled at 4°C and kept at this temperature overnight. Purification of the collected bright yellow powder was performed through several washings with iced water, MeOH and diethyl ether to get rid of side products. Centrifugation allowed to collect the final product (**11**) in 75% yield. With compound **11** in hands, we exploited the presence of two hydroxyl groups to form two ester bonds using 4 equiv. of succinic anhydride in dry DMSO, we lyophilized and crystallized the crude from acetone at 50°C. We repeated the crystallization three times to totally remove the succinic acid formed during the reaction to obtain prodrug **12** as a light yellow powder in 30% yield (Scheme 1.4).
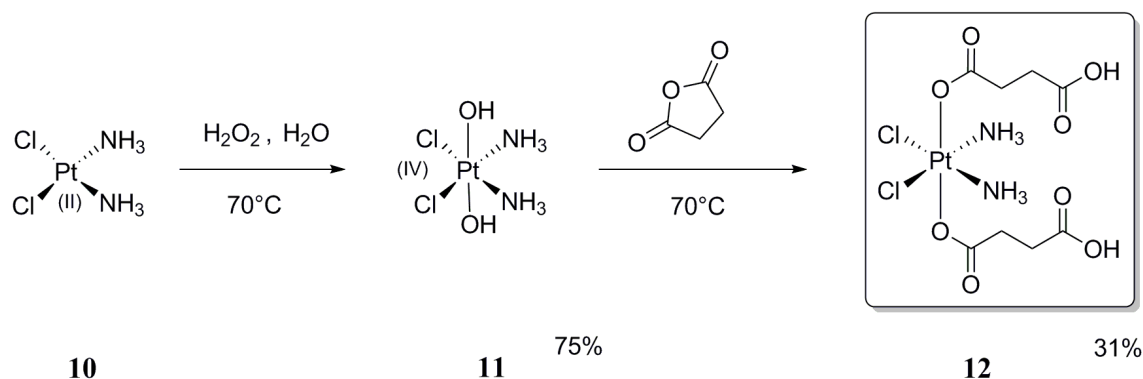
Scheme 1.4.

In 2009 *Lippard et al.*[112] reported the synthesis of monosuccinate Pt(II) derivative **14**, a pro-drug that seemed to be more suitable than compound **12** for linking on the peptide. We tried synthesizing a Pt(IV)-complex with only one ester bond, using 1 equiv. of succinic anhydride, we lyophilized and crystallized the crude from acetone but we didn't obtain **14** due to problems occurring during the purifying procedure. In fact, during the recrystallization the crude becomes a hardly filterable oil from which is not possible to retrieve the pure product (Scheme 1.5).
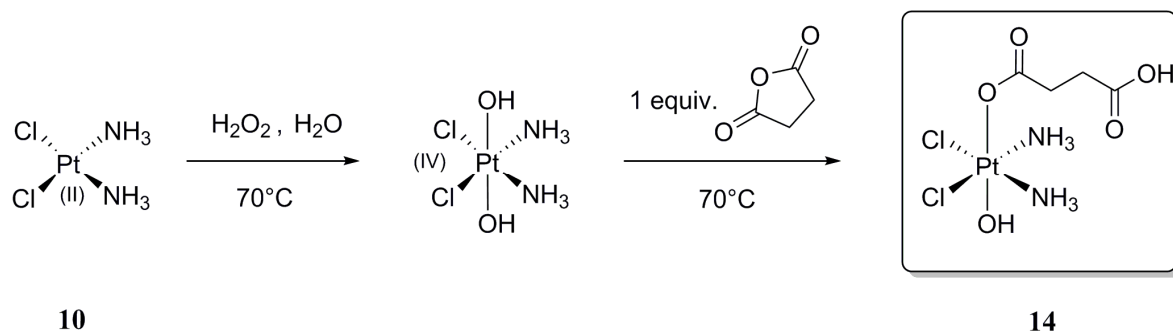
Scheme 1.5.

Thus, at the university of Siena compound **12** has been attached on tetrabranched peptide exploiting solid phase reaction. Unfortunately, from mass spectrometry data the prodrug seemed not to be linked to the peptide at the end of the synthetically procedure, so it couldn't be used in *in vivo* tests. We hypothesize that functionalized cisplatin could detach from the peptide during the cleavage of this from the resin, due to the use of TFA or scavenger agent like TIPS that interfered with the stability of the complex. Thus, we envisage an alternative strategy to overcome this experimental problem, as described in the next chapter of this thesis (§ 2).

C. Estrogens

Estrogens have been recommended as treatment for breast cancer since 1960 but have fallen out of favor clinically in recent years because of the emergence of a variety of antiestrogen agents and the use of chemotherapy.[114]

Despite a declining incidence, breast cancer remains the most common cancer among women in the United States. More than two-thirds of all patients with breast cancer present with tumors that express estrogen receptors, progesterone receptors, or both, and the modulation of estrogen receptor signaling has been one of the most successful strategies for these patients. In recent years, the most commonly used forms of endocrine therapy have included the competitive inhibition of the estrogen receptors with an antiestrogen (selective estrogen receptor modulators [SERMs], eg, tamoxifen,[115] or selective estrogen-receptor down-regulators, [SERDs], eg, fulvestrant)[116] and the decrease in estrogen production from precursor steroid hormones using an aromatase inhibitor.[117]

Estradiol

Estradiol, E_2, (**15**) (Figure 1.24) is the most potent estrogen of a group of endogenous estrogen steroids which includes estrone and estriol. In women estradiol is responsible for growth of the breast and reproductive epithelia, maturation of long bones and development of the secondary sexual characteristics. Estradiol is produced mainly by the ovaries with secondary production by the adrenal glands and conversion of steroid precursors into estrogens in fat tissue.[118]
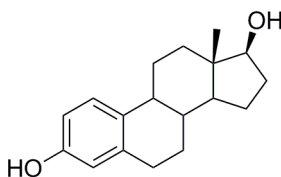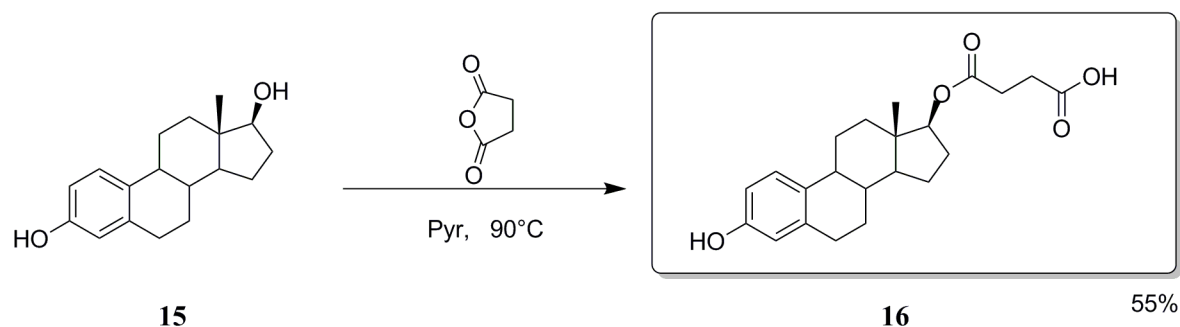

Figure 1.24. β-estradiol, **15**

Estrogen deprivation therapy with aromatase inhibitors has been hypothesized to paradoxically sensitize hormone receptor-positive breast cancer tumor cells to low-dose estradiol therapy. In 2009 *Ellis et al.*[119] determine that 6 mg of estradiol daily, which produces estradiol levels similar to those in ovulating premenopausal women, is an active low-cost treatment for postmenopausal women with advanced breast cancer and acquired resistance to aromatase inhibitor treatment. Estradiol treatment not only stops disease progression in about a third of patients, but in some patients, metastatic tumours become resensitized and again responded to antiestrogen treatments.

For the prodrug synthesis we exploited the difference of reactivity of the two hydroxilic group of **15** to form an ester using succinic anhydride. We could avoid protecting phenolic group that results to be less nucleophilic than aliphatic hydroxilc one and unable to react with succinic anhydride. We started the procedure from the commercially available β-estradiol **15** which was treated with succinic anhydride (2.7 eq.) in pyridine at 90°C for a day, than poured onto MeOH overnight. The yellow syrup obtained was kept in refrigerator for two days, allowing it to become a white powder in 55% yield, without further purification (Scheme 1.6).

15 → **16** 55%

Pyr, 90°C

Scheme 1.6.

2-Methoxyestradiol

An estimated 186,000 new cases of breast cancer will be diagnosed, and 46,000 women in the US will die from breast cancer in 1999 (Figure 1.25).[120]
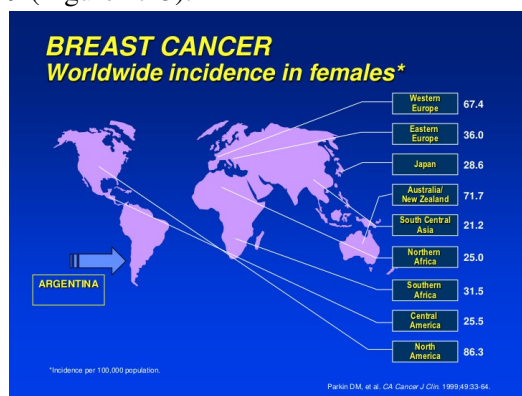

Figure 1.25. Worldwide incidence of breast cancer in 1999

The development of new drugs that facilitate better management and control of breast cancer is warranted, particularly with the increased incidence of breast cancer in the past two decades and the development of resistance to current chemotherapeutic agents. Recently, 2-methoxyestradiol (**23**) (2-MeOE$_2$), one of the endogenous metabolites of estradiol (E$_2$), was shown to demonstrate *in vitro* inhibition of angiogenesis and suppress tumor growth (Figure 1.26).[121]
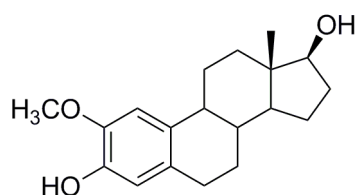
Figure 1.26. 2-methoxyestradiol, **23**

The formation of new blood vessels (angiogenesis) is critical for the growth of tumours and 2-MeOE$_2$ is a potent inhibitor of endothelial cell proliferation and migration as well as angiogenesis *in vitro*.[122] Moreover, when administered orally in mice, it strongly inhibits the neovascularisation of solid tumours. This tumor-suppressing effect seems to be due to the inhibition of tumor-induced angiogenesis, rather than direct inhibition of proliferation of tumor cells. The treated mice show no apparent signs of toxicity and are all alive after 12 days of daily treatment. They don't show hair loss, intestinal disturbance or infection, all toxic side-effects associated with conventional chemotherapy.

37

The lack of toxicity is consistent with the *in vitro* results, showing no effects on quiescent non-dividing cells. Unlike the angiostatic steroids of corticoid structure, 2-MeOE$_2$ does not require the co-administration of heparin or sulphated cyclodestixtrins for activity. Thus, 2-methoxyestradiol is the first steroid to have high antiangiogenic activity by itself and it could be used in the treatment of solid tumours and other angiogenic deseases such as psoriasis and pediatric haemangiomas.[123]

Also in 1994, *D'Amato et al.*[124] reported that 2-methoxyestradiol, a normal mammalian metabolite inhibits in vitro tubulin polymerization. These studies suggested that abnormal microtubule assembly may be responsible for the antiangiogenic activity. It has long been postulated that the colchicine site of tubulin is a regulatory domain that interacts with endogenous substances affecting microtubule assembly. The fact that 2-MeOE$_2$ binds to the colchicines site of tubulin and inhibits assembly provides evidence that endogenous molecules similar in size to colchicine could serve such functions. Their observations with 2-MeOE$_2$ suggest that other, perhaps unknown, steroid compounds could play important roles in microtubule assembly, possibly functioning as negative regulators. In vitro experiments have demonstrated that certain estrogen metabolites covalently bind to the C-terminal region of the β-subunit of tubulin,[125] suggesting that the interactions of estrogens and/or estrogen metabolites with tubulin and microtubule assembly may play an important epigenetic role. Important questions of whether this effect on tubulin and microtubules is due to the estrogen itself, the formation of a hydroxylated metabolite, or further metabolism of the 2-hydroxyestrogen via oxidative or peroxidative pathways remains unanswered.[126]

Furthermore, demethylation of 2-methoxyestrogens is an additional pathway of estrogen metabolism and may complicate the *in vivo* investigations of 2-methoxyestradiol as a potential anticancer agent. Further investigations on possible mechanisms for this antiangiogenic effect have focused on the interactions of 2-MeOE$_2$ with 2-MeOE$_2$ inhibiting nucleation and propagation of tubulin assembly and being a competitive inhibitor of colchicines binding (K_i of 22 μM). Additionally, 2-MeOE$_2$ has been reported to produce metaphase arrest and interfere with mitotic spindle dynamics.[127] Other mechanisms for 2-MeOE$_2$ antitumor activity have also been proposed that do not involve tubulin and microtubules. Several studies have implicated p53-mediated mechanisms responsible for apoptosis induced by 2-MeOE$_2$, including upregulation and stabilization of p53 in lung cancer cells. According to litterature following 2-MeOE$_2$-mediated increases in wildtype p53 protein, cells bypass the G$_1$-S checkpoint of the cell cycle with 30 to 40% undergoing apoptosis.[128] Increased phosphorylation of Bcl-2 has also been reported.[129] Alterations of enzymes in various intracellular signaling pathways, including nitric oxide synthase and mitogen-activated protein kinase , have also been observed upon treatment with 2-MeOE$_2$.[130]

Currently, encapsulation of 2-methoxyestradiol within multifunctional dendrimers[131] and combination with bevacizumab[132] have been investigated for targeted therapy of metastatic carcinoid tumors.

Synthesis started by protecting both the alcohols using chloromethyl ethyl ether and DIPEA in dry THF. Then, we exploited a one step reaction to insert another hydroxylic group on the phenolic ring. First of all, sec-BuLi 1.3 M in cyclohexane deprotonated carbon 2 (the use of n-BuLi was not successful since it's a not strong enough base) and a borate was insert in this position thanks to the reaction between the new formed anion and the trimethylborare at -75°C degrees (a). We observed that if the reaction was led at a lower temperature (-65°C), the yield will increase (b) Then, the borate was oxidized to hydroxilic group using sodium perborate at 35°C degrees. Unfortunately, the methylation of carbon 2, in the next step, resulted to have a low yield either using CH$_3$I, or dimethyl sulphate, due to the hindrance of the protecting group on carbon 1. Moreover, we were not able to purify the crude by flash chromatography because Rf of **18** and **19** are very similar (Scheme 1.7).
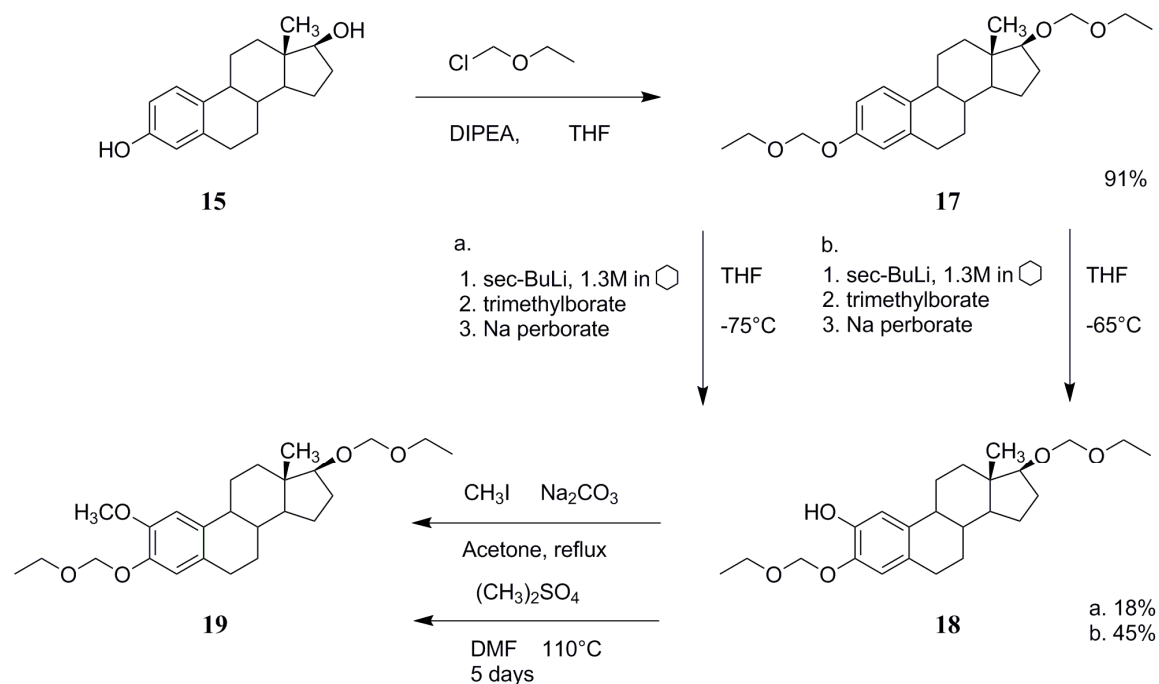
Scheme 1.7.

According to literature, we decided to use the less hindered protecting group chloromethyl methyl ether and the methylation of hydroxilic group on carbon 2 resulted to be successful, using dimethyl sulphate and Na_2CO_3 in dry acetone. A solution of MeOH and HCl was used to obtain 2-methoxyestradiol **22**, which was treated with succinic anhydride (2.7 equiv.) in pyridine for a day, than poured onto MeOH overnight. The yellow syrup obtained was kept in refrigerator for two days, allowing it to become a white powder in 55% yield, without further purification (Scheme 1.8).
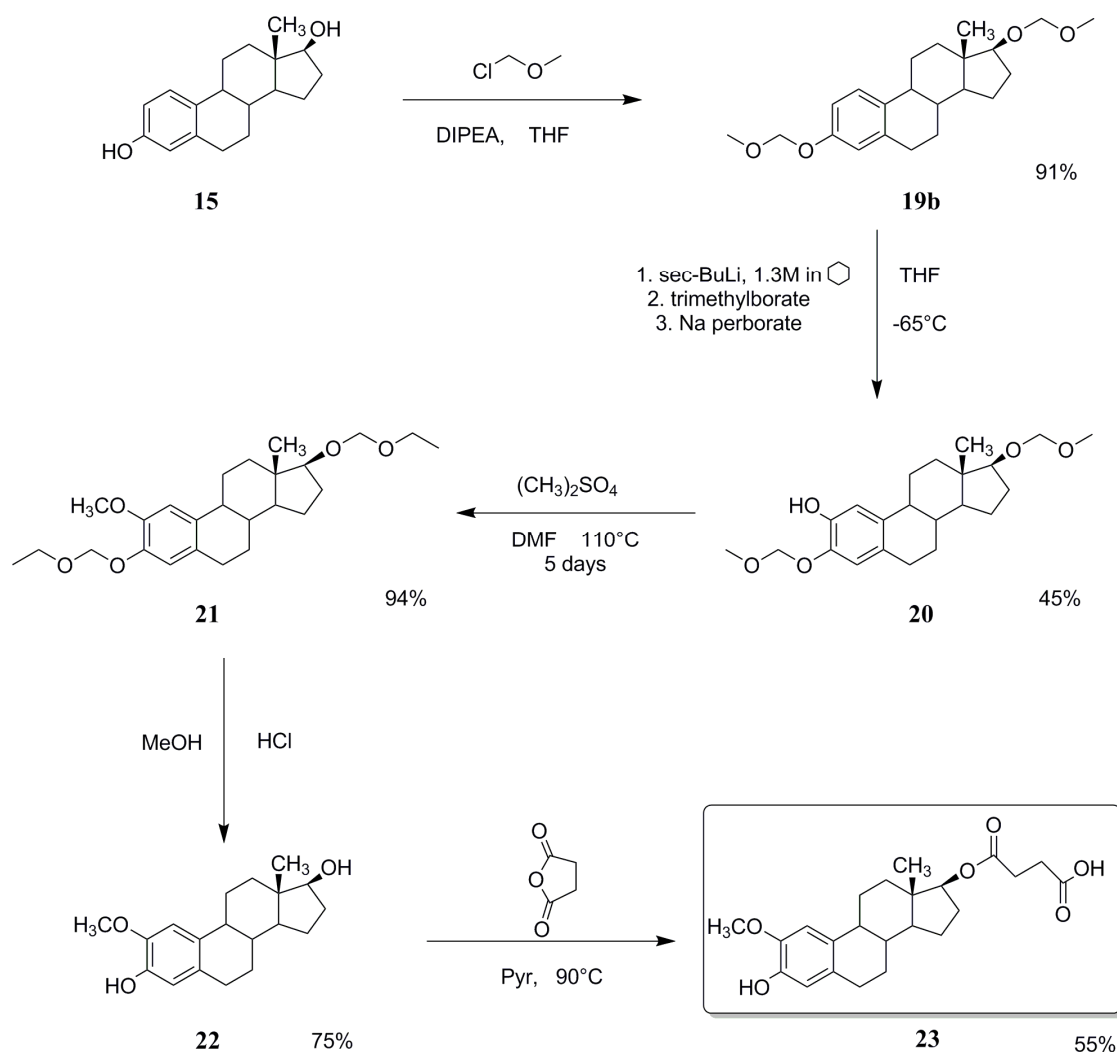
Scheme 1.8.

D. Mitosis Inhibitors

Drugs that interfere with the normal progression of mitosis belong to the most successful chemotherapeutic compounds currently used for anti-cancer treatment. Classically, these drugs are represented by microtubule binding drugs that inhibit the function of the mitotic spindle in order to halt the cell cycle in mitosis and to induce apoptosis in tumor cells, which is the desired outcome of chemotherapy.[133]

Although anti-microtubule drugs have been used in the clinic for many years, the mechanisms of how these drugs induce tumor cell death are not well understood. At clinically relevant concentrations, they suppress the dynamics of the mitotic spindle and thereby inhibit chromosome alignment. The presence of partially aligned chromosomes that lack microtubule attachment chronically activates the mitotic spindle checkpoint leading to the mitotic arrest in a prometaphase-like state. In fact, the mitotic arrest observed upon treatment with anti-microtubule drugs is dependent on the spindle checkpoint, but is not permanent. Instead, upon prolonged treatment, cells exit from mitosis in the presence of misaligned chromosomes, a process known as mitotic slippage.[134]

The primary target of microtubule binding drugs is the mitotic spindle, however, these compounds act not only on proliferating tumor cells, but exhibit significant side effects on non-proliferating cells

including neurons that are highly dependent on intracellular transport processes mediated by microtubules. Peripheral neuropathy might be explained by a disruption of microtubule mediated axonal flow and includes numbness, jaw pain, vocal cord dysfunction, constipation and abdominal cramps. Suppression of the mitotic microtubule function also inhibits the proliferation of non-transformed cells including hematopoetic precursor cells, which might explain the severe myelosuppression and neutropenia observed in patients during therapy.[135]

Despite rapid progress made in understanding the biological mechanism regulating developmental and tumor vasculature, the clinical success of targeted therapeutics that interfere with key molecular and cellular pathways of angiogenesis has been limited by a lack of improved patient survival when these agents were administered as single agents. In contrast, *vascular disruptive agents* (VDAs) induced rapid regression of established tumors in preclinical studies.[136] Recently, it has been established that some tubulin binding agents selectively target the vascular system of tumors. These compounds induce morphological changes in the endothelial cells of the tumour's blood vessels, resulting in their occlusion and interruption of blood flow.[137] These agents has been termed *antivascular* agents, in contrast with antiangiogenic agents, which can act by inhibiting proliferation of new tumour vasculature. Vascular targeting drugs instead specifically and rapidly act on preexisting tumour blood vessels.

Tubulin binding molecules have gained much interest among cytotoxic agents due to its success in clinical oncology, in recent time. Tubulin binding drugs have been classified on the basis of their mode of action and binding site (Figure 1.27) as:[138]

- **I.** Tubulin polymerization inhibitors

  a) *Paclitaxel site ligands*, includes the paclitaxel, epothilone, docetaxel, discodermolide; they are also called taxanes.

- **II**. Tubulin polymerization inhibitors

  a) *Colchicine binding site*, includes the colchicine, combretastatin, methoxy benzenesulfonamides (E7010);

  b) *Vinca alkaloids binding site*, includes vinblastine, vincristine, vinorelbine, vinfluine, dolastatins, halichondrins, hemiasterlins, cryptophysin 52.
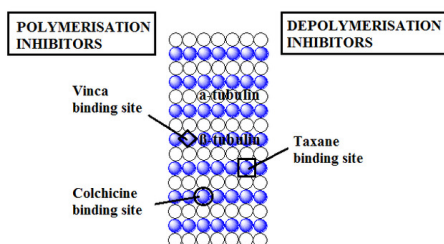

Figure 1.27. Tubulin inhibitors binding site

The taxanes represent the first class of antimicrotubule agents with a new mechanism of cytotoxic action since the introduction of the vinca alkaloids several decades ago. These compounds may prove to be the "anticancer drugs of the 1990s", just as the anthracyclines and the platinum compounds were the "anticancer drugs" of the 1970s and 1980s.[139] After only a brief period, the taxanes have not only

demonstrated a unique ability to palliate the symptoms of many types of advanced cancers, including carcinoma of the ovary, lung, head and neck, bladder, and esophagus, they have also demonstrated effectiveness in the initial therapy of earlier stages of cancer, a setting in which any new therapy is likely to make its greatest impact.[140] Taxanes are diterpenes produced by the plants of the genus *Taxus* (yews) and include Paclitaxel (Taxol) and Docetaxel (Taxotere) as well as taxanes homologs, which are derived from natural sources.

Paclitaxel appeared to be an ideal candidate for derivatisation, as it possesses one more reactive function among the others (the OH at position 2'); this remarkably simplifies prodrug design strategies. The failure of pre-coupling strategy led us to develop a successful alternative strategy, exclusively tailored for Paclitaxel, as below described in a dedicated chapter (§ 1.2.2).

Among tubulin polymerization inhibitors, combretastatins are a class of natural stilbenoids. These molecules generally share three common structural features: a trimethoxy "A"-ring, a "B"-ring containing substituent often at C3′ and C4′, and an ethane bridge between the two rings, which provides necessary structural rigidity. Members of the combretastatin family possess varying ability to cause vascular disruption in tumors. Combretastatin A4, in particular, attracted our attention since its molecular scaffold only brings one reactive OH function, rendering it perfectly suitable for our aim.

Paclitaxel

Paclitaxel (**24**) is one of the more used mitotic inhibitor used in cancer chemotherapy. Paclitaxel is a diterpenoid pseudoalkaloid, having molecular formula $C_{47}H_{51}NO_{14}$, corresponding to the molecular weight of 853 Da. It has a tetracyclic 17-carbon (heptadecane) skeleton, with a total of 11 stereocenters. The active stereoisomer is (-)-paclitaxel. It was discovered in a US National Cancer Institute program at the Research Triangle Institute in 1967 when Monroe E. Wall and Mansukh C. Wani isolated it from the bark of the Pacific yew tree,*Taxus brevifolia* and named it *taxol* (Figure 1.28).[141]
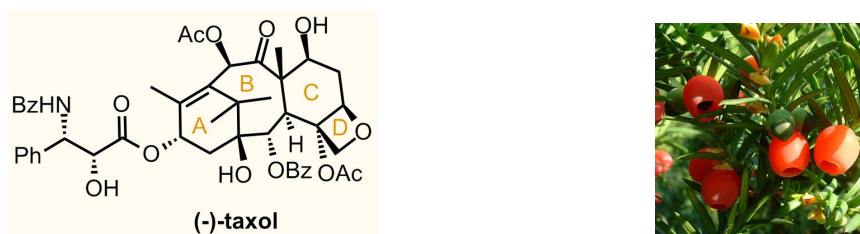

Figure 1.28. (-)-paclitaxel (**24**) (left) and *taxus brevifolia* (right)

In 1971 Paclitaxel was found to be having cytotoxic effects on solid tumors and leukemic cells[145] and in early 1879 Dr. Horwitz Susan and her group delineated its main mechanism of action (since then unknown) involving the stabilization of microtubules.[143] After numerous *in vivo* studies, in 1992, Bristol-Myers Squibb marketed the drug as TAXOL® with the approval of the FDA where it was used for treatment of breast, ovary and AIDS-related Kaposi sarcoma; furthermore, its combination with cisplatin is used in the treatment of advanced ovarian cancer and NSCLC.[144]

Mechanism of action and current use

Taxanes currently known to suppress and inhibit cell growth, differentiation and proliferation in indefinitely known cancer cell lines are the most preferred anticancer drugs by physicians. They are commonly known as mitotic inhibitors or microtubule inhibitors as they cause a frozen mitosis; hence they are also sometimes called as mitotic poisons.[145] Paclitaxel, inspite of its excellent anti-tumor activity is still not cell specific and not all concentrations have similar effects on the microtubules; higher concentrations cause microtubule arrangement into bundles, while at lower concentrations, there is suppression and stabilization of microtubule dynamics without alteration of the polymer mass formed.[146] Further studies have even demonstrated that at very low concentrations, Taxol can inhibit cell proliferation with no mitotic arrest.[147] Low concentrations of paclitaxel induce cell type-dependent p53, p21 and G1/G2 arrest instead of mitotic arrest: molecular determinants of paclitaxel-induced cytotoxicity. Unlike other microtubule agents, such as *Vinca* alkaloids, which induce the disassembly of microtubules, paclitaxel promotes the polymerization of tubulin; the resulting tubules are extraordinarily stable and dysfunctional, thereby causing the death of the cell by disrupting the normal tubule dynamics required for cell division and vital interphase process. Moreover, taxanes have been found to be potential angiogenic inhibitors either as single agents, together with chemotherapeutic drugs or combination therapies, such as endogenous estrogens (2-methoxyestradiol)[148] and bevasizumab[149] which regulated VEGF (vascular endothelial growth factor) in an agonistic manner.

For past two decades, Taxol has been undergoing infinite number of clinical studies in many cancer patients, in order to know about several factors regarding their usefulness as potential anti-neoplastic agents. Paclitaxel has neoplastic activity particularly against primary epithelial ovarian carcinoma breast cancer, colon, head, non-small cell lung cancer, and AIDS related Kaposi's sarcoma. This has led, in recent time, to the approval of the drug in many countries for its use as second line treatment of ovarian and breast cancers.[150] Despite of the primary importance of several paclitaxel-based monotherapies, conjoint terapie with platinum derivatives is, nowadays, a first line of treatment of ovarian cancer. In particular, carboplatin-paclitaxel combination is an emerging therapeutic protocol for advanced ovarian carcinoma, replacing the older and more toxic cisplatin-paclitaxel one.[151] The same trend that envisages a more effective cancer management with combined therapies is found in treatments of breast cancer, for which, binary association with anthracyclines and triple with doxorubicin and gemcitabine prolonge patients' survival rates.[152] In general, thus, in order to achieve disease free survival taxol should be tried with several adjuvants to meet up to its expectancy.

Drawbacks of paclitaxel therapy and alternative approaches for taxol formulation

There is no question that Paclitaxel is one of the more effective weapon we have in hands to treat a broad range of cancers that are generally considered to be refractory to conventional therapy. Unfortunately, its extended use have underlined several limitations, mainly related to: a) *availability*, b) *solubility*, c) *resistance*, as below discussed:

a) *Availability*. Paclitaxel is extracted from the bark of Pacific Yew Although the extraction has increased yields to 0.04% w/w, 4 trees have to be sacrificed to produce 2 g of the drug for the chemotherapy of one patient and this is not affordable from the environmental point of view.[153] Paclitaxel is currently formulated in a vehicle composed of 1:1 blend of Cremophor EL (polyethoxylated castor oil) and ethanol which is diluted with 5-20-fold in normal saline or dextrose solution (5%) for administration. lots of problems employing this vehicle have been reported. For instance, Cremophor vehicle required to solubilize it has a toxicity that includes hypersensitivity reactions, nephrotoxicity and neurotoxicity.[154] Moreover, the recommended concentration of the drug

in the properly diluted clinical formulation is 0.3-1.2 mg ml^{-1} (0.35-14 mM) and has only short-term physical stability as some particles slowly tend to precipitate out of the aqueous media;

b) *Solubility*. Paclitaxel is poorly soluble in an aqueous medium (approx. 0.6 mM), but can be dissolved in organic solvents. Its solutions can be prepared in a milimolar concentration in a variety of alcohols, such as methanol, ethanol, tertiary-butanol as well as in DMSO;

c) *Resistance*. Acquired resistance to taxanes has become a serious clinical issue with increasing prescription. Though there have been a lot of successful outcomes with taxanes involved in the treatment of endless number of cancers but nevertheless, drug resistance remains a major obstacle which needs to be combated urgently. For years, profound researches have been going on just to understand the mechanisms related to MDR (multidrug resistance). Few of the mechanisms that have been highlighted includes P-glycoprotein which pumps out intracellular accumulation of respective drugs.[155]

Considering the above mentioned limitations, the main challenge of actual research is to develop alternative and safer strategies for an appropriate deliver of paclitaxel. The primary goal of formulation development for paclitaxel is to eliminate the Cremophor vehicle by reformulation of the drug in a better-tolerated vehicle. Reformulation also provides the possibility of improving the efficacy of paclitaxel based anticancer therapy. Moreover, a great deal of effort is being directed towards the development of aqueous based formulations for paclitaxel, including soluble semi-synthetic paclitaxel derivatives that do not require solubilisation by Cremophor and that decrease the systemic clearance of the drug. Overall, 'carrier delivery systems', including liposomes, micelles and particulate drug delivery systems, seem to be the best possible approach towards the ideal dosage form which would bypass all the present limitations and provide a desirable means and cure.[150] The approaches (Figure 1.29) being used for a desired formulation of paclitaxel by various methods are below summarized:

✓ *Increased aqueous solubility*. Weak electrolytes and non-polar drug molecules frequently have poor water solubility.Their solubility can be increased by the addition of water miscible solvent in which the drug has a good solubility (*co-solvency* strategy). In this case, the vehicle consisting of ethanol and polysorbate-80, to be diluted in glucose solution before use, was found to be suitable for the administration of paclitaxel.[156]
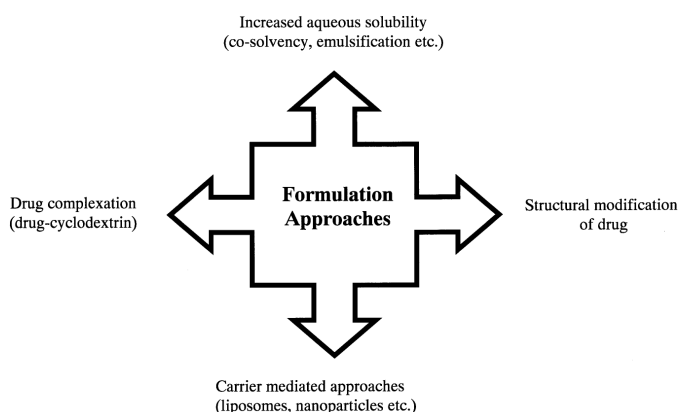

Figure 1.29. Alternative approaches for taxol formulation

✓ *Drug complexation.* Ciclodextrins are cyclic oligosaccharides, which have been used extensively to increase the solubility, dissolution rate and the bioavailability of poorly soluble drugs. An enhancement in solubility of paclitaxel from an inclusion complex with hydroxy propyl-β-CD (HPβCD) was demonstrated by Cserhati et al. They stated that the complex formed was more hydrophilic than the uncomplexed drug indicating that the solubility of the drug can be enhanced by by 950-fold or more and clinically useful concentration (1-4 mM) of paclitaxel can be easily achieved.[157]

✓ *Carrier mediated approach.*

- Among the drug carrier systems, *liposomes* represent a mature versatile technology with a considerable potential for encapsulation of both the lipophilic and the hydrophilic drugs and are in clinical trials for a number of neoplastic and infectious diseases. A liposomal drug delivery systems containing paclitaxel and phospholipid in molar ratio of 1:33 from phosphatidylglycerol and phosphatidylcholine (1:9 molar ratio) was developed and was found to be stable for more than 2 months at 4 °C, and for 1 month at 20 °C. These formulations retained growth inhibitory activity of the free drug in-vitro against a variety of tumor cell lines.[158] Unfortunatelly, the use of liposomes in drug targeting is found to be limited mainly due to problem of low entrapment efficiency, drug instability, rapid drug leakage and poor storage stability.

- Alternatively, non-liposomal drug carrier systems, such as *nanoparticles*, have been studied since on one hand, due to their extremely small size, can extravasate at the pathological site such as solid tumors through passive targeting mechanism; on the other hand they possess the advantages gained by the use of liposomal delivery additionally overcoming the limitations faced by them, including low entrapment efficacy, drug instability and leakage. *Wang et al.*[159] purposed paclitaxel loaded microspheres using a lactic-co-glycolic acid copolymer with a lower molecular weight from which faster release of paclitaxel is expected. Recently, *Si-Shen Feng*[160] developed the paclitaxel-loaded nanospheres of biodegradable polymers with freeze dry solvent extraction/evaporation technique. In 2005, FDA approved Abraxane®, a nanoparticle paclitaxel (nab-paclitaxel) from Abraxis Bioscience in breast metastasis and in June 2010, outcome in NSCLC (non-small cell lung cancer) proved its efficacy in clinical trials.[145]

✓ *Structural modifications.* The fear that Paclitaxel was derived from an exhaustible source, made an urge to develop new semisynthetic taxol analogues: TAXOTERE®. Licenced by Sanofi- Aventis, it derives from *Taxus Baccata*, a European yew being a renewable source and is approved by the FDA for breast, head and neck, prostate and gastric carcinomas.[144] Taxotere differs from taxol at two positions in its chemical structure; a hydroxyl functional group on carbon 10 where instead Taxol has an acetate ester and a tert-butyl carbamate ester exists on the phenylpropionate side chain instead of bezyl amide in taxol. Hence, it is the carbon 10 functional group that causes Taxotere to be more water soluble. During the course of time, many new taxanes from the parent molecule has been developed and entered clinical trials so as to give early diagnosed cancer patients a chance to live longer, remain cancer free and patients with advanced cancers some more months to live if not years.

Since its approval from FDA and introduction on the market, Paclitaxel has also received extensive chemical studies during its development. Various chemical transformations have been carried out, which provided structure-activity relationships (SAR). Due to the poor crystalline property of paclitaxel and its analogs, the first X-ray crystal structure of paclitaxel was not available until 1995.[161]
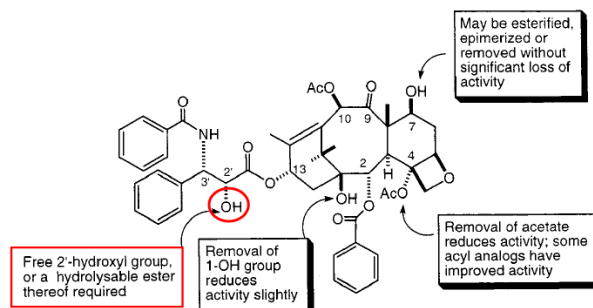

Figure 1.30. Some structure-activity relationships of paclitaxel

Kingston et al.[161] have studied the importance of the various hydroxyl groups of the taxane ring system on the activity of taxol (Figure 1.30). In these investigations it was shown that both the C-10 and C-7 positions could be deoxygenated without significant loss of activity, but that deoxygenation of the C-4 and C-2' positions did result in a significant activity loss. The use of esters as prodrugs has been extensively employed for modifying biologically active molecules containing either hydroxyl or carboxyl functionalities. In case of paclitaxel, the simplicity of synthesis coupled with facile enzymatic hydrolysis dictates esters as a first choice when considering prodrug strategies. Studies of 2′-taxol esters as prodrugs demonstrated that esters without α-substituents hydrolyzed only to the extent of 10% over a 24 h period, while those with electron-withdrawing substituents in the α-position showed remarkable enhancement in their rates of hydrolysis.[163] Among the most notable paclitaxel derivatives synthesized so far are those in which the C-2 and C-7 hydroxyl groups of the molecule are engaged in a functional group that collapses, upon in vivo activation, releasing paclitaxel.[164]

For our aim we decided to exploit the more reactive OH function at position 2' to insert a succinate linker, strategy that allowed us to have the desired prodrug in one step, without protecting the other hydroxylic groups on the scaffold (Scheme 1.9).
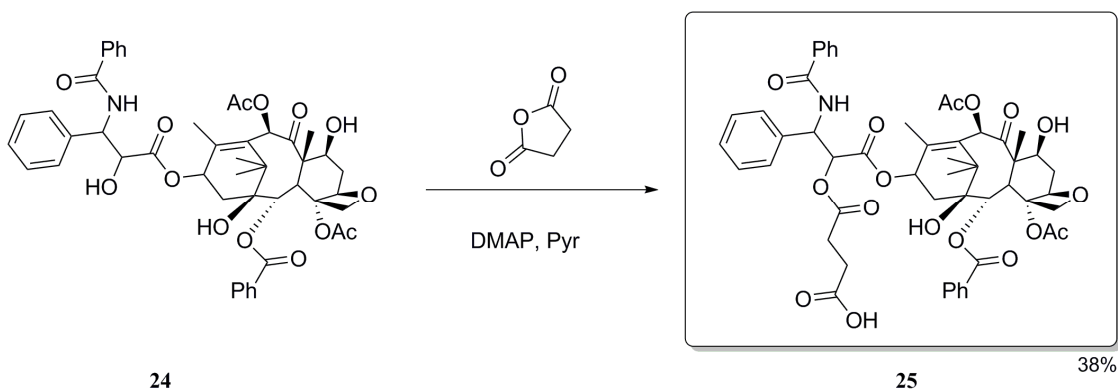
Scheme 1.9

The one step reaction started treating a solution of taxol (**24**) in 4 mL of dry pyridine with an slight excess of succinic anhydride (1.1 equiv.) and DMAP (2 equiv.) for 3 h under a N_2 atmosphere. After several washings of the crude with a saturated solution of NH_4Cl to get rid of pyridine, the desired prodrug (**25**) was obtained without further purification in 38% yield. The paclitaxel-MAP peptide complex resulted not to be stable to TFA, thus, even in this case, we envisaged an alternative strategy to overcome this experimental problem, as described in § 1.2.2.

Combretastatin A4

Combretastatins are a family of natural phenols, contained in plants belonging to the *Combretum* genus, notably in *Combretum caffrum*, the Eastern Cape South African bushwillow tree [165] and *Combretum leprosum*, the Brazilian "mofumbo" tree.[166] Several molecules belonging to the combretastatin family have been found in the extracts of said plants, among which combretastatin A-4 (**33**) and combretastatin A-1 (Figure 1.28). Both have interesting biological activity but the one on which we decided to focus our research is combretastatin A-4, because of the promising results of clinical trials it has undergone.[167]

Figure 1.31. a. Combretastatin A-4; **b.** Combretastatin A-1

Combretastatin (**33**) (*Cis*-CA-4) is a small organic molecule with stilbenoid structure, found in the bark of the African bush willow tree *Combretum caffrum* (Figure 1.31), identified 21 years ago by Professor George R. Pettit.[168]
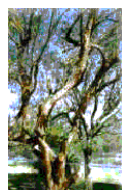
Figure 1.32. Combretum caffrum

Cis-CA-4, a tubulin binding agent currently undergoing phase I clinical trials, is a potent antimitotic and cytotoxic agent which strongly inhibits the polymerization of tubulin by binding to the colchicine site and causes vascular disruption in some experimental primary tumours and in vascularized metastatic tumour deposits.[169] Actually, the exact mechanism of action of combretastatin A-4 hasn't been fully elucidated yet, but several structural analogies with colchicines (Figure 1.32), the most

known mitosis-inhibiting toxin,[170] can be highlighted and support the above stated hypothesis involving the colchicines site.

Figure 1.33. Analogies of combretastatin A-4 (a) with colchicine (b)

Many *in vitro* studies have proposed a heterogenous variety of possible mechanisms through which CA4 may exert its anticancer activity. In an early study, *Iyer et al.* has shown that CA4 causes death by apoptosis in human umbilical vein endothelial cells (HUVECs) by inducing proteolytic conversion of CPP32 into caspase-3, a pro-apoptotic enzyme,[171] although various mechanisms through which this action is performed have been proposed.[172] However, Nabha *et al.*, who tested CA4P on a panel of malignant human B-lymphoid cell lines, observed that the mechanism through which the drug led to cell death was mitotic catastrophe,[173] a sort of fatal response to a failed apoptosis process. [174]

In addition, *Cis*-CA-4 differentially affects quiescent and tumour vasculature, as indicated by the greater magnitude of transient changes induced in vascular pressure and resistance in tumors compared with those in normal tissues. The mechanism of action of *cis*-CA-4 remains to be elucidated but it has been hypothesized that it manifests a selective toxicity for tumour endothelial cells,[175] because their proliferative activity renders them more susceptible to the drug than the quiescent vasculature which predominates in the adult. The anti-vascular activities of *cis*-CA-4 have been reported to be specific for tumor vasculature. Although the inhibition of angiogenesis is an elegant concept in cancer therapy, there are concerns about its implementation. Antiangiogenesis therapy-induced tumoral hypoxia upregulates genes that can significantly reduce the pro-apoptotic effect of chemotherapy leading to 'reactive resistance'. Furthermore, the activation of the hypoxic response can enhance the metastatic and invasive potential of tumour cells, although this has not been resolved clinically.[176]

Furthermore, CA4 exhibits strong cytotoxicity against a broad spectrum of cancer cell lines, such as murine melanoma, human ovarian and colon cancer cells, and even those with multidrug resistance, which makes CA4 a potent cancer drug.[177] Despite its pharmacodynamic advantages, combretastatin A-4 has a pharmacokinetic limit: it is has a very poor water solubility, that in biological media significantly impair its bioavailability and its antitumor activity for clinical applications.[178] These limitations have led to the development of water-soluble structural analogue, such as *CA4P*.

Figure 1.34. a. Combretastatin A-4 (*Cis*-CA4 **33**) and **b.** its prodrug Combretastatin A-4 phosphate (CA4P)

Phosphate CA4P, is a water soluble prodrug of CA4 (Figure 1.34 b), now in phase II of clinical trials and classified like a VDAs (tumour vascular disrupting agents) that target the existing vasculature of tumours to cause rapid vascular shutdown in the tumour, leading to cell death.[179] It is rapidly hydrolyzed to the active phenol form (combretastatin A-4 itself) by nonspecific alkaline phosphatases, which is particularly interesting, as these enzymes are overexpressed on endothelial cells in proliferating vasculature. Moreover, when CA4P is combined with a variety of cytotoxic agents (carboplatin and paclitaxel),[180] as well as with radiotherapy and antiangiogenesis inhibitors, enhanced tumour control is achieved *in vivo*. CA4P is currently under investigation in phase I trials with bevacizumab for extracranial human tumours[181-182] and in phase II trials for ovarian, lung, and anaplastic thyroid cancer.[183] In *in vitro* tests, CA4P has been shown to be selectively cytotoxic to proliferating HUVECs, while being reported not to be toxic neither to quiescent HUVECs (which can represent a good model for sane endothelial cells in physiological conditions) nor to other proliferating cells, such as dermal fibroblasts.[184] As proliferating endothelial cells are a feature which is almost exclusive to tumor tissue, combretastatin can be classified as a remarkably selective tumor targeting agent.

Combretastatin A-4 as a functional moiety in a targeted drug delivery system

Having an intrinsically tumor-targeting mechanism of action, combretastatin A-4 lacks the side effects which are peculiar to classic, non-specific chemotherapeutical agents (see Introduction); nevertheless, this drug is still characterised by a non irrelevant toxicological profile. *Young* and *Chaplin* have reported CA4 to have a certain cardiotoxicity (in particular, QTc interval prolongation) during one of the earliest clinical trials undergone by this drug,[185] side effect which could be a consistent drawback in treatment of cancer in patients also suffering from cardiovascular diseases. Other reported side effects, although not severe as in classical chemotherapy, are lymphopenia and headache; moreover, combretastatin A-4 peculiarly increases tumor pain,[186] a negative effect which could dramatically diminish compliance with patients.

Despite CA4 toxicity and side effects are in no way comparable to those exhibited by classical chemotherapeutical agents, they still have not to be underestimated, since any improvement of quality life in oncological patients has to be firmly pursued. For all these reasons, the development of a combretastatin-based targeted therapy appears to be highly desirable. In addition, the simple chemical structure of combretastatin A-4 makes it an ideal candidate for derivatisation, as it just possesses one reactive function (the phenolic OH); this remarkably simplifies prodrug design strategies.

Total synthesis and introduction of the suitable linker will allowed the delivery of the drug by the branched-peptide. We imagined to exploit the same releasing mechanism adopted for 5-FdUrd, gemcitabine and lapachone derivatives (**1**, **4** and **7**), transforming the free phenolic OH of **33** in a functionalized ester. Combretastatin was prepared by a modification of previous methods developed by *Pettit et al.*, that exploits a Wittig reaction between an aldehyde and the ylide **29** as the key step (Scheme 1.10).
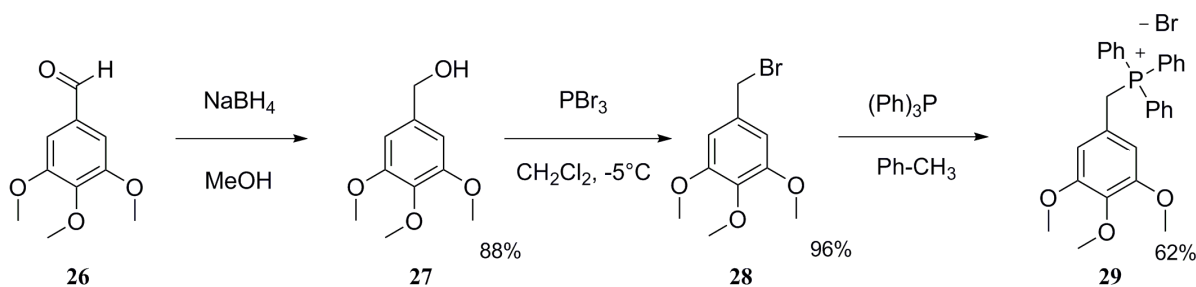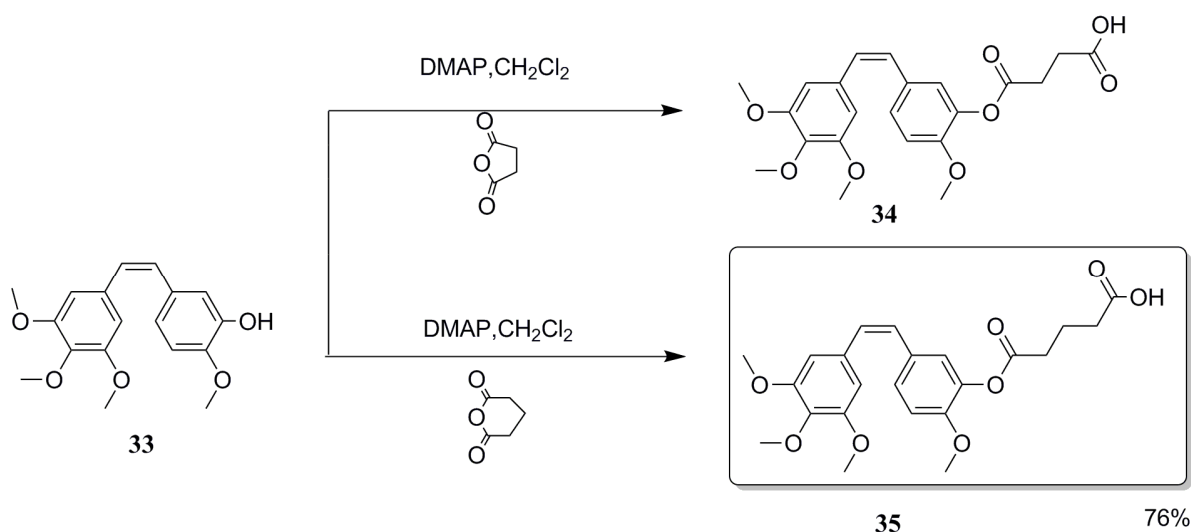
Scheme 1.10.

The synthesis of the phosphonium salt **29** started from the reduction of 3,4,5-trimethoxybenzaldehyde **26** (1.0 equiv.) by the addition of NaBH$_4$ (1.2 equiv.) in MeOH at 0 °C to yield benzyl alcohol **27** in 88% yield. To a solution of **27** (1.4 eqiv.) in dry CH$_2$Cl$_2$, cooled to -5 °C, a solution of PBr$_3$ (1.0 equiv.) in dry CH$_2$Cl$_2$ was added dropwise to give bromide **28** in 96% yield. Finally, a solution of triphenylphosphine (1 equiv.) in toluene was added to a solution of bromide **28** (1 equiv.). The reaction mixture was stirred for 24 h at r.t. and the precipitate formed filtered and dried to obtain phosphonium bromide **29** in 62% yield.
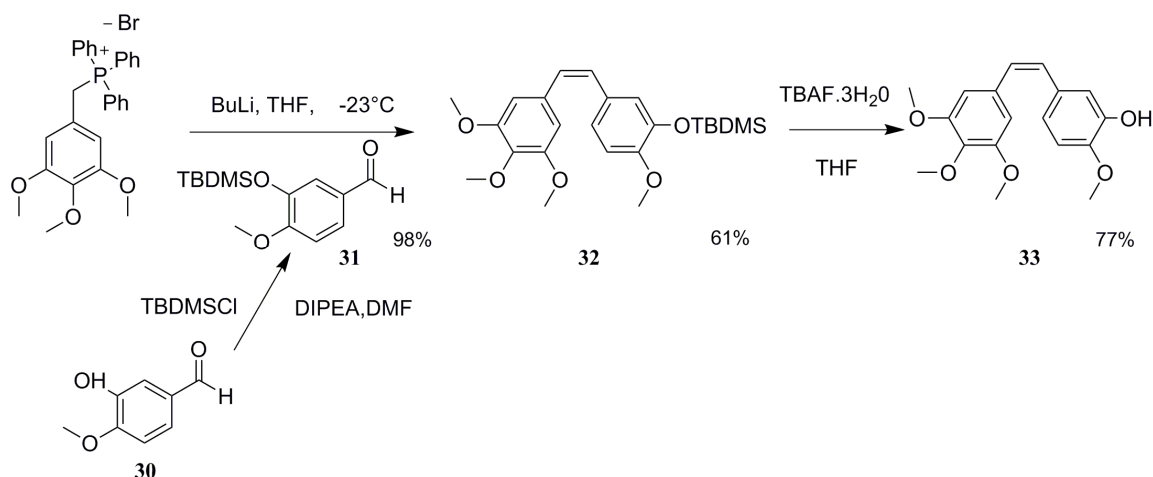
Scheme 1.11.

Isovanillin (**30**) had to be protected to undergo the Wittig reaction and we chose *tert*-butylsilyl (TBDMS) as protecting group. To a solution of isovanillin (1.0 equiv.) in dry DMF, DIPEA (2.0 equiv.) and TBDMSCl (1.6 eqiv.) were added. The crude product, obtained after 4 h of reaction, was purified by flash chromatography to give **31** in 98% yield. A suspension of phosphonium bromide **29** (1.0 equiv.) in dry THF is cooled to -23 °C under a N$_2$ atmosphere and retained at that temperature for 2 h. Butyllithium (1.0 equiv.) was added dropwise, the resultant orange solution was stirred at the same temperature for 1 h and finally **31** (1.04 equiv.) was added. The reaction mixture was stirred at -23 °C for 4 h and at r.t. for 18 h, ice-water was added and two phases separated. The aqueous phase was washed with Et$_2$O and the etheral solution added to the THF layer. The combined organic phase was washed with water and dried. The crude product was purified by flash chromatography to give both the desired *Z* isomer in 61% yield and a 20% of the corresponding *E* product. The careful control

of temperature was critically correlated with the obtainment of an excess of *Z* isomer. Deprotection of **32** (1 equiv.) occurred in dry THF in the presence of TBAF 3H$_2$O (1 equiv.) after 20 min stirring. The residue was then chromatographed to obtain the natural product CA4 **33** in 77% yield (Scheme 1.11).

Scheme 1.12.

The next reaction with succinic anhydride, led as usual with DMAP in CH$_2$Cl$_2$, gave ester **34**, as verified by NMR analysis, but this derivative turned out to be instable even in silica gel, making impossible not only the purification but also the coupling with the dendrimeric peptide. Since the other succinate derivatives prepared (**1**, **4** and **25**) were stable even in harsh acid conditions, we realized that the aromatic ring promotes the ester cleavage because it stabilizes the resulting phenate ion. Therefore, we imagined the formation of a more stable derivate, just increasing the ester chain length. Glutaric anhydride (4 equiv.) was added to a solution of combretastatin **33** (1 equiv.) in dry CH$_2$Cl$_2$. The mixture was stirred for 16 h at r.t., refluxed for 24 h and poured onto ice/water/NaHCO$_3$. The suspension was washed several times to remove other glutaric derivatives and gave the desired acid **35** in 76% yield. This product was much more stable than the corresponding compound obtained by the reaction with succinic anhydride (Scheme 1.12).

Citotoxycity of compound **35** has been tested in PC-3, PANC-1 and HT-29 human cancer cell lines. The pharmacological results will be discussed in § 1.3.

E. DNA topoisomerase I inhibitors

Topoisomerase inhibitors are agents designed to interfere with the action of topoisomerase enzymes[187](topoisomerase I and II), that control the changes in DNA structure by catalyzing the breaking and rejoining of the phosphodiester backbone of DNA strands during the normal cell cycle. DNA topoisomeras are ubiquitous enzymes in eukaryotic cell and prokaryotic cell. They are crucial for cellular genetic processes, such as replication, recombination, transcription, chromosome condensation, and the maintenance of genome stability by catalyzing the passage of individual DNA strands (topoisomerase I) or double helices (topoisomerase II) through one another.

Topoisomerase I (Topo I), in particular, plays a crucial role in the normal replication of DNA. In its physiological state in the chromosome, the DNA helix is supercoiled and tightly packed into chromatin. Replication requires transient relaxation and unwinding of the parent DNA to allow the replication fork to proceed down the DNA strand and serve as a template for synthesis of new strands of DNA. In order to achieve this without creating extreme torsional stress on the parent DNA, transient cleavage of the DNA is required. This transient cleavage also allows passage of newly synthesized DNA without it becoming irretrievably tangled in the parent strands. Topo I subserves this process through a reversible trans-esterification reaction which yields a covalent intermediate form with the tyrosine of the enzyme bound to the 3' end of the DNA strand. This 'cleavable complex' normally lasts only long enough to allow passage of the newly synthesized strand through the cut, after which topo I reseals the cleavage (Figure 1.35).[188]
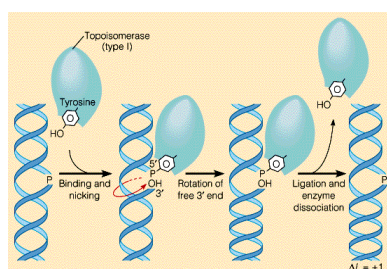
Figure 1.35. Topoisomerase I relaxing the Super coiled DNA

It is known in literature that topoisomerases are over expressed in cancer cell growth and thus are important cellular targets for anticancer drugs,[189] thus in recent years, topoisomerases have become popular targets for cancer chemotherapy treatments. It is thought that topoisomerase inhibitors block the ligation step of the cell cycle, generating single and double stranded breaks that harm the integrity of the genome. Introduction of these breaks subsequently leads to apoptosis and cell death. Regarding cancer therapy, topoisomerase inhibitors are often divided according to which type of enzyme it inhibits:[190]

- Topoisomerase I inhibitors: irinotecan, topotecan, camptothecin and lamellarin D; all target type IB topoisomerases;

- Topoisomerase II inhibitors: etoposide, teniposide, doxorubicin , daunorubicin, mitoxantrone and HU-331, a quinolone synthesized from cannabidiol.

The topoisomerases were discovered in 1971 but it was not until the 1980s that the significance of these enzymes as potential therapeutic targets was appreciated. Over the past two decades, there has been an explosion of interest in topo I and the development of compounds that can selectively inhibit this enzyme. DNA topoisomerase are particularly vulnerable to topisomerase I inhibitors during their cleavage intermediate step. TOP1 cleavage complexes (TOP1ccs) are normally so transient that they are not detectable, but it is these complexes that are specifically and reversibly trapped by camptothecin and its pharmaceutical derivatives.[191]

Camptothecins are among the most effective anticancer agents recently introduced into clinical practice. They are pharmacologically unique for several reasons:

- First, TOP1 is the only target of camptotechins, as has been shown using yeast cells, which become totally resistant to camptothecin when the *TOP1* gene is removed and by the existence of single point mutations that render TOP1 immune to camptothecins in vertebrate cell lines selected for resistance to camptothecin.[192]

- Second, changing the stereochemistry of camptothecin by inverting its chiral centre at position 20 completely inactivates camptothecin. Therefore, it is remarkable that the natural alkaloid exists as the active 20-S-camptothecin enantiomer (referred to as camptothecin for simplicity) (Figure 1.36).
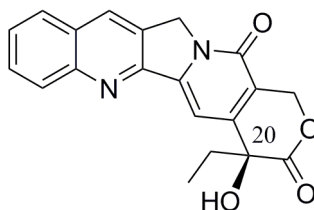
Figure 1.36. The active 20-*S*-camptothecin enantiomer

- Third, camptothecins penetrate vertebrate cells readily and target TOP1 within minutes of exposure. Camptothecin then binds reversibly to TOP1ccs. Because the cleavage complexes reverse within minutes of camptothecin removal, camptothecin is an incisive pharmacological tool, as drug exposure and the trapping of TOP1ccs can be precisely controlled.

- Finally, camptothecin and its derivatives have a relatively low affinity for TOP1ccs, as micromolar drug concentrations are required to detectably trap TOP1cc in biochemical assays, which indicates that camptothecin (which might function as an antibiotic in plants) was naturally selected for on the basis of its selectivity rather than its potency.[191]

In this regard, the camptothecin derivative topotecan (Hycamtin) was the first campotechin approved in 2007 by the U.S. FDA for the treatment of ovarian and lung cancer. Another camptothecin derivative, irinotecan (CPT11) was approved for the treatment of colon cancer. There are, however, certain clinical limitations of the camptothecin derivatives. These include: 1) spontaneous inactivation to a lactone form in blood, 2) rapid reversal of the trapped cleavable complex after drug removal, requiring prolonged infusions, 3) resistance of cancer cells overexpressing membrane transporters, and 4) dose-limiting side effects of diarrhea and neutropenia. Moreover, although camptothecins are therapeutically effective, they are not curative as single agents. Several approaches need to be considered to improve the effectiveness of TOP1 inhibitors, such as a rationale for the combination of TOP1 inhibitors with other drugs or biological treatments on the basis of the molecular network of individual tumors and reliable, sensitive and non-invasive biomarkers to follow the early response or lack of response to TOP1 inhibitors in combination with other treatments so that therapies can be rapidly and effectively adapted.

Camptotechin

Camptothecin (CPT, **36**, Figure 1.36) is a cytotoxic quinoline alkaloid which inhibits the DNA enzyme topoisomerase I. Camptothecin was first isolated from the bark of the Chinese tree, *Camptotheca acuminata*. It was discovered and developed by the US National Cancer Institute (NCI)

at about the same time and by the same groups that were also working on paclitaxel (Taxol).[142] Camptothecin carboxylate was tested clinically in the mid 1970s and showed anticancer activity, but was discontinued because of its side effects22. It was not until after the discovery that TOP1 was the cellular target of camptothecin that the water-soluble derivatives of camptothecin (topotecan and irinotecan) (also known as CPT-11) were successfully developed.[193]

CPT has a planar pentacyclic ring structure, that includes a pyrrolo[3,4-β]-quinoline moiety (rings A, B and C), conjugated pyridine moiety (ring D) and one chiral center at position 20 within the alpha-hydroxy lactone ring with (S) configuration (the E-ring). Its planar structure is thought to be one of the most important factors in topoisomerase inhibition. SAR of CPT has been deeply investigated, highlitning that the lactone ring in CPT is highly susceptible to hydrolysis. The open ring form is inactive and it must therefore be closed to inhibit topo I. The closed form is favored in acidic condition, as it is in many cancer cells microenvironment, rendering this molecule suitable for cancer treatment.[194]

We decided to consider it for our design of prodrugs synthesis (Scheme 1.13).

36 **37** 18%
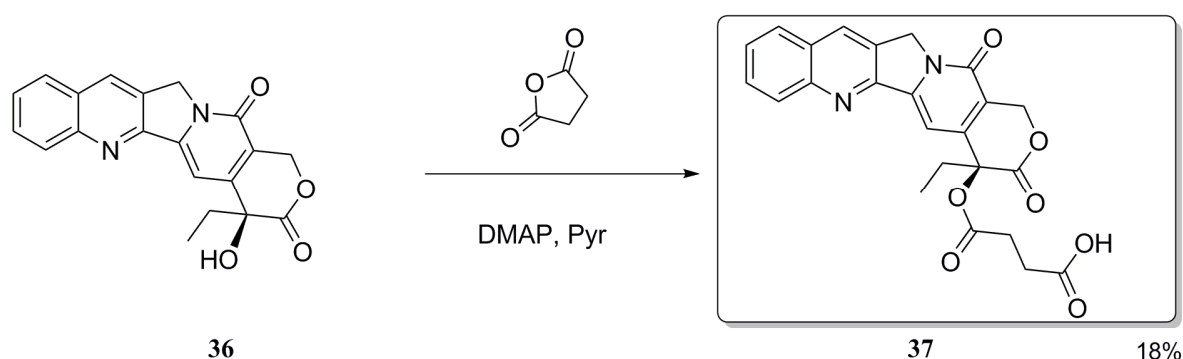
Scheme 1.13.

Derivative **37** was synthesized, according to the procedure reported in literature.[195] A suspension of Camptothecin (**36**) (1 equiv.) in pyridine was treated with a large excess of succinic anhydride (8 equiv.) and a catalytic amount of DMAP (0.3 equiv.) under a N_2 atmosphere at 50°C for tow days. The solid obtained upon adding of HCl was recrystallised by MeOH to give a mixture of starting material and desired product. The crude was, then purified by flash chromatography using DCM : MeOH 20 : 1 as eluent to obtain the final product (**37**) in 18% yield.

A stability test to acid was performed on derivative (37), that resulted to be stable overnight upon exposure to 95% TFA solution. For this reason design a 'post-cleavege coupling' strategy fo Camptotechin was not necessary.

Conjugation to the tetrabranched peptide (NT4)

We have synthesized, as described above, a variety of carboxylic derivatives decorating the most common anticancer drugs (Combretastatin A-4 (CBTST), 5-Fluoro-2'-deoxyuridine (5-FdUrd),

Gemcitabine, Cis-Platinum, Estradiol, β-hydroxy Lapachone). The accessible COOH groups of these Functional Units should be then coupled with the tetrameric NT peptide in order to provide a tumor targeting system for diagnostic or therapeutic applications. The conjugation with the NH_2 group, introduced *ad hoc* on the dendrimer, was carried out by standard solid phase synthesis for most of the derivatives prepared.

Operatively, peptide synthesis was performed on a MultiSynTech Syro automated multiple peptide synthesizer (Witten Germany), employing 9- fluorenylmethoxycarbonyl (Fmoc) chemistry with 2-(1H-benzotriazole-1-yl)-1,1,3,3- tetramethyluronium hexafluorophosphate (HBTU) / N,N-diisopropylethylamine (DIPEA) activation. Side chain protecting groups were trityl for His, 2,2,4,6,7-pentamethyldihydro-benzofuran-5-sulfonyl for Arg, tert-butyl ether for Ser and Tyr, tert-butyl ester for Asp and Glu, and tert-butyloxycarbonyl for Trp.

Considering the large variety of molecules to be conjugated with the dendrimeric peptide, prof. Bracci's group tested different approaches to find the most simple and versatile way to prepare tetramers. Tetra-branched analogues were synthesized on resin NovaSyn TGR. A mixture of 5 equiv. of Fmoc protected aminoacid, 5 equiv. of HBTU dissolved in DMF and 10 equiv. of DIPEA were added to the resin beads. The reaction was automatically performed at r.t. for 40 minutes and the coupling step repeated twice. After each aminoacid addition the Fmoc protecting group was removed with a 40% solution of piperidine in DMF and extensively washed with DMF before adding the next one.

All tetrameric peptides were built employing two consecutive Fmoc-Lys(Fmoc)-OH coupling steps to form the branched core. Fmoc-Lys(Fmoc)-OH was used to build the three-lysine branched core. C-terminal stepwise automated elongation [(Arginine (R), Arginine (R), Proline (P), Tyrosine (Y), Isoleucine (I), Leucine (L)] was then carried out by the above described HBTU/DIPEA method. Boc-Arg(Pbf)-OH was used as last amino acid of the neurotensin sequence, so that the last step occurred selectively on the side chain arm. In fact, Dde protective group was removed with 2% hydrazine for 10 min at r.t. and the free amino group was coupled with all the new functional units, which are provided with a carboxylic acid function. Moreover, the side chain amine group to be used for the functional unit coupling was rendered more accessible stretching it with Fmoc-PEGOH. After deprotection of the Fmoc group on PEG, the functionalized peptide was finished by activation and coupling of the carboxylic acid of the Functional Unit (R'- OH), (Scheme 1.14).
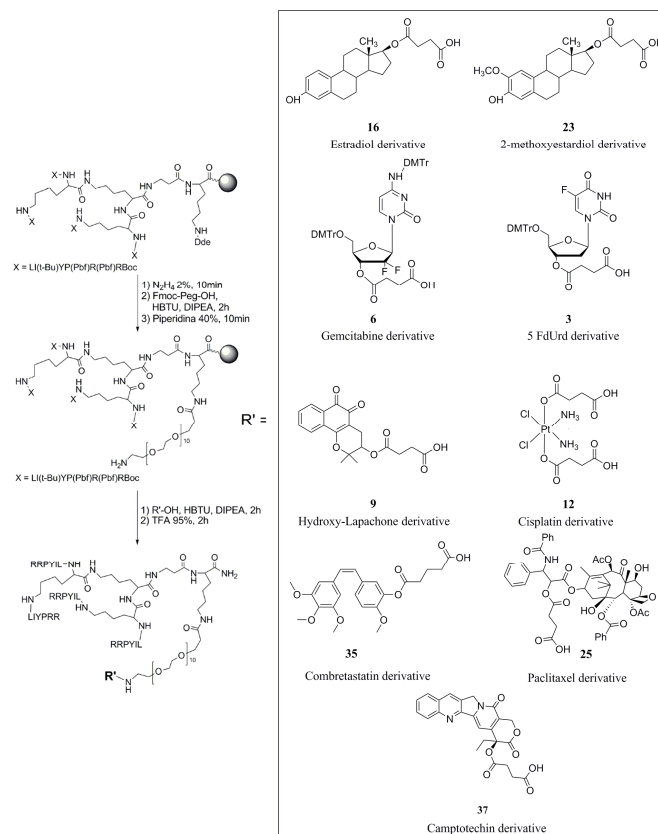
Scheme 1.14.

Peptides were cleaved from the resin and deprotected by treatment with trifluoroacetic acid (TFA) containing water and triisopropylsilane (95/2.5/2.5), and precipitated with diethyl ether (Scheme 14). The final isolation was obtained through lyophilisation. All compounds were characterized by MS on a Ettan MALDI-TOF mass spectrometer and purified by HPLC on a C18 Vydac column.

For instance, Combretastatin derivative (**35**) in a DMF solution of DIPEA (10 equiv.) was activated with an excess of HBTU (5 equiv.). The mixture was reacted with MAP-NT peptide in solid phase.The reaction was automatically performed at r.t. for 1 h and the coupling step repeated twice, followed by several washings with DMF to get rid of the excess of (**35**). The obtained complex was cleaved from the resin with a mixture 95:2.5:2.5 of TFA:water:TIPS, shaking for 2 h, allowed to precipitate with diethyl ether and finally liophylised to give the desired drug-peptide complex (Scheme 1.15).
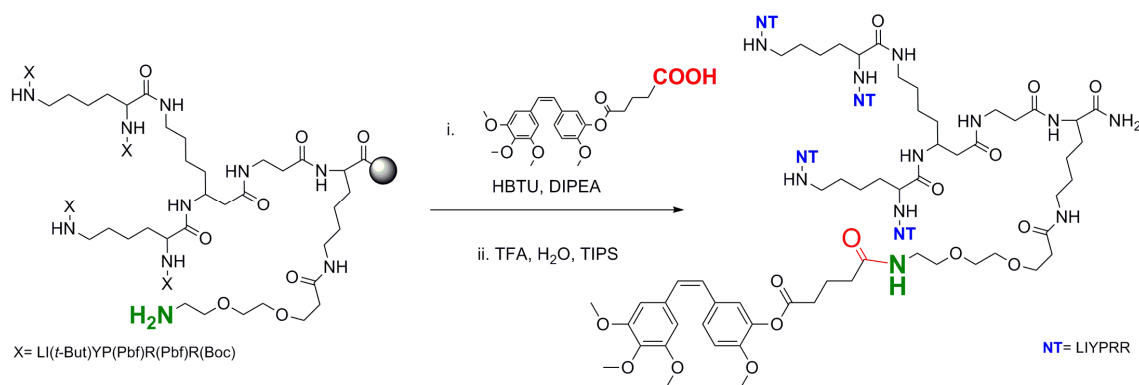
Scheme 1.15.

1.2.2 Cytotoxin: post-cleavage coupling

As stated above, we envisaged an alternative protocol of coupling of our therapeutical units to MAP NT, since some of them resulted not to be stable to the cleavage conditions, required in the 'pre-cleavage coupling'. This need was born, in particular, with the failure of the latter strategy with compounds such as cisplatin and paclitaxel derivative (**12** and **25** respectively). In both cases, the correct mass peak of the desired drug-peptide complex was not observed after removal from the resin. Considering that the decoration of these drugs was straightforward and the presence of compounds **12** and **25** was confirmed with different spectroscopical methods, we imagined an instability of such derivatives in drastic acid conditions. We, thus, performed stability tests of the drugs in exam, exponing them to a 95% solution of TFA in water for 2 h. (simulating in this way the cleavage condition from solid phase). After evaporating the acid solution we recorded NMR spectra (data not shown), that confirmed the chemical degradation of our compounds. Starting from this experimental evidence, we opted for the so called 'click chemistry reactions' for post removal coupling as possible solution to overcome the synthetical problem we run into.

<u>Click chemistry</u>

'Click chemistry' was first fully described by *Sharpless* and *Fokin* at the Georgia Institute of Technology in 2001 and describes chemistry tailored to generate substances quickly and reliably by joining small units together. Click chemistry is not a single specific reaction, but was meant to mimic nature, which also generates substances by joining small modular units. It describes reactions that are high yielding, wide in scope, create only byproducts that can be removed without chromatography, are stereospecific, simple to perform, and can be conducted in easily removable or benign solvents. This concept was developed in parallel with the interest within the pharmaceutical, materials, and other industries in capabilities for generating large libraries of compounds for screening in discovery research. Several types of reaction have been identified that fulfill these criteria, thermodynamically-favored reactions that lead specifically to one product:[196]

✓ [3+2] cycloadditions, such as the *Huisgen 1,3-dipolar cycloaddition*.[197] It fulfills many of the prerequisites, since many of the starting monosubstituted alkynes and organic azides are available commercially, many others can easily be synthesized with a wide range of functional groups, and their cycloaddition reaction selectively gives 1,2,3-triazoles. Unfortunately, the thermal Huisgen reaction of alkynes to azides requires elevated temperatures and often

produces mixtures of the two regioisomers when using asymmetric alkynes. In this respect, the classic 1,3-dipolar cycloaddition fails as a true click reaction. A copper-catalyzed variant[198] that follows a different mechanism can be conducted under aqueous conditions, even at room temperature (Scheme 1.16).
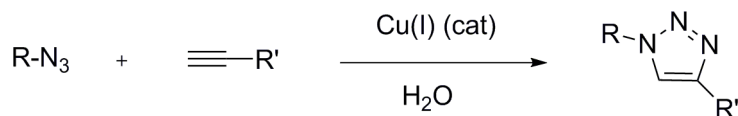
Scheme 1.16.

Additionally, whereas the classic Huisgen 1,3-dipolar cycloaddition often gives mixtures of regioisomers, the copper-catalyzed reaction allows the synthesis of the 1,4-disubstituted regioisomers specifically. Thus, this catalyzed reactions comply fully with the definition of click chemistry and have put a focus on azide-alkyne cycloaddition as a prototype click reaction.

✓ Addition reactions to carbon-carbon double bonds like the alkynes in the *thiol-yne reaction* (Scheme 1.17).
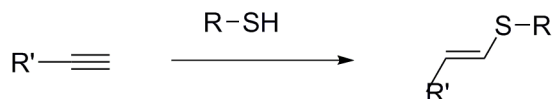
Scheme 1.17.

The thiol-ene reaction (also alkyne hydrothiolation) is an organic reaction between a thiol and an alkyne. The reaction product is an alkenyl sulfide.[199] The reaction was first reported in 1949 with thioacetic acid as reagent and rediscovered in 2009. It is used in click chemistry and in polymerization, especially with dendrimers.

✓ *Diels-Alder reaction* and inverse electron demand Diels-Alder reaction. The Diels–Alder reaction is an organic chemical reaction (specifically, a cycloaddition) between a conjugated diene and a substituted alkene, commonly termed the dienophile, to form a substituted cyclohexene system.[200] The reaction can proceed even if some of the atoms in the newly formed ring are not carbon . Some of the Diels-Alder reactions are reversible; the decomposition reaction of the cyclic system is then called the retro-Diels–Alder. According to the cis principle or the Alder–Stein rules, the reaction is steroselective: stereochemistry of substituents in the starting material is retained in the product.

✓ [4+1] *cycloadditions* between isonitriles (isocyanides) and tetrazines.

✓ *Nucleophilic substitution* especially to small strained rings like epoxy and aziridine compounds.

✓ Carbonyl-chemistry-like formation of ureas but not reactions of the aldol type due to low thermodynamic driving force.

Among the above described reactions, we chose to focus our attention on the first two strategies, since they appeared to be the most suitable for the functionalisation of our drugs and peptides. It implied to reconsider either the solid phase reaction protocol of MAP-NT and the liquid phase reaction protocol of therapeutical units, in order to insert complementary moieties on both of them. The aim of the following section is to summarized all the attempted strategies of drug functionalisation in order to lead a coupling in solution after removal of the peptide from the resin. We imagined to start from some of the therapeutical compounds above described, introducing a proper variability on their scaffolds. The screening was based on the pharmacological results obtained in *in vitro* tests (as reported in PHAR): drug-peptide complexes with comparable or higher citotoxicity than the uncojugate ones were selected as suitable candidates for the purposed click chemistry strategy.

A. Antimetabolites

5-Fluoro-2'-deoxyuridine (5-FdUrd)

As stated in the previous paragraph, 5-FdUrd (**1**) has a relevant role in the treatment of metastatic cancers. In order to realize a Huisgen 1,3-dipolar cycloaddition with MAP-NT, we attempted to insert an alkyne moiety through esterification.
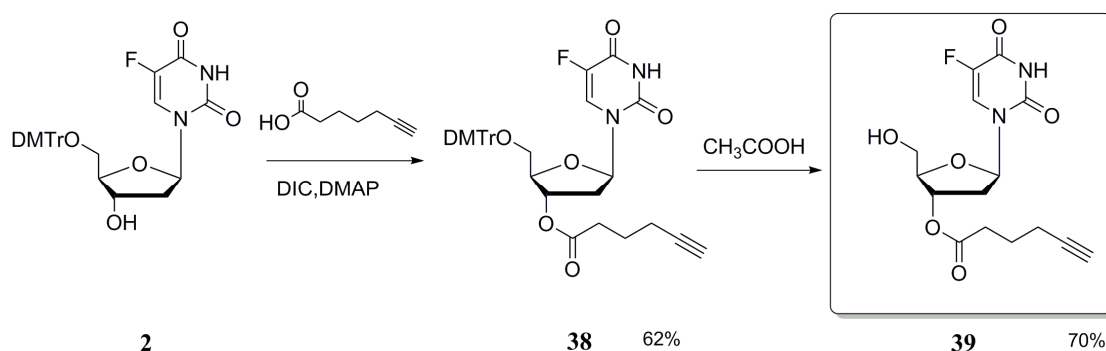
Scheme 1.18.

Thus, the strategy used recalled the one used to prepare derivative **3** and the desired moiety is inserted forming an ester bond. Synthesis started protecting the primary alcohol of 5-Fluoro-2'-deoxyuridine (**1**) to give intermediate **2** as previousely reported (Scheme 1). The free hydroxylic group was, then, reacted with an excess of 5-hexynoic acid (1.1 equiv.) and of DIC (1.1 equiv.) and with a catalytic amount of DMAP (0.1 equiv.) in dry DCM for 3 h. The crude was washed several times with a saturated solution of NH$_4$Cl to get rid of DCU to give **38** in 62 % yield. Compound **38** was finally deprotected by stirring for 3 h with a 80% solution of acetic acid in water. and purified by flash chromatography using CH$_2$Cl$_2$: MeOH 25 : 1 as eluent to give the desired product (**39**) in 70% yield (Scheme 1.18).

Furthermore, we decided to play with the chemical nature of the bifunctional linker to modulate the *in vivo* release rate of the therapeutic unit. Indeed, we investigated the effect of a more stable linker in physiological conditions. The ester bond was, thus, replaced by an ether one, a much more stable linkage that does not undergo hydrolysis from proteases and esterases of serum (Scheme 1.19)
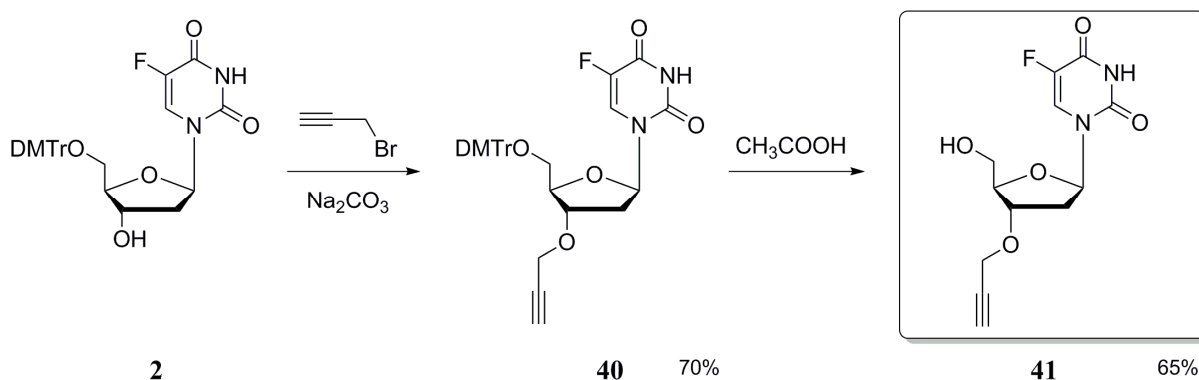
Scheme 1.19.

In this case, the protected derivative **2** was treated with propargyl bromide (3 equiv.) in dry DMF, in the presence of Na_2CO_3 (3 equiv.) as base. The reaction took 19 h stirring to be completed and intermediate **40** was isolated after purification by flash chromatography, using CH_2Cl_2 : MeOH / 50 : 1 as eluent, in 70% yield. The obtained compound turned out to be not stable to storage, since it spontaneously started releasing the DMTr protecting group after a few days. The spontaneous conversion of intermediate **40** into **41** could be easily observed by the orange coloration that (**40**) develops in DCM solution. Compound **40** was completely deprotected with CH_3COOH as above described to give prodrug **41** in 65 % yield. Cytotoxicity assays to determine whether or not our hypotesis on chemical stability is correct will be performed at University of Siena.
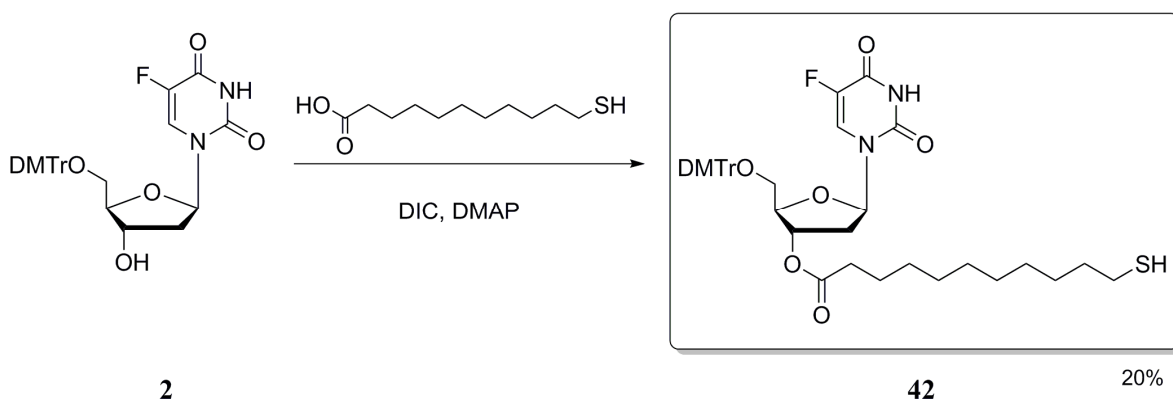
Scheme 1.20.

Moreover, we imagined to bind 5-Fluoro-2'-deoxyuridine to properly functionalized MAP-NT (for instance, with a maleimido terminal group) through a thiol-ene reaction. For this aim we decided to use an α-thiol-ω-carboxylic linker that, on one hand, allows the anchorage on drug through a selectively *in vivo* cleavagable ester bond on the other hand provides a suitable thiol group for the

purposed click chemistry reaction. In order to realize that, derivative **2** was treated with 11-mercaptoundecanoic acid (1.5 equiv.) under the DIC-DMAP protocol above described for the synthesis of compound **39**. Final pro-drug **42** was obtained after purification by flash chromatography using EtP : AcOEt 2 : 1 as eluent in 20% yield (Scheme 1.20). The poor yield is due to the easy oxidation of the thiol to the corrisponding disulphur on silica gel, during purification.

Gemcitabine

Gemcitabine (**4**) is a milestone for treatment of pancreatic cancer. Synthetical approaches used were similar to the ones investigated for 5-Fluoro-2'-deoxyuridine, since the chemical structures of these two antimetabolites resemble each other.
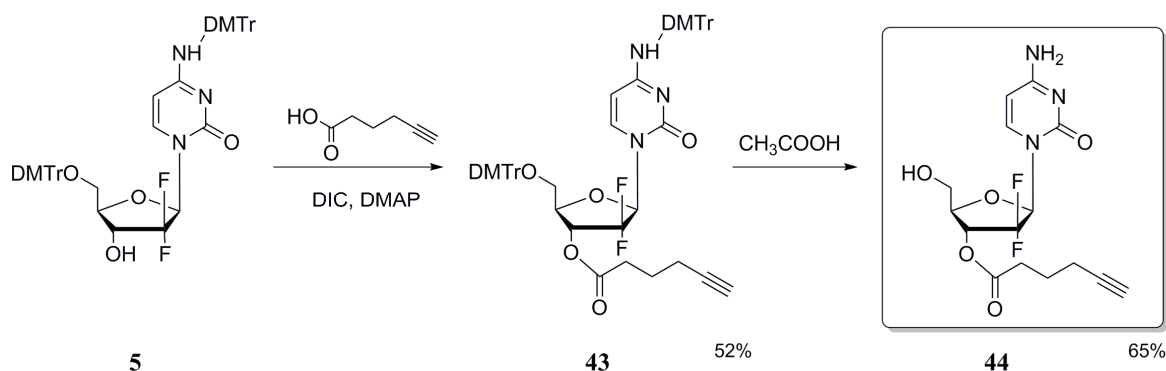
Scheme 1.21.

After required protections to synthesize intermediate **5**, as previousely described, the alkyne moiety was inserted on the free OH group treating it with 5-hexanoic acid (1.1 equiv.) and following the DIC-DMAP protocol. After several washings of the crude with a saturated solution of NH_4Cl, intermediate **43** was obtained in 52% yield. We attempted the final deprotection with a 80% solution of CH_3COOH in water, as for compound **38**. In this case, the reaction was not successful; deprotection required more harsh acid condition to be completed, such as treatment with a 90% solution of TFA at 40°C for 2 hours. Final compound **44** was obtained after purification by flash chromatography, using DCM : MeOH 5 : 1 as eluent in 65% yield (Scheme 1.21)
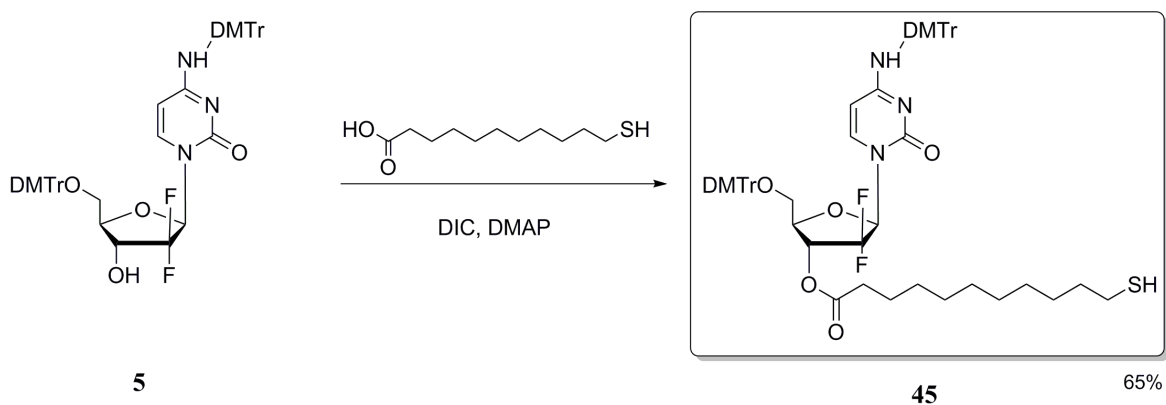
Scheme 1.22.

In this case, as well, we decided to use an α-thiol-ω-carboxylic bifunctional linker. The experimental procedure was the same above described for 5-Fluoro-2'-deoxyuridine, except that DCM : AcoEt 7 : 1 was used as eluent for flash chromotagraphy and this time the final compound (**45**) was obtained in pretty much higher yield (65%). Oxidation process was not that consisting, allowing a good final yield (Scheme 1.22)

B. Bioreductive drugs

Cisplatin

As previousely mentioned, platinum derivatives complexation is a relevant challenge in inorganic synthesis, since the isolation of the desired compound is, most of the time, far from being straightforward. Moreover, Pt(IV) coumpounds are less stable than Pt(II) ones in which they easily tend to convert. Pre-cleavage coupling between prodrug (**12**) and MAP-NT peptide failed due to the instability of this complex to acid conditions (as reported in § 1.2.1).
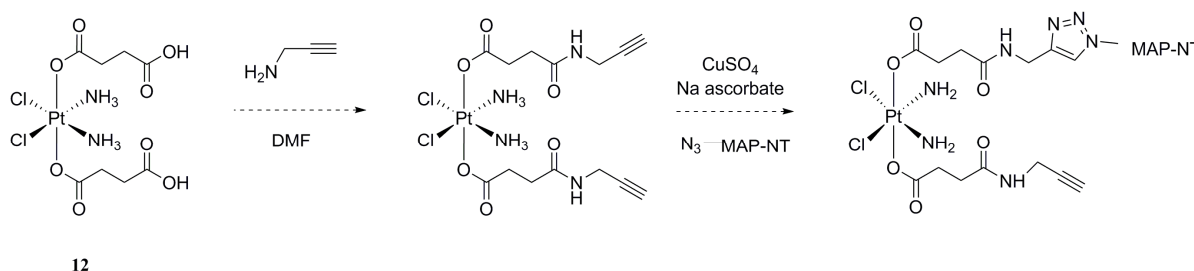
Figure 1.37.

A post-cleavage coupling strategy, involving a Huisgen 1,3-dipolar cycloaddition was envisaged, as suggested in scheme 22. Unfortunatelly, reaction between derivative (**12**) and propargylamine for inserting an alkyne moiety on cisplatin was not successful (Figure 1.37), since we have had problem in isolating the final desired compound. Moreover, the classical Huisgen reaction requires copper catalysis in a reductive environment, not compatible with Pt(IV) derivatives stability. As future perspective, a copper free version of this cycloaddition has to be imagined for this kind of metal-based drugs. In the next chapter (§ 2) a possible solution to link cisplatin on peptides will be extensively discussed.

C. Estrogens

Estradiol

On the way of the previous esterification reactions, we inserted an alkyne terminal linker on hydroxylic group at position C17 of β-estradiol. Exploiting the higher reactivity with anhydride of the

latter, compared to the phenolic one, we easily synthesized derivative **16** (Scheme 1.6), that was used as anchorage for the alkyne moiety. This strategy allowed to obtain the desired compound (**46**) in a two steps reaction.

54%

16   **46**
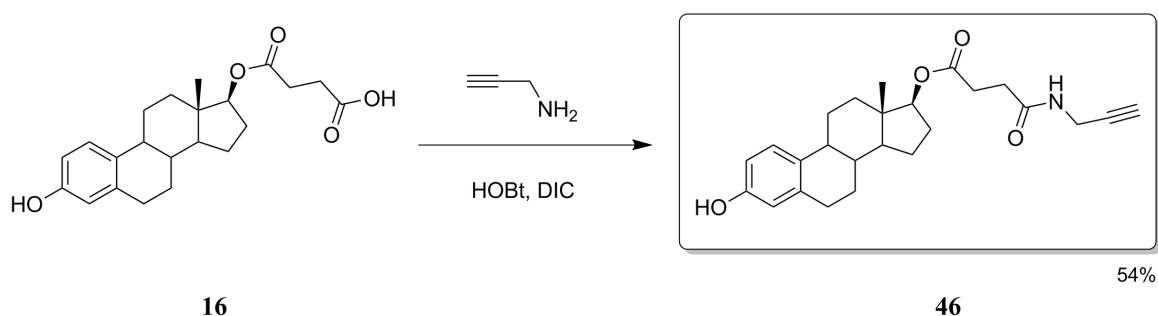
Scheme 1.23.

Synthesis started activating a solution of estradiol-17-β-O-carbonylpropionic acid (**16**) in dry THF with equimolar, stechiometric amount of HOBt and DIC at 0°C for 0.5 h. After the allotted time, propargylamine (1 equiv.) was added, the pH was adjusted to 8 with TEA and the reaction mixture stirred for 22 h. The crude was purified by flash chromatography using DCM : AcOEt 2 : 1 as eluent to obtain derivative **46** as white powder in 54% yield (Scheme 1.23).

Considering our handy at preparing prodrugs through esterification reactions and with 11-mercaptoundecanoic acid in hands we envisaged to insert it at position C17 of estradiol, following the purposed protocol, reported in scheme 1.24.

63
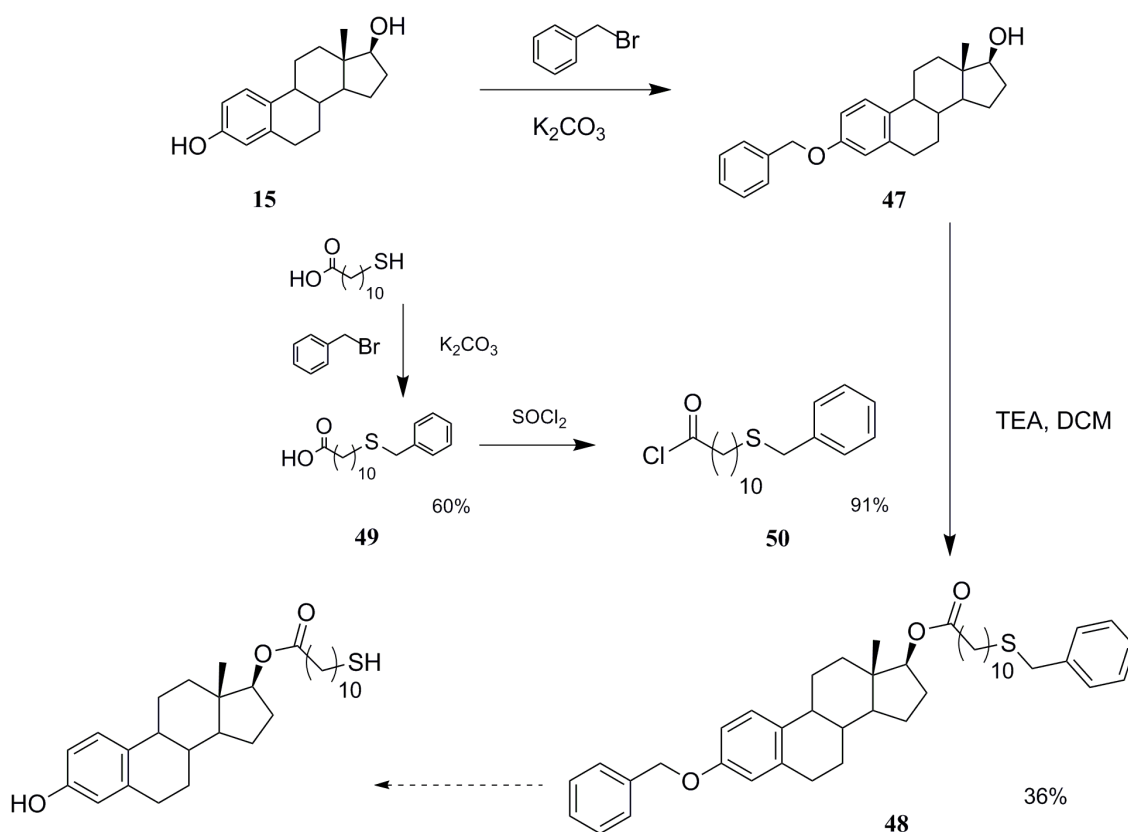
Scheme 1.24.

According to literature,[201] to achieve our synthetical target, we started protecting phenolic OH of estradiol (**15**) as benzyl group, using an excess of benyl bromide (2 equiv.) in dry acetone in the presence of K_2CO_3 (4 equiv.) as base, with a 60% yield of the reaction. The protection turned out to be strictly necessary because hydroxylic group at C17 tipically shows a higher reactivity than phenolic one only in reactions with anhydrides and not with carboxylic acid. At the same time, we protected the thiol moiety of the bifunctional linker with a benzyl group, exploiting the same procedure reported for **16**, obtaining intermediate **49** in 60% yield. This step was mandatory to avoid side reactions in the next step of the procedure, since the thiol group could compete with acid group, during the activation of the latter. The terminal carboxylic acid moiety was, thus, activated to the correspondent chloride with an excess of oxalyl chloride (1.5 equiv) in dry DCM, obtaining chloride intermediate **50** in 91% yield. The latter turned out not be stable, so that ^{13}C NMR spectrum was not recordable. We reacted a freshly prepared solution of **50** in dry DCM with a stechiometric amount of protected estradiol **47** in the presence of TEA (2 equiv.) as base, to have the diprotected compound **48** in 36% yield. Despite of the poor yield of the last coupling described, the procedure was straightforward until this stage. Unfortunately, we have faced problems in the last step of the strategy.

We attemped to simultaneously deprotect the OH at position 17 and the thiol group with a Pd/C catalized hydrogenation at ordinary pressure that only resulted in the removal of the benzyl group on the phenyl ring. We, then, tried to stress the conditions, leading the reaction at 10 Atm in autoclave, not obtaining any improvement. The failure of SH deprotection was attributed to the well-known capability of sulfur containing compounds to poison palladium-based catalysts. As alternative way of deprotection we attempted to convert derivative **48** in the correspondent sulfoxide with a slight excess of m-chloroperoxybenzoic acid (1.3 equiv.), in order to obtain a more easily cleavable compound via Pummerer rearrangement. Unfortunatelly, the desired benzyl deprotection reaction, led at reflux in CH_3COOH, didn't occur.

As a consequence of these problems we run into during the final stage of the purposed protocol, we step back to the tested strategy used for derivative **46** as escamotage to avoid protecting phenolic OH and thiolic linker (Scheme 1.25).

16 → **51** 30%
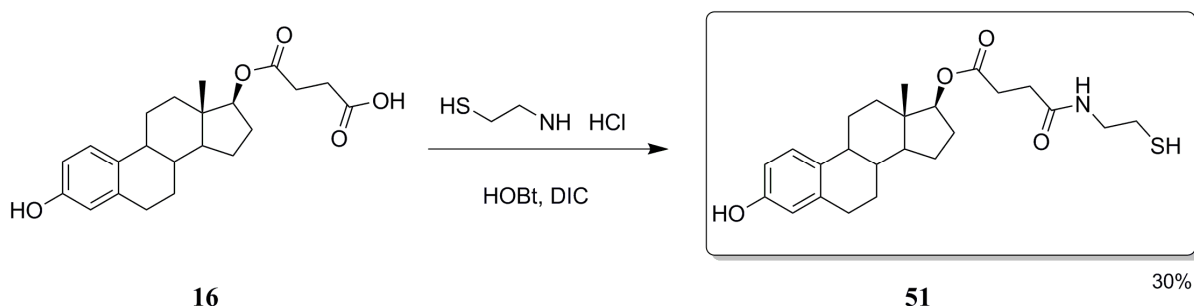
Scheme 1.25.

Synthesis started activating a solution of estradiol-17-β-O-carbonylpropionic acid (**16**, see Sheme 1.23) in dry THF with equimolar, stechiometric amount of HOBt and DIC at 0°C for 0.5 h. After the

allotted time, cysteamine hydrochloride (1 equiv.) was added, the pH was adjusted to 8 with TEA and the reaction mixture stirred for 21 h. The crude was purified by flash chromatography using DCM : AcOEt 1 : 8 as eluent to obtain thiolic derivative **51** as white powder oil in 30% yield (Scheme 1.25).

D. Mitosis Inhibitors

Paclitaxel

Paclitaxel (**24**) is among that pool of drugs that are not stable in harsh acid conditions, rendering impossible the complexation with NT peptide directly on solid phase. Nevertheless, we were absolutely not willing to opt it out from our tests only for an experimental problem we run into, considering that Paclitaxel is nowadays a first line treatment for numerous cancerous deseases. Indeed, designing a suitable 'post-cleavage coupling' strategy for Paclitaxel resulted to be of extreme importance.

As previousely discussed (§ 1.2.1), paclitaxel has a scaffold that is ideal for our prodrug strategy since we could exploit the more reactive OH function at position 2' to insert the desired linker, in a one step reaction and without protecting the other hydroxy groups. The 2'-hydroxy and 7'-hydroxy groups of paclitaxel are suitable sites for conjugation to a targeting ligand, with preferential modification occurring at the 2'-hydroxy group due to steric hindrance at the 7'-hydroxy group. Synthesis started with the add of an equimolar amount of 5-hexynoic acid and DIC (1 equiv.) to a dry DCM solution of Paclitaxel (**24**), in the presence of DMAP as catalytic base (0.1 quiv.). The reaction mixture was stirred at r.t. for 18 h and purified by flash chromatography using EtP : AcoEt 2 : 3 as eluent to obtain the alkyne derivative **52** in 46% yield (Scheme 1.26).
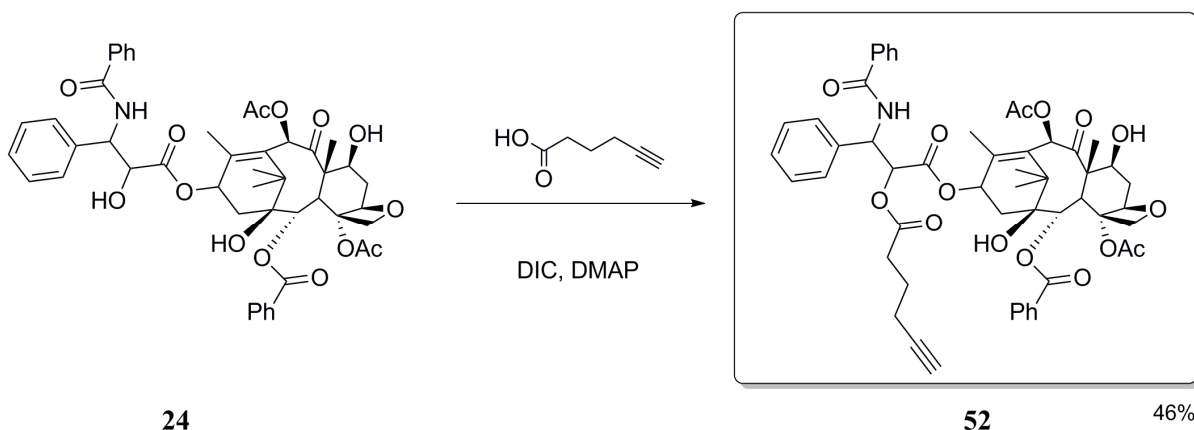
Scheme 1.26.

Among the interesting and up-to-date delivery systems for cancer therapy, use of gold nanoparticles (AuNPs) as inert and efficient carriers for cargo such as drugs is an emerging strategy. AuNPs are gaining in importance also thanks to the relative simplicity with which they can be synthesized and functionalized. A preferential strategy for AuNPs functionalization consists of exploiting the great

affinity presented by thiols and disulfides for gold $^{(0)}$. We originally imagined to functionalise AuNPs with Paclitaxel disulfide derivatives. Indeed, a variation on the so called Brust's method allows the simultaneous reduction of a golden salt (HAuCl$_4$) and the disulfide respectively to AuNPs and thiol analogues, as extensively discussed in § 1.2.3c. The main advantage of this method is that a one pot reaction is able to provide the desired drug functionalised AuNPs overnight. On the other hand the fundamental requisite for drug is stability to NaBH$_4$, the reductive agent used. We, thus, decided to perform preliminary stability tests of Paclitaxel, dissolving it in DCM and treating it with an excess of NaBH$_4$ at r.t. After only two hours, proton NMR spectrum clearly showed its degradation. Nevertheless, we proceeded in the synthesis of a Paclitaxel disulfide derivative to eventually anchorate it on AuNPs with a different method, such as 'ligand-exchange (alkylthiol-for-disulfide) reactions. This method consists of preparing gold nanoparticles, by following the Brust-Schiffrin two phase method using 1-pentanethiol as capping ligand. Ligand place exchange reaction is then carried out, mixing AuNPs with disulphide derivative in 1:3 ratio in weight, in DCM.[202]

Synthesis of disulphide derivative **53** was led as a variation of the procedure reported in literature.[203] A solution of Paclitaxel (**24**) in dry DCM was reacted with DL-α-lipoic acid (1 equiv.) and purified, following the DIC-DMAP protocol above reported for compound **52** to give the desired pro-drug **53** in 25% yield (Scheme 1.27).

DIC, DMAP

24 **53** 25%
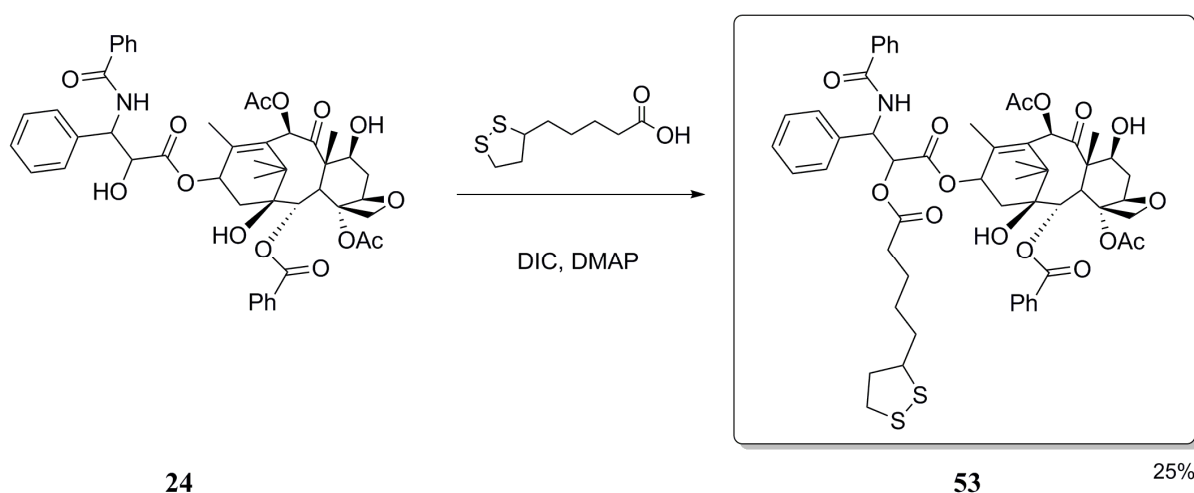
Scheme 1.27.

Although the bond strength between anchoring groups and the gold surface plays a critical role in determining the subsequent functionality, packing density and surface energetics make equally important contributions. While dithiolates are often viewed as preferable to their mono-thiolate counterparts due to multivalent binding avidity, these molecules are actually more prone to oxidative desorption due to inefficient packing. On the other hand, thiolates, most commonly employed for attachment to gold nanoparticles in non-labile biomedical applications, can remain stably adsorbed for up to 35 days under physiologic conditions.This suggests that thiolates may be a preferred functional group for attachment of biological molecules to gold surfaces in many biomedical applications. For this reason, we are planning to realize a thiolate derivative of Paclitaxel.

Preliminary tests of thiol-ene coupling

Considering the feseability of one pot reactions to functionalise Paclitaxel, we investigate the possibility to exploit a thiol-ene coupling between this drug and tetrabranched neurotensin peptide as 'post-cleavage' coupling strategy. Paclitaxe-peptide complexes are largely described in literature,[204] but in most of the cases an amidation coupling is reported, while we envisaged an alternative strategy of anchorage.

A suitable linker should bind to the drug molecule in a labile manner at one end and to the carrier at the other end and thus be employed in order to liberate the drug at the receptor. Interestingly, the maleimide group was found to be a very useful component of such bifunctional spacer since it very cleanly bound to the free thiol groups present in the carrier.[205] At the time we started working on this idea, in our laboratory we were synthesizing maleimido derivatives of Combretastatin A4 for AuNPs and we had in hands a useful bifunctional maleimido linker (**63**) (for details, see § 1.2.3a). We, thus, decided to use it for decorating Paclitaxel.

Moreover,in literature,[206] the use of a tetrameric peptide specifically targeting $\alpha_v\beta_6$ receptor to actively deliver paclitaxel to cancer cells is reported. *Brown et al.* synthesized a water soluble paclitaxel-peptide conjugate in which the position 2 of paclitaxel is attached to the tetrameric peptide via an ester linkage. On the basis of the aforementionated paper, 2-Maleimido-paclitaxel (**54**) was prepared in 46% yield through, coupling paclitaxel with an equimolar amount of 3-maleimidopropionic acid (1 equiv.), following DIC-DMAP protocol above described. The achievement of the final compound required several washing with a saturated solution of NH_4Cl to get rid of DCU and purification by flash chromatoghraphy using EtP : AcoEt 2 : 3 as eluent.

In parallel, at the University of Siena, a modified version of neurotensin tetrabranched peptide was assembled on resin in order to adapt it to our thiol-ene coupling strategy. The modification consisted of inserting on the PEG moiety a cystein residue that introduced a free SH group on peptide, useful to be linked with maleimido moiety on paclitaxel (as below described in details). Its realisation was successful. Anyway, since only a few milligrams of desired peptide could be obtained (as usual with the adopted method), before attempting the final coupling with maleimide-derivative (**54**) we planned a simulation of the said reaction. In our laboratories, we envisaged a in liquid phase coupling between maleimido-paclitaxel and a costless compound that mimics the chemical nature of MAP-NT peptide.
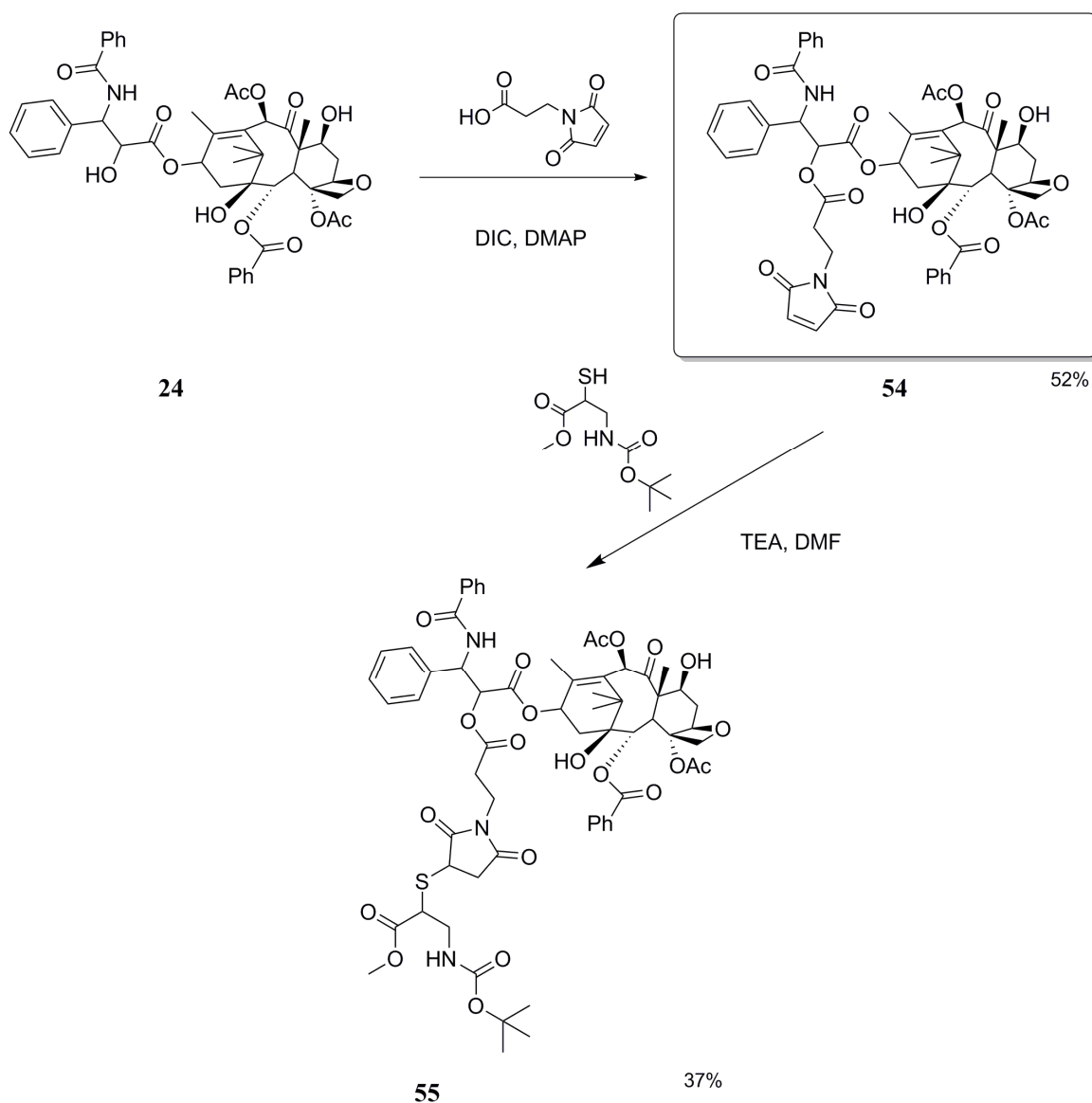
Scheme 1.28.

We chose N-Boc cysteine methylester (1 equiv.), that closely resembles the terminal hindered cysteine residue on the peptide, presenting the same functional thiol group. The reaction was led in dry DMF, in the presence of TEA (1 equiv.) as base, stirred at r.t for 1 h. and purified by flash chromatography (EtP : AcOEt 1 : 3 as eluent) to obtain compound (**55**) in 37% yield (Scheme 1.28).

The ^{1}H NMR spectrum of the final compound (**55**) was pretty complicated due to the presence of 4 diasteroisomers (cysteine derivative was, indeed, used as racemic mixture). Anyway, the disappearing of the signal related to the double bond of maleimido acid at 6.4 ppm and the shift of the presence of a new signals related to the new formed thiolether moiety were clear evidences of the successful coupling (Figure 1.38).
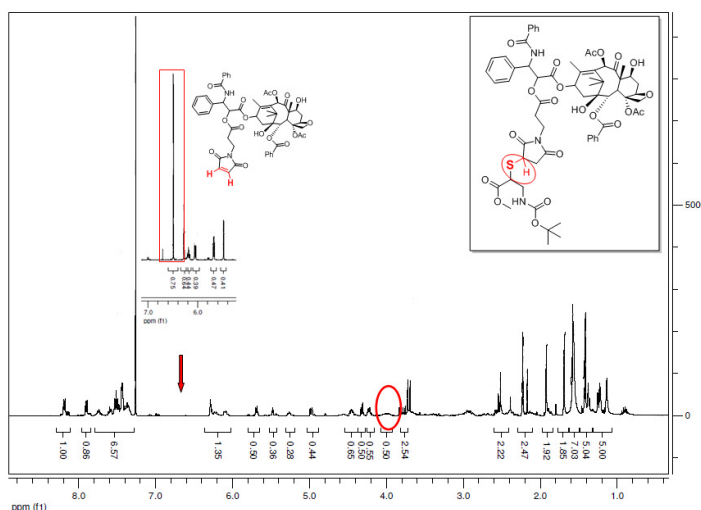
Figure 1.38. ¹H NMR spectrum of compound **55**, showing the signal of the new formed thiolether moiety and the disappearing of the double bond signal. Inset: double bond region of ¹H NMR spectrum of maleimido-paclitaxel (**54**).

Demonstrating the efficiency of thiol-ene coupling strategy for our compounds, the success of this test encouraged us to apply the same protocol of reaction to the modified neurotensin peptide, as below described. Nevertheless, once again we decided to also preliminary investigate the tumor targeting capability of a peptide-cargo complex such assembled. In fact, we would like to convalidate the hypothesis that replacing an amidic bond with a thiolether moiety would not impair, or in the worst case prevent, recognition of MAP from neurotensin receptors on cancer cells. We, thus, envisaged an imaging study to track the *in vivo* distribution of the complexes, after injection. For this aim a fluorophore molecule functionalised with a maleimido moiety, Alexa Fluor 750, was chosen to be linked to the NT thiol-modified peptide. Post-cleavage coupling reaction was then realised in liquid solution exploiting the experimental conditions we imagined to use for Paclitaxel derivative to give NT4-ALEXA 750 complex, as below described.

Conjugation to the tetrabranched peptide (NT4)

Peptide synthesis was performed with an automated multiple peptide synthesizer (MultiSynTechSyro, Witten, Germany) by standard Fmoc chemistry. Protected L-amino acids, coupling reagents (DIPEA and HBTU) and NovaSyn TGR resin were purchased from Merck Chemicals (Darmstadt, Germany). Tetra-branched peptides were built using two consecutive Fmoc-Lys(Fmoc)-OH coupling steps to form the branched core. NT4-ALEXA 750 were synthesized using Fmoc-Cys(Trt)-OH as first and Fmoc-PEG-OH as second amino acid on Novasyn TGR resin. NT4 sequence is pyroELYENKPRRPYIL. Once cleaved from the resin, deprotected and purified the intermediate peptide NT4-PEG-Cys was conjugated to the maleimide group of Alexa Fluor 750 (Invitrogen) via the Cysteine sulfhydryl group. The intermediate was dissolved in DMF (1mg / 10ml) and Alexa Fluor 750 (1.5 equiv.) and finally DIPEA (0.2 equiv) were added. The reaction mixture was kept stirring for 3 h at r.t., then concentrated under reduced pressure and purified (Scheme 1.29).
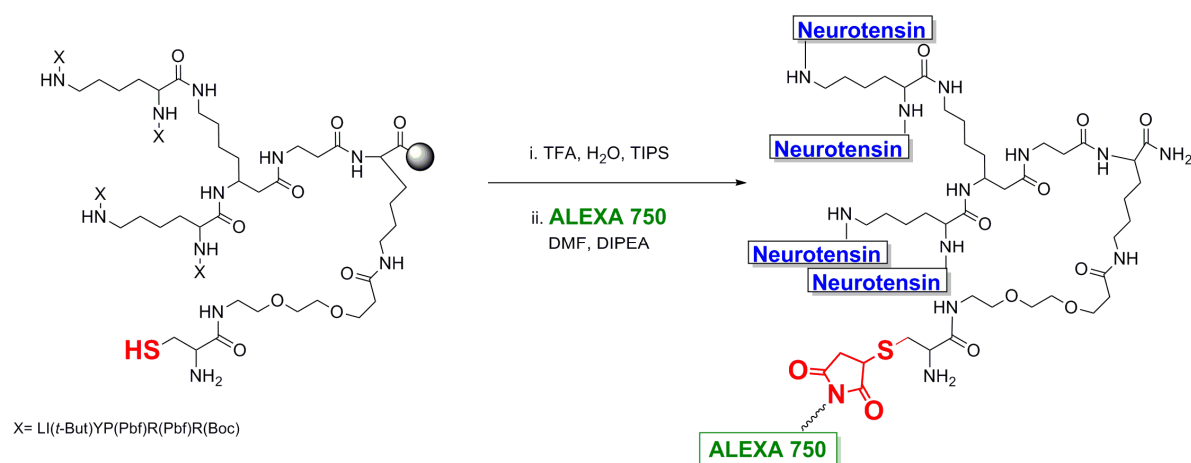
Scheme 1.29.

HPLC purification was performed on a C18 Vydac column. Water (A) containing 0.1% TFA and methanol (B) were used as eluents, gradients of B in 30 min were run at flow rates of 0.8 ml/min and 4 ml/min for analytical and preparatory procedures, respectively. All compounds were also characterized on an Ettan MALDI-TOF mass spectrometer (Amersham Biosciences, Buckinghamshire, UK). Obtained NT4-ALEXA 750 was used for *in vivo* imaging test as below reported.

Preliminary *in vivo* cancer imaging test of NT4-ALEXA 750

Three naked mice (CD-1 nude mice-Harlan Lab.) were xenografted with 10^6 HT29 tumor cells, in order to obtain a subcutaneous tumoral mass of colon carcinoma. After 4 days tumor has a diameter of 6 mm and two mice bearing HT-29 xenograft were injected with a 10 nmol solution of NT4-ALEXA 750 in the tail vein, while another tumor bearing mouse was injected with saline (control mouse). After 72 hours mice were anesthetized with isofluorane and images were taken with Odyssey Infrared Imaging System (Licor, Lincoln, Nebraska 68504 USA). Mice were then sacrificed with CO_2.
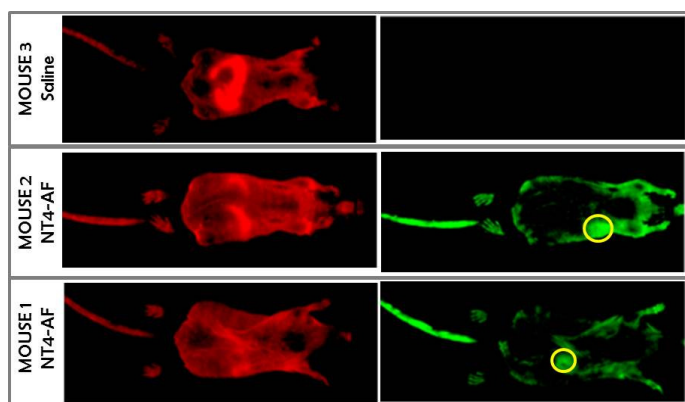
Figure 1.39. *In vivo* imaging of HT29 tumor bearing mice, i.v. injected with NT4-ALEXA 750 or with saline solution. Tissues autofluorescence on left panels and fluorophore emission on right panels. Tumors are indicated by the yellow rings.

Imaging results showed that at wavelength of 700 nm excitation the autofluorescence of the mice tissues was evident, while at 800 nm the fluorophore highlighted the tumor. Indeed, except from tail that was the site of injection, the fluorescence was particularly intense in the area in which the tumor mass was placed, indicating that efficient tumor targeting capability of NT4-ALEXA 750 (Figure 1.39).

Encouraged by the promising results obtained either for the efficiency of the click coupling of maleimido-paclitaxel and tetrameric NT peptide and the efficiency of tumor targeting of their complex, we finally assembled NT4-Paclitaxel. Experimental conditions and purification were the same described above for the synthesis of NT4-ALEXA 750 (Scheme 1.30).
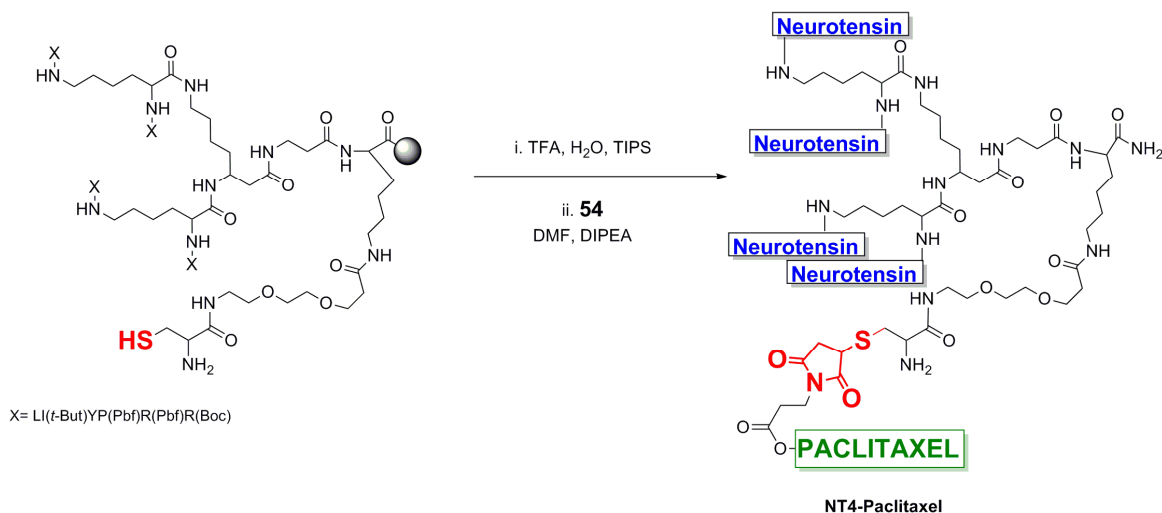
Scheme 1.30.

NT4-Paclitaxel has been successfully synthesized and *in vitro test* on HT-29 cancer cells are in progress at the moment, but preliminary data showed a promising cytotoxicity of this complex, compared to the unconjugated drug. If final results will confirm these data, we could assert that an efficient and alternative drug delivery system for paclitaxel has been achieved.

1.2.3 Development of a strategy to achieve a MAP NT-nanoparticle-drug conjugate

A three-step strategy towards the realisation of a three-unit nanosystem

As previously said (see § Introduction), during my PhD project I have worked on the development of several kinds of tumor-targeted drug delivery nanosystems whose core (represented by a metallic nanoparticle) is functionalised both with a targeting unit (consisting in a MAP-NT dendrimer) and a chemotherapeutic unit. Among all drugs taken in exams and previously described, Combretastatin A4

was the one we chose as cargo for NPs, on the basis of the promising cytotoxicological results in cancer cells upon conjugation with MAP-NT (see § 1.3).

A consistent part of my PhD project consisted in drawing up the first step of the strategy which will eventually lead us to the achievement of the three-unit nanosystem; this first step implied the functionalisation of the three types of nanoparticles (NPs) with combretastatin A-4 (CA4). The thus obtained NP-CA4 adducts have then been characterised and tested before moving on towards the next step, which was represented by the addition of the targeting unit.

The first problem we had to face was the development of a suitable synthetic strategy which could both ensure the effective drug-loading of the nanoparticles and allow a future functionalisation of the two-unit nanosystem with MAP-NT.

A two-phases functionalisation of the nanoparticles, using orthogonal linkers, could have been theoretically feasible. Pursuing such a strategy, as a first step we would have introduced a combretastatin A-4 selective linker, then a MAP-NT selective one. After coating the NPs with such orthogonal linkers, the following step would have been the subsequent introduction of the drug -which would have bound only with the first linker- and, eventually, the addition of the MAP-NT targeting unit, which would have selectively reacted with the second linker, as schematised in figure 1.40.
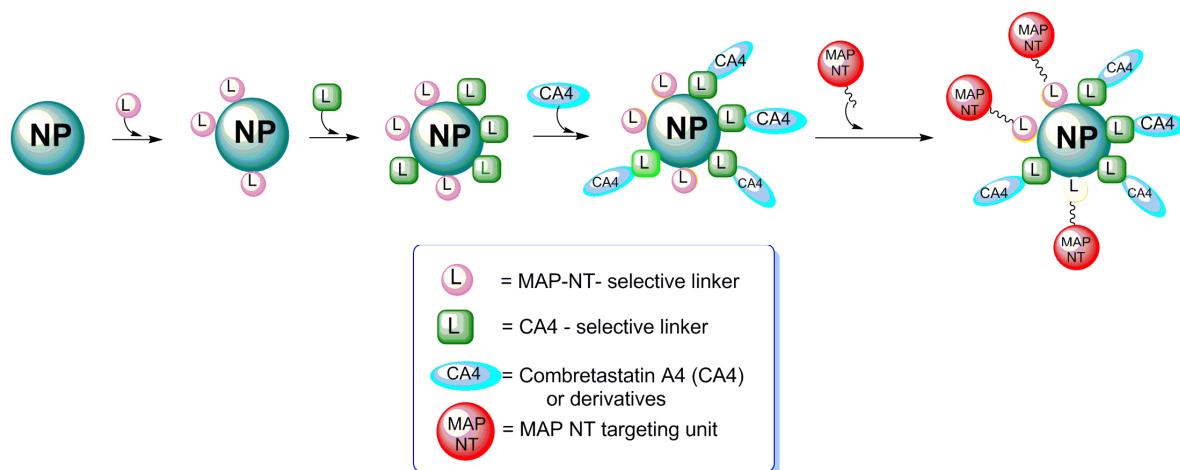
Figure 1.40. A four-step strategy to attain the NP-peptide-drug conjugate using orthogonal linkers.

This strategy exhibited some major problems, such as the constitutional difficulties which lied in the mere functionalisation of the nanoparticles; moreover, the complexity of the MAP NT structure, which, as a polypeptide, presented many different, reactive functions, complicates the development of a linker which could selectively bind to combretastatin A-4 (or a derivative) without reacting with the targeting unit.

Since this four-step strategy presented evident limits, we subsequently decided to adopt a simpler- although less selective- approach. We decided to coat the nanoparticles' surface with a linker which could bind both to combretastatin A-4 and to MAP-NT; to ensure the effective functionalisation of the nanoparticles through the two steps, we coupled the linker-coated nanoparticles with less than 1 equivalent of drug, so that a consistent share of free linker could remain available for the binding with MAP-NT, as schematized in figure 1.41.
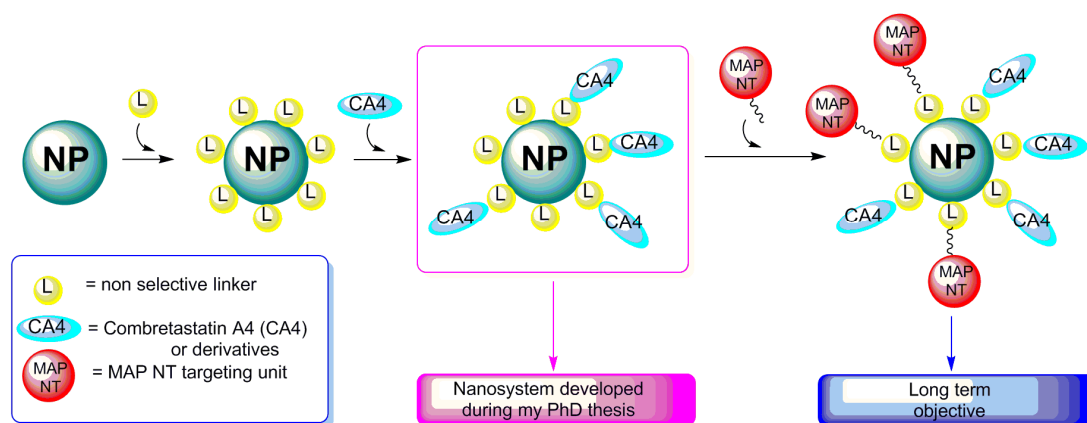
Figure 1.41. The three-step strategy we chose to pursue. Actual PhD thesis work ended at step 2, with the achievement of a CA4-loaded nanosystem.

Choice of suitable linkers and drug derivatisation for nanoparticles drug-loading

In order to pursue the above mentioned strategy, the first problem was to ensure that both combretastatin A-4 and MAP NT have the same reactivity. In order to make them bind with the same linker. For this reason, both the drug and the targeting unit have been derivatised so that they present the same affinity for the linkers which the nanoparticles' surface is coated with.

As for the choice of said linkers, every kind of nanoparticle has been treated in a different way:

- **Superparamagnetic Iron Oxide Nanoparticles (SPIONs)** have been functionalized with a linker which carries a terminal N-maleimido function (Figure 1.42):
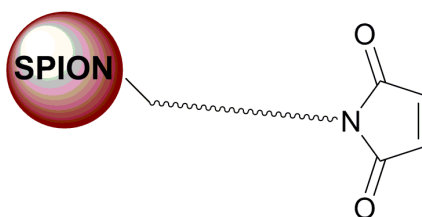
Figure 1.42. Maleimidic linker-loaded SPIONs

The maleimidic linker has been chosen because of its capacity to give 1,4-Michael addition with strong nucleophiles like thiols in the so called thiol-ene reaction (Scheme 1.31)
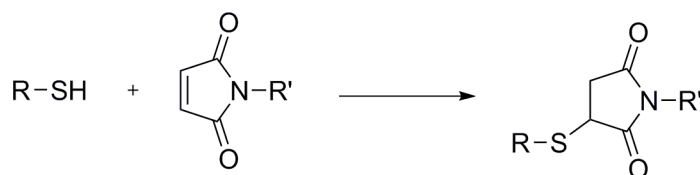
Scheme 1.31.

The Michael addition between a maleimide and a thiol can be considered a *click* reaction; as a matter of fact, the term *click chemistry*, designs a series of very efficacious reactions characterized by a remarkable performing simplicity, stereoselectivity and high yields, all features which are presented by this reaction. Indeed, this reaction constitutes the base of a routine method for thiol detection in clinical and environmental analysis.[207] Traditionally, a wide variety of catalysts have been used to initiate the thiol-Michael addition reaction, including strong bases, metals, organometallics, and Lewis acids. In the case of thiol-maleimide reactions, usually a tertiary amine (TEA) is used as catalyst.

Thus, coating the SPIONs with a maleimidic linker (for details see § 1.2.3a), a thiol function had to be introduced on both combretastatin A-4 and MAP-NT. The insertion of a sulfydryl group on MAP-NT has been performed by Dr. *Falciani*'s group at the University of Siena, by coupling the polypeptide with a cysteine residual, as already discussed above. The synthesis of a thiol-derivative of combretastatin A-4 has therefore turned out to be a necessary step towards the attainment of the desired drug-NP conjugate (Scheme 1.32).
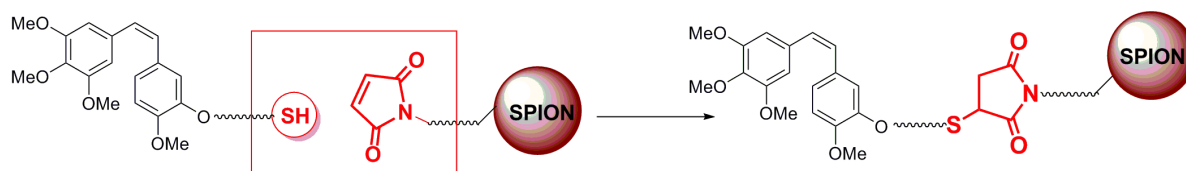
Scheme 1.32. Click Michael addition between a thiolic derivative of CA4 and a maleimidic linker-loaded SPION.

- **Cobalt *TurboBeads Click* © (CoNPs)** do not need previous functionalization to undergo drug loading, as they are commercialized as ready-to-use coated nanoparticles. The metal core is covered with an azido or amino-group functionalised graphene coating (Figure 1.43).

Figure 1.43. A schematic image of TurboBeads Click © as presented on their selling company's website. [208] " M" stands for cobalt. a. azido functionalisation, b. amino functionalisation.

The azido group is a very useful function, as it can undergo Copper(I)-catalyzed Azide-Alkyne Cycloaddition (CuAAC), a particular click reaction which occurs between an azide and an alkyne (Scheme 16) and which constitutes a variation on the traditional Huisgen cycloaddition. This reaction has been increasingly raising universal scientific interest for its specificity and efficacy and appeared to be very promising in the light of our project.[209] Therefore, the synthesis of an alkyne derivative of CA4 has been realized in our laboratory, in order to proceed with the coupling with CoNPs (Scheme 1.33); for what concerns MAP-NT, an alkyne-terminal PEGylated derivative is being developed at University of Siena.
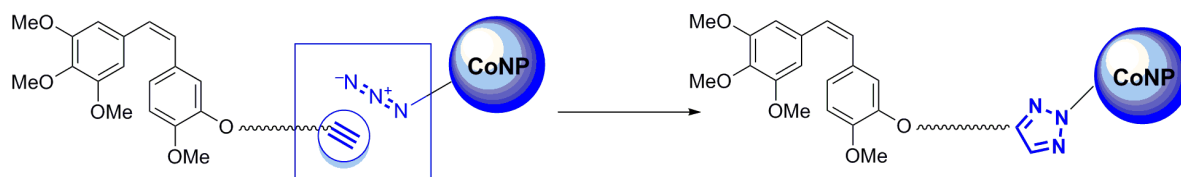
Scheme 1.33. CuAAC between an alkyne derivative of CA4 and CoNPs.

Another interesting coupling in biological field is the one that exploits an amidation reaction, since it mimics the formation of a peptidic bond. The reaction does not spontaneiusely occur in laboratory, as it on the contrary does *in vivo*, thus carboxylic acid moiety involved need to be activated. Indeed, we envisaged the synthesis of a N-hydroxysuccinimide ester of CA4 as activated form, suitable to easily react with amines on the surface of Turbobeads (Scheme 1.34), as suggested on their selling company's website.[208]
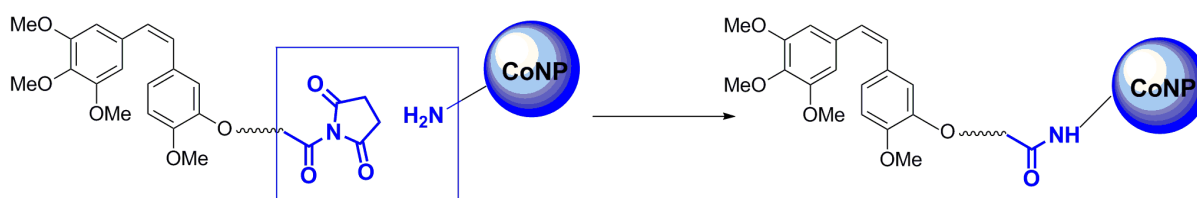
Scheme 1.34. Amidic coupling between activated CA4 derivative and amine-gropu coated Turbobeads.

- **Gold nanoparticles (AuNPs)** do not need previous functionalization either. As a matter of fact, gold possesses a strong affinity for sulfydryls, which can be exploited for the functionalisation of this kind of nanoparticles. This can be realized by means of a one-pot process (see § 1.2.3c for a detailed explanation) which involves the simultaneous *in situ* formation and functionalisation of AuNPs. For the realization of AuNPs-conjugates, thus, thiol derivatives of combretastatin have been used and further development of new CA4-based prodrugs was not necessary (Scheme 1.35).
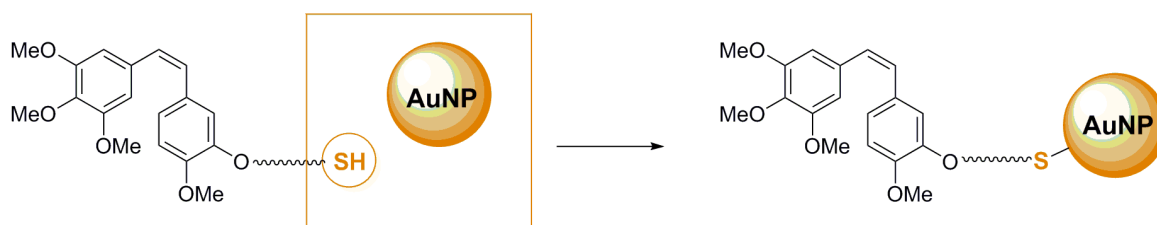
Scheme 1.35. AuNPs functionalisation with a CA-4-thiol derivative. AuNPs are generated in situ from the reduction of $HAuCl_4$.

As a result, in order to attain the NP-drug conjugates which could eventually open the door to the development of the three-unit nanosystem, suitable derivatives of combretastatin A-4 had to be synthesized.

Below the results of the related synthetical efforts will be presented, together with a short outline of the chemical modifications operated on combretastatin A-4, in order to realize suitable derivative for NPs decoration.

Combretastatin A-4 derivatives for NPs decoration

As above stated, the simple chemical structure of combretastatin A-4 makes it an ideal candidate for derivatisation, as it just possesses one reactive function (the phenolic OH); this remarkably simplifies prodrug design strategies. The first combretastatin A-4 prodrug we decided to synthesize was the thiol derivative (**56**) for the functionalisation of maleimidic linker-loaded SPIONs. We chose to perform the esterification of combretastatin A-4 phenolic OH with an aliphatic α-mercapto acid, namely 11-mercaptoundecanoic acid (Scheme 1.36), with DIC as a coupling agent.
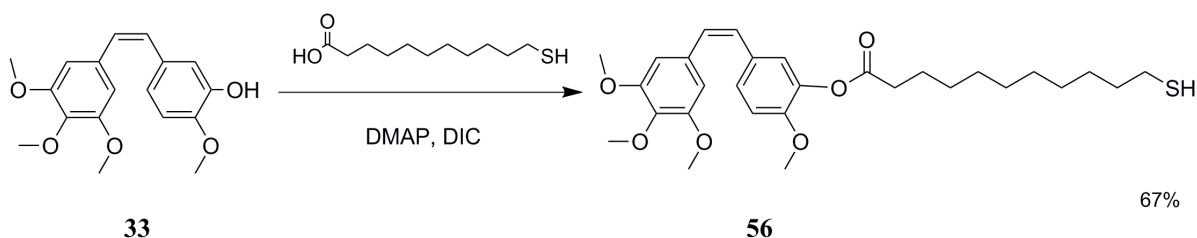
Scheme 1.36.

In detail, to a solution of combretastatin A-4 (**33**) (1.0 equiv.) in dry DCM, DMAP (0.1 equiv.) and 11-mercaptoundecanoic acid (1.0 equiv.) were added under a N_2 atmosphere. After 5', DIC (1.1 equiv.) was added dropwise at 0°C and the mixture was then allowed to stir for 19 h. at r.t. Additional DIC (2.2 equiv.) and DMAP (0.1 equiv.) were then added and the solution was stirred again for 1h. The reaction mixture was diluted with Et_2O and the organic phase was washed with a saturated aqueous solution of NH_4Cl, then with a saturated aqueous solution of $NaHCO_3$. The combined organic layer was dried, filtered and evaporated and the crude product was purified by flash chromatography to obtain combretastatins' ester (**56**) in 67% yield.

Secondly, we needed an alkyne derivative to functionalise azide-coated *TurboBeads* CoNPs. We decided to synthetise an ester of combretastatin with 5-hexynoic acid, adapting the aforementioned esterification procedure (Scheme 1.37).
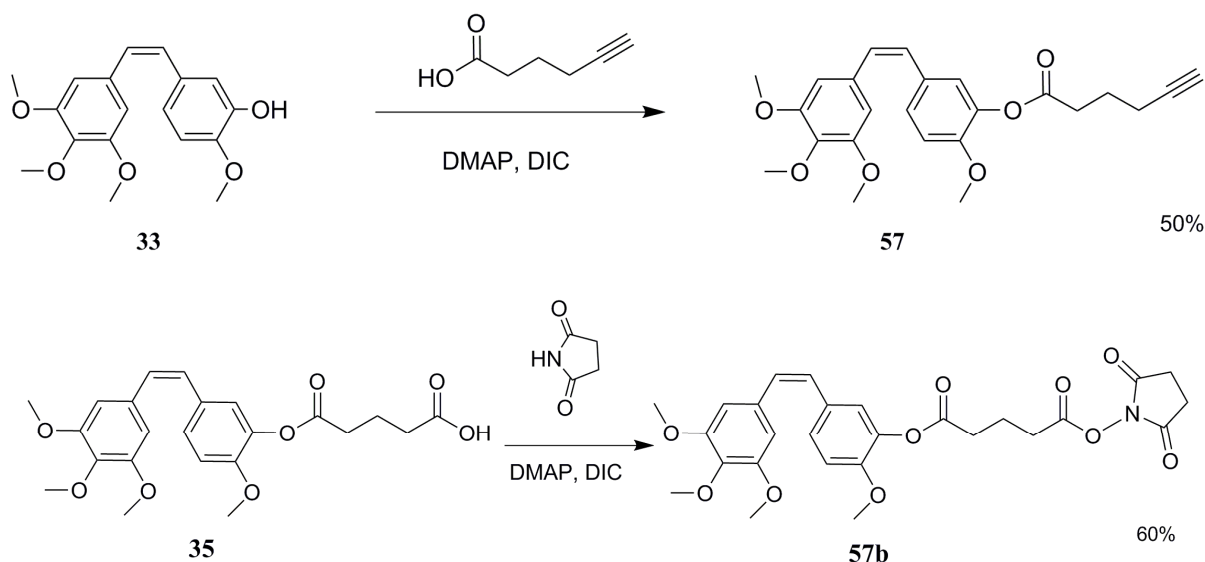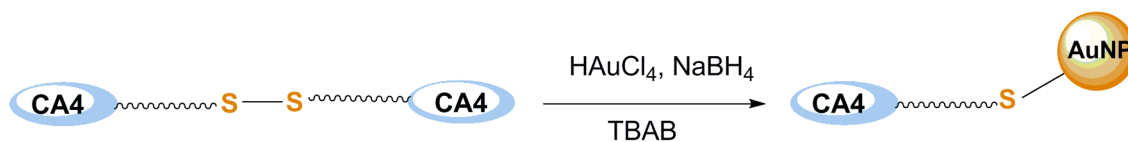
Scheme 1.37.

To a solution of combretastatin A-4 (**33**) (1.0 equiv.) in dry DCM, DMAP (0.1 equiv.) and 5-hexynoic acid (1.1 equiv.) were added under a N_2 atmosphere, DIC (1.1 equiv.) was then added dropwise at 0°C and the mixture was allowed to stir for 24 h at r.t. DIC (0.5 equiv.) and DMAP (0.1 equiv.) were then added and the solution was allowed to stir again for 1h. The crude product was purified by flash chromatography to afford ester (**57**) in 50 % yield (Scheme 1.37).

Finally, having in hands amine-coated *TurboBeads* CoNPs, we decide to alternatively attempt the coupling of the combretastatin derivative through an amidation. Indeed, we operated an activation of the terminal carboxylic group of compound **35**, with a slight excess of DIC and N-hydroxysuccinimide (1.1 equiv.) in the presence of a catalytic amount of DMAP (0.1 equiv.). We thus obtained compound **57b**

For what concerns gold nanoparticles (AuNPs), a brief preamble has to be made.

The thiol derivative of combretastatin necessary to carry out the functionalisation of AuNPs (**56**) was very susceptible to oxidation and tended to form disulfide analogues very rapidly. In order to avoid handling such short-lifed derivatives, we chose to directly use the more stable disulfide derivative. As a matter of fact, the desired thiol can be formed *in situ* during the one-pot reductive process of AuNPs formation and drug-loading (see §1.2.3c, for more details) from a disulfide. Obviously, this could not occur while functionalizing SPIONs, as the disulfide could not be reduced anymore: therefore, in that case we were forced to use the thiol, trying to prevent its oxidation. AuNPs were generated by the reduction of $HAuCl_4$ by means of $NaBH_4$, which was also responsible for the simultaneous reduction of the disulfide to the thiol (Scheme 1.38). As the thiol is generated, it instantly binded to the AuNP, due to sulfur's strong affinity for gold; therefore, it was not isolated.

Scheme 1.38. *In situ* generation of CA4-thiol derivative during AuNPs formation and functionalisation.

The simplest way to obtain a CA4-disulfide was to esterify 2 equivalents of combretastatin A-4 (**33**) with 1 equivalent of a dithioaliphatic diacid.

A first trial was carried out esterifying CA4's phenolic OH with 4,4' dithiobutyric acid, following the previously described acylation procedure; this allowed to obtain diester (**58**) in 45% yield (Scheme 1.39) in a three days' time.
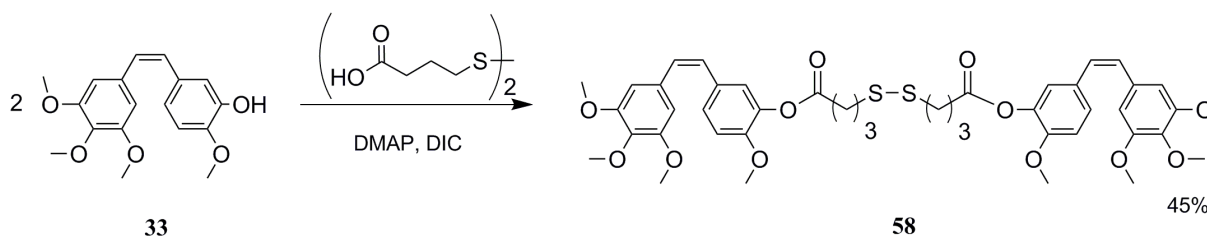
Scheme 1.39.

After this successful attempt, we decided to esterify combretastatin A-4 with a longer chain dithioacid, 11-11' dithioundecanoic acid (**60**). This would allow to have a more spacing linker, hence a minimized risk of loss of pharmacological activity due to steric hindrance issues. Before obtaining the disulfide derivative, however, we had to synthetize the dithioacid (**60**) from 11-mercaptoundecanoic acid by oxidation (Scheme 1.40).
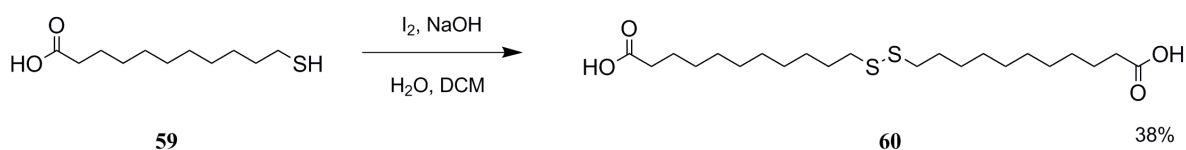
Scheme 1.40.

11-Mercaptoundecanoic acid (**59**) (1.7 equiv.) was suspended in a 1:1 mixture of NaOH 0.1 M: DCM and a solution of I_2 (1.0 equiv.) in DCM was added dropwise. After 30 minutes' stirring the reaction mixture was diluted with AcOEt and the pH of the solution adjusted to 5 with a saturated aqueous solution of NH_4Cl. After separating the two phases, the organic layer was washed with an aqueous solution of 10% $Na_2S_2O_3$, dried, filtered and evaporated to afford dithioacid (**60**) in 38% yield.

Esterification of combretastatin A-4 (**33**) (2.0 equiv.) with dithioacid (**60**) (1.0 equiv.) was performed by means of the already mentioned acylation procedure, using DIC (2.0 equiv.) as a coupling agent and catalytic DMAP (0.2 equiv.). Diester (**61**) was obtained after 3 days at r.t. in 40% yield (Scheme 1.41).
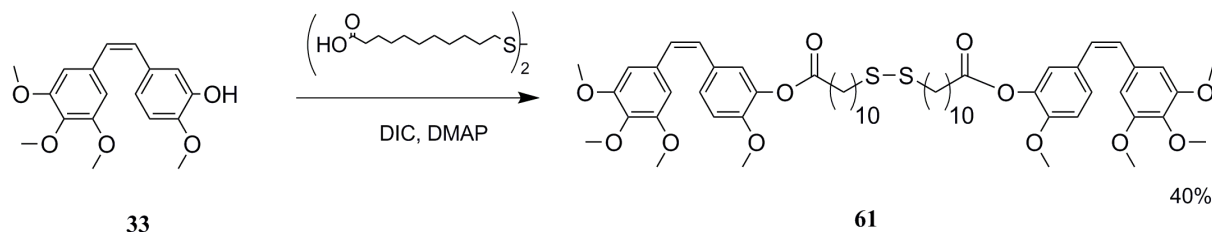
Scheme 1.41.

Following the above procedures, we have obtained four combretastatin A-4 derivatives **56**, **57**, **58** and **61**, suitable for nanoparticles' functionalisation (Figure 1.44). In the next paragraph the three NP-prodrug conjugates will be described individually, with regard either to their chemical and pharmacological properties.
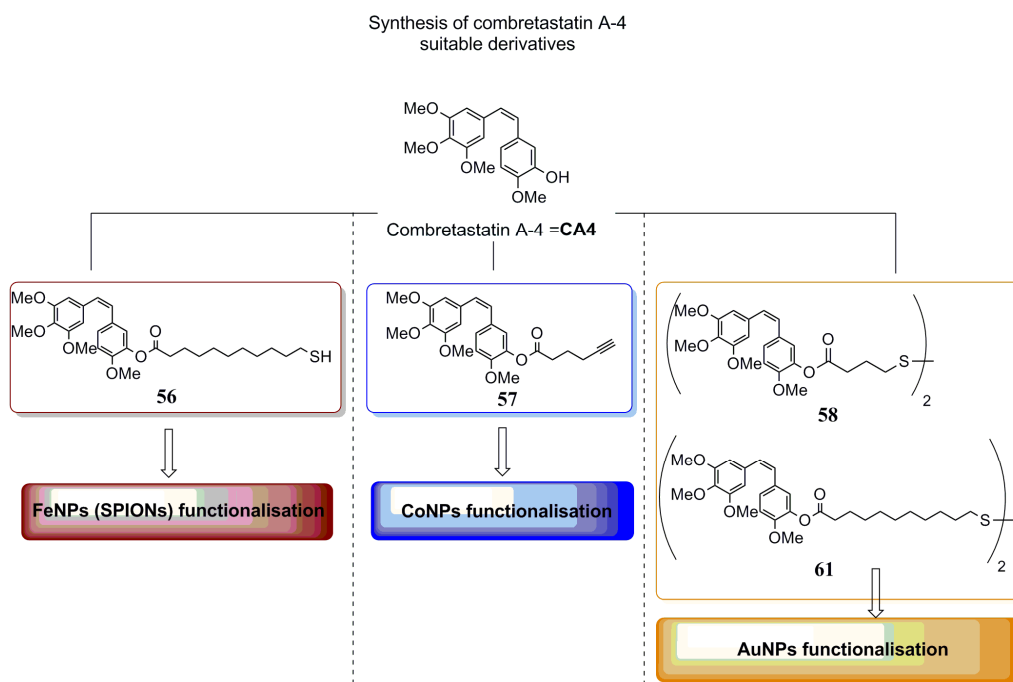
Figure 1.44. A summary of the synthetised CA4 derivatives.

1.2.3a Development of SPIONs-CA4 conjugates

3.1 SPIONs: structure, chemical properties and pharmacological applications

Many iron oxides fall under the category of Superparamagnetic Iron Oxide Nanoparticles (SPIONs), namely magnetite (Fe_3O_4), maghemite (γ-Fe_2O_3) and hematite (α-Fe_2O_3);[210] the SPIONs on which we worked are constituted by a mixture of the two ferric oxides (Fe_2O_3).

SPIONs usually present an external layer of ferric hydroxide (Figure 1.45), which can be exploited for covalent surface functionalization,[211] as the iron-bonded hydroxyl is characterised by peculiar reactivity features.
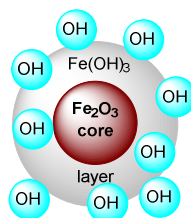
Figure 1.45. Composition of a ferric oxide nanoparticle

As previously said (see § Introduction), SPIONs are the only clinically approved nanoparticles: as a matter of fact, two SPIONs agents are clinically approved as magnetic resonance imaging (MRI) contrast agents, namely: ferumoxides (Feridex in the USA, Endorem in Europe) with a particle size of 120 to 180 nm, and ferucarbotran (Resovist) with a particle size of about 60 nm.[212]

SPIONs' success as MRI contrast agents is due to their superparamagnetic properties: in fact, in magnetic resonance imaging, under an applied magnetic field, induced magnetic spins in magnetic nanoparticles perturb the nuclear spin relaxation processes of protons of water molecules surrounding magnetic nanoparticles. This effect leads to the shortening of spin-spin relaxation time of the proton due to inhomogeneities in local magnetic field and fluctuating magnetic fields at molecular level, which results in darkening of MR images (Figure 1.46), hence the "negative contrast" properties of SPIONs. Traditional contrast agents are usually paramagnetic gadolinium (Gd^{3+}) chelates; since iron oxide nanoparticles have markedly higher value of the magnetic moment and thus, present much higher relaxivities than Gd^{3+}-chelates, they are increasingly replacing these more traditional contrast agents.[213]
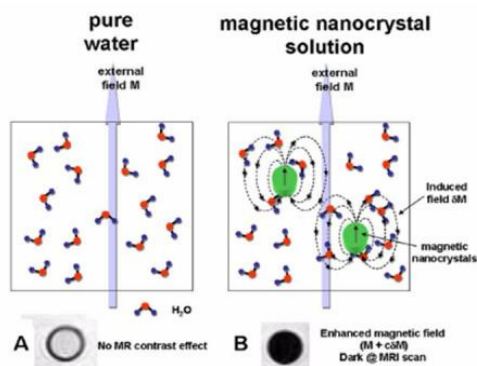

Figure 1.46. SPIONs' mechanism of action as MRI contrast agents

SPIONs' suitability for clinical application makes them very attractive also for the development of therapeutic systems: as aforementioned, SPIONs possess theranostic properties, that is to say they have both diagnostic and therapeutic qualities. For what concerns therapeutic applications, in fact, thanks to their superparamagnetic properties, SPIONs could be a promising magnetic vector for magnetic field assisted radionuclide therapy and for localised hyperthermic application (see § Introduction). Recently, a folate-SPION conjugate designed for targeted hyperthermia has achieved promising theranostic results, as it constituted an excellent device for tumor cell marking, targeting (thanks to the folate moiety) and killing.[214]

Besides having many favourable properties which are typical to almost every kind of nanoparticle, such as EPR effect-mediated passive tumor targeting and enhanced drug loading allowed by the high surface area / volume ratio, SPIONs have recently showed some peculiarities which render them particularly apt for tumor therapy. For instance, it has been observed by *Kievit et al.*[215] that SPIONs are able to circumvent multidrug resistance, since they seem not to be subject to tumor cell pump-mediated drug efflux. As a matter of fact, polymer-coated SPIONs loaded with doxorubicine, an antineoplastic anthracyclin, showed greater retention time inside tumor cells compared with the free drug.[216] As a result, a SPIONs based therapy could be helpful in the treatment of chemotherapy-resistant cancers.

Moreover, SPIONs are characterised by a better biocompatibility compared with other paramagnetic nanoparticles, such as nickel oxide nanoparticles. As previously said (see Introduction), SPIONs have a mild cytotoxic activity, due to the formation of reactive oxygen species (ROS) deriving from the reduction of Fe(III).[217] In fact, SPIONs' Fe(III) can be bio-reduced to Fe(II) (e.g. by ascorbic acid), which can undergo Fenton reaction and generate ROS. At any rate, this toxicological profile is in no way comparable to the one presented by the aforementioned nickel oxide nanoparticles, as it is demonstrated by the fact that SPIONs are the only magnetic NPs approved by FDA for clinical use. In addition, this kind of toxicity may presumably lead to severe consequences only if the contact with SPIONs is chronical and prolonged, which is not the case of nanoparticle-based acute cancer therapy. However, this toxicity may vary considerably depending on the route of administration and on the coating of the nanoparticle, not to mention the fact that this toxicological profile may be tuned by means of magnetic field assisted targeted therapy which could exploit the cytotoxicity of SPIONs for tumor cell killing. Furthermore, iron nanoparticles are preferable to other metallic nanoparticles inasmuch as metal from degraded NP cores may enter physiological iron methabolic pathways; phenomenon which does not occur, for instance, in the case of other metals.[218]

As a result, SPIONs appear to be particularly interesting in the light of the development of an innovative targeted drug delivery system. In the next paragraph the strategies we adopted to develop SPIONs-based nanosystems and the related synthetic results will be presented.

Synthetical strategies for the development of SPIONs-combretastatin A-4 conjugates

As previously stated, we chose to coat SPIONs with a maleimidic linker which could allow the further functionalization of the nanoparticles with a thiol derivative of combretastatin A-4 (see Scheme 1.32). In order to do that, the synthesis of a linker able to bind with SPIONs was required. We decided to

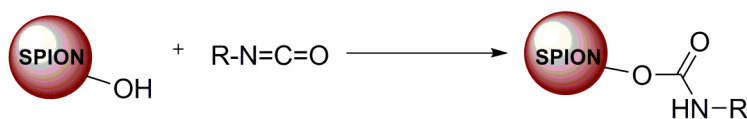exploit the reaction between isocyanates and SPIONs which has been recently described (Figure 1.47).[219]

Figure 1.47. Schematisation of the reaction between SPIONs and a generic isocyanate

This reaction appears to be particularly favourable for a series of reasons. First of all, the isocyanate selectively reacts with the iron-bonded hydroxyls in mild conditions, actually milder in comparison with the ones used in reactions between alcohols and isocyanates.

Secondly, the thus obtained carbamate may have some interesting pharmacokinetic properties. In fact, in medicinal chemistry, a carbamate function is usually considered as a good isosteric substitute for esters, as they can resist *in vivo* hydrolysis better than these latters. One of the biggest drawbacks in SPIONs-based therapy is the burst effect,[213] that is to say the sudden detachment of the drug moiety from the nanosystem core due to *in vivo* hydrolysis, making any targeting efforts useless, as the drug would suddenly undergo a systemic distribution. A carbamate linker could instead render the drug moiety hydrolysis slower. Therefore, an intracellular hydrolysis might be more probable than an extracellular one, considering the fact that, thanks to the several aforementioned targeting mechanisms (magnetic field application, EPR effect…) the time spent by the therapeutic device in the systemic circulation is minimal in comparison with the time spent inside the tumor cell.

Thirdly, this reaction is easily monitorable by means of IR spectroscopy. The possibility to follow a reaction's evolution via IR spectroscopy is crucial when working with superparamagnetic nanoparticles, as this spectroscopic technique is one of the few methods which can be used to characterize them. In fact, besides the several complexities related to heterogeneous phase synthesis (as a matter of fact, SPIONs are not soluble in any solvent), the superparamagnetism of SPIONs impedes any kind of *in solution* NMR analysis. On the other hand, the disappearance of the N=C=O stretching bands, which belong to the very diagnostic zone 2 in IR spectrum (at about 2270 cm^{-1}) and the appearance of the very strong band of carbamate's C=O stretching (at about 1700 cm^{-1}) is an unmistakable proof of carbamate's formation.

Our purpose was therefore to develop a synthetic strategy which could allow the functionalisation of SPIONs with a maleimidic linker, bound to SPIONs' hydroxyl through a carbamate bond (Figure 1.48).
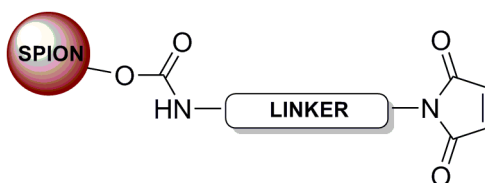

Figure 1.48. SPIONs functionalised with a maleimidic linker by means of a carbamate bond

We attempted at functionalising SPIONs pursuing several strategies, whose description will be briefly provided.

First attempt at functionalising SPIONs

Our first attempt at functionalising SPIONs implied a reaction between SPIONs and 4-chlorosulfonylphenylisocyanate, in order to obtain carbamate (**62**) (Scheme 1.42).
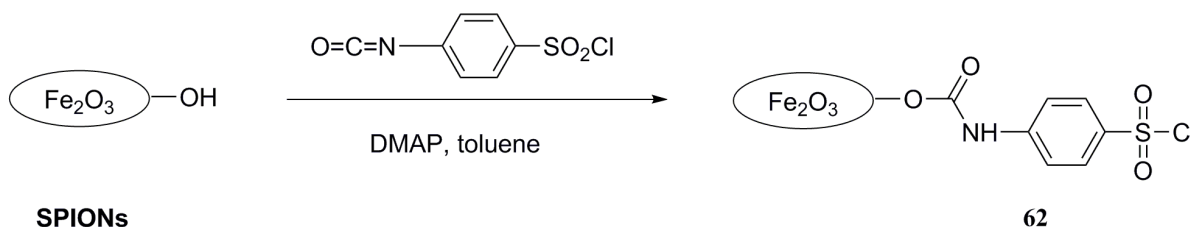
Scheme 1.42.

To obtain adduct **62**, SPIONs (1.0 equiv. in weight, as SPIONs' hydroxyl loading is unknown) were washed 3 times in dry toluene and suspended in this solvent by sonicating. To the suspension, 4-chlorosulfonylphenilisocyanate (1.0 equiv. in weight) and DMAP (0.1 equiv. in weight) are added, and the thus obtained suspension is sonicated for 4 h at r.t., under a N_2 atmosphere. The solvent has been eliminated by magnetic separation and the solid residue has been washed for three times with toluene. Residual toluene was eliminated by vacuum evaporation to afford carbamate **62**.

4-Chlorosulfonylphenylisocyanate has been chosen because the presence of the electrophile chlorosulfonic function could allow the insertion of a maleimidic-bearing moiety. As a matter of fact, sulfonyl chlorides can react with amines to give sulfonamides, whose *in vivo* stability is remarkable. We thus decided to develop the second moiety of the maleimidic linker by coupling mono Boc-hexamethylenediamine with N-maleoyl-β-alanine (**63**), in order to obtain the α-amino, ω-maleimido amidic moiety (**64**), suitable for the reaction with the sulfonyl chloride- functionalised SPIONs (Scheme 1.43).
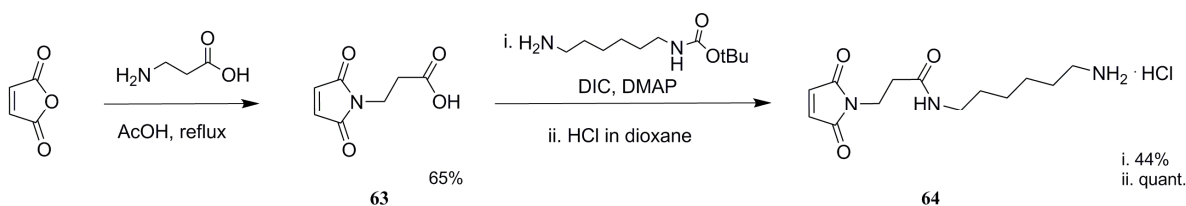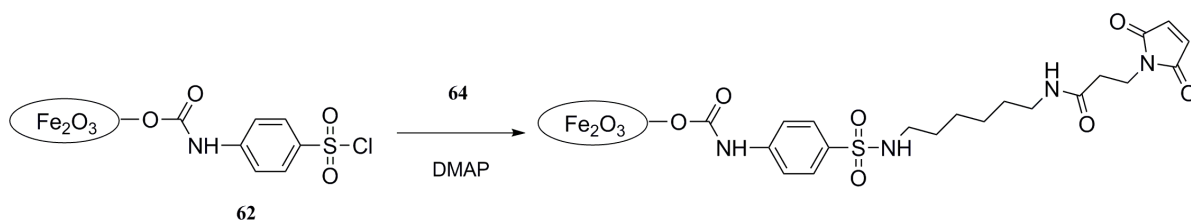

Scheme 1.43.

The synthesis of amide **64** started from the preparation of N-maleoyl-β-alanine (**63**). To a suspension of maleic anhydride (1.0 equiv.) in AcOH, β-alanine (1.0 equiv.) was added. The reaction mixture was heated at reflux for 5 h, then AcOH was removed by azeotroping with toluene. The obtained residue was then poured on water and extracted with AcOEt; the combined organic layer was dried, filtered

and evaporated to give N-maleoyl-β-alanine (**63**) in 65% yield. In order to prevent the formation of diamides, we chose to couple it to mono-Boc (abbreviation for tert-butyloxycarbonyl) hexamethylenediamine. The coupling between carboxylic acid (**63**) and mono-Boc hexamethylenediamine was performed using the acylation procedure already mentioned in above, which allowes the obtainment of Boc-protected amide in 15 h at r.t., in 44% yield. The tert-butyloxycarbonyl protecting group was removed using HCl (4 M in H_2O/dioxane, 13.5 equiv.). The reaction mixture was allowed to stir for 3 h to afford amino chlorhydrate (**64**) in quantitative yield. The product was used without further purification, due to the difficulties in retrieving protonated amines from aqueous solutions such as those used for washing organic layers (Scheme 1.43).

Amine chlorhydrate (**64**) (1 equiv. in weight) has then been added to chlorosulfonyl-SPIONs (1 equivalent in weight) (**62**) in order to obtain the desired maleimidic linker-functionalised SPIONs through the formation of a sulfonamidic bond. The reaction was performed in excess of DMAP, which served both as a catalyst and as a base to deprotonate amine chlorydrate (Scheme 1.44).
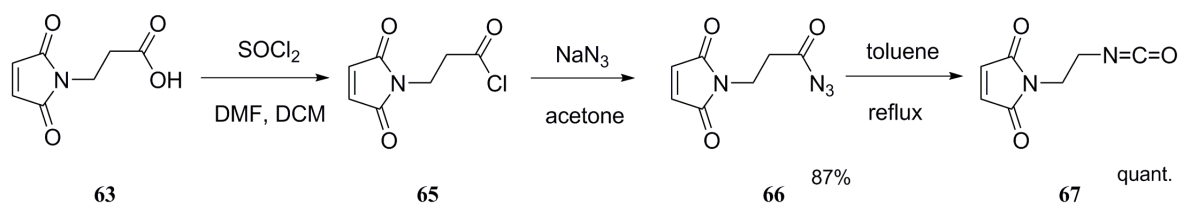

Scheme 1.44.

Nevertheless, the reaction between a sulfonyl chloride and an amine is not easily monitorable via IR spectroscopy, which constitutes (as previously said) the only method to understand the chemical nature of NPs adducts; as a matter of fact, the sulfonamide stretching bands belong to a scarcely diagnostic zone (1350-1300 cm^{-1} and 1150-1100 cm^{-1}) and it is not possible to establish whether the desired product has been formed beyond reasonable doubt. For this reason, we did not manage to understand if the effective functionalisation of SPIONs had taken place. Furthermore, the results of the following synthetic step, that is the conjugation with combretastatin A-4 thiolic derivative (**56**), would have been limited by the same characterisation issues, therefore we decided to develop a new functionalisation strategy.

Second attempt at functionalising SPIONs: homogeneous phase synthesis of the linker

The new strategy we developed was aimed at synthesizing the maleimidic linker in homogenous phase, in order to reduce the number of steps which require IR spectroscopy for full characterisation. Thus, we could characterise by means of NMR spectroscopy a greater number of synthetic intermediates, therefore ensuring a more certain identification of the final NP-conjugate. Following this strategy, instead of building the maleimidic linker on the nanoparticle through two steps, an α-maleimido ω-isocyanate linker has been synthesized and has been linked to the SPIONs hydroxyl only in the final step.

As a result, we chose to insert an isocyanate function direct on N-maleoyl-β-alanine, whose synthesis had always been optimized while developing the first strategy, in order to obtain the desired

bifunctional linker in few steps. The easiest way to attain an isocyanate from a carboxylic acid group is undoubtedly Curtius' transposition,[220] which when applied on N-maleoyl-β-alanine (**63**) allows to obtain the maleimido-isocyanate linker (**63**) in just 3 steps (Scheme 1.45).

Scheme 1.45.

In detail, to a solution of N-maleoyl-β-alanine (**63**) (1.0 equiv.), SOCl$_2$ (2.0 equiv.) and catalytic DMF (0.1 equiv.) were added at r.t. The solution ws stirred for 24 h under a N$_2$ atmosphere, then SOCl$_2$ (1.0 equiv.) and DMF (0.1 equiv.) were added again. The solution was stirred for 24 h under the same conditions to afford acyl chloride (**65**). Chloride **65** was converted into the acyl azide (**66**) by adding a saturated aqueous solution of NaN$_3$ at 0°C under N$_2$. The reaction mixture was stirred at 0°C for 10', then allowed to reach r.t. and stirred for 2'. The reaction mixture was poured onto water and extracted with DCM: the organic layer was dried, filtered and evaporated to afford acyl azide (**66**) in 87% yield. Once dissolved in dry toluene, acylazide was then converted into isocyanate (**67**), promoting the Curtius' transposition by refluxing for 90' and stirring at r.t. for three days (Scheme 45). Isocyanate (**67**) has been obtained in quantitative yield and has been easily characterised via IR spectroscopy, as this product presents a very diagnostic, strong band (N=C=O stretching) at 2270 cm^{-1}. Isocyanate (**67**) is a very promising linker for SPIONs functionalization (Figure 1.49), as in just one step it is able to derivatize SPIONs surface (thanks to the isocyanate group) and to bind thiols such ad CA4-derivative (**56**).
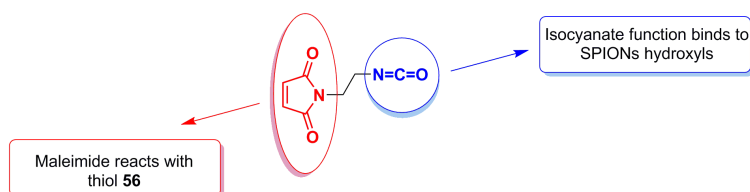

Figure 1.49. The bifunctional linker **67**

SPIONs can be then functionalised with isocyanate (**67**) under the same conditions used in the reaction with 4-chlorosulphonylphenylisocyanate, to afford functionalised SPIONs (**68**) in 4 h. of sonication at r.t. (Scheme 46). The reaction has been repeated without sonicating, in order to elucidate the role of sonication in the formation of the carbamate. Adduct (**68**) could be obtained even without sonicating, simply by leaving the reaction mixture for 16 h. between two magnetic stirrers, as this procedure allows to stir magnetic NPs without sonicating (Scheme 1.46).
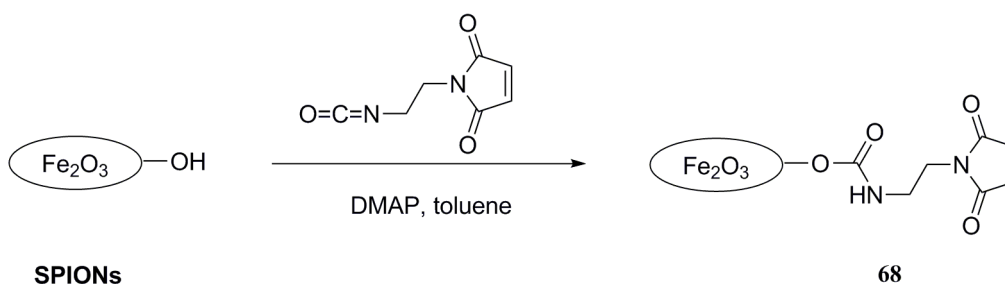
Scheme 1.46.

The relevant advantage brought by the utilisation of bifunctional linker (**67**) consisted in the fact that the whole process of SPIONs surface coating with maleimides was easy to supervise by means of IR spectroscopy; as a matter of fact, the formation of the carbamate necessarily implied the derivatisation of SPIONs with maleimidic functions. As said before, the disappearance of the stretching bands of the isocyanate (2274 cm^{-1}, Figure 1.50a) and the appearance of the C=O stretching of the carbamate (1703 cm^{-1}) is a proof of the successful functionalisation of SPIONs (Figure 1.50b).
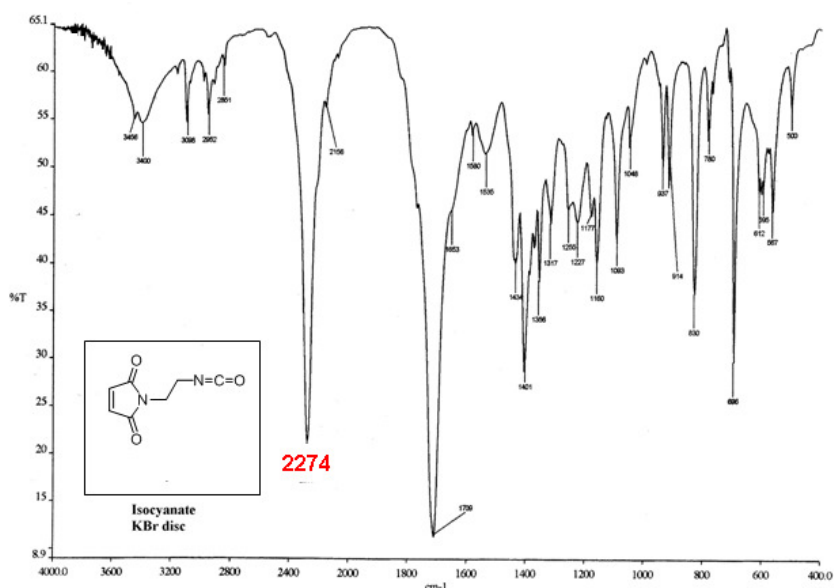
Figure 1.50a. IR spectrum of isocyanate **67**
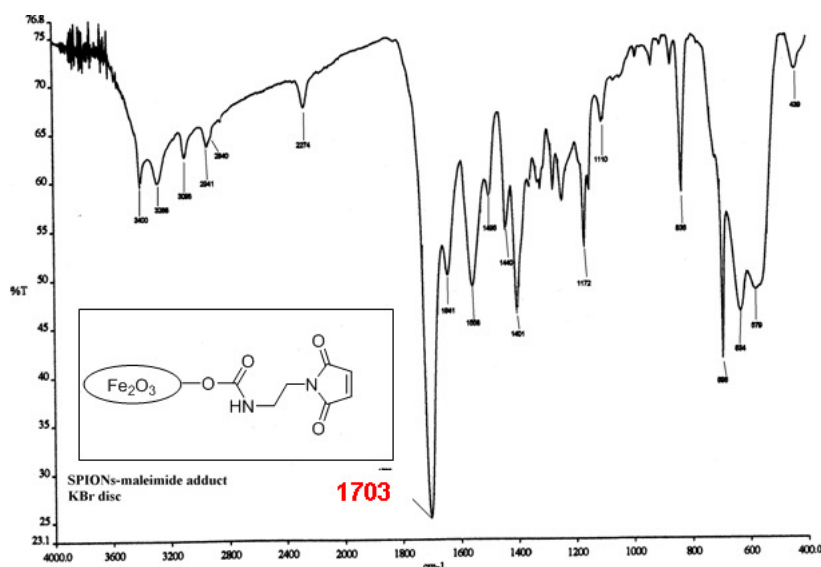
Figure 1.50b. IR spectrum of SPIONs-maleimide adduct **68**

Further proofs of the functionalisation of the SPIONs were given by thermogravimetric analysis (TGA, performed by Dr. Utzeri at ISMAC, Genova), which showed the effective adhesion of an organic moiety, demonstrated by a loss of adduct **68**'s weight on SPIONs' surface (see later in the same paragraph, Figure 1.51). The loss of weight increased proportionally with temperature in nitrogen atmosphere (from 30°C to 700°C), presumably due to the thermal degradation of almost the whole organic moiety; insertion of oxygen (700°C to 800°C) increased the slope of the loss of weight function until it reaches a plateau, phenomenon which we attributed to a total oxidative degradation of the organic residue. The esteemed total weight loss amounted to 51.3% (Figure 1.51).
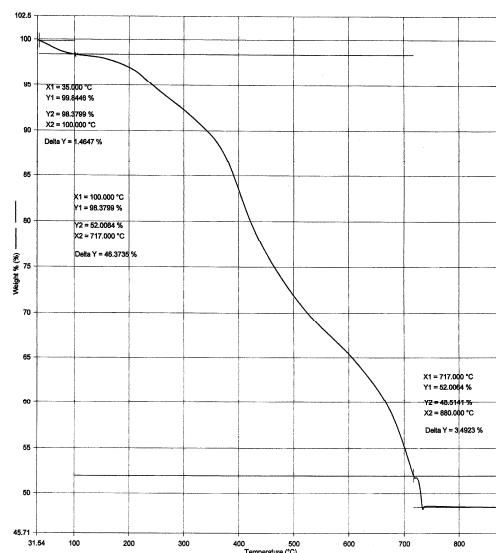

Figure 1.51. TGA thermogram for adduct **68**

Elemental analysis on (**68**) reported carbon, hydrogen and nitrogen percentages on total weight which were in line with our expectations (see § 1.4).

We have then studied the reactivity of isocyanate (**67**) towards various kinds of organic nucleophiles, namely benzylic alcohol, propargilic alcohol and propargilamine, in order to compare the related synthetic results with those obtained from the reaction with SPIONs. The reactions between isocyanate (**67**) and these nucleophiles were performed at r.t., under a N_2 atmosphere, using DMAP or TEA as a catalyst and suitable dry apolar solvents (DCM, toluene). It was interesting to observe that, although being carried out under the same conditions used with SPIONs, none of these reactions allowed the formation of the expected products (Scheme 1.47).
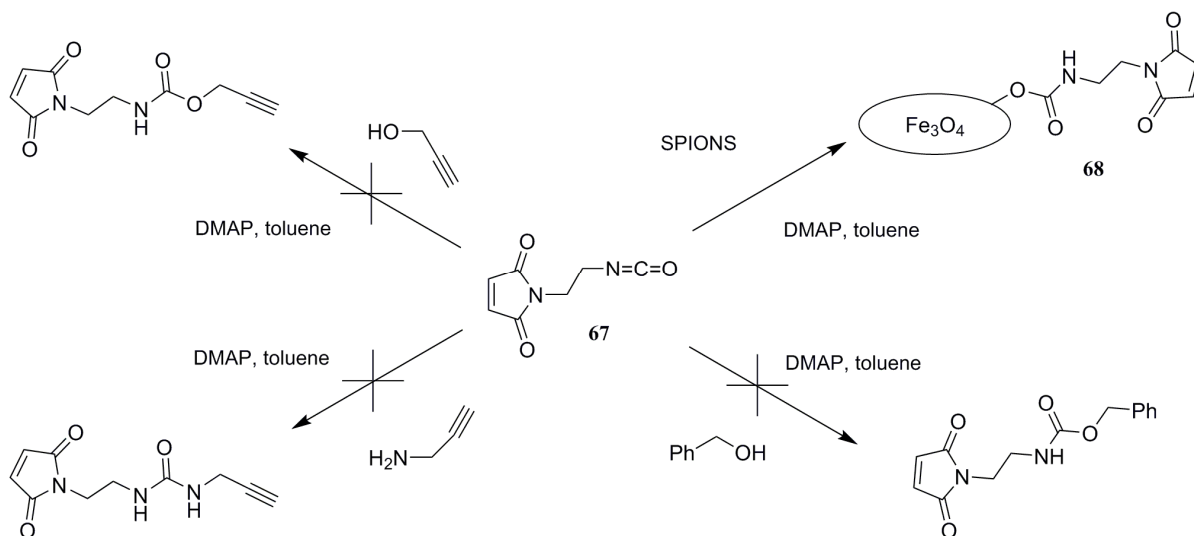
Scheme 1.47.

An even more striking proof of the efficacy of the reaction between SPIONs and isocyanate was provided by a successive test we performed on isocyanate (**67**). Isocyanate (**67**) was grounded in a mortar together with a comparable quantity of SPIONs and 10:1 KBr for 2'. The thus obtained co-grounded powder was then analysed by IR spectroscopy, which showed that, after just 2' of co-grinding, a consistent percentage of isocyanate had already reacted with SPIONs to give carbamate (**68**) (Figure 1.52).

This highlights the great potential showed by the reaction between SPIONs and isocyanate.
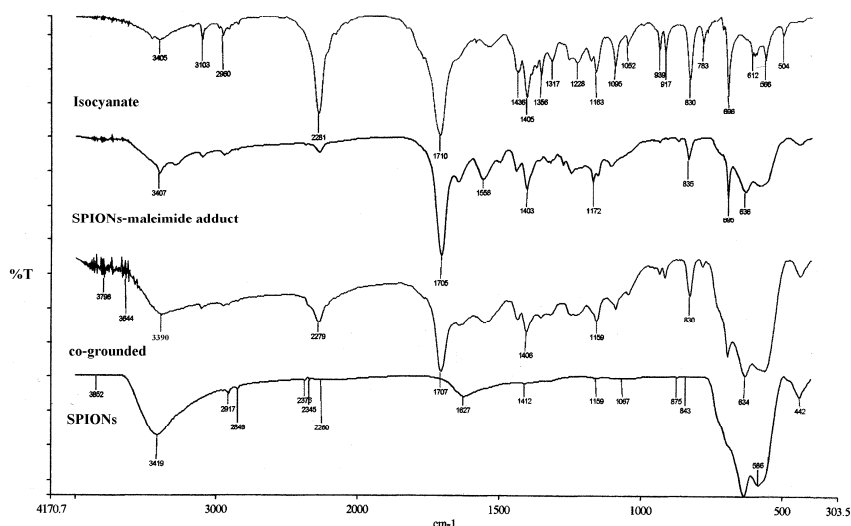
Figure 1.52. IR (KBr) analysis of co-grounded, isocyanate, adduct **68** and SPIONs.

Having obtained SPIONs-maleimidic linker conjugate (**68**), we proceeded to the final step of the synthetic strategy, namely the conjugation between SPIONs' maleimido group and the sulfydryl function of combretastatin A-4 thiolic derivative (**56**) through a 1,4-Michael addition.

To obtain the SPIONs-CA-4 conjugate, **69** (1.0 equiv. in weight) was suspended in dry, deoxygenated DCM under a N_2 atmosphere. The absence of oxygen in the reaction environment was critical, in order to avoid the oxidation of the thiol to a disulfide. A solution of thiol (**56**) in dry DCM (1.0 equiv. in weight) and TEA (1.3 molar equivalents in respect to thiol) were then added and the suspension was sonicated at room temperature for 4 h, then it was left to stir for 16 h under the same conditions. The solvent was eliminated by magnetic separation and the solid residue was washed three times with fresh DCM. Residue solvent elimination was performed by vacuum evaporation, to obtain NPs-adduct (**69**) (Scheme 1.48).
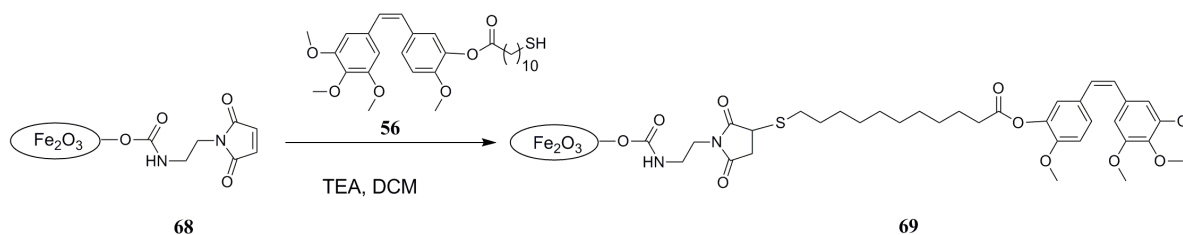
Scheme 1.48.

To characterise this adduct, we made use of three techniques: a) elemental analysis, b) IR spectroscopy, c) TGA, although obviously, given the aforementioned difficulties in characterising SPIONs-containing species, further tests will be needed.

89

a) Elemental analysis on adduct **69** reported very low carbon, hydrogen and nitrogen percentage on total weight compared to those found in adduct (**67**) (see § 1.4). This led us to think that probably, in Michael addition's conditions, some of the carbamate bond present in SPIONs-maleimide conjugate may have been damaged, causing the loss of the whole organic moiety and leaving some iron bonded hydroxyl free. The remaining maleimide functions, however, may have been functionalised with the thiol, as it is suggested by the altered C/H/N ratio.

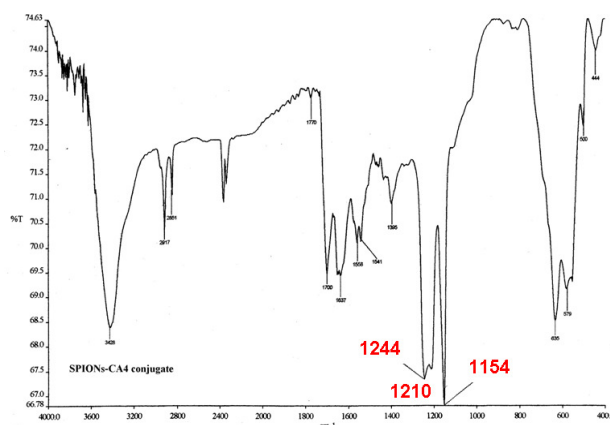b) FT-IR spectroscopy provided further information to support this theory (Figure 1.53).

Figure 1.53. IR spectrum of adduct **69**, recorded in KBr discs

The strong bands at 3428 (FeO-H stretching), 635 and 579 cm^{-1} (Fe-O stretching) are typical of free SPIONs, thus demonstrating the hypotheses of a loss of a part of carbamate bonds. However, a relevant percentage of carbamoylic moieties has survived Michael addition's conditions and has been functionalised. In fact, the IR fingerprint pattern peculiar to adduct **69** (Figure 1.53) has disappeared, showing the alteration of the pre-existing structure. Other important signals are the bands at 1244, 1210, 1154 cm^{-1}. These strong bands (although their intensity may considerably vary depending on the acquistition conditions) have been described in literature and attributed to a succinidimyl thioether structure, which actually results from thiol addition to maleimides.[221] Further proof of the obtainment of a succinidimyl thioethereal structure was given by the comparison of the IR spectra (Figure 1.54) of two compounds previously synthesized in our laboratory deriving from thiol addition to maleimides.
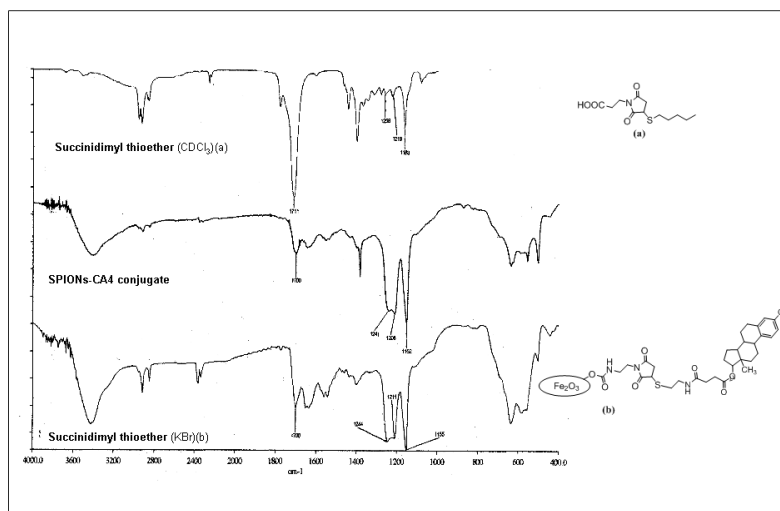
Figure 1.54. IR spectra of adduct **69**, succinidimyl thioethers (a) and (b), recorded in KBr discs (left); the structure of succinidimyl thioethers (a) and (b) (right).

c) <u>TGA</u> thermogram on product **69** reinforced the previously formulated hypotheses (Figure 1.55, right). The esteemed weight loss, in this case, amounted to 25.5%, leading us to think that a relevant percentage of the maleimidic linker on carbamate has been lost during the Michael addition. Another interesting phenomenon, however, was the weight increase (7.48%) registered as oxygen was inserted. Free SPIONs thermogram (Figure 1.55, left) highlighted a slight weight gain under the same conditions which was presumably due to the oxidation of Fe° and FeO impurities to Fe_2O_3. At any rate, this weight increase was in no way comparable to the one showed by adduct **69**.
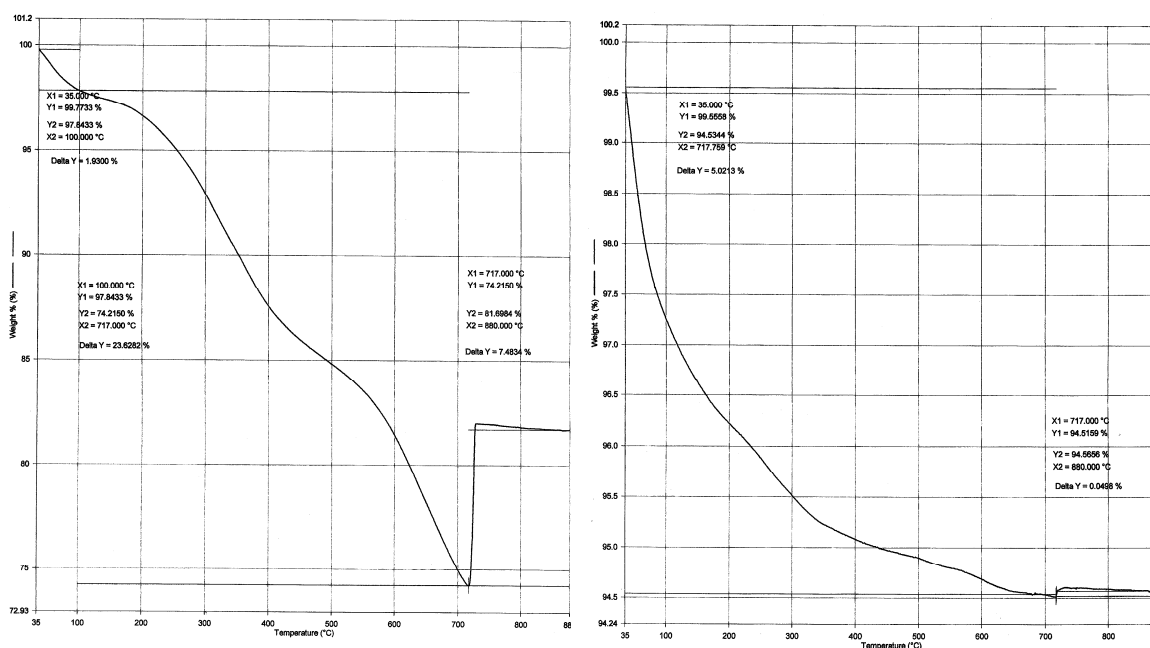

Figure 1.55. Right: thermogram of adduct **69**. Left: thermogram of blank SPIONs

We supposed that during Michael addition of thiolic derivative (**56**) to adduct **68**, the thiol may reduce Fe(III) to Fe(II). Fe(II) may undergo subsequent oxidation during TGA as soon as oxygen is inserted, leading to a significant weight gain. On the other hand, thiol-mediated Fe (III) reduction has been often reported in literature; for instance, Doong et colleagues have studied cysteine-mediated iron (III) reduction, which can occur both in abiotic and biological conditions.[222]

In conclusion, we had sufficient proofs to state that NP functionalisation with CA4-thiolic derivative (**56**) has been achieved, although it was evident that this procedure has to be optimized and further identification tests have to be performed.

Third attempt of functionalising SPIONs: insertion of an isocyanate function on CA4

As described in the previous paragraph, we managed to attain a NP-CA4 conjugate (adduct **69**). However, the characterisation of the thus obtained nanosystem presents relevant difficulties, not to mention the fact that further identification studies which could help us in the precise determination of its structure still have to be made. Therefore, we decided to develop another synthetic strategy which could allow to reduce the number of SPIONs-involving steps further, so that the characterisation of our products could raise fewer doubts. For instance, the insertion of an isocyanate function of combretastatin A-4 would have permitted one-step SPIONs functionalisation, process which could have been easily monitorable by IR spectroscopy.

We decided to perform Curtius' transposition on a carboxylic derivative of combretastatin whose synthesis had already been optimized in our laboratory, combretastatin monoglutarate (**35**). The synthesis of this derivative has already been discussed and reported in scheme 1.12. We subsequently proceeded with the cloruration of the free carboxylic function with $SOCl_2$, in order to follow the isocyanate synthesis strategy we had successfully pursued while synthetising isocyanate (**67**) (Scheme 1.45). However, glutarate derivative(**35**) was not stable to the required acidic reaction conditions and we had to quit this synthetic strategy (Scheme 1.49). We also attempted to synthesize combretastatin monoglutaryl azide, starting material for Curtius' transposition, avoiding cloruration. We followed a procedure (described by *Kim et al.*)[222], which allowed to perform the reaction in milder conditions. As a matter of fact, this procedure implies the use of Cl_3CCN, NaN_3 and PPh_3, with no acidity development. Nevertheless, neither this strategy has been successful, as no formation of the desired acyl azide was observed (Scheme 1.49).
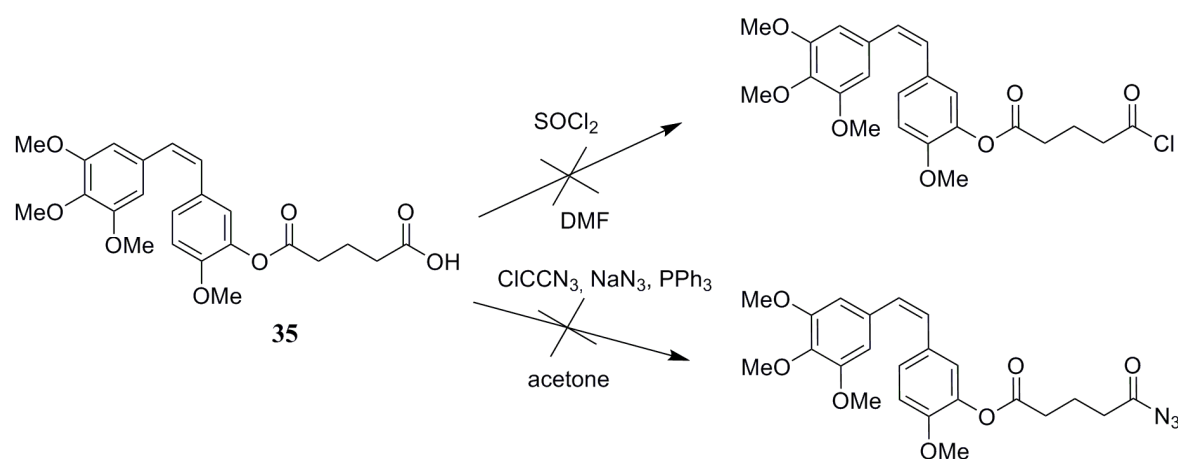
Scheme 1.49.

Furthermore, we tried to synthetise an acyl chloride derivative of combretastatin by esterificating it with malonyl dichloride, in order to avoid aggressive cloruration (Scheme 1.50), but the thus formed ester was not stable on silica gel. Moreover, while the esterification of combretastatin A-4 phenolic OH was demonstrated by NMR spectroscopy, the presence of the terminal acyl chloride function was not certain, as IR analysis did not show the typical, very diagnostic bands of acyl chloride's C=O stretching above 1800 cm^{-1}.

33
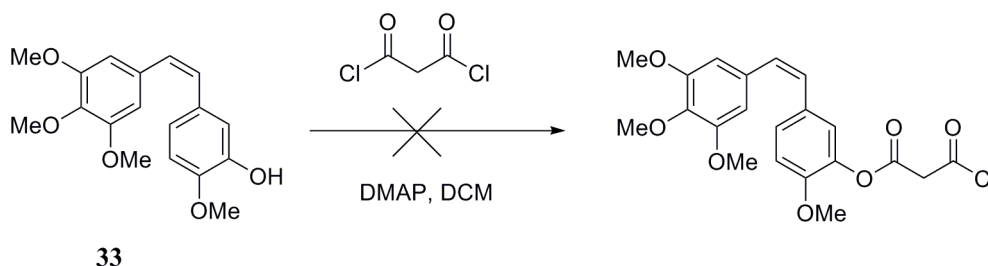
Scheme 1.50.

In conclusion, we did not manage to develop a one-step strategy for SPIONs functionalisation, thus we decided to focus on the characterisation of conjugate (**69**). At any rate, it might be interesting to investigate further on other simpler, faster synthetic routes for the achievement of SPIONs conjugates and their characterisation.

1.2.3b Functionalisation of Cobalt TurboBeads Click with combretastatin A-4

Cobalt TurboBeads Click: structure, properties and applications

TurboBeads are highly magnetic cobalt nanoparticles with diameters of below 50 nm. The surface of the particles is coated with a graphene shell, which is covalently functionalised with primary aliphatic azido or amino groups (≥0.1 mmol/g).[223]

Figure 1.56. A schematisation of the structures of TurboBeads: left, *Click*; right, amine coated

Their strong paramagnetism has been exploited for the development of a breakthrough purification technique, which allows the magnetic separation of chemicals of various nature from a reaction mixture as well as bulk samples. In fact, quick and efficacious separation of TurboBeads-conjugates from other chemical species can be achieved by using a laboratory-scale neodymium magnet. The magnet is put on the outside of the flask containing the sample and attracts the NP-conjugates, which

gather in its proximity. As NP-conjugates can't be removed from this position, other species present in the reaction mixture can be simply washed away. Also other kinds of paramagnetic nanoparticles (such as SPIONs, see §1.2.3a) can undergo magnetic separation, but in the case of TurboBeads this process is particularly fast and efficient.

This novel kind of cobalt nanoparticles, on the market since 2007, is being applied in an increasing number of science fields: for instance, they play an important role in biochemical assays when bound to targeting moieties of biomolecular interest.[224] Moreover, they are increasingly gaining in importance for what concerns organic synthesis, as they can be further functionalised with expensive catalysts to improve their recovery from the reaction mixture, in order to recycle them. In addition, if functionalised with heavy metal chelators, they constitute very useful tools in clinical and environmental toxicology.

For what concerns theranostic applications, the use of TurboBeads or, more in general, of cobalt nanoparticles (CoNPs) is currently being the object of many pharmacological studies. Thanks to their elevated magnetic moment, CoNPs could be the ideal candidate for magnetic field assisted targeted drug delivery or hyperthermia. Actually, it has been observed that CoNPs' magnetic moment is twice as high as that of SPIONs,[225] property which could render them suitable for applications in magnetic resonance imaging. For instance, they could replace SPIONs-based contrast media in the diagnosis of hidden, scarcely detectable tumors. Furthermore, being the metal with the highest Curie point, cobalt firmly maintains its magnetic properties also in stress conditions: this could allow the development of nanosystems characterised by a very prolonged shelf-life.[226]

At any rate, the development of *in vivo* applicable CoNPs-based theranostic systems is being held back by non negligible toxicological issues. If SPIONs' ROS-mediated toxicity still has to be unanimously acknowledged, it is commonly known that cobalt may induce oxidative stress *in vivo*:[213] metallic cobalt can, in fact, be oxidised to generate various oxidation state cobalt ions. This newly generated reactive species can in turn be reduced again, hence cobalt's oxidizing activity. Recently, it has been observed by *Jiang et al.* that CoNPs exposure induces cytotoxicity and genotoxicity in human T cells *in vitro*.[227] Moreover, CoNPs have a remarkable ability to permeate membranes[228] and they can be easily accumulated by cells and exert their oxidative DNA damage activity. However, CoNPs toxicity may be fine-tuned by the application of a suitable coating which could limit their systemic oxidative activity; this relevant cytotoxic activity could be even addressed towards tumor cells by means of the already described targeting techniques. The modulation of CoNPs' toxicity by the addition of a protective coating seems however to constitute the most promising strategy: it has been observed, for instance, that CoNPs coated with graphitic shells (feature presented also by TurboBeads) can be applied in hyperthermia therapy to generate thermally localized cellular damage, which can induce cell death and necrosis in cancerous tissue.[229]

Our work thus consisted in the functionalisation of cobalt TurboBeads, by means of copper (I)-catalyzed alkyne-azide cycloaddition (CuAAC) reaction or amidation reaction, with the previously described combretastatin A-4 alkyne derivative (**57**) or NHS-activated derivative (**57b**), in order to achieve a new, promising, theranostic CoNPs-based system.

Synthesis and characterisation of CoNPs-CA4 conjugate

The functionalisation of cobalt TurboBeads *Click* was achieved by carrying out an adapted version of copper-catalyzed azide-alkyne cycloaddition, or CuAAC, described by *Sharpless et al.*[197] In this reaction, the azide reacts specifically with the alkyne to give a triazole, as discussed in § 1.2.3.

To functionalise azide-coated CoNPs with combretastatin A-4 hexynoate (**57**), we activated the nanoparticles by washing them in dry toluene and sonicating for 10' at r.t. for 3 times. This procedure consented a fine particle dispersion, which facilitated access to the azido functions on the NPs' coating. Once washed, CoNPs were suspended in dry toluene under a N_2 atmosphere and combretastatin hexynoate (**57**) (10 equiv.), CuI (0.5 equiv.) and triethylamine (1 equiv.) were added. As TurboBeads *Click*'s azide loading is known (0.1 mmol azide/g), other reagents could be added in molar ratio instead of weight ratio, as it was for SPIONs. The suspension was sonicated for 16 h. at r.t. under N_2, then the nanoparticles were retrieved from the reaction mixture by magnetic separation and solvent was eliminated. The solid residue was washed with fresh toluene, then residual solvent was eliminated under vacuum to afford NP-conjugate (**70**) (Scheme 1.51).
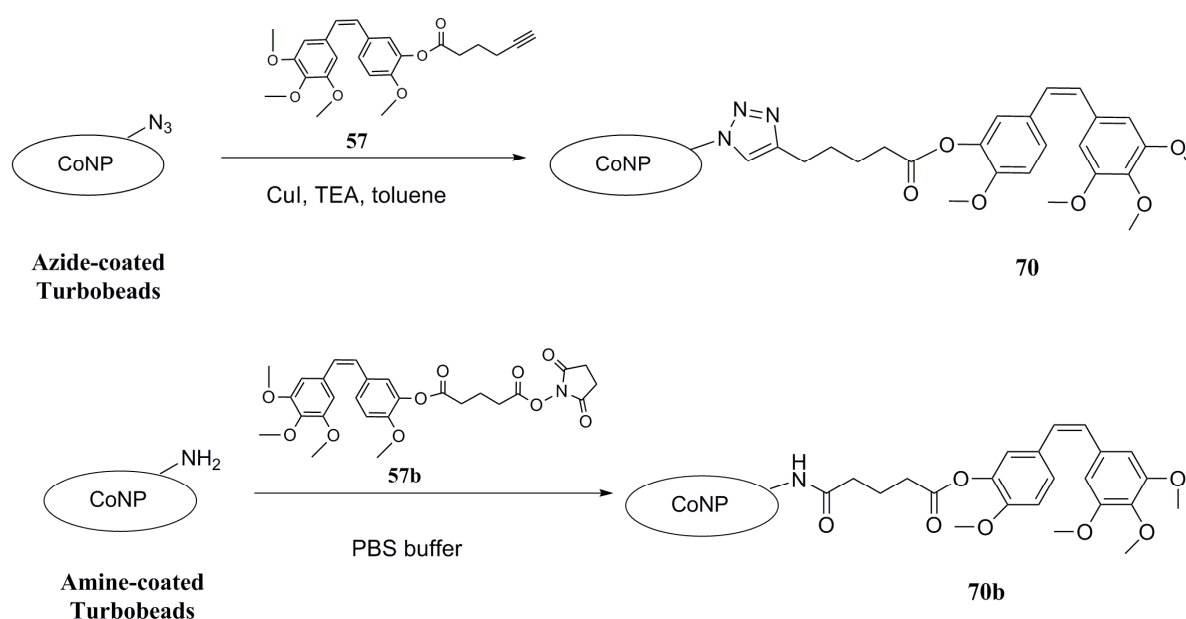
Scheme 1.51.

The functionalisation of cobalt amine-coated TurboBeads was achieved by carrying out a preliminary activation of the carboxylic derivative of Combretastatin (**35**) to a reactive NHS-ester compound (**57b**), followed by an amidation reaction. This strategy has been widely used to bind to proteins, peptides, DNA fragments or customized linking chemicals utilizing EDC/NHS chemistry.

In details, to functionalise amine-coated CoNPs with combretastatin A-4 derivative (**57b**), we activated the nanoparticles by washing them in a freshly prepare Tris buffer and sonicating for 10' at r.t. for 3 times. After these preliminary ones, we performed two more washing with a freshly prepared PBS buffer, as suggested on the website of Turbobeads company.The amidation reaction was thus carried out in this solvent that suspended either compound **57b** and CoNPs. The suspension was sonicated for 2 h at r.t. under N_2, then the nanoparticles were retrieved from the reaction mixture by

magnetic separation and solvent was eliminated. The solid residue was washed with fresh PBS followed by DCM, then residual solvent was eliminated under vacuum to afford NP-conjugate (**70b**) (Scheme 1.51).

NP-CA4 conjugate (**70**) has been analysed by means of: a) IR spectroscopy and b) thermogravimetric analysis.

a) <u>FT-IR</u> control of the reaction was particularly appropriated, as azide N=N=N stretching band could be found at 2090 cm^{-1} (Figure 1.57, left). While the IR spectrum of blank TurboBeads is characterised by the presence of the azide stretching band, adduct **70**'s spectrum (Figure 1.57, right) did not present any signal in that zone. This may be a convincing proof that functionalisation has successfully taken place.
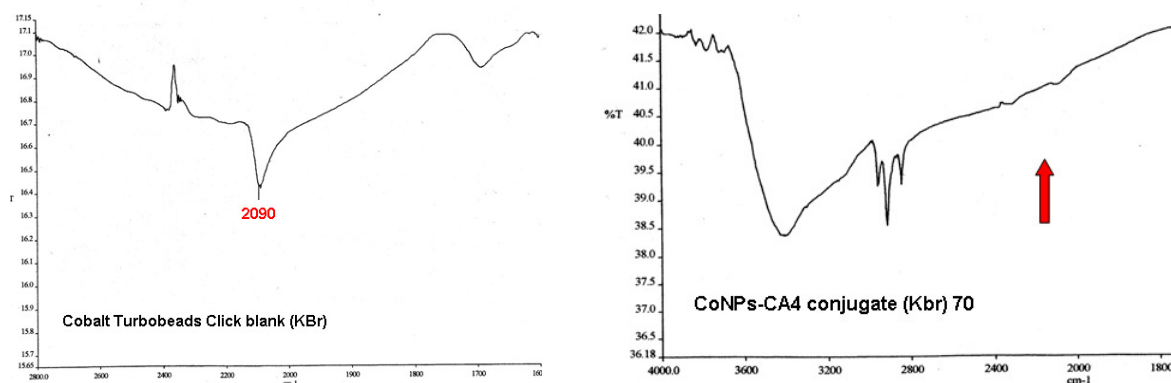

Figure 1.57. Left: IR spectra of blank TurboBeads. Right: IR spectra of CoNPs-CA4 conjugate **70**

b) *TGA*. For what concerns TGA analysis, a thermogram of CoNPs-CA4 conjugate (**70**) has been recorded and compared to that of blank TurboBeads (Figure 1.58). In the thermogram of the blank nanoparticles, a first, non-oxidative 3.8% weight loss is observed from 30°C to 700°C, under a nitrogen atmosphere.

The slope of the weight loss function brusquely increases as oxygen is inserted, leading to a further 1.45% weight loss. Therefore, a total 5.2% weight loss has been recorded, due to the thermal and oxidative degradation of NPs' graphene coating. From 770°C a 2% weight increase is observed. This is presumably due to the oxidation of the metal cobalt core to cobalt oxides, once exposed to the oxygen-rich atmosphere after the degradation of the protective organic shell.
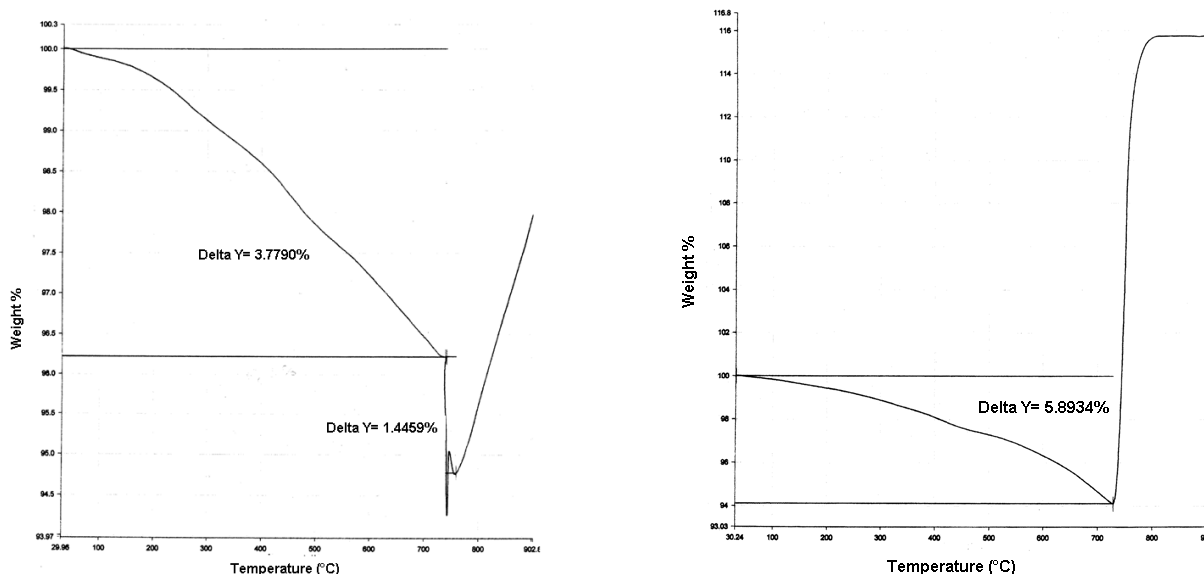
Figure 1.58. Left:Thermogram of blank TurboBeads. Right: thermogram of conjugate (**70**)

Adduct **70**'s thermogram showed instead an interesting phenomenon. From 30°C to 700°C, under a N_2 atmosphere, a 5,9% weight loss has been observed. As the non-oxidative weight loss was greater in the case of the adduct (5.9% against 3.8% of the blank) it could be inferred that the addition of an organic, thermodegradable portion on nanoparticles has occurred. The non-oxidative weight loss of adduct **70** was even greater than the total weight loss of the blank, both oxidative and not. At any rate, as oxygen was inserted, a sudden weight increase, amounting to 21%, was observed: this weight increase wass much more relevant than the one recorded in the case of the blank. Instead of showing a first oxidative weight loss and, only afterwards, a weight gain as in the case of the blank, adduct **70** just underwent a weight increase (Figure 1.58, right).

This led us to suppose that the prolonged sonication might have damaged the graphene shell on the NPs coating: in this case, cobalt would have been exposed to the oxidizing atmosphere from the very moment of oxygen insertion. However, an external coating damage would have seriously compromised the final achievement of the desired system, so we studied this phenomenon further. In order to verify whether sonication had actually affected the integrity of the graphene coating, we sonicated a sample of blank TurboBeads for 16 h. in the same conditions described in the synthesis of product (**70**). This new sample was then analysed by TGA (Figure 1.59).
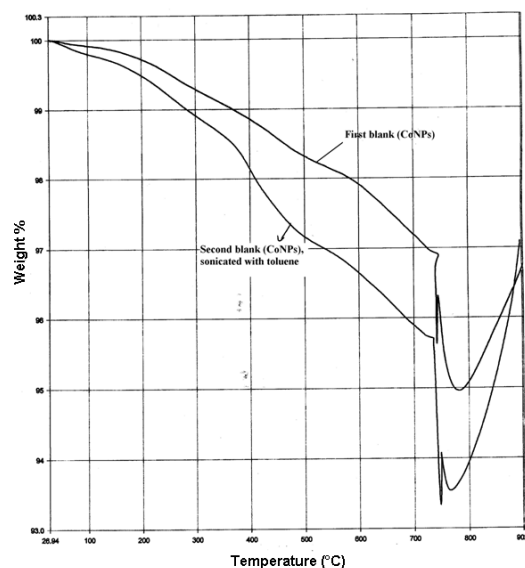
Figure 1.59. Thermogram of sonicated blank compared with that of the first blank.

The thermograms of the first blank and the one of the sonicated blank were absolutely comparable, from which we can infer that sonication did not disrupt NPs' coating. The weight gain observed in **70**'s thermogram may thus be attributed to other phenomenons which do not invalidate the achievement of the final conjugate system. Moreover, a similar TGA weight increase in oxidizing atmosphere has also been reported for other kinds of commercial TurboBeads.[230] For all these reasons, we suppose that the functionalisation of TurboBeads has successfully occurred.

Characterization of adduct **70b** is still in progress and it is not reported here.

1.2.3c. Synthesis of combretastatin A-4-loaded gold nanoparticles

Gold nanoparticles: properties, synthesis and applications

Gold nanoparticles (AuNPs, or colloidal gold) have been known since ancient times; the first empirical synthesis of colloidal gold dates back to 4th century B.C. In fact, gold nanoparticles have been extensively used as pigments for glass staining for centuries, thanks to their spectacular chromatic properties. This obviously occurred without much understanding of the synthesis process or of the actual nature of AuNPs, which Paracelsus described as "*Aurum potabile*". The first who took a properly scientific interest in colloidal gold was no less than Michael Faraday, who developed the first rational gold nanoparticles' synthesis procedure. He used phosphorus to reduce gold (III) chloride to nano-sized metallic gold particles, thus preparing the ground for modern AuNPs synthesis procedures.[231]

Currently, several AuNPs synthesis methods have been developed, either in aqueous or organic medium. The first AuNPs in organic solvents was achieved by *Brust* and colleagues[232] in the 1990s: according to this procedure, $HAuCl_4$ is dissolved in water, then the thus obtained solution is poured in a toluene solution of tetraoctylammonium bromide, which works both as a phase-transfer catalyst and as a particle stabilizer. The biphasic system is stirred, then $NaBH_4$ is added to reduce gold (III) to

metallic gold. Other methods are carried out by variations on Brust's procedure or by sonication of solutions of $HAuCl_4$.

Gold has been widely used in medicine for years, thanks to its biocompatibility and relatively acceptable toxicological profile, compared with that of other heavy metals. Gold complexes with thiols (e.g. pharmaceutical active ingredients such as Auranofin, Myocrisin) are still used for the treatment of arthritic pain, demonstrating the suitability of this metal for clinical applications.[233] Furthermore, a combination of AuNPs and microwave irradiation is achieving promising results in Alzheimer's disease therapy, as this treatment has been proved to disrupt β-amyloid plaques *in vitro*.[234] Great clinical interest raised by metallic gold is, as said, due to their favourable toxicological profile. However, as nanoparticles' properties may differ by definition from the those of the bulk material (see § Introduction), extensive study on AuNPs' toxicity is currently being carried out. AuNPs' *in vivo* toxicity has been proved to depend strictly on size and administration route. In particular, a study conducted by *Chen et al.*[235] has showed that intraperitoneal injection of naked AuNPs, ranging from 8 to 37 nm, induced severe hepatotoxicity in mice. Nevertheless, as said for TurboBeads (see §1.2.3b), toxicity can be relevantly improved by coating engineering.

Furthermore, AuNPs have recently emerged as an attractive candidate for theranostic delivery applications. AuNPs have interesting Raman effect enhancing properties (200 times more intense than that of quantum dots) and surface enhanced Raman spectroscopy (SERS) may be exploited to develop an innovative oncologic diagnosis technique. Tumoritropic targeted AuNPs could be used to reach cancerous tissue and to detect it by means of SERS, as molecules surrounding the nanoparticle give a consistently intensified Raman effect.[236] For what concerns therapy, AuNPs' ability to vectorize drugs and genes is being extensively investigated. Like the previously described nanoparticles (see §1.2.3b and 1.2.3c), AuNPs may target tumoral tissue by both passive (EPR effect, see § Introduction) and active targeting if conjugated with a suitable moiety (such as our MAP-NT unit). AuNPs are also considered as one of the most suitable vectors for gene therapy, thanks to their capacity to permeate cell nucleus.[237] Interestingly, *Gibson* and colleagues have recently achieved satisfying pharmacological results by developing a paclitaxe-AuNPs conjugate.[238]
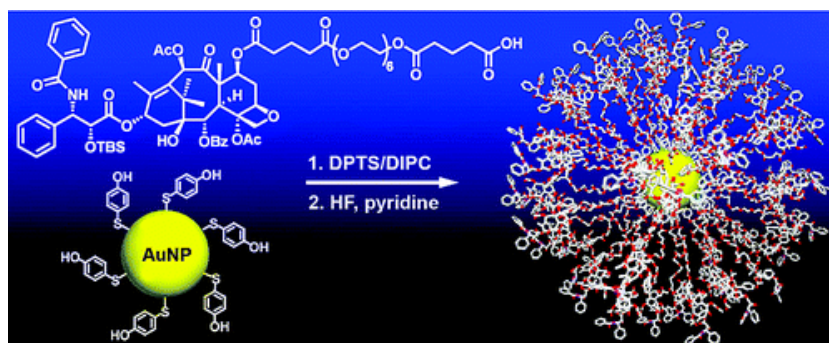

Figure 1.60.

In their paper, they describe the first example of 2 nm gold nanoparticles (AuNPs) covalently functionalized with paclitaxel, through a flexible hexaethylene glycol linker at the C-7 position of paclitaxel. Beyond presenting a new alternative for the design of nanosized drug-delivery systems, they furnish an approach that gives a rare opportunity to prepare hybrid particles with a well-defined amount of drug (Figure 1.60).

Moreover, AuNPs may be indicated in radionuclide cancer therapy by virtue of their radiosensitising effect. Although AuNPs' radiosensitising mechanism has not been fully elucidated yet, their capacity to enhance radiotherapy's cytotoxic effect on tumor cells is unanimously acknowledged.[239] Another characteristic which renders AuNPs a promising nanovector in oncology is the fact that ultra small nanoparticles can trespass the blood brain barrier (BBB), thus allowing the delivery of chemotherapeutics in the central nervous system (CNS). This could be relevantly helpful in the treatment of resistant cancers (for example, chemotherapy-resistant leukaemia) who established tumor sanctuaries in the CNS.[12]

AuNPs are gaining in importance also thanks to the relative simplicity with which they can be synthesized and functionalized. A preferential strategy for AuNPs functionalization consists in exploiting the great affinity presented by sulfydryls for gold (see §1.2.3c, Results and Discussion) and we decided to adopt it to achieve a CA4-AuNP conjugate.

Development of the CA4-AuNP conjugate

The purpose of our work was to functionalise AuNPs with combretastatin A-4 disulfide derivatives **58** and **61**. As already mentioned, we adopted a synthetic strategy (consisting in a variation on the aforementioned Brust's method) which allowed the simultaneous reduction of $HAuCl_4$ and the disulfide respectively to AuNPs and thiol analogues. This two *in situ* generated species reacted mutually, giving an Au-S adduct. An Au-S conjugate appeared to be particularly suitable for pharmacological applications, as the functional unit could be released *in vivo* by means of other endogenous thiols' action, namely GSH or cysteine. Nevertheless, during my PhD project we managed only to attain the conjugate deriving from disulfide **58** due to time reasons: conjugate deriving from disulfide **61** will be at any rate developed in the future.

To achieve the desired CA4-AuNP conjugate, a golden colored aqueous solution of $HAuCl_4$ (1.5 equiv.) was added to a solution of tetrabutylammonium bromide (2.2 equiv.) in toluene. The biphasic system was stirred for 10', then a solution of disulfide derivative (**58**) (1.0 equiv.) was added. The reaction mixture was cooled to 0°C. A freshly prepared aqueous solution of $NaBH_4$ (29 equiv.) was added dropwise, after a few drops the aqueous layer turned to black and bubble were observed. The mixture is stirred at r.t for 24 h. to give a biphasic system with black organic layer and colourless aqueous layer. The organic layer was isolated, evaporated and washed with Et_2O to afford AuNP-drug conjugate (**71**) as a black oil with purple glare (Scheme 1.52).
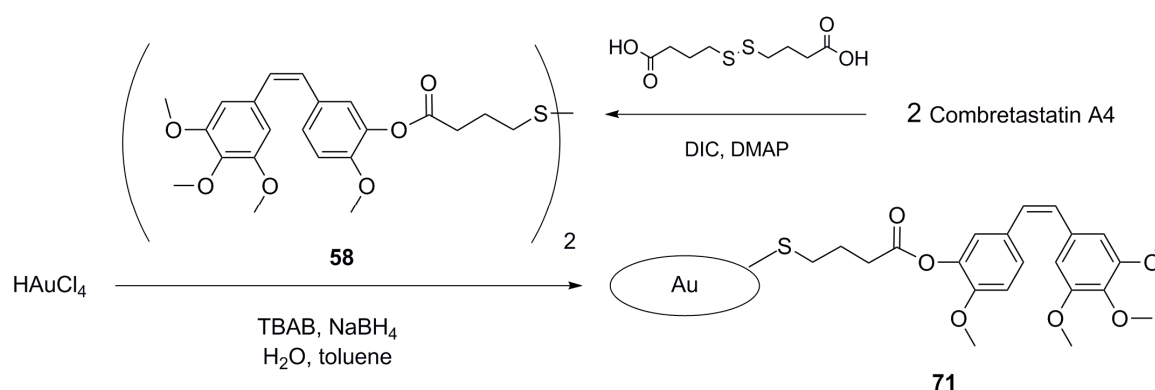
Scheme 1.52.

In comparison with paramagnetic NPs derivatives above described, AuNPs presented a big advantage: these adducts could be characterized by means of NMR spectroscopy (a), as gold $^{(0)}$ is not magnetic. Furthermore, AuNP-drug conjugate (**71**) is perfectly soluble in CDCl$_3$, (giving an homogeneous purple solution) even allowing an IR analysis (b) and TEM imaging investigations (c), in addition to TGA (and DTGA) analysis (d).

This notably simplifies the elucidation of the structure of conjugate **71**, as below reported.

a) <u>Proton NMR</u>. Comparing the proton spectrum of derivative **58** with the one of AuNPs adduct (**71**) (Figure 1.61), it was crystal clear at first sight that thiolated CA4 was successfully anchorated onto gold nanoparticles.
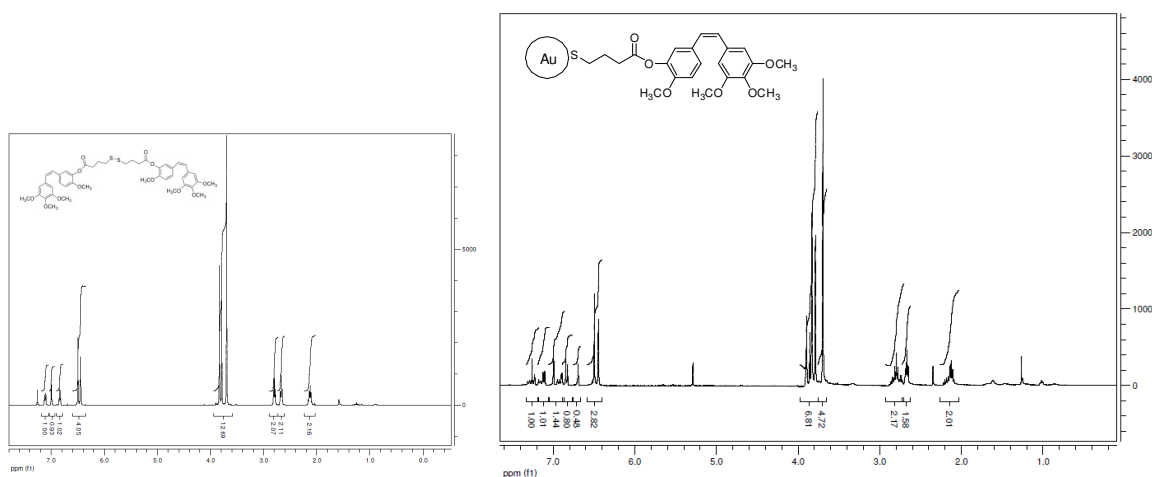
Figure 1.61. ^{1}H NMR spectra of: left, combretastatin disulphide **58**; right, AuNPs adduct **71**

^{1}H NMR spectra of **58** and **71** were recorded in the same conditions, dissolving the samples in CDCl$_3$ and obtaining, in the case of **71** an homogeneous purple solution. Despite the spectrum of the latter appeared to be pretty much more complicated than the one of the starting materials, due to the fact that signals tend to split or to lose their molteplicity, it unequivocally showed the precence of the organic drug onto AuNPs. Indeed, all the signals of combretastatin disulphide mantened the correct chemical schift and integration in the conjugates' spectrum. The same situation was mirrored by carbon NMR analysis (data not shown).

Moreover, in order to calculate the organic loading of combretastatin derivative on AuNPs, we recorded the ^{1}H NMR spectrum of a known quantity of adduct **71**, in the presence of a known amount of DCM, as internal standard. Considering that AuNPs cannot be detected by NMR, the obtained spectrum only showed signals related to DCM and combretastatin derivative. Making a quantitative comparison between the integration values of signals of the two species allowed us to calculate the precise amount of derivative **58**. In details,to a solution of 38 mg of adduct **71** in CDCl$_3$ 20 mg of DCM were added. The ratio between the singlet of methylene group of DCM and singlets of 4 methoxy groups of combretastin adduct was found to be 3.12: 1 (Figure 1.62). Considering that the

former integrated for 2 protons while the latter for 12 protons, the desired amount of thiolated combretastatin was calculated as below reported:

1.00 DCM/2 protons= 0.5, integration value DCM per proton

1.97 derivative **58**/12 protons= 0.16, integration value of adduct **71** per proton

0.5/0.16= 3.12 ratio DCM/ adduct **71**

20 mg DCM/84.93 M.W. DCM= 0.23 mmol DCM/3.12= 0.075 mmol adduct **71**

0.075 mmol x 432 (M.W. compound **58**)= 32.5 mg compound **58**

38 mg adduct **71** : 100 = 32.5 mg compound **58** : x

x= 85% loading
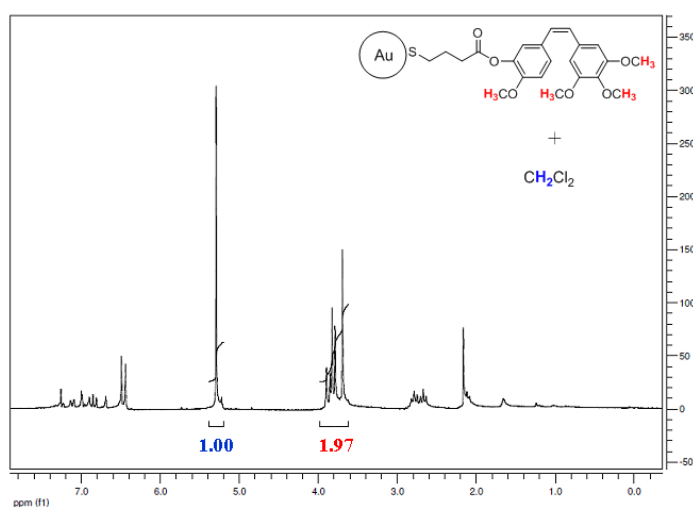
Figure 1.62. Methoxy groups' area of ^{1}H NMR spectrum of adduct **71** in the presence of DCM.

The final loading of AuNPs resulted to be 85%, a value consistent with the one calculated on the basis of TGA analysis, as reported below.

b) IR. IR spectroscopy analysis provided a clear evidence of the presence of our drug derivative on nanoparticles. In this sense, two diagnostic peaks have to be highlighted: at 1756 cm^{-1} the one related to the C=O stretching of the ester moiety we have strategically inserted on CA4 to realise its prodrug; the one at 1507 cm^{-1}, related to C-O stretching of the same functional group (Figure 1.63). The sample was prepared as a solution in CDCl$_3$. After examined the results from NMR and IR analysis a doubt raised about the validity of the date we were looking at. In fact, it could be that we were observing the spectra of the excess of unconjugated CA4 derivative **71**, that easily passed in organic solution. To esclude this possibility, we performed several washing of the adduct with water in which compound (**58**) is soluble. We thus repetead the aforementioned analysis, obtaining the same results and confirming the effective anchorage of CA4 on AuNPs.
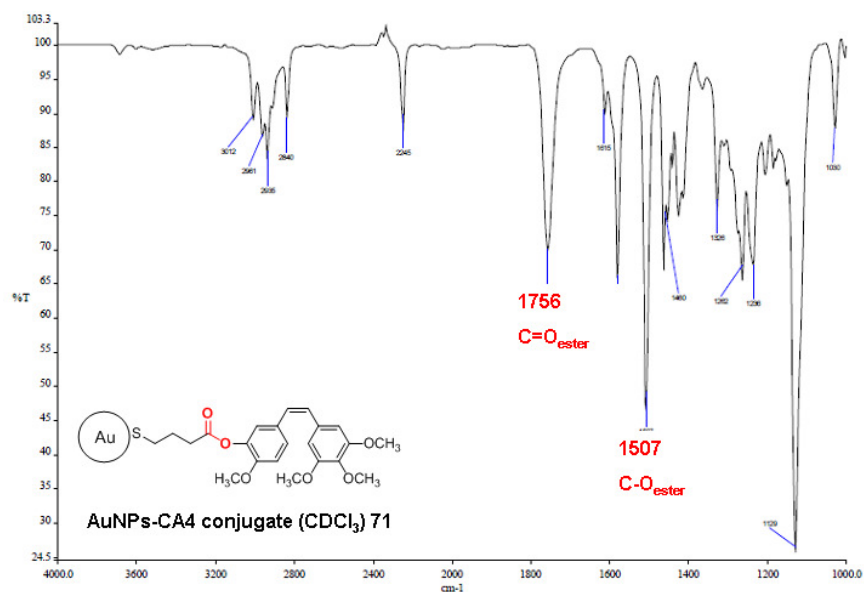
Figure 1.63. IR spectrum of adduct **71**, with characteristic signals highlighted in red color.

c) <u>TEM imaging</u>. We performed a TEM imaging analysis in order to evaluate shape and dimension of the above described fuctionalised nanoparticles. The image showed black, spheroidal shape NPs, surrounded by a grey shade, typical of organic funcionalization of metallic cores (Figure 1.64).
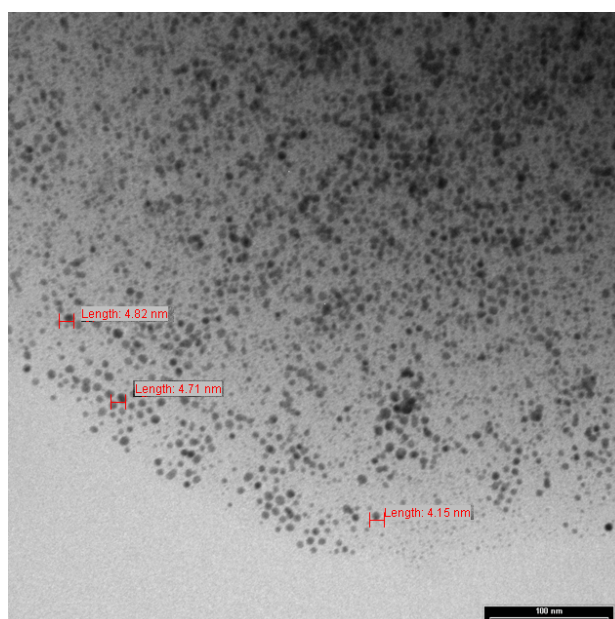

Figure 1.64. TEM imaging, showing the dimensions of functionalised AuNPs

Gold nanoparticles have numerous medical applications and traditionally have been thought of as bioinert since bulk gold has been deemed as such. However, more studies are suggesting potential toxicity concerns for gold nanoparticles due to their size, surface charge, and shape,the same unique

properties that make them so appealing for medical applications.[240] For instance, several studies have examined the effect of gold nanoparticle size on toxicity. From this investigations emerged that gold nanoclusters of 1.4 nm selectively and irreversibly bind to the major grooves of B-DNA, causing increased cytotoxicity compared to larger particles (18 nm).[241] Similarly, *Pan et al.* studied the size-dependent cytotoxicity of gold nanoparticles (water soluble and stabilized with triphenylphosphine derivatives) on several different cell lines. They discovered that nanoclusters of 1.4 nm exhibited increased cytotoxicity (IC_{50}=30 and 46 μM), whereas larger sizes ones (15 nm) exhibited no cytotoxicity even at high concentrations (6.3 mM).[242]
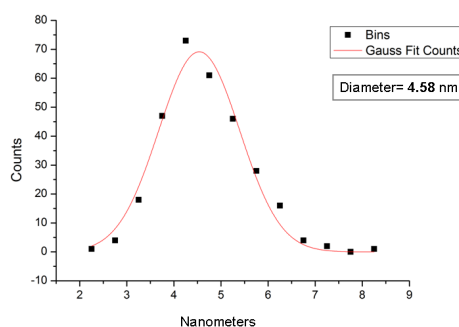

Figure 1.65. Gaussian distribution of AuNPs diameter.

AuNPs synthesized in our laboratory had dimensions that are a good compromise between low toxicity and efficiency as drug delivery systems. In fact, medium diameter was found to be of 4.58 nm, feature which should lower typical gold nanoparticles' size-dependent hepatotoxicity,[235] on one hand and which allows cellular uptake in cancer cells on the other hand.[243] Medium diameter was calculating from TEM image as mean of more than 300 nanoparticles and their distribution of size fitted with a Gaussian curve, as shown in figure 1.65.

d) <u>TGA</u>. A thermogravimetric analysis of adduct **71** was performed (Figure 1.66). It has shown an initial weight loss of 3.5% (from r.t to 200°C), due to the loss of volatiles (such as moisture and hydratation water) of the sample. Then, a non-oxidative weight loss of 83.5% (from 30 to 700°C, nitrogen atmosphere) was observed with max. speed at 339°C and assigned to the thermal decomposition of the organic fraction of adduct **71**. In the end, an oxidative weight loss of 7.72% (from 700 to 900°C) was recorded, due to the a residual carbon fraction, with max speed at 736 °C in the presence of oxigen. This data are perfectly in line with our expectations, as extimated loading from ^{1}H NMR spectrum amounted around to 86%.
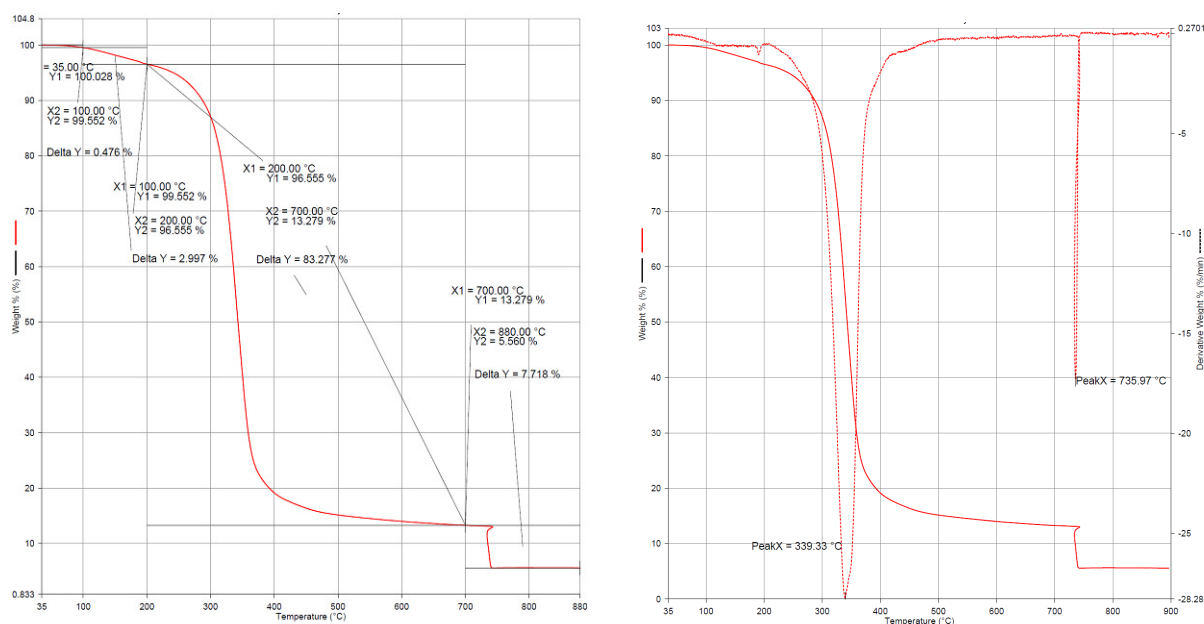
Figure 1.66. Left: thermogram of AuNP-CA4 conjugate **71**. Right: DTGA thermogram

Despite of the good matching between experimental results from two different tecniques (NMR and TGA), these data are not consistent with loading that can be inferred from calculations based on geometrical considerations, that turned out to be sensibly lower, as it is shown below.

Calculation of maximum possible loading of derivative 58

AuNps can be approximately considered as spheroidal shape entities, whose geometrical parameters such as volume, superficial area and mass can be estimated, knowing their diameter. At any rate, in order to calculate the maximum possible loading, several features of cargo molecule have to be kept in account, first of all, sterical hindrance on gold surface. In our case, capping molecule is combretastatin derivative **58**, a planar (Z)-stilbene scaffold, decorated with a pending thiolated chain. The presence of this chain between sufu atom and combretastatins' core plays a fundamental role of spacer, keeping the hindered portion of the drug far away from gold surface and thus enhancing the loading surface.

Assuming to treat **58** as a long chain linear thiol, the estimated superficial area was found to be about 21 Å. Regarding AuNPs, considering a medium diameter of 3 nm and the gold density of 19.32 g/cm^3, the estimated superficial area, volume and mass of a single NPs are 2826 Å, 14.3 nm^3 and 2.76 x 10^{-19} g, respectively. Ratio between superficial area of NP and combretastatin derivative (2826 Å/21 Å) give a loading of 135 drug molecules for each NPs, that corrensponds to a total amount of 0.6 x 10^{-19} g of derivative **58** per nanoparticle. Finally, percentual ratio between masses of compound **58** and AuNPs give a maximum possible loading of 25%. This data resulted to be considerably underestimated in respect of the ones from NMR and TGA analyses.

To further confirm the validity of the low percentage obtained, we decided to performed more sofisticated calculations, using specific softwares able to realistically simulate the distribution of cargoes on nanoparticles' surface. With the intent of calculating the *maximum possible loading*, softwares required preliminary data such as medium diameter of AuNPs and the length of the spacer that separe cargoes from gold surface, to estimate the proper diameters' correction. The former was

obtain from TEM analysis as above reported (4.58 nm), while the latter was calculated through crystallographic simulation of derivative **58**. Moreover, it was important to determine in the same way the dimensions of (Z)-stilbene moiety, in order to determine its superficial area. Starting from that, we envisaged two different kind of simulations. In the first case (a), we kept in account possible chemico-phisical interaction between capping molecules that could alterate the loading capability of our systems; in the second one (b), we ignored them. Herein are reported the obtained results from both the calculations:

a. The presence of a (Z)-stilbene moiety rose, indeed, the doubt of possible π- π stacking interactions between aromatic rings of combretastatins, once anchorated on gold surface through thiolated linker. If this happens, capping molecules can tightly pack one on the other as a series of rectangles, whose area was calculated to be 0.09 nm^2. Software simulation resulted in 233 capping molecules per NP coverage with a maximum possible loading of 25%. Despite of a slight mismatch in estimated coverage, the date was perfectly consistent with the one obtain from geometrical calculation above described.

b. In case π- π stacking interactions were not considered, the aromatic portion of compound **58** could not be regarded as a rectangle, since in this case there's not a complete overlapping of aromatic rings. Indeed, gaps between molecules had to be taken in account, thus, we thought to be more appropriate to treat (Z)-stilbene moiety as an ellipse whose area was calculated to be 0.28 nm^2. Software simulation resulted in 93 capping molecules per NP coverage with a maximum possible loading of 12%.

The fact we obtained a lower loading value in the second simulation was not that surprising, since lack of interactions between capping agents is known to impair nanoparticle's coverage. Nevertheless, in our case the total absence of π- π stacking interactions seemed to be unlikely. Indeed, the peculiar pattern of ^{1}H NMR spectrum of adduct **58**, showing splitting of the majority of signals, could be an evidence of this kind of interactions. Moreover, it could be indicative of the presence of a network of combretastatin molecules stabilized by non covalent attractions, some of them directly anchorated on gold surface through their thiol moieties and the others trapped in the abovementioned net through π- π stacking interactions. In addition to clarify the unexpected NMR signals' splitting, this hypothesis provides a reasonable explanation for the observed mistmach in loading values, obtained with different techniques. In fact, an additional amount of drugs trapped onto AuNPs could justify the sensibly higher percentage of loading (86%) detected by TGA than the one (25%) obtained through softwares' calculations.

In conclusion, detecting and quantifying organic coating of AuNPs turned out to be a challenging task. Eventhough, at first glance, inconsistency of data pushed us to draw the wrong conclusion we have used not appropriate techniques to calculate it, the above suggested hypothesis cast new light on this topic, reasonably explaining the mistmach of data.

1.3 Pharmacological results

Cytotoxicity of drug-conjugated tetra-branched NT peptides

The experiments have been carried out in different cell lines to represent the diverse tumours that over-express NT receptors : HT-29 (colon adenocacinoma), PANC-1 (pancreas epitheloid carcinoma), T24 (bladder carcinoma) and PC-3 (prostate carcinoma) and TE-671 (human rhabdomyosarcoma cell).

Our tumor targeting system is based on the specific delivery of the functional unit into the tumor cell by peptide binding and subsequent internalization of the receptor-ligand complex by endocytosis. In order to validate NT branched peptides as possible targeting agents for therapy of either colon or pancreas or prostate adenocarcinoma, binding of tetra-branched NT peptides to human tumor cell lines, was analysed and their rate of internalization was quantified. Peptide binding and internalization of tetra-branched NT(8-13) conjugated to Biotin (NT(8-13)4-Biotin) was analysed by confocal microscopy in HT-29, PANC-1 and PC-3 cell lines. NT(8-13) is considered the active fragment of the tetrameric peptide. It was found that NT4 conjugated to different fluorophores or to biotin, followed by fluorophore-conjugated streptavidin, specifically bind to the three cell lines, which express the NT receptors.[244] Peptide binding on membrane receptors was observed after 30 minutes incubation at room temperature. Cells were then washed and further incubated for 1, 2 or 4 hours to follow peptide internalization by confocal microscopy as it is shown in Figure 1.67.
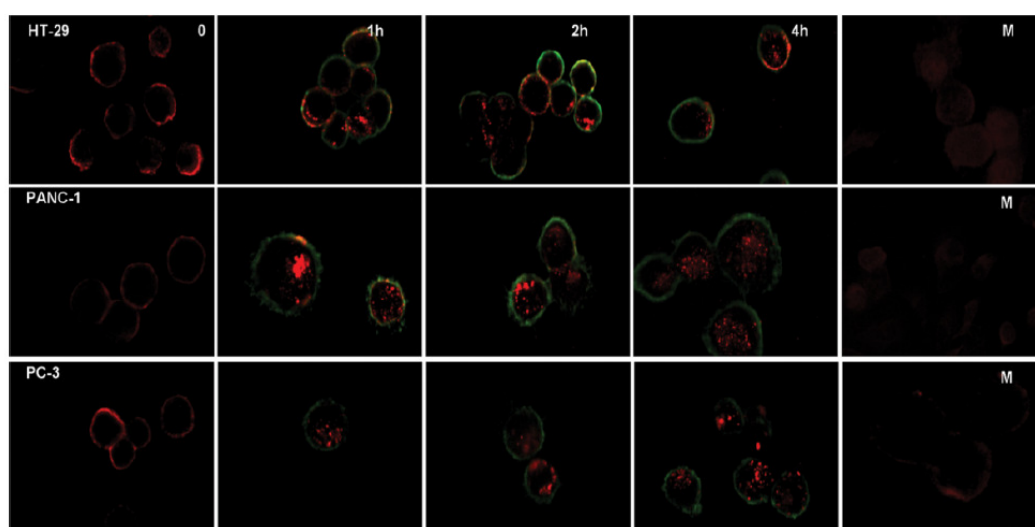

Figure 1.67. Binding and internalization in tumor cell lines. HT-29, PC-3 and PANC-1 were exposed for 30 minutes (time 0) to NT(8-13)4-Biotin or monomeric NT(8-13)-Biotin (M) followed by Streptavidin-Cy3. Internalization of NT(8-13)4-Biotin was observed after 1, 2 and 4 hours of further incubation in medium at 37°C. Cell membrane was stained with Lectin-FITC.

Peptides are degraded inside the cells within 18 h. Binding of tetra-branched NT(1-13) and NT(8-13) was clear in all the cell lines, whereas that of corresponding monomeric peptides was scarcely evident, which demonstrated the higher binding efficiency of branched peptides. NT(1-13) and NT(8- 13) branched peptides were completely internalized by the three cell lines, despite different internalization rates among the cell lines. Internalization of both tetrabranched NT(1-13) and NT(8-13) was quicker in PANC-1 and PC-3 than in HT-29. As a matter of fact HT-29 still showed a considerable amount of peptide on the cell membrane after a 2-hour incubation, whereas in PANC-1 and PC-3, peptides were completely internalized after a 1-hour incubation. No binding was observed either with an analogously conjugated branched peptide containing an unrelated sequence (DDHSVA) or with equivalent concentrations, in terms of peptide units, of the conjugated monomeric NT(1-13) or NT(8-13)

sequences.[245] Drug-conjugated tetra-branched NT peptides' internalization rate PANC-1 cells were incubated with tetra-branched NT conjugated to Functional Units and with the unrelated peptide (DDHSVA). Cells were centrifuged, washed and then lysed. The presence of uncleaved peptides was assessed by MALDI spectrometry both in the cell supernate and in cell lysate. Functional Units were detected as uncleavedmolecules in cell supernate and cell lysate even after 48 h. Unrelated peptides were found intact after 48 hours in the supernate and never detected in the lysed cells. Linear NT(1-13) (Sigma) was detectable in cell supernate after 2 h but was undetectable in the lysed cells.

The ability of tetrabranched peptides conjugated to a functional unit to bind cancer cell lines through NT receptors, to be rapidly internalized in cells and still detectable after 4 hours, is an important feature for possible therapeutic applications of these molecules. Finally we tested the possible application of these new NT-based molecular tools, conjugated to different drugs, for personalized therapy by determining their cytotoxicity in different human cancers.

Cytotoxicity of drug-conjugated NT4 in different tumor cell lines

It is well known that classical chemotherapeutics used in the clinical practice have different activity on different tumors. This is due to natural resistance of cancer cells to the drugs, determined by different mechanisms, including a decreased uptake or increased export of drugs by the cell, increased inactivation of drugs inside the cell or enhanced repair of the DNA damage produced by DNA-alkylating agents.

Previously reported cytotoxicity experiments, performed by the Prof. Bracci's research group on HT-29,[244] demonstrated that conjugation of methotrexate (MTX) or of the photosensitizer, chlorine-e6, to tetra-branched NT(8-13) produces pro-drugs like molecules. Such molecules can no longer be transported across plasma membranes by the mechanism of the corresponding free drug and can only be 'activated' via peptide receptor binding, thus profoundly decreasing non-specific drug toxicity.

Introduction of a novel, peptide receptor-mediated, mechanism of cell internalization of the drug might allow by-passing natural mechanism of cell resistance. As already shown, we designed and synthesize several derivatives of different drugs, commonly used in traditional tumor chemotherapy. Almost all these molecules were tested either as free drugs or conjugated to the tetra-branched NT(1-13) on HT-29,PANC-1 and PC-3 tumor cell lines.

In details, HT-29, PANC-1 or PC-3 cells were plated at a density of 2.5 x 104 per well in 96-well microplates. Different medium were used: DMEM medium fo PANC-1, McCOY's medium for HT-29 and HAM's F12 medium for PC3 cancer cell lines. Different concentrations of free or NT(8-13)-conjugated drugs, from 0.15 to 30 µmol/L, were added 24 h after plating. Cells were grown without changing the medium for 6 days. Growth inhibition was assessed by 3-(4,5- dimethylthiazol-2-yl)-2,5-diphenyltetrazolium bromide (MTT test). EC_{50} values were thereby calculated by non-linear regression analysis. The cellular toxicity of all the drug-conjugated NT4 was tested on the three cell lines and compared with the cytotoxicity of corresponding free drugs and also with that of an unrelated tetra-branched peptide, identically conjugated to the same drug. Stability of the conjugated molecule was then assessed by incubation with HT-29 for different time intervals and the supernatant and cell lysate

analysed by HPLC and MS resulting in a complete release of the drug moiety after 2 hours (data not shown). The ester bond allows a faster release of the drug and all the branched derivatives prepared were then classified as *fast releasing*.

When cells were incubated with the fast releasing peptide drugs in experimental protocol of six days of incubation without washing part of the chemotherapeutic moiety was released outside the cell and internalized via a different mechanism, probably by membrane diffusion. This was proved since unrelated conjugated peptides had a cytotoxic effect that could only be ascribed to the release of the 5-FdUrd **1**, Combretastatin **33** or Gemcitabine **4**, since we demonstrated that the unrelated peptide cannot be internalized. The washing procedure was then essential to follow the activity of fast releasing adducts so to exclude the additive effect of the released free drug. Cytotoxicity of fast releasing drug-conjugated tetra-branched peptides was then tested[245] in HT-29, PANC-1 and PC-3 in experiments where cells were exposed to a 1 hour pulse of free or NT-conjugated drug, washed and incubated for 6 days or, alternatively incubated for 6 days with the peptides, without additional washing. The additional washing was performed in order to avoid diffusion of free drug inside the cells during the following 3 or 6 days.

Below the results of *in vivo* tests, performed at the University of Siena are herein discussed.

a) *Cytotoxicity of **3**, NT4 derivatives of 5-Fluorodeoxyuridine*

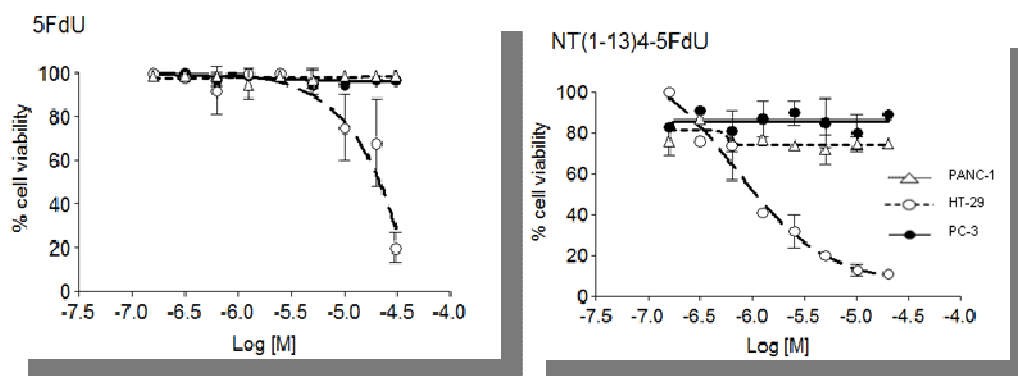5-FdUrd (5-fluorodeoxyuridine, **1**), as already said is a thymidylate synthase inhibitor.

Figure 1.68. Cytotoxicity of conjugate [NT4-**3**] (indicated like NT4-5FU) compared to free 5FdU

Drug **1** has a relevant role in the treatment of metastatic cancers, either by exerting an appropriate antitumor activity via blocking thymidylate synthase to inhibit DNA synthesis or by incorporation of its metabolite (5-Fluorouracyl) into DNA or RNA. Its principal uses are in colorectal cancer, and pancreatic cancer, in which it has been the established form of chemotherapy for decades. It is also sometimes used in the treatment of inflammatory breast cancer, an especially aggressive form of breast cancer. 5-Fluorouracile was used as a control in the experiment of cytotoxicity and showed analogue activity on PC-3, PANC-1 and HT-29 cell lines. The conjugated molecule NT4-5FU showed increased

activity with respect to the free drug especially on HT-29 where the IC_{50} drops to 1.0 nM, whereas in PC-3 and PANC-1, IC_{50} is in the micromolar range, respectively 3.8 μM and 1.6 μM (Figure 1.68).
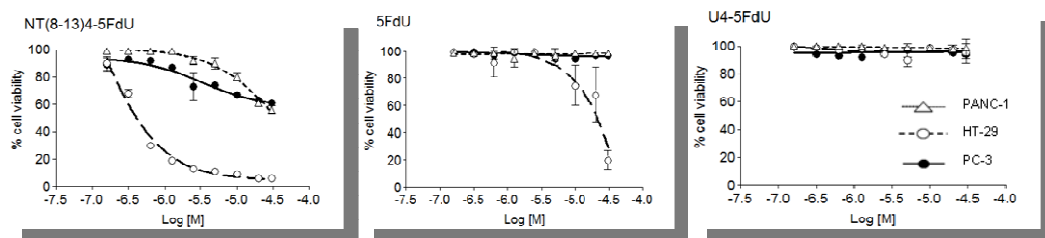

Figure 1.69. Cytotoxicity of conjugate [NT4-**3**] (indicated like NT4-5-FU) compared to free 5FU and the unrelated conjugate U4-3 (indicated like U4-5FU) after washing

An additional washing was performed, after 2 h of incubation, in order to avoid the diffusion of free 5-FdU released by hydrolysis of the ester bond of compound (**3**) during the 6 day incubation period and the data obtained with this procedure are reported above (Figure 1.69). They basically were in agreement with the previous ones, confirming the increased activity of the conjugated molecule NT4-5FU showed with respect to the free drug and the absence of cytotoxicity of conjugate with an unreleated sequence peptide.

b) *Cytotoxicity of 6, NT4 derivatives of Gemcitabine*

Gemcitabine (**4**) (dFdC) is a new anticancer nucleoside, a deoxycytidine analog. Postoperative gemcitabine significantly delayed the development of recurrent disease after complete resection of pancreatic cancer. Its main ues is as adjuvant chemotherapy in resectable carcinoma of the pancreas. Now gemcitabine is also used to treat certain types of breast, pancreatic, ovarian, and lung cancer and is being studied in the treatment of other types of cancer.
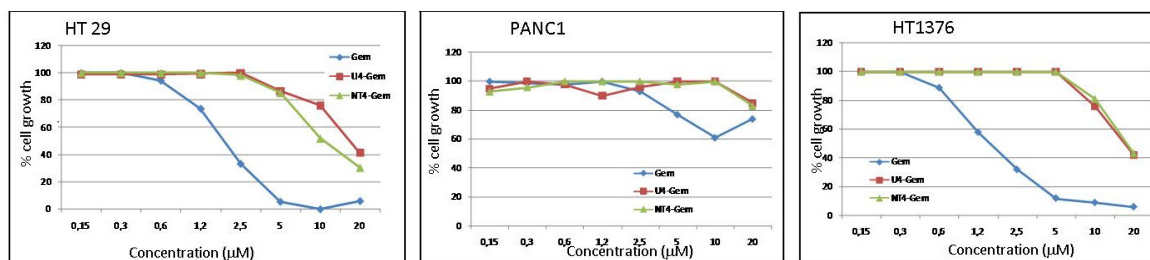

Figure 1.70. Cytotoxicity of conjugate [NT4-**6**] (indicated like NT4-Gem) compared to the free Gem and the unrelated conjugate U4-Gem

Gemcitabine (**4**) was used as a control in the experiment of cytotoxicity and showed different citotoxic activity on HT-29, HT1376 (bladder carcinoma) and PANC-1 cell lines. Indeed PANC-1 showed complete resistance to Gemcitabine, even when used as free drug (Figure 1.70). This result suggested that PANC-1 are not the suitable model for this test. In HT1376 and HT-29, free Gemcitabine was

active, though it lost most of its activity upon conjugation with the peptide. On top of that the activity of NT4-**6** and that of the non-internalizing U4-**6** analogue are comparable, and this effect is due to the weakness of the ester link which allows the release of free Gemcitabine before internalization and then its free diffusion into the cells. Thus, we should consider the possibility to synthesize gemcitabine analogues decorated with longer ester chains or with another kind of moiety (creating a *slow releasing system*) so to stabilize the linkage with the peptide.
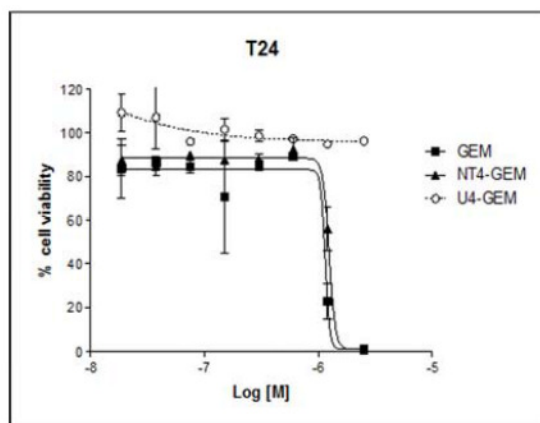
Figure 1.71. Cytotoxicity of conjugate **6** compared to the free Gem and the unrelated conjugate U4-Gem in T24 (bladder carcinoma) cells

In more recent time, conjugate's **6** activity has been tested in T24 (bladder carcinoma) cells, highlitening a promising cytotoxicity, comparable with the one of the free drug. Moreover, U4-Gem didn't show any anti-cancer activity, confirming that MAP NT4 is the portion responsible for tumor targeting and able to enhance the intrinsic cytotoxicity of gemcitabine (Figure 1.71).

c) *Cytotoxicity of **35**, NT4(8-13) derivative of Combretastatine*

Cis-CA-4 (Figure 20 a), a tubulin binding agent currently undergoing phase I clinical trials, is a potent antimitotic and cytotoxic agent which strongly inhibits the polymerization of tubulin by binding to the colchicine site and causes vascular disruption in some experimental primary tumours, and in vascularized metastatic tumour deposits. The anti-vascular activities of *cis*-CA-4 have been reported to be specific for tumour vasculature. Moreover, Combretastatin A-4 inhibits cell growth even at low nanomolar concentrations and exhibits inhibitory effects on multidrug resistant cancer cell lines.
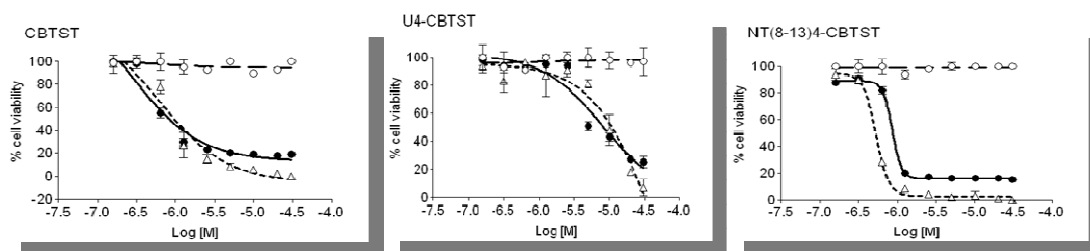
Figure 1.72 Cytotoxicity of conjugate [NT4-**35**] (indicated like NT4-CBST) compared to the free CBST and the unrelated conjugate U4-CBTST

The strong toxic activity of the free drug was evident in these human tumors cell lines and especially against PANC-1 and PC-3. The conjugated derivative NT4-**35** preserves its activity in the three cell lines and reflects the same trend, in facts, the IC_{50} is 3.5 μM on HT-29 and drops to 0.5 and 0.4 nM respectively on PANC-1 and PC-3 (Figure 1.72).

As for [NT4-**3**] the additional washing was performed and the results compared. Compound **35** deserved major interest, since the activity of the drug is clearly increased by conjugation to branched NT4 through a fast releasing linker (Figure 1.73) and this is evident though the unfavourable conditions of the additional washing. Nevertheless, free combretastatin and both conjugated analogues were found to be not cytotoxic in HT-29 cell line, that are well known to be resistant to this drug. Resistance to combretastatin and a possible solution to overcome this problem through conjugation with nanoparticles is broadly discussed below.
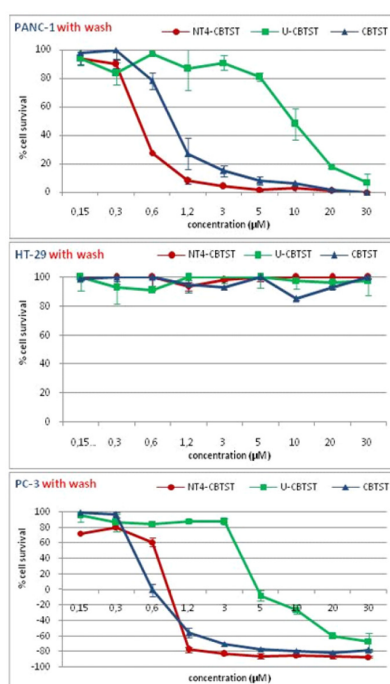

Figure 1.73. Cytotoxicity of conjugate [NT4-**35**] (indicated like NT4-CBST) compared to the unrelated conjugate (indicated like U-CBST) and free CBST after washing

c) *Cytotoxicity of **54**, NT4 derivative of Paclitaxel*

Paclitaxel is nowadays considered a first line treatment for numerous cancer deseases. This drug has neoplastic activity particularly against primary epithelial ovarian carcinoma breast cancer, colon, head,

non-small cell lung cancer, and AIDS related Kaposi's sarcoma. Despite of the primary role it plays in cancer therapy, several limitations has been ascribed to Palitaxel. On top of all, the poor bioavailability *in vivo*, because of its low aqueous solubility. For this reason, Paclitaxel is usually administered in polyethoxylated castor oil (Cremophor EL) and ethanol, a vehicle that is often associated with severe hypersensitivity reactions. This limitation triggered our effort to realize a drug delivery system able to overcome pharmacokinetic problems.
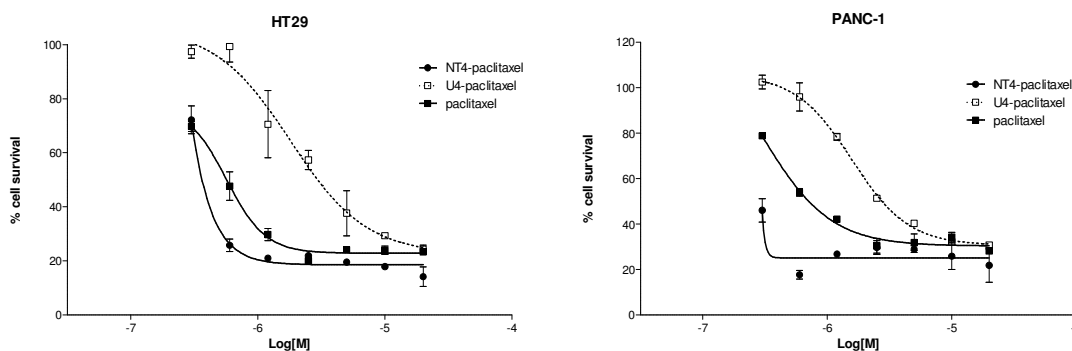
Figure 1.74. Results of MTT test on HT-29 (left) and PANC-1 (right) tumor cells. Cytotoxicity of conjugate [NT4-**54**] (indicated like NT4-paclitaxel) compared to the one of free drug (paclitaxel) and the one of a conjugated to a peptide with unreleated sequence (U4-paclitaxel)

Considering the feseability of one pot reactions to functionalise Paclitaxel, we investigated the possibility to exploit a thiol-ene coupling between a maleimido derived of the drug and thiol derivative of tetrabranched neurotensin peptide, as 'post-cleavage' coupling strategy. After validating its tumor targeting capability (as described in Results and Discussion section), NT4-paclitaxel conjugate's activity has been tested in in HT-29 and PANC-1 cells (Figure 1.74). In both cancer cell lines, obtained results were promising. While unrelated conjugate showed no activity as expected, free drug and conjugate [NT4-**54**] showed a strong toxic activity. In addition, for the first time since we have been working with NT4 peptide derivatives, we have observed a higher activity of the conjugate than the free drug currently on the market. This improvement in efficacy could open the way to an alternative delivery strategy of Paclitaxel, overcoming solubility problems and increasing its bioavailability.

IC_{50} values could not be calculated at this stage since the concentrations of conjugate [NT4-**54**] incubated with cells were too high to obtain an accurate sigmoidal shaped curve from which inferred them. In fact, the range of concentration we usually used to performed our assays turned not to be appropriate for Paclitaxel, considering the unexpected good activity of the conjugate in exam. With the current results in hands, we are planning to set up a more accurate cytotoxic test that will allow us to have precise IC_{50} values for both the free drug and comjugate [NT4-**54**].

Cytotoxicity of drug-conjugated nanoparticles in different tumor cell lines

While *in vitro* pharmacological tests CoNPs-conjugates are still being carried out at University of Siena, SPIONs-CA4 conjugate (**69**) and AuNPs-CA4 conjugate (**71**) have already completed their early pharmacological screenings.

a) *Cytotoxicity of **69**, SPIONs-CA4 conjugate*

The citotoxicity of product **69** has been tested on HT-29, PC-3 and PANC-1 tumor cell lines and compared with the ones exhibited by naked SPIONs (the commercially available compound) and by SPIONs functionalized with the maleimido linker (adduct **68**), above described in Results and Discussion section. The comparison with the latters blank compounds was done in order to demonstrate the biological inactivity of the metallic carrier, allowing us to exclusively attribute the observed citotoxicity to the organic fraction of adduct **69**.
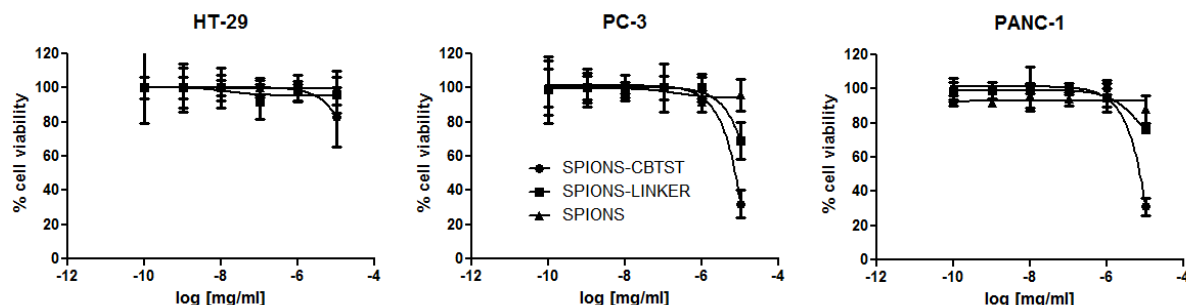
Figure 1.75. Results of MTT test on: left, HT-29, center: PC-3, right: PANC-1 cell lines. Cytotoxicity of SPIONs conjugate (**69**) is compared to the one of naked SPIONs and maleimido functionalised adduct **68**

As desired, adduct **68** and naked SPIONs were found not to be toxic even at high concentration. On the opposite, growth inhibition by conjugate **69** was shown in all the considered cell lines, even if more pronounced in PC-3 and PANC-1 cells (Figure 1.75). This data was not totally unexpected since HT-29 tumor cell line are reported in literature to be a resistant to combretastatin, as we also experimentally confirmed with citotoxic tests above described. A certain, even though poor, activity of adduct **69** on HT-29 cells has, thus, to be considered as an important starting point for a new strategy of delivering combretastatin, that overcomes resistance, with relevant clinical implications.

Literature about pharmacological screenings of nanometric particles is lacking of accurate descriptions of experimental protocol to test their activity *in vitro*. Beyond doubt, the insolubility of these systems in aqueous buffer represents a limitation in dosing the exact amount of nanoparticles, and thus drug, incubated with cells. Since obtaining a solution was not possible, we decided to calculate concentrations as ratio between weight of NPs and volume of buffer. Nevertheless, ongoing studies have been performing to set up a more consistent protocol.

b) *Cytotoxicity of **71**, AuNPs-CA4 conjugate*

The cellular toxicity of product (**71**) has been tested on HT-29 and TE 671 tumor cell line and compared with the one exhibited by CA4-disulphide (**58**).

Growth inhibition was assessed by 3-(4,5- dimethylthiazol-2-yl)-2,5-diphenyltetrazolium bromide (MTT test). Cytotoxicity results appear to be more promising in the case of TE-671 cell lines than in the case of HT-29, as it is evident from figure 1.76.
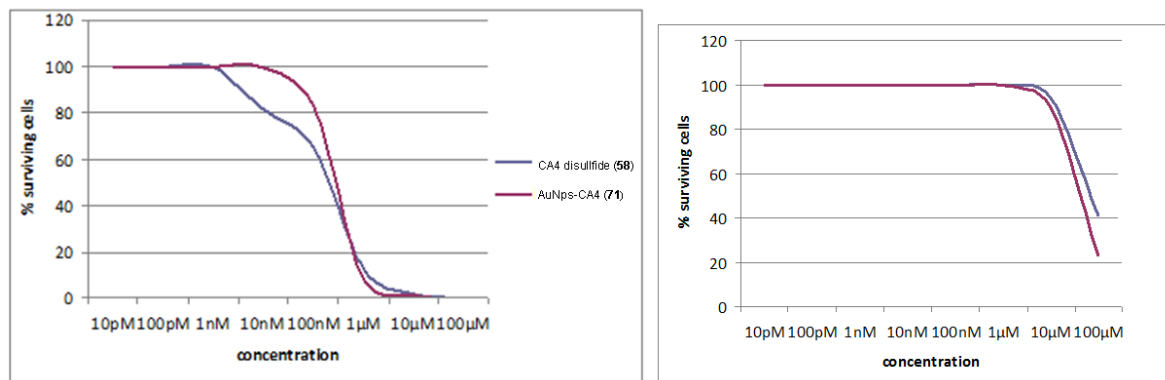

Figure 1.76. Results of MTT test on: left, TE-671 (human rhabdomyosarcoma cell line)and right: HT-29. Cytotoxicity of AuNPs conjugate (**71**) is compared to the one of free drug (CA4 disulfide **58**)

In the case of TE-671 cells, conjugate (**71**) attained a 50% growth inhibition at a sub-micromolar dose: this result has surely to be improved, but it constitutes a satisfactory starting point towards the development of the three-unit targeted drug delivery system.

Nevertheless, product (**71**) approximately presented the same cytotoxic profile as free pro-drug (**58**) and caused greater cell growth inhibition in TE-671 cell line, due to the above mentioned resistance of HT-29 cells to combretastatin.

At any rate, the fact that AuNP-conjugate (**71**) achieves slightly worse results on TE-671 cells in comparison with pro-drug (**58**) should not curb enthusiasm, as the advantages of NPs-conjugates in respect to free drug can be fully revealed only in *in vivo* tests, where EPR effect-mediated targeting occurs. At University of Siena, further investigations are in progress at the moment to better determinate IC_{50} values of conjugate in exam.

1.4 Conclusions and ongoing investigations

The aim of my PhD project has been to synthesize tetrabranched NT peptides (NT4) conjugated to different functional units for selective imaging and killing of cancer cells. Indeed, NT4 peptides efficiently discriminate between tumor and healthy tissue in human surgical samples of colon and pancreas adenocarcinoma from many patients and are, thus, ideal targeting units for drug delivery system in tumor targeted therapy. We decided to work with a large variety of anticancer drugs, all currently used in first-line treatment of cancerous deseases, presenting different mechanism of action and different chemical structures, as therapeutic units.

Following a well-consolidated solid-phase assembling protocol of the aforementioned conjugates, we managed to realize the desired complexes and to *in vitro* test the latters in cancer cell lines, in order to prove the enhanced cytotoxicity respect to the free drug. Mainly,we had to face two limitations of different nature: chemical instability of conjugates to acid conditions required from the used method and lack of multiplicity. The first one was overcome setting up an alternative synthetical procedure that avoided the exposure of conjugates to strong acids (see § 1.2.1), while the second one required the use of nanodevices with high loading of drugs (see § 1.2.3). In both cases, we successfully achieved the prefixed goals.

At the same time, at the University of Siena, in-depth investigations about mechanism of action of neurotensin and its tetrabranched form has been performed. As reported in a recent paper,[248] *Bracci* et all. demonstrate that synthesis of the neurotensin sequence in a tetrabranched form induces a switch of receptor selectivity by decreasing affinity to highaffinity NTR1 (the first biological target identified for neurotensin) and simultaneously allowing binding to additional receptors such as LRP6, and LRP1, belonging to the low density lipoprotein receptors (LDLR) and Sortilin (NTR3, belonging to Vps10d family) which have already been described as important tumor markers.[249] Membrane receptors belonging to the Vps10d family2 or the contiguous family of low density lipoprotein receptors (LDLR)[250] are endocytic receptors that share multiple ligands. Most ligands of LDLR, such as ApoE, are heparin-binding proteins, which bind LDLR and heparan sulfate proteoglycans (HSPGs) by means of repeated pairs of positively charged residues, establishing multimeric ionic interactions with highly repeated negatively charged residues on LDLR or HSPG.[251] Since the neurotensin sequence has one lysine at position 6 and two contiguous arginines at positions 8 and 9, repeated four times in the branched structure of NT4, it seemed reasonable to test whether NT4 bound heparin and other glycosaminoglycans (GAGs). The final confirmation arise from a systematic substitutions of residues in the NT sequence of NT4 (Alanine scan protocol), that proved that binding of NT4 to the protein receptors sortilin, LRP6, and LRP1 is mediated by the same residues, which are also responsible for heparin binding. The determinant role of the cluster of positively charged residues of the NT sequence for NT4 binding to protein receptors and heparin was, thus, clearly confirmed.

1.5 Experimental Section

General synthetic procedures

All the reactions were monitored by TLC on commercially available precoated plates (silica gel 60 F 254) and the products were visualized with acidic vanillin solution.

Silica gel 60, 230–400 mesh, was used for column chromatography, unless otherwise stated. EtP refers to light petroleum, bp 40–60 °C and EtOAc to ethylacetate. ^{1}H and^{13}C NMR spectra were recorded at 400, 200 and 100, 50 MHz, respectively. Melting points were measured on a microscopic apparatus and are uncorrected. FTIR spectra were recorded in KBr pellets or in CDCl$_3$ solutions. Mass spectra were measured with a Shimadzu QP5050 or by FAB (*m*-nitrobenzyl alcohol as matrix) or by ESI using JEOL MStation JMS700.

THF was distilled from sodium in the presence of the blue colour of benzophenone kethyl, toluene was distilled from sodium, CH$_2$Cl$_2$ was distilled from CaH$_2$ and MeOH from Mg.

Commercial available reagents, catalysts and ligands were used as obtained, unless otherwise stated, from freshly opened container without further purifications.

Synthesis of 2'-deoxy-5'-O-[bis(4-methoxyphenyl)phenylmethyl]-5-fluorouridine (2)


2
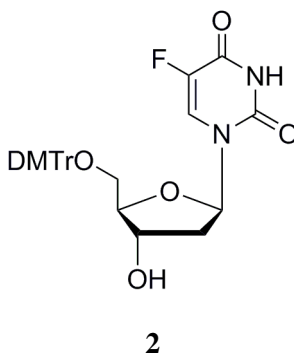
2'-Deoxy-5-fluorouridine (**1**) (0.2 g, 0.81 mmol) was evaporated 3 times with 1 mL of dry pyridine and finally dissolved in 2,7 mL of anhydrous pyridine. Drop wise a solution of 4-4'dimethoxytriphenylmethyl chloride (0.413 g, 1.22 mmol) in 5 mL of dry pyridine was added at 0°C, under stirring. The reaction was stirred at r.t. for 20 h, its colour turned to green. Ice and a saturated solution of $NaHCO_3$ (50 mL) were added, the solution was extracted with CH_2Cl_2 (3x50 mL).The recollected organic phase was dried over dry Na_2SO_4, filtered and evaporated. The crude product was purified by flash chromatography using CH_2Cl_2 : MeOH 25 : 1 as eluent, obtaining the product in 82% yield. ^{1}H NMR, 400MHz, $CDCl_3$, δ: 2.20-2.25 (m, 1H, 2'-H); 2,65-2.70 (m, 1H,2'-H); 3.42-3.38 (m, 2H, 5'-H_2); 3.76 (s, 6H, 2OCH_3); 4.20-4.12 (m, 1H, 4'-H); 4.60-4.45 (m, 1H, 3'-H); 6.31 (at, 1H, J=6,1'-H); 6.90-6.78 (m, 4H, CH_{arom}); 7.15-7.4 (m, 9H, H_{arom});7.83 (d, 1H, J=4.4Hz, 6-H,F).^{13}C NMR, 100MHz, $CDCl_3$, δ: 41.1 (1C, 2'-C); 55.3 (2C, CH_3); 63.4 (1C, 5'-C); 72.0 (1C, 3'-C); 85.6 (1C, 1'-C); 86.5 (1C, Cquat); 87.1 (1C, 4'-C); 113.2 (4H, CH_{arom}); 123.7; 124.4; 126.9; 127.8; 129.8; (10C, C_{arom}+ 6-C); 135.2; 135.0 (2C, C_{quat}); 140.4 (d, 1C, J =236.1Hz, 1-CF); 144.0 (1C, C_{quat}); 148.9 (1C, 4-CO); 157.1; 156.6 (2C, C_{quat}-OCH_3); 158.5 (1C, 2-CO).

Synthesis of 2'-Deoxy-5'-O-[bis(4-methoxyphenyl)phenylmethyl]-5-fluoro-3'-O-(3-carboxypropanoyl)uridine (3)

3
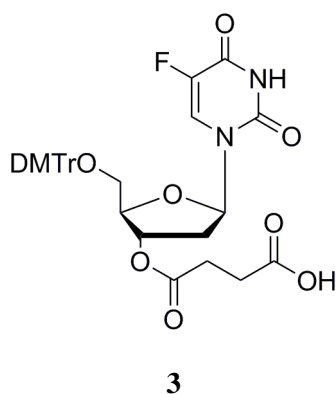
To a solution of compound (**2**) (0.18g, 0.33 mmol) in 4 mL of dry CH$_2$Cl$_2$ DMAP (0.06 g, 0.49 mmol) and succinic anhydride (0.131g, 1.31 mmol) were added. The solution was stirred for 24 h under a N$_2$ atmosphere at r.t. Then the reaction mixture was poured onto 10 mL of water and acidified to pH=3. The solution was extracted with DCM (3x20mL) and the organic phase was washed with water (3 x 50mL), dried over Na$_2$SO$_4$,filtered and evaporated to give compound **3** in 90% yield. ^{1}H NMR,4 00MHz, (CD$_3$)$_2$CO, δ: 2.60-2.40 (m, 6H, 2'-H$_2$ + CH$_2$CH$_2$); 3.58-3.33 (m, 2H, 5'-H2); 3.78 (s, 6H, OCH$_3$); 4.22-4.19 (m, 1H, 4'-H); 5.50-5.43 (m, 1H, 3'-H); 6.28 (at, 1H, J =6.2 Hz, 1'-H); 6.91-6.89 (m, 4H, CH$_{arom}$); 7.50-7.24 (m, 9H, H$_{arom}$); 7.88 (d, 1H, J = 6.8Hz, 6-H,F). ^{13}C NMR, 100 MHz, (CD$_3$)$_2$CO, δ: 29.4; 30.2 (2C, Succ-CH$_2$), 38.2 (C-2); 55.4 (2C, OCH$_3$); 64.5 (C-5); 75.4 (C-3); 84.6 (C-4); 85.7 (C-1); 87.6 (C-Ph$_3$); 113.9 (2C, C$_{arom}$); 124.6 (C-6); 127.6 (1C, C$_{arom}$); 128.6 (1C, C$_{arom}$); 128.7 (1C, C$_{arom}$); 130.8 (2C, C$_{arom}$); 136.1; 136.3 (2C, C$_{arom}$); 141.3 (C-5); 145.6 (1C, C$_{arom}$); 150.3 (C-2); 157.3 (C-4); 159.5 (2C, C$_{arom}$); 172.4; 173.4 (2C, Succ-CO). ESI-MS: m/z = 648 [M+H]$^+$.
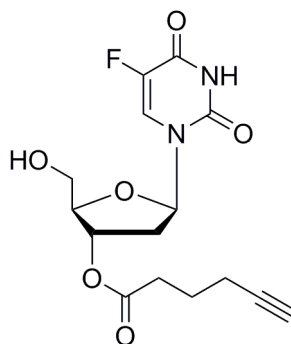
Synthesis of 2'-deoxy-5'-O-[bis(4-methoxyphenyl)phenylmethyl]-5-fluoro-3'-O-(hex-5-ynoate)uridine (38)

38
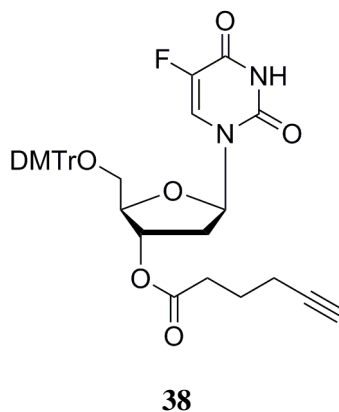
To a solution of 2'-deoxy-5'-O-[bis(4-methoxyphenyl)phenylmethyl]-5-fluorouridine (**2**) (0.60 g, 0.11 mmol) in 2 mL of dry CH$_2$Cl$_2$ 5-hexynoic acid (0.013 g, 0.12 mmol), DMAP (0.001 g, 0.01 mmol) and diisopropylcarbodiimide (19 µL, 0.12 mmol) were added at 0°C, under a N$_2$ atmosphere. A white precipitate was observed. The reaction mixture was stirred for 3 h. at r.t. then poured onto 20 mL of diethyl ether and washed with a saturated solution of NH$_4$Cl (3x50 mL), followed by a saturated

solution of NaHCO$_3$ (2x70 mL). The recollected organic layer was dried over Na$_2$SO$_4$, filtered and evaporated to obtain a white solid (0.04 g). The ^{1}H NMR spectrum still showed the presence of diisopropylurea, removed washing the crude, dissolved in 20 mL of ether, with a saturated solution of NH$_4$Cl (6x30 mL). The organic layer was dried over Na$_2$SO$_4$, filtered and evaporated to obtain a colourless oil (0.90 g) as pure product (**38**) in 62% yield. ^{1}H NMR, 300MHz, acetone-*d*, δ: 1.76-1.87 (m, 1H, CH$_\beta$); 2.05-2.82 (m, 2H, CH$_\beta$ + H$_{vinylic}$); 2.21-2.30 (m, 1H, CH$_\gamma$); 2.36-2.41 (m, 2H, 2'-H); 2.42-2.58 (m, 1H, CH$_\gamma$); 2,74-2.92 (m, 2H, CH$_{2\alpha}$); 3.35-3.60 (m, 2H, 5'-H$_2$); 3.79 (s, 6H, 2OCH$_3$); 4.18-4.22 (m, 1H, 4'-H); 5.55-5.60 (m, 1H, 3'-H); 6.38 (at, 1H, *J*=6,1'-H); 6.89-6.92 (m, 4H, CH$_{arom}$); 7.21-7.51 (m, 9H, H$_{arom}$);7.89 (d, 1H, J=6.6Hz, 6-H,F); 10.20 (bs, 1H, NH).

Synthesis of 2'-deoxy-5-fluoro-3'-*O*-(hex-5-ynoate)uridine (39)

39

2'-deoxy-5'-O-[bis(4-methoxyphenyl)phenylmethyl]-5-fluoro-3'-*O*-(hex-5-ynoate)uridine (**38**) (0.04 g, 0.07 mmol) was dissolved in 2 ml of CH$_3$COOH 80% to obtain a bright orange solution. The reaction mixture was stirred at room temperature for 3 h, then concentrated in vacuum. The crude product was purified by flash chromatography using CH$_2$Cl$_2$: MeOH 25 : 1 as eluent, obtaining the product (**39**) in 70% yield. ^{1}H NMR, 400MHz, CDCl$_3$, δ: 1.82-1.90 (m, 2H, CH$_\beta$); 2.00 (t, 1H, *J*= 2.64Hz, H$_{vinylic}$); 2.26-2.31 (m, 3H, CH$_{2\gamma}$ + 2'-H); 2.42-2.58 (m, 3H, CH$_{2\alpha}$ + 2'-H); 3.95-3.98 (m, 2H, 5'-H$_2$); 4.11-4.14 (m, 1H, 4'-H); 5.35-5.38 (m, 1H, 3'-H); 6.32 (at, 1H, *J*=7.2Hz, 1'-H); 8.04 (d, 1H, J=6.4Hz, H-F); 8.95-8.98 (m, 1H, NH). ^{13}C NMR, 100MHz, CDCl$_3$, δ: 17.76; 23.28; 32.70; 37.80; 62.59; 69.50; 74.90; 82.87; 85.30; 85.78 (10C, C$_{aliphatic}$); 124.51 (1C, C$_{vinylic}$); 140.65 (d, 1C, *J* =235.6Hz, C-F); 148.84 (1C, C=O); 156.54 (1C, C=O); 172.82 (1C, C=O$_{est}$).
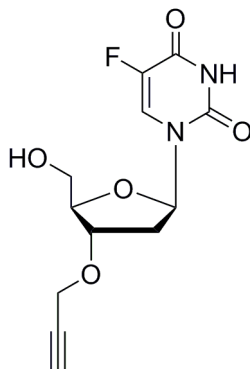
Synthesis of 2'-deoxy-5'-O-[bis(4-methoxyphenyl)phenylmethyl]-5-fluoro-3'-*O*-(prop-2-ynyloxy)uridine (40)
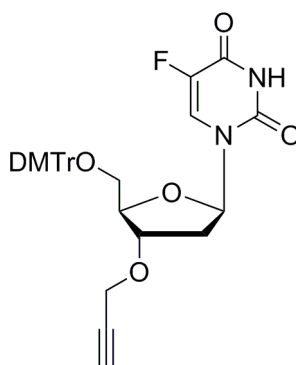
40

2'-deoxy-5'-O-[bis(4-methoxyphenyl)phenylmethyl]-5-fluorouridine (**2**) (0.15 g, 0.27 mmol) was dissolved in 4 mL of dry DMF, obtaining a yellow solution to which Na_2CO_3 (0.07g 0.68 mmol) and propargyl bromide (75 µL, 0.68 mmol) were added, under a N_2 atmosphere. The reaction mixture was stirred for 19 h, then poured onto 30 mL of water and extracted with DCM (3x50 mL). The organic layer was washed with water (3x100 ml) to get rid of the precipitate formed during the extraction, dried over dry Na_2SO_4, filtered and evaporated. The crude product was purified by flash chromatography using CH_2Cl_2 : MeOH 50 : 1 as eluent, obtaining the product in 71% yield. The crude turned out to be not stable to storage since it spontaneousely released the protecting group with time. We, thus proceded to the next synthetical step without isolating it.

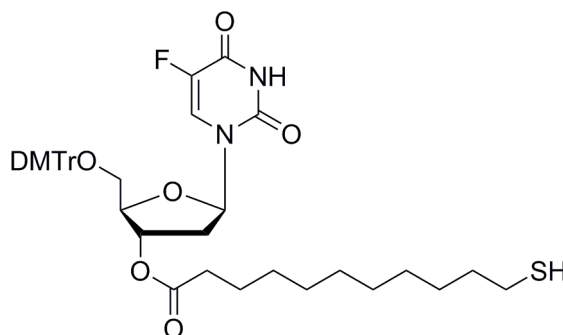**Synthesis of 2'-deoxy-5-fluoro-3'-*O*-(prop-2-ynyloxy)uridine (41)**

41

2'-deoxy-5'-O-[bis(4-methoxyphenyl)phenylmethyl]-5-fluoro-3'-*O*-(prop-2-ynyloxy)uridine (**40**) (0.03 g, 0.06 mmol) was dissolved in 2 ml of CH_3COOH 80%, the solution immediately turned to bright orange. The reaction mixture was stirred at r.t. for 3 h, then poured onto 10 mL of water and extracted with AcOEt (3x20 mL). The organic phase was washed with a saturated solution of $NaHCO_3$ (4x20 mL), the aqueous layer was acidified to pH=4 and extracted with AcOEt (3x40 mL). The recollected organic layer was dried over dry Na_2SO_4, filtered and evaporated to obtain the desired product (**41**) without further purification in 65% yield. ^{1}H NMR, 400MHz, $CDCl_3$, δ: 2.20 (t, 1H, *J*= 2.40 Hz, H$_{vinylic}$); 2.26-2.36 (m, 1H, 2'-H); 2,38-2.48 (m, 1H,2'-H); 3.86-4.10 (m, 2H, 5'-H$_2$); 4.25-4.28 (m, 1H, 4'-H); 4.58-4.62 (m, 1H, 3'-H); 4.72 (d, 2H, *J*= 2.40Hz, CH$_2$); 6.35 (at, 1H, *J*= 6,6 Hz,

1'-H); 7.98 (d, 1H, *J*= 6.3Hz, H-F). IR (CDCl$_3$), cm^{-1}: 3306.03 (m, C-H$_{vinylic}$ stretch.); 2254.31 (m, C-C$_{vinylic}$ stretch.); 1718.27 (s, C=O stretch.); 1666.66 (s, C=O stretch.); 1266.66 (m, C-F stretch.).

Synthesis of (2R,3R,5R)-2-((bis(4-methoxyphenyl)(phenyl)methoxy)methyl)-5-(5-fluoro-3,4-dihydro-2,4-dioxopyrimidin-1(2H)-yl)-tetrahydrofuran-3-yl 11-mercaptoundecanoate (42)


42

To a solution of 2'-deoxy-5'-O-[bis(4-methoxyphenyl)phenylmethyl]-5-fluoro-3'-*O*-(prop-2-ynyloxy)uridine (**2**) (0.072g, 0.13 mmol) in 3 mL of dry DCM, DMAP (0.0016 g, 0.013 mmol) was added, in a N$_2$ atmosphere. The yellowish solution was cooled at 0°C, then11-mercaptoundecanoic acid (0.043 g, 0.2 mmol) was added, followed by DIC (22 µL, 0.14 mmol). The reaction mixture was stirred for 22 h at r.t., then poured onto 20 mL of diethyl ether and washed with a saturated solution of NH$_4$Cl (3x40 mL), then a saturated solution of NaHCO$_3$ (2x40 mL) followed by a saturated solution of NH$_4$Cl (5x40 mL). The recollected organic layer was dried over Na$_2$SO$_4$, filtered and evaporated to obtain a colourless oil (90 mg). The crude was purified by flash chromatography using EtP : AcOEt 2 : 1 as eluent to obtain the final pure product (**42**) as colourless oil in 20% yield. ESI-MS: *m/z* = 747.43 [M-H]$^-$. IR (CDCl$_3$), cm^{-1}:3383.62 (w, N-H stretch.); 3064.64 (w, C-H$_{arom}$ stretch.); 2926.72 (m, C-H$_{alifph}$ stretch.); 2857.75 (w, S-H stretch.); 1722.58 (s, C=O$_{ester}$ stretch.);1705.37 (bs, C=O$_{ketone}$ stretch.+ C=O$_{amide}$ stretch.); 1606.45 (m, N-H bend.).

Synthesis of 2'-deoxy-5'-O-[bis(4-methoxyphenyl)phenylmethyl] 4(bis(4methoxyphenyl)(phenyl)methylamino)-2',2'-difluoro-3'-O-(3-carboxypropanoyl)cytidine (5)
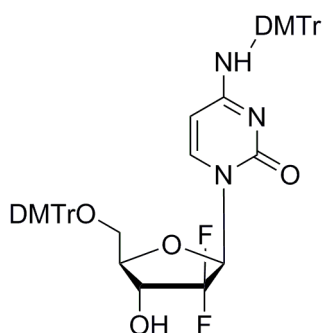
Gemcitabine (**4**) (1.00 g, 3.8 mmol) was dissolved in 8 mL of dry pyridine and evaporated 3 times. The foam was finally dissolved in 54 mL of dry pyridine. A solution of 4,4'dimethoxytriphenylmethyl chloride (3.86 g, 11.4 mmol) in pyridine (54 mL) was added drop wise at 0°C, under a N_2 atmosphere. The reaction mixture was stirred at r.t. for 16 h. The yellow solution was, then, poured onto 100 mL of water and extracted with DCM (3 x 150 mL). The yellow organic layer was washed with water (3 x 200mL) to take pyridine off and dried over Na_2SO_4, filtered and evaporated. The crude product was purified by flash chromatography using AcOEt as eluent to obtain the final product in quantitative yield. ^{1}H-NMR, 200MHz, CDCl$_3$, δ: 3.38-3.52 (m, 2H, 5'-H2); 3.69-3.73 (m, 12H, OCH$_3$); 4.02-4.06 (m, 1H, 4'-H); 4.40-4.45 (m, 1H, 3'-H); 4.88 (d, 1H, J=6.8, H$_{vinyl}$); 6.30-6.42 (m, 1H, 1'-H); 6.70-6.81 (m, 8H, H$_{arom}$); 7.01-7.32 (m, 20H, H$_{arom}$); 7.57 (d, 1H, J=6.8, H$_{vinyl}$). ^{13}C NMR, 100MHz,CDCl$_3$, δ: 55.3 (4C, CH$_3$); 61.2 (1C, 5'-C); 70.4 (1C, 3'-C); 80.4 (2C, C$_{quat}$); 84.5 (1C,1'-C); 86.7 (1C, 4'-C); 95.5 (1C, C$_{vinyl}$); 113.2; 113.6; 127.4; 127.8; 128.3; 128.4; 129.9;130.2 (14C, C$_{arom}$+ 6-C); 135.0; 135.1; 135.7; 136.1 (4C, C$_{quat}$); 141.0 (1C, C$_{vinyl}$); 144.2; 144.8 (2C, C$_{quat}$); 155.1 (1C, CO); 158.4; 158.5 (4C, C$_{quat}$-OCH$_3$); 165.3 (1C, 2-CO). M.p= 143-147°C.

Synthesis of 2'-deoxy-5'-O-(bis(4-methoxyphenyl)phenylmethyl)-4-(bis(4-methoxyphenyl)(phenyl)methylamino)-2',2'-difluoro-3'-O-(3-caroxypropanoyl)cytidine (6)


6
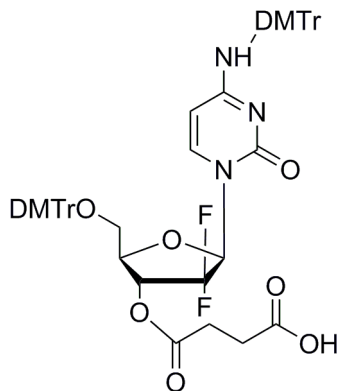
To a solution of compound (**5**) (0.84 g, 0.97 mmol) in 18 mL of dry DCM was added DMAP (0.17 g, 1.45 mmol) and then succinic anhydride (0.39 g, 3.88 mmol). The reaction was stirred at r.t. for 4 h under a N_2 atmosphere. The reaction mixture was poured onto 20 mL of water and acidified to pH=3. The solution was extracted with CH$_3$Cl$_2$ (3x50 mL) and the organic layer was washed with water (3x40mL), dried over Na$_2$SO$_4$, filtered and evaporated. The ester prodrug (**6**) was obtained without further purification in 83% yield. ^{1}H NMR, 400MHz, (CD$_3$)$_2$CO, δ: 2.60-2.70 (m, 4H, CH$_2$CH$_2$); 3.28-3.41 (m, 2H, 5'-H$_2$); 3.73;3.74; 3.75; 3.76 (s, 12H, OCH$_3$). 4.06-4.09 (m, 1H, 4'-H); 4.92 (d, 1H, J=7.6 Hz, H$_{vinyl}$); 5.45-5.51 (m, 1H, 3'-H); 6.39 (at, 1H, J = 6.2 Hz, 1'-H); 6.73-6.82 (m, 8H, CH$_{arom}$); 7.50-

7.24 (m, 18H, H_{arom}); 7.40 (d, 1H, $J=7.6$, H_{vinyl}). ^{13}C NMR, 100 MHz, $(CD_3)_2CO$, δ : 28.7 (2C, Succ-CH_2); 55.1; 55.2 (4C, OCH_3); 60.9 (C-5); 69.7-69.8 (1C, 3'-C); 70.4(C_{quat}); 78.2 (C-4); 83.5-83.7 (C-1); 86.6 (C-Ph_3); 95.6 (1C, C_{vinyl}); 113.2; 113.5 (4C,C_{arom}); 123.5 (C-2); 126.8; 127.4; 127.7;127.9; 128.3; 128.5; 129.1; 129.9; 130.1 (18C,Carom), 134.9; 135.7; 140.0 (4C, C_{arom}); 140.8 (CH); 144.1; 144.4 (2C, C_{arom}); 154.6 (C_{arom}); 158.5; 158.6 (4C, C_{arom}); 165.4 (1C, C-NH); 170.6; 175.3 (2C, Succ-CO). ESI-MS: m/z = 967 [M+H]$^+$.

Synthesis of 2'-deoxy-5'-O-(bis(4-methoxyphenyl)phenylmethyl)-4-(bis(4-methoxyphenyl)(phenyl)methylamino)-2',2'-difluoro-3'-*O*-(hex-5-ynoate) cytidine (43)
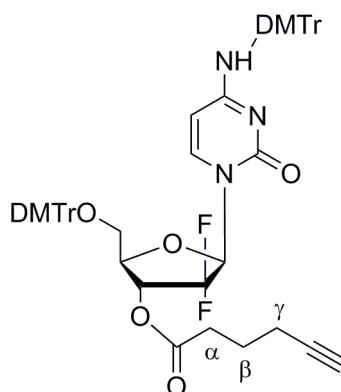
43

To a solution of **5** (0.63 g, 0.72 mmol) in 7 mL of dry DCM, DMAP (0.009 g, 0.072 mmol) was added. The yellow solution was cooled at 0°C, then 5-hexanoic acid (0.09 g, 0.80 mmol) and DIC (0.1 g, 0.8 mmol) were added. The white suspension was stirred at r.t for 2 h, poured onto 50 ml of diethyl ether and filtered. The white solid was dissolved in 25 mL of DCM and washed with a saturated solution of NH_4Cl (6 x 30 mL) to get rid of the side product, DCU. The organic layer was dried over Na_2SO_4, filtered and evaporated to obtain the final pure product, as white solid in 52% yield. ^1H NMR, 400MHz, $CDCl_3$, δ: 1.81-1.89 (m, 2H, $CH_β$); 1.96 (t, 1H, $J= 2.64Hz$, $H_{vinylic}$); 2.22-2.27 (m, 2H, $CH_{2γ}$); 2.05-2.55 (m, 2H, $CH_{2α}$); 3.28-3.32 (m, 1H, 5'-H_2); 3.39-3.44 (m, 1H, 5'-H_2); 3.74; 3.75; 3.76(4s, 12H, $4OCH_3$); 4.05-4.10 (m, 1H, 4'-H); 4.94 (d, 1H, $J= 7.71$ Hz, =H); 5.43-5.50 (m, 1H, 3'-H); 6.42 (at, 1H, $J=8.0Hz$, 1'-H); 6.63-6.83 (m, 8H, $H_{arom.}$); 7.10-7.33 (m, 18H, $H_{arom.}$); 7.39 (d, 1H, J=7.9 Hz, =H). ^{13}C NMR, 100MHz, $CDCl_3$, δ: 17.64 (1C, $C_β$); 23.32 (1C, $C_γ$); 32.24 (1C, $C_α$); 55.13 (4C, CH_3); 61.21 (1C, 5'-C); 69.51 (1C, CH_{vinyl}); 70.30 (1C, 3'-C); 78.05 (2C, C_{quat}); 82.66 (1C,1'-C); 86.73 (1C, 4'-C); 95.27 (1C, C_{vinyl}); 113.20; 113.60; 126.86; 127.46; 127.84; 128.37; 129.83; 129.90;130.03

(14C, C_{arom}+ 6-C); 134.95; 135.91; 136.13 (4C, C_{quat}); 140.95 (1C, C_{vinyl}); 144.34 (2C, C_{quat}); 154.71 (1C, CO); 158.61; 158.69 (4C, C_{quat}-OCH$_3$); 165.47 (1C, C=O); 171.25 (1C, C=O$_{est}$). IR (CDCl$_3$), cm^{-1}: 3392.24 (m, N-H stretch.), 3306.03 (m, C-H$_{vinylic}$ stretch.); 2237.06 (m, C-C$_{vinylic}$ stretch.); 1752.68 (s, C=O$_{est.}$ stretch.); 1662.36 (s, C=O stretch.); 1253.76 (m, C-F stretch.).

Synthesis of 2'-deoxy-2',2'-difluoro-3'-O-(hex-5-ynoate) cytidine
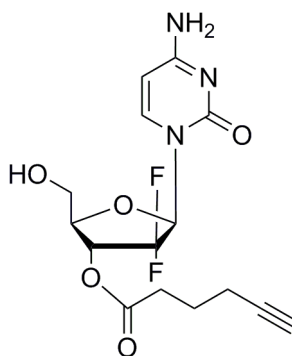
44

Compound **43** (0.13 g, 0.13 mmol) was dissolved in 2 mL of 80% aqueous solution of CH$_3$COOH. The orange solution was stirred for 3 h at r.t., then evaporated to obtain a bright red oil. This oil was dissolved in 1 mL of DCM and 1mL of an aqueous solution of TFA 90% was added. The red solution was stirred at 40°C for 2 h then poured onto 5 mL of EtOH and evaporated. This procedure was repeated two times to obtain a red oil. The crude was purified by flash chromatography using DCM : MeOH 8 : 1 as eluent, followed by DCM : MeOH 5 : 1 after the second spot came out, obtaining the product **44** in 65% yield. ^{1}H NMR, 400MHz, acetone-d, δ: 1.84-1.89 (m, 2H, CH$_\beta$); 2.27-2.31 (m, 2H, CH$_{2\gamma}$); 2.38 (t, 1H, J= 2.6, H$_{vinylic}$); 2.60-2.64 (m, 2H, CH$_{2\alpha}$); 3.82-3.86 (m, 1H, 5'-H$_2$); 3.97-4.01 (m, 1H, 5'-H$_2$); 4.29-4.32 (m, 1H, 4'-H); 4.40 (bs, 1H, OH); 5.49-5.56 (m, 1H, 3'-H); 6.27 (d, 1H, J= 7.71 Hz, =H); 6.33 (at, 1H, J=8.4, 1'-H); 8.02 (d, 1H, J=7.6Hz, =H); 8.25 (bs, 1H, NH); 9.25 (bs, 1H, NH). ^{13}C NMR, 100MHz, acetone-d, δ: 17.13; 23.50; 31.95; 59.46; 69.51; 69.83; 69.97; 79.93; 82.91 (9C C$_{aliphatic}$); 95.46 (1C, C$_{vinylic}$); 121.75 (t, 1C; J= 259 Hz, F-C-F); 142.70 (1C, C$_{vinylic}$); 152.10 (1C, C$_{quat}$); 163.72 (1C, C=O); 171.22 (1C, C=O$_{est}$).

Synthesis of (2R,3S,5R)-2-((bis(4-methoxyphenyl)(phenyl)methoxy)methyl)-5-(4-(bis(4methoxyphenyl)(phenyl)methylamino)-2-oxopyrimidin-1(2H)-yl)-4,4-difluoro-tetrahydrofuran-3-yl 11-mercaptoundecanoate (45)
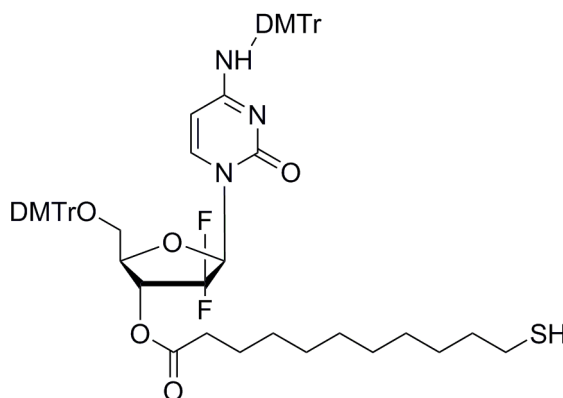

45

To a solution of 2'-deoxy-5'-O-[bis(4-methoxyphenyl)phenylmethyl]-4-(bis(4-methoxyphenyl)(phenyl)methylamino)-2',2'-difluoro-3'-O-(3-carboxypropanoyl)cytidine (**5**) (0.061g, 0.07 mmol) in 2 mL of dry DCM, DMAP (0.001 g, 0.077 mmol) was added, in a N_2 atmosphere. The colourless solution was cooled at 0°C, then11-mercaptoundecanoic acid (0.017 g, 0.077 mmol) was added, followed by DIC (12 µL, 0.077 mmol). After 3 h of stirring, the suspension became a solution. The reaction mixture was stirred for 24 h at r.t.. After the allotted time, the TLC analysis still showed the starting material's spot so 0.4 equiv. of 11-mercaptoundecanoic acid (0.006 g, 0.028 mmol) were added and the reaction mixture was stirred for 14 h, then poured onto 20 mL of diethyl ether and washed with a saturated solution of NH_4Cl (3x40 mL), then a saturated solution of $NaHCO_3$ (2x40 mL) followed by a saturated solution of NH_4Cl (5x40 mL). The recollected organic layer was dried over Na_2SO_4, filtered and evaporated to obtain a colourless oil (65 mg). The crude is purified by flash chromatography using DCM : AcOEt 7 : 1 as eluent to obtain the final pure product as colourless oil (**45**) in 63% yield. ^{1}H NMR, 400MHz, CDCl$_3$, δ: 1.25-1.39 (m, 14H, 7CH$_2$); 1.51-1.62 (m, 2H, CH$_2$); 2.36 (aq, 2H, J= 7.2 Hz, CH$_2$SH); 2.51 (aq, 2H, J= 7.2 Hz, CH$_2$COO); 3.28-3.32 (m, 1H, 5'-H$_2$); 3.39-3.44 (m, 1H, 5'-H$_2$); 3.74; 3.75; 3.76; 3.77(4s, 12H, 4OCH$_3$); 4.05-4.10 (m, 1H, 4'-H); 4.93 (d, 1H, J= 8.0 Hz, =H); 5.41-5.52 (m, 1H, 3'-H); 6.42 (at, 1H, J=8.4 Hz, 1'-H); 6.73-6.82 (m, 8H, H$_{arom.}$); 7.10-7.32 (m, 18H, H$_{arom.}$); 7.39 (d, 1H, J=8.0 Hz, =H). IR (CDCl$_3$), cm^{-1}: 3392.24 (w, NH stretch.); 3064.65 (w, CH$_{arom}$ stretch.); 2926.72 (m, CH$_{aliph}$ stretch.); 2849.13 (m, SH stretch.); 1752.68 (m, C=O$_{est}$); 1658.06 (s, C=O$_{keton}$); 1627.95 (s, C=O$_{amide}$); 1606.45 (m, NH bend).

Synthesis of 4-(2,2-dimethyl-5,6-dioxo-3,4,4a,5,6,10b-hexahydro-2H-benzo(h)chromen-3-yloxy)-4-oxobutanoic acid (8)
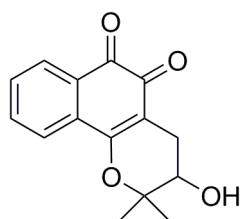
To a solution of Lapachol (**7**) in 7 mL of dry DCM, 1,4 eq. of MCPBA in 8 mL of DCM was added. The dark red solution was stirred under a N_2 atmosphere for 18 h, after the allotted time we decided to add 0,7 eq. of MCPBA because TLC still showed the lapachol spot. The solution turned to green and became a suspension after few minutes. After 1 h the reaction was stopped, pouring it (in a separating funnel) onto a solution of $NaHCO_3$ saturated (50 mL) and extracted with DCM (3x20mL). The recollected organic layers was dried over dry Na_2SO_4, filtered and concentrated whit evaporating rotator. The yellow oil was purified by flash chromatography with EtP : AcOEt 4 : 1 followed by EtO : AcOEt 3 : 1 after the first spot came out, to obtain the final product (**8**) in 49% yield. ^{1}H NMR, 400 MHz, CDCl$_3$, δ: 1.45 (s, 3H, CH$_3$); 1.53 (s, 3H, CH$_3$); 1.90 (s, 1H, OH); 2.64 (dd, 1H, J = 19 and 5.7 Hz, H-4); 2.82 (dd, 1H, J = 19 and 5.3 Hz, H-4); 3.91 (dd, 1H, J = 5.7 and 5.3 Hz, H-3); 7.60-7.66 (m, 3H, H$_{arom}$); 8.02 (d, 1H, J = 6.2 Hz, H$_{arom}$). ^{13}C NMR, 400 MHz, CDCl$_3$, δ: 21.0; 22.6; 23.2; 69.0; 79.7; 110.0; 124.3; 128.8; 130.1; 131.0; 132.0; 135.0; 161.2; 178.6; 179.4. IR, (CDCl$_3$), cm^{-1}: 1700 (OH stretch.), 1630 (C=O stretch.). Mp 203-205°C.

Synthesis of succinic acid mono,(2-dimethyl-5,6-dioxo-3,4,5,6,-tetrahydro-2H-benzo(h)chromen-3-yloxy) ester (9)
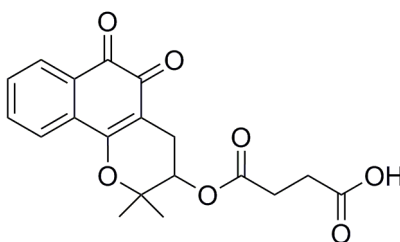
9

To a solution of β-lapachone (**8**) in 18 mL of dry DCM, DMAP and succinic anhydride were added under a N_2 atmosphere,in a two necks flask. The reaction mixture was stirred for 22 h at r.t, then we decided to add 1 equiv. of DMAP and 1 equiv. of succinic anhydride, since starting material's spot on TLC was still visible. The reaction was stirred for 24 h, the solution became a dark yellow suspension. The reaction mixture was poured into 25 mL of water , ice and $NaHCO_3$ ($NaHCO_3$ dissolved the suspension) and extracted with DCM (1x30 mL). The collected yellow water layer was acidified to pH=5 and extracted with DCM (2x100mL). The organic layer was dried over dry Na_2SO_4, filtered and evaporated to give the product (**9**) in 60% yield. ^{1}H NMR, 200 MHz, CDCl$_3$, δ: 1.43 (s, 3H, CH$_3$); 1.48 (s, 3H, CH$_3$); 2.62-2.74 (m, 6H, H-4 and CH$_2$); 5.17 (t, 1H, J= 4.8 Hz, H-3); 7.53 (dt, J = 1.0 and 6.4 Hz 1H, H$_{arom}$); 7.64 (dt, J = 1.6 and 6.0 Hz 1H, H$_{arom}$); 7.84 (dd, J = 1.0 and 6.0 Hz, 1H, H$_{arom}$); 7.64 (dt, J = 1.4 and 6.6 Hz, 1H, H$_{arom}$). ^{13}C NMR, 400 MHz, CDCl$_3$, δ: 22.5; 23.2; 24.9; 29.0; 29.7; 69.4; 79.7; 109.9; 124.3;128.8;130.0;131.0; 134.9; 137.4; 171.2; 179.2.

Synthesis of dihydroxy cisplatin (11)
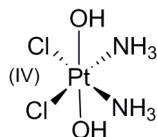
11

A mixture of cisplatin (0.54 g, 1.8 mmol), H_2O_2 (30 wt%, 3.2 mL, 27.4 mmol) in water (24,7 mL) was heated at 65°C for 2 h with vigorous magnetic stirring. Then the heating was removed and the reaction mixture was kept at 4°C for 1 h, allowing a light yellow suspension to precipitate. Water was removed through centrifugation and the obtained powder was crystallized in water at reflux, then kept at 4°C overnight. The bright yellow powder was washed with 25 mL of ice water, 10 mL of EtOH and 10 ml of diethyl ether and vacuum dried to obtain compons **11** in 75% yield. IR (KBr), cm^{-1}: 3518 (O-H free stretch.), 3260 (N-H free stretch.), 2980;2902 (N-H bonded stretch.), 1589 (NH_3^+ bend.), 1034 (Pt-OH bend.), 559 (Pt-O bend), 453 (Pt-N bend).

Synthesis of disuccinate cisplatin (12)
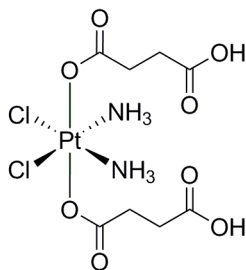
12

In a vial 0,4g of succinic anhydride and 0,345 g of **11** were added to 1,1 mL of dry DMSO deut (we use activated molecular sieves). The suspension was heated at 70°C and stirred for 24 h in the dark. The solvent was removed via lyophilisation. The crude product (pale yellow powder) was crystallized from acetone and allowed to precipitate at -20°C. The powder was isolated via vacuum filtration and washed with ice cold acetone to isolate the product **12** in 31% yield. ^{1}H NMR, 400 MHz , DMSO-d, δ: 2.33-2.38 (m, 4H, CH$_2$); 2.46-2.51 (m, 4H, CH$_2$); 6.4 (bs, 6H, NH$_3$); 12.00 (bs, 2H, COOH). ^{13}C NMR, 100 MHz, DMSO, δ: 30.28 (2C, CH$_2$); 30.91 (2C, CH$_2$); 174.23 (2C, C=O$_{ester}$); 180.02 (2C,COOH). IR (KBr), cm^{-1}: 3400-3000 (broad, stretch. COO-H), 1717 (stretch. C=O$_{ester}$), 1670 (stretch. C=O$_{acid}$). ESI-MS:m/z = 530.97 (90) [M-2H]$^-$.

Synthesis of Estradiol-17-β-O-carbonylpropionic acid (16)
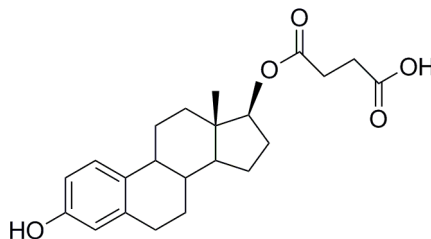
16

To a solution of succinic anhydride (0.1 g, 1.0 mmol) in 1 mL of pyridine heated at 90°C in a vial, estradiol (**15**) (0.1 g, 0.37 mmol) was added. The reaction mixture was stirred at 90°C overnight, then TLC (CHCl$_3$: MeOH : CH$_3$COOH, 10 : 0.5 : 0.2) indicated the complete disappearance of the blue spot of estradiol. The solution was cooled to r.t., mixed with 20 mL of Brine and stirred for 5 minutes. The mixture was, then, extracted with AcOEt (3x30 mL), the collected organic layers were dried over Na$_2$SO$_4$ for 2 h, filtered and evaporated to obtain a light yellow syrup. The syrup was dissolved in 1 mL of MeOH, basified to pH=8-9 with a solution of Na$_2$CO$_3$ (10%) and stirred for 20 h at r.t. The pH was adjusted to 6 with CH$_3$COOH (50%) and the solution was evaporated with evaporating rotator. The residual syrup was suspended in 2 mL of Brine and extracted with AcoEt (3x20 mL); the organic phase was washed with ice water (3x20 mL), dried over Na$_2$SO$_4$, filtered and evaporated. The yellow syrup obtained was kept in refrigerator for two days, allowing it to become a white powder (**16**) in 55% yield. ^{1}H NMR, 400MHz, DMSO-d, δ: 0.82 (s, 3H, CH$_3$); 1.26-1.45 (m, 7H); 1.50-1.60 (m, 1H); 1.68-1.75 (m, 1H); 1.79-1.86 (m, 2H); 2.08-2.18 (m, 3H); 2.13-2.25 (m, 1H); 2.52-2.56 (m, 2H CH$_2$ + DMSO); 2.79-2.73 (m, 2H, CH$_2$); 4.67 (t, 1H); 6.50 (d, J=2.6Hz, 1H$_{arom}$); 6.54 (dd, J$_1$=1.3Hz, J$_2$=10.5Hz, 1H$_{arom}$); 7.08 (d, J=9.2Hz, 1H$_{arom}$); 9.02 (s, 1H, OH$_{phenolic}$); 12.24 (s, 1H, OH$_{acid}$). ^{13}C NMR, 100MHz, DMSO-d, δ: 11.86 (1C, CH$_3$); 22.78; 26.83; 27.05; 28.80 (4C, C$_{aliph.}$); 29.01 (2C, 2CH$_2$); 38.28; 38.89; 40.14; 42.64; 43.23; 49.04; 81.92 (7C, C$_{aliph}$); 112.73; 114.92; 126.00; 130.12; 154.93 (6C$_{arom}$); 171.84 (1C, C$_{ester}$); 173.41 (1C, C$_{acid}$). IR (CDCl$_3$): 3400.56 (OH$_{phenolic}$ stretch.); 3253.03; 3035.12; 2918.76; 1709.09 (C=O$_{ester}$ stretch.); 1619.58 (C=O$_{acid}$ stretch.); 1502.09; 1446.15; 1356.64; 1283.91; 1205.59; 1121.67; 869.93 cm^{-1}. Mp: 148-150°C.
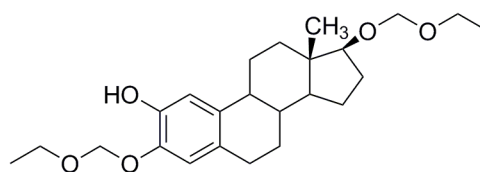
Synthesis of 3,17 β-Estradiol-3,17-bis (ethoxymethyl) ether (17)
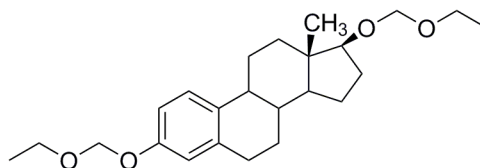
17

To a solution of 3,17 β-estradiol (**15**) (1.0 g, 3.67 mmol) in 5,8 mL of anhydrous THF under a N$_2$ atmosphere, DIPEA (3.8 mL, 22.0 mmol) and chloromethyl ethyl ether (1.7 mL, 18.3 mmol) were added. The mixture was heated at 55°C and stirred for 24 h, during which the colour turned to orange. The suspension was cooled to less than 40°C, then 3 mL of aqueous solution of NH$_4$Cl (20%) were added and magnetic stirring allowed DIPEA hydrochloride to dissolve. The mixture was diluted with 10 mL of AcOEt and the two layers were separated. The organic phase was washed with the solution of NH$_4$Cl previously prepared (3x40 mL) followed by Brine (2x40 mL), dried over Na$_2$SO$_4$, filtered and evaporated. The orange oil was purified by flash chromatography, using CH$_2$Cl$_2$: AcOEt 20 : 1 as eluent to obtain a colourless oil (**17**) (1.3g) in 91% yield. ^{1}H, NMR, 400MHz, CDCl$_3$, δ: 0.80 (s, 3H, CH$_3$); 1.23 (t, 6H, J=7.3Hz, 2 CH$_3$); 1.30-1.36 (m, 2H); 1.36-1.40 (m, 2H); 1.40-1.44 (m, 1H); 1.44-1.46 (m, 1H); 1.44-1.50 (m, 1H); 1.50-1.54 (m, 1H); 1.54-1.56 (m, 1H); 1.56-1.62 (m, 1H); 1.64-1.74 (m, 1H); 1.84-1.90 (m, 1H); 1.99 (dt, 1H); 2.02-2.12 (m, 1H); 2.14-2.24 (td, 1H); 2.28 (dq, 1H); 2.80-2.88 (m, 2H); 3.62 (qd, 2H, CH$_2$); 3.73 (q, 2H, J$_1$=7.3Hz, J$_2$=14Hz, CH$_2$); 4.65 (s, 2H, CH$_2$); 5.20 (s, 2H, CH$_2$); 6.73 (d, J=2.6Hz, 1H$_{arom}$); 6.84 (dd, J$_1$=8Hz, J$_2$=2.6Hz, 1H$_{arom}$); 7.21 (d, J=8Hz, 1H$_{arom}$). ^{13}C NMR, 100MHz, CDCl$_3$, δ : 11,73 (2C, 2CH$_3$); 15.09; 15.13; 23.09; 26.19; 26.27; 28.08; 29.76; 37.29; 38.57; 43.00; 44.01,50.01 (11C$_{aliph.}$); 62.99 (1C, CH$_2$ of $_{aliph}$ CH$_2$CH$_3$); 64.07 (1C, CH$_2$ of $_{phenolic}$ CH$_2$CH$_3$); 86.45 (1C, C-17); 93.22 (1C, CH$_{2aliph.}$); 94.58 (1C, CH$_{2phenolic}$); 113.67; 116.21; 126.31; 133.86; 138.04 (5C, C$_{arom}$); 155.24 (1C, C-3).

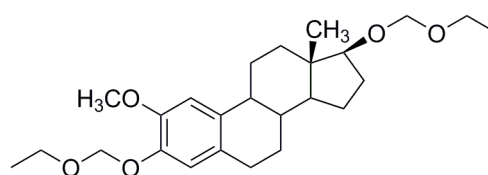**Synthesis of 2-Hydroxyestra-3,17 β-Estradiol-3,17-bis (ethoxymethyl) ether (18)**

18

In a Schlenk linked to vacuum-nitrogen line 3,17 β-Estradiol-3,17-bis (ethoxymethyl) ether (**17**) (1.30 g, 3.35 mmol) was dissolved in 6,5mL of THF anhydrous at -75°C, under a N$_2$ atmosphere. To the obtained solution, sec-butyllithium 1.3M in cyclohexane (4.5 mL, 5.83 mmol) was added drop wise at a rate such that the reaction temperature did not exceed -65°C. The reaction was stirred for 2 h between -70°C and -75°C, then trimethyl borate (1.38g, 13.3mmol) was added maintaining temperature under -60°C. The reaction was allowed to stir for 15 minutes between -70°C and -75°C and then allowed to warm to 0°C. The suspension was quenched with 13 mL of an aqueous solution of NH$_4$Cl (10%) and stirred for 1 h at r.t. Sodium perborate tetrahydrate (2.05 g, 13.30 mmol) was added in portions maintaining the temperature under 35°C and the suspension was stirred for 15 h at r.t. The reaction was filtered to remove inorganic salts and the filtered cake was washed with AcOEt (10x2mL), the layer were then separated. The aqueous layer was extracted with AcOEt (2x20mL). The combined organic phases were washed with Brine (2x50mL), dried over Na$_2$SO$_4$, filtered and

evaporated. The dark yellow oil was dissolved in 3 mL of toluene and filtered to remove inorganic salts and then concentrated in vacuum to give a orange oil. The crude was purified by flash chromatography using EtP : AcOEt 5 : 1 as eluent, to obtain 2-Hydroxyestra-3,17 β-Estradiol-3,17-bis (ethoxymethyl) ether (**18**) in 45% yield as colourless oil. ^{1}H NMR, 400MHz, CDCl$_3$, δ: 0.80 (s, 3H, CH$_3$); 1.23 (t, 6H, J=7.3Hz, 2 CH$_3$); 1.30-1.36 (m, 2H); 1.36-1.40 (m, 2H); 1.40-1.44 (m, 1H); 1.44-1.46 (m, 1H); 1.44-1.50 (m, 1H); 1.50-1.54 (m, 1H); 1.54-1.56 (m, 1H); 1.56-1.62 (m, 1H); 1.64-1.74 (m, 1H); 1.84-1.90 (m, 1H); 1.99 (dt, 1H); 2.02-2.12 (m, 1H); 2.14-2.24 (td, 1H); 2.28 (dq, 1H); 2.80-2.88 (m, 2H); 3.62 (qd, 2H, CH$_2$); 3.73 (q, 2H, J$_1$=7.3Hz, J$_2$=14Hz, CH$_2$); 4.7 (s, 2H, CH$_2$); 5.20 (s, 2H, CH$_2$);5.80-5.90 (bs, 1H, OH); 6.79 (s, 1H$_{arom}$); 6.89 (s, 1H$_{arom}$). ^{13}C NMR, 100MHz, CDCl$_3$, δ: 11,73 (2C, 2 CH$_3$); 15.09; 15.13; 23.09; 26.19; 26.27; 28.08; 29.76; 37.29; 38.57; 43.00; 44.01;50.01 (11C$_{aliph.}$); 62.99 (1C, CH$_2$ of $_{aliph}$ CH$_2$CH$_3$); 64.07 (1C, CH$_2$ of $_{phenolic}$ CH$_2$CH$_3$); 86.45 (1C, C17); 94.55 (1C, CH$_{2aliph.)}$; 94.93 (1C, CH$_{2phenolic}$); 112.35; 116.12; 128.35; 133.86 (4C, C$_{arom}$); 135.19 (1C,C2); 144.17 (1C, C3).

Synthesis of 2-methoxyestra-3,17 β-Estradiol-3,17-bis (ethoxymethyl) ether (19)

19

In a vial to a solution of 2-Hydroxyestra-3,17 β-Estradiol-3,17-bis (ethoxymethyl) ether (**18**) (0.12 g, 0.30 mmol) in 1.0 mL of dry DMF was added Na$_2$CO$_3$ (0.13 g, 1.20 mol) and dimethyl sulfate (57 μL, 0.6 mmol) under a N$_2$ atmosphere. The vial was stopped up and the suspension is stirred at 80°C for 2 days. The reaction mixture was poured onto water and extracted with CH$_2$Cl$_2$ (4 x 20mL). The organic layer was washed several times with water, then dried over Na$_2$CO$_3$, filtered and evaporated to give a brown oil. The crude was purified with flash chromatography, using EtP : AcOEt 5 : 1 as eluent to obtain not totally pure **19**. ^{1}H NMR, 400MHz, CDCl$_3$, δ: 0.80 (s, 3H, CH$_3$); 1.23 (t, 6H, ˏJ=7.3Hz, 2 CH$_3$); 1.30-1.36 (m, 2H); 1.36-1.40 (m, 2H); 1.40-1.44 (m, 1H); 1.44-1.46 (m, 1H); 1.44-1.50 (m, 1H); 1.50-1.54 (m, 1H); 1.54-1.56 (m, 1H); 1.56-1.62 (m, 1H); 1.64-1.74 (m, 1H); 1.84-1.90 (m, 1H); 1.99 (dt, 1H); 2.02-2.12 (m, 1H); 2.14-2.24 (td, 1H); 2.28 (dq, 1H); 2.80-2.88 (m, 2H); 3.62 (qd, 2H, CH$_2$); 3.73 (q, 2H, J$_1$=7.3Hz, J$_2$=14Hz, CH$_2$); 3.84 (s, 3H, OCH$_3$); 4.71 (s, 2H, CH$_2$); 5.20 (s, 2H, CH$_2$); 6.79 (s, 1H$_{arom}$); 6.89 (s, 1H$_{arom}$).
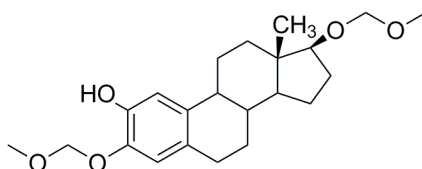
Synthesis of 3,17 β-Estradiol-3,17-bis (methoxymethyl) ether (19b)
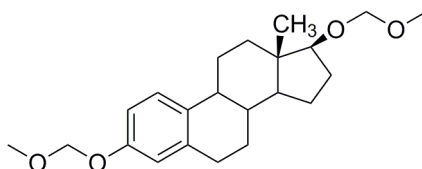
19b

To a solution of 3,17 β-estradiol (**15**) (0.90 g, 3.36 mmol) in 5,3 mL of dry THF under a N$_2$ atmosphere, DIPEA (3.5 mL, 20.1 mmol) and chloromethyl methyl ether (1.26 mL, 16.8 mmol) were added. The mixture was heated at 55°C and stirred for 24 h, during which the colour turned to orange. The suspension was cooled to less than 40°C, then 3 mL of aqueous solution of NH$_4$Cl (20%) were added and magnetic stirring allowed DIPEA hydrochloride to dissolve. The mixture was diluted with 10 mL of AcOEt and the two layers were separated. The organic phase was washed with the solution of NH$_4$Cl previously prepared (3x40 mL) followed by Brine (2x40mL), dried over Na$_2$SO$_4$, filtered and evaporated. The orange oil was purified by flash chromatography, using CH$_2$Cl$_2$: AcOEt 20 : 1 as eluent to obtain a colourless oil (**19b**) (1.3g) in 91% yield. ^{1}H NMR, 400MHz, CDCl$_3$, δ: 0.80 (s, 3H, CH$_3$); 1.30-1.36 (m, 2H); 1.36-1.40 (m, 2H); 1.40-1.44 (m, 1H); 1.44-1.46 (m, 1H); 1.44-1.50 (m, 1H); 1.50-1.54 (m, 1H); 1.54-1.56 (m, 1H); 1.56-1.62 (m, 1H); 1.64-1.74 (m, 1H); 1.84-1.90 (m, 1H); 1.99 (dt, 1H); 2.02-2.12 (m, 1H); 2.14-2.24 (td, 1H); 2.28 (dq, 1H); 2.80-2.88 (m, 2H); 3.62 (qd, 2H, CH$_2$); 3.73 (q, 2H, J_1=7.3Hz, J_2=14Hz, CH$_2$); 4.65 (s, 2H, CH$_2$); 5.20 (s, 2H, CH$_2$); 6.73 (d, J=2.6Hz, 1H$_{arom}$); 6.84 (dd, J_1=8Hz, J_2=2.6Hz, 1H$_{arom}$); 7.21 (d, J=8Hz, 1H$_{arom}$). ^{13}C NMR, 100MHz, CDCl$_3$, δ: 11,73 (2C, 2CH$_3$); 15.09; 15.13; 23.09; 26.19; 26.27; 28.08; 29.76; 37.29; 38.57; 43.00; 44.01; 50.01 (11C$_{aliph.}$); 62.99 (1C, CH$_2$ of $_{aliphatic}$ CH$_2$CH$_3$); 64.07 (1C, CH$_2$ of $_{phenolic}$ CH$_2$CH$_3$); 86.45 (1C, C17); 93.22 (1C, CH$_{2aliph.}$); 94.58 (1C, CH$_{2phenolic}$); 113.67; 116.21; 126.31; 133.86; 138.04 (5C, C$_{arom}$); 155.24 (1C, C-3).

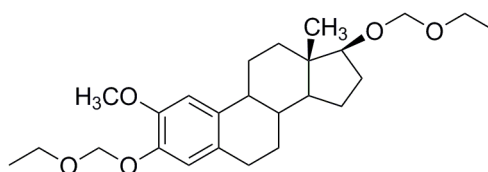**Synthesis of 2-Hydroxyestra-3,17 β-Estradiol-3,17-bis (methoxymethyl) ether (20)**

20

In a Shlenk linked to vacuum-nitrogen line 3,17 β-Estradiol-3,17-bis (ethoxymethyl) ether (**19b**) (1.16 g, 3.22 mmol) was dissolved in 5, 8mL of dry THF at -65°C, under a N$_2$ atmosphere. To the solution obtained sec-butyllithium 1.3M in cyclohexane (4.3 mL, 5.6 mmol) was added drop wise at a rate such that the reaction temperature did not exceed -55°C. The reaction was stirred for 3 h between -60°C and -65°C, then trimethyl borate (1.38 g, 13.3 mmol) was added maintaining temperature under -55°C. The reaction was allowed to stir for 30' between -60°C and -65°C and then allowed to warm to 0°C. The suspension was quenched with12mL of an aqueous solution of NH$_4$Cl (10%) and stirred for 1 h at r.t. Sodium perborate tetrahydrate (1.97 g, 12.8 mmol) was added in portions maintaining the temperature under 35°C and the suspension was stirred for 17 h. The reaction was filtered to remove

inorganic salts and the filtered cake was washed with AcOEt (2x25mL), the layer were then separated. The aqueous layer was extracted with AcOEt (2x50mL). The combined organic phases were washed with Brine (3x100mL), dried over Na_2SO_4, filtered and evaporated. The dark yellow oil was dissolved in 3 mL of toluene and filtered to remove inorganic salts and then concentrated in vacuum to give a orange oil. The crude was purified by flash chromatography using EtP : AcOEt 5 : 1 as eluent, to obtain 2-Hydroxyestra-3,17 β-Estradiol-3,17-bis (ethoxymethyl) ether (**20**) in 45% yield as colourless oil. ^{1}H NMR, 300MHz, CDCl$_3$, δ: 0.80 (s, 3H, CH$_3$); 1.30-1.36 (m, 2H); 1.36-1.40 (m, 2H); 1.40-1.44 (m, 1H); 1.44-1.46 (m, 1H); 1.44-1.50 (m, 1H); 1.50-1.54 (m, 1H); 1.54-1.56 (m, 1H); 1.56-1.62 (m, 1H); 1.64-1.74 (m, 1H); 1.84-1.90 (m, 1H); 1.99 (dt, 1H); 2.02-2.12 (m, 1H); 2.14-2.24 (td, 1H); 2.28 (dq, 1H); 2.80-2.88 (m, 2H); 3.60 (t, 1H, J=8.6Hz, CH$_2$); 3.37 (s, 3H, OCH$_3$); 3.51 (s, 3H, OCH$_3$); 4.65 (s, 2H, CH$_2$); 5.15 (s, 2H, CH$_2$); 5.80-5.90 (bs, 1H, OH); 6.79 (s, 1H$_{arom}$); 6.89 (s, 1H$_{arom}$). ^{13}C NMR, 100MHz, CDCl$_3$, δ: 11,73 (2C, 2CH$_3$); 15.09; 15.13; 23.09; 26.19; 26.27; 28.08; 29.76; 37.29; 38.57; 43.00; 44.01; 50.01 (11C$_{aliph.}$); 62.99 (1C, CH$_2$ of $_{aliphatic}$ CH$_2$CH$_3$); 64.07 (1C, CH$_2$ of phenolic CH$_2$CH$_3$); 86.45 (1C, C17); 94.55 (1C, CH$_{2aliph.}$); 94.93 (1C, CH$_{2phenolic}$); 112.35; 116.12; 128.35; 133.86; (4C, C$_{arom}$); 135.19 (1C,C); 144.17 (1C, C).

Synthesis of 2-Methoxyestra-3,17 β-Estradiol-3,17-bis (methoxymethyl) ether (21)

21

In a vial, to a solution of 2-Hydroxyestra-3,17 β-Estradiol-3,17-bis (methoxymethyl) ether (**20**)(0.55 g, 1.45 mmol) in 3mL of dry acetone were added powdered Na_2CO_3 (0.62 g, 5.80 mmol) and dimethyl sulfate(0.21 mL, 2.20 mmol), under a N$_2$ atmosphere. The reaction was heated at reflux and stirred for 23 h, then filtered to remove Na_2CO_3. The solution was poured onto 20 mL of NH$_4$Cl and extracted with diethyl ether (2x50mL). The organic layer was washed with water (3x70mL), dried over Na_2SO_4, filtered and evaporated to obtain a orange oil as final product (**21**) in 94% yield. ^{1}H NMR, 300MHz, CDCl$_3$, δ: 0.81 (s, 3H, CH$_3$); 1.30-1.36 (m, 2H); 1.36-1.40 (m, 2H); 1.40-1.44 (m, 1H); 1.44-1.46 (m, 1H); 1.44-1.50 (m, 1H); 1.50-1.54 (m, 1H); 1.54-1.56 (m, 1H); 1.56-1.62 (m, 1H); 1.64-1.74 (m, 1H); 1.84-1.90 (m, 1H); 1.99 (m, 1H); 2.02-2.12 (m, 1H); 2.14-2.24 (m, 1H); 2.28 (m, 1H); 2.80-2.88 (m, 2H, H-17); 3.37 (s, 3H, OCH$_3$); 3.51 (s, 3H, OCH$_3$); 3.60 (t, 1H, J=8.6Hz, CH$_2$); 4.65 (s, 2H, CH$_{2aliph.}$); 5.15 (s, 2H, CH$_{2phenolic}$); 6.79 (s, 1H$_{arom}$); 6.89 (s, 1H$_{arom}$). ^{13}C NMR, 100MHz, CDCl$_3$, δ: 11,73 (2C, 2CH$_3$); 15.09; 15.13; 23.09; 26.19; 26.27; 28.08; 29.76; 37.29; 38.57; 43.00; 44.01; 50.01 (11C$_{aliph.}$); 62.99 (1C, CH$_2$ of $_{aliphatic}$ CH$_2$CH$_3$); 64.07 (1C, CH$_2$ of $_{phenolic}$ CH$_2$CH$_3$); 86.45 (1C, C-17); 94.55 (1C, CH$_{2aliph.}$); 94.93 (1C, CH$_{2phenolic}$); 112.35; 116.12; 128.35; 133.86 (4C, C$_{arom}$); 135.19 (1C,C-2); 146.7 (1C,-1).

## Synthesis of 2-Methoxyestra-3,17β-Estradiol (22)
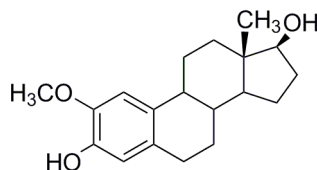
22

A solution of 2-Methoxyestra-3,17β-diol-3,17-bis(methoxymethyl)ether (**21**) (0.54 g, 1.37 mmol) in 0. 8 mL of THF was added drop wise, over a period of 10', to a solution of MeOH (5.34 mL) and HCl 6M (2.5 mL). The resulting yellow solution was stirred at r.t for 21 h, then 9 mL of water were added to allow the precipitation of the product. The white solid was filtered off via vacuum and washed several times with water. The crude product was purified by flash chromatography using CH_2Cl_2 : AcOEt 2 : 1 as eluent to obtain the final product (**22**) as white powder in 75% yield. ^{1}H NMR, 400MHz, DMSO-d, δ: 0.65 (s, 3H, CH_3); 1.00-1.40 (m, 6H); 1.50-1.60 (m, 1H); 1.70-1.80 (m, 2H); 1.81-1.96 (m, 2H); 2.00-2.15 (m, 1H); 2.20-2.35 (m, 1H); 2.58-2.70 (m, 2H); 3.3.45-3.58 (m, 1H, H17); 3.69 (s, 3H, OCH_3); 4.46 (s, 1H, $O_{haliph.}$); 6.42 (s, $1H_{arom}$); 6.74 (s, $1H_{arom}$); 8.54 (s, 1H, $OH_{phenolic}$). ^{13}C NMR, 100MHz, DMSO-d, δ: 11,74 (1C, CH_3); 23.23; 26.69; 27.51; 28.87; 30.38; 37.09; 39.11; 43.28; 44.31; 49.99; 56.22 ($11C_{aliph.}$); 80.51 (1C, OCH_3); 110.18; 116.02, 128.75; 130.87 ($4C_{arom}$); 144.74 (1C, C-1); 146.00 (1C, C-2).

## Synthesis of 2-Methoxyestra-3,17-β-O-carbonylpropionic acid (23)
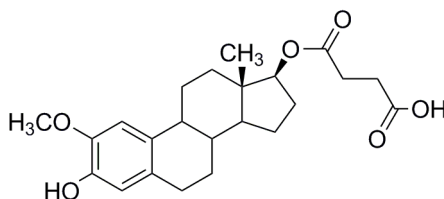
23

To a solution of succinic anhydride (0.12 g, 3.60 mmol) in 1 mL of pyridine, heated at 90°C in a vial 2-methoxyestradiol (**22**) (0.4 g, 1.32 mmol) was added. The reaction mixture was stirred at 90°C overnight, then TLC ($CHCl_3$: MeOH : CH_3COOH, 10 : 0.5 : 0.2) indicated the complete disappearance of the blue spot of 2-methoxyestradiol. The solution was cooled to r.t., mixed with 80 mL of Brine and stirred for 5 minutes. The mixture was then extracted with AcOEt (3x100 mL), the collected organic layers were dried over Na_2SO_4 for 2 h, filtered and evaporated to obtain a light yellow syrup. The syrup was dissolved in 1 mL of MeOH, basified to pH=8-9 with a solution of

Na$_2$CO$_3$ (10%) and stirred for 20 h at r.t. The pH was adjusted to 6 with CH$_3$COOH (50%) and the solution was evaporated with evaporating rotator. The residual syrup was suspended in 8 mL of Brine and extracted with AcOEt (3x100 mL); the organic phase was washed with ice water (3x70 mL), dried over Na$_2$SO$_4$, filtered and evaporated. The yellow syrup obtained was kept in refrigerator for 2 days, allowing it to become a yellow powder (**23**) in 55% yield. ^{1}H NMR, 400MHz, DMSO-d, δ: 0.83 (s, 3H, CH$_3$); 1.26-1.45 (m, 7H); 1.50-1.60 (m, 1H); 1.68-1.78 (m, 1H); 1.81-1.90 (m, 2H); 2.08-2.18 (m, 3H); 2.13-2.25 (m, 1H); 2.59-2.71 (m, 8H CH$_2$+DMSO); 2.73-2.80 (m, 2H, CH$_2$); 3.85 (s, 3H, OCH$_3$); 4.71 (t, 1H, J=8Hz, H-17); 6.63 (s, 1H$_{arom}$); 6.78 (s, 1H$_{arom}$).^{13}C NMR, 100MHz, CDCl$_3$, δ: 12.04 (1C, CH$_3$); 23.20; 26.44; 27.24; 27.47; 28.91 (5C, C$_{aliph.}$); 29.03; 29.13 (2C, 2CH$_2$); 36.88; 38.50; 43.00; 44.04; 49.71; 56.07; 83.20 (7C, C$_{aliph.}$); 108.14; 114.61; 129.4; 131.57; 143.44; 144.58 (6C$_{arom}$); 172.09 (1C, C$_{ester}$); 177.74 (1C, C$_{acid}$). ESI-MS: m/z = 401.18 [M-H]$^-$; 803.09 [2M-H]$^-$.

Synthesis of 3-hydroxy-13-methyl-7,8,9,11,12,13,14,15,16,17-decahydro-6H-cyclopenta[a]phenanthren-17-yl 4-oxo-4-(prop-2-yn-1-ylamino)butanoate (46)
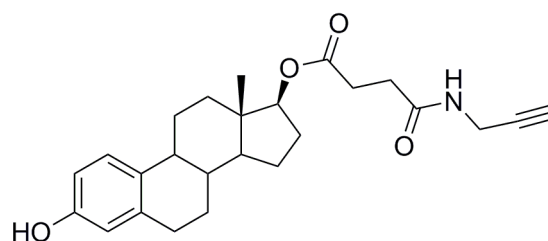

46

To a solution of Estradiol-17-β-O-carbonylpropionic acid (**16**) (0.103 g, 0.276 mmol) in 7 mL of anhydrous THF, HOBt (0.037, 0.276 mmol) and DIC (0.035, 0.276 mmol) were added at 0°C and stirred at this temperature for 0.5 h to provide solution. At 0 °C, propargylamine (18 µL, 0.276 mmol) was added, the pH was adjusted to 8 with TEA (40 µL) and the reaction mixture was stirred at r.t for 22 h. The white suspension was filtered and evaporated to obtain a colourless oil that was solubilised in DCM (20 mL) and washed with a saturated solution of NH$_4$Cl (3x40 mL), then a saturated solution of NaHCO$_3$ (2x40 mL) followed by a saturated solution of NH$_4$Cl (5x40 mL). The recollected organic layer was dried over Na$_2$SO$_4$, filtered and evaporated to obtain a colourless oil. The crude was purified by flash chromatography using DCM : AcOEt 2 : 1 as eluent to obtain the final pure product as white powder oil (**46**) in 54% yield. ^{1}H NMR, 400MHz, CDCl$_3$, δ: 0.81 (s, 3H, CH$_3$); 1.20-1.97 (m, 11H); 2.14-2.21 (m, 2H); 2.28 (t, J= 2.4 Hz, C$H_{vinylic}$, X part of ABX system); 2.29-2.31 (m, 1H); 2.43-2.58 (m, 2H), 2.61-2.68 (m, 2H, CH$_2$); 2.79-2.82 (m, 2H, CH$_2$); 4.05- 4.07 (m, AB part of ABX system); 4.70 (t, J= 8.4 Hz, 1H, H-17); 4.82-5.83 (bs, 1H, OH$_{phenolic}$); 5.84-5.87 (bs, 1H, NH); 6.56 (d, J=2.8 Hz, 1H$_{arom}$); 6.62 (dd, J_1=8.4 Hz, J_2=2.8 Hz, 1H$_{arom}$); 7.12 (d, J=8.4 Hz, 1H$_{arom}$). ^{13}C NMR, 100 MHz, CDCl$_3$, δ: 12.09; 23.23; 26.19; 27.15; 27.51; 29.31; 29.56; 29.61; 30.93; 36.90; 38.53; 43.03; 43.75;

49.74 (14C, C$_{aliph}$); 71.66 (1C, C$_{vinylic}$); 83.22 (1C, C-17); 112.67; 115.22; 126.50; 132.41; 138.14; 153.44 (6C, C$_{arom}$); 171.18 (1C, C=O$_{amide}$); 172.92 (1C, C=O$_{ester}$). ESI -MS: *m/z* = 817.49 [2M-H]$^-$; 852.64 [2M+Cl]$^-$; 841.44 [2M+Na]$^+$.

Synthesis of 3-benzyloxyestra-1,3,3(10).trien-β-ol (47)

47
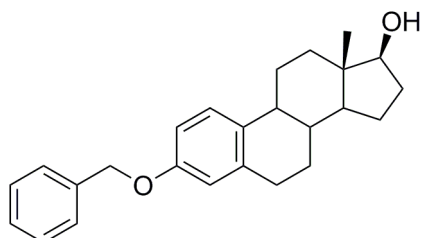
To a solution of β-estradiol (**15**) (0.05 g, 0.18 mmol) in 5 mL of dry acetone, K$_2$CO$_3$ (0.10 g, 0.73 mmol) and benzyl bromide (41 μL, 0.346 mmol) were added, under a N$_2$ atmosphere. The suspension was refluxed for 24 h, then poured onto 20 mL of DCM and filtered. The organic phase was washed with Brine (3 x 40 mL), dried over Na$_2$SO$_4$, filtered and evaporated to obtain a yellowish oil (60 mg), which solidified on standing. The crude was purified by flash chromatography using DCM : AcoEt 8 : 1 as eluent to obtain the final pure product (**47**) as colourless oil in 78% yield. The obtain compound was used in the next step of the procedure, without any further characterization.

Synthesis of 11-(benzylthio)undecanoic acid (49)
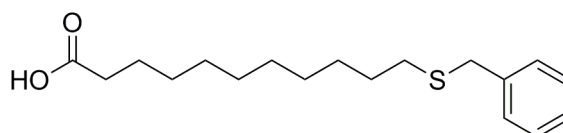
49

To a solution of 11-mercaptoundecanoic acid (0.30 g, 1.37 mmol) in 10 mL of dry EtOH, Na (0.062 g, 2.75 mmol) was added, at 0°C, under a N$_2$ atmosphere. The suspension was stirred 1 h, then again cooled at 0°C and benzyl bromide (16 μL, 1.37 mmol) was added drop wise. The reaction mixture was stirred at r.t overnight, then diluted with 30 ml of cold water and 30 mL of AcoEt. The two layers were separated, the aqueous phase was acidified to pH=2 with 0.1 M HCl and extracted with AcoEt (3 x 50 mL). The recollected organic phase was dried over Na$_2$SO$_4$, filtered and evaporated to obtain a white powder (300 mg). The crude was purified by flash chromatography using DCM : AcoEt 10 : 1 as eluent to obtain the final pure product as white powder (**49**) in 60% yield. ^{1}H NMR, 400MHz, CDCl$_3$, δ: 1.21-1.37 (m, 12H, 6 CH$_2$); 1.54 (quintet, 2H, *J*= 7.6 Hz, CH$_2$); 1.62 (quintet, 2H, *J*= 7.6 Hz, CH$_2$);

2.35 (t, 2H, J= 7.6 Hz, CH$_2$COOH); 2.40 (t, 2H, J= 7.6 Hz, CH$_2$SH); 3.70 (as, 2H, CH$_{2benzylic}$), 7.21-7.32 (m, 5H, H$_{arom.}$). ^{13}C NMR, 100MHz, CDCl$_3$, δ: 24.65; 28.83; 29.02; 29.15; 29.18; 29.02; 29.32; 29.39; 31.39; 34.03 (10C, C$_{aliph.}$); 36.30 (1C, C$_{benz}$); 126.84; 128.42; 128.81; 138.68 (6C, C$_{arom}$); 180.00 (1C, C=O$_{acid}$). IR (CDCl$_3$), cm^{-1}: 3060.34; 3025.86 (w, CH$_{arom}$ stretch.); 2922.41 (s, CH$_{aliph.}$ stretch.); 1707.52 (s, C=O$_{acid}$ stretch.). ESI-MS: m/z = 307.40 [M-H]$^-$.

Synthesis of 11-(benzylthio)undecanoyl chloride (50)
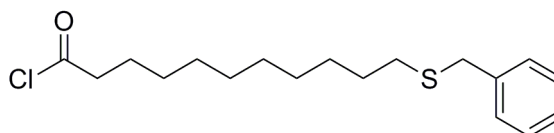
50

To a solution of 11-(benzylthio)undecanoic acid (**49**) (0.19 g, 0.63 mmol) in 10 mL of dry DCM, one drop of dry DMF was added, under a N$_2$ atmosphere. The reaction mixture was cooled at 0°C and a solution of oxalyl chloride (81 µL, 0.95 mmol) in 2 mL of dry DCM was added. The obtained yellow solution was stirred at reflux for 5 h, then dried in vacuum to get rid of the excess of oxalyl chloride, to obtain a bright yellow oil (**50**) (188 mg) in 91% yield. The desired product was not stable enough to record a ^{13}C NMR spectrum. ^{1}H NMR, 300MHz, CDCl$_3$, δ: 1.19-1.41 (m, 12H, 6 CH$_2$); 1.54 (quintet, 2H, J= 7.5 Hz, CH$_2$); 1.70 (quintet, 2H, J= 7.5 Hz, CH$_2$); 2.40 (t, 2H, J= 7.5 Hz, CH$_2$SH); 2.88 (t, 2H, J= 7.5 Hz, CH$_2$COCl); 3.70 (as, 2H, CH$_{2benzylic}$), 7.21-7.31 (m, 5H, H$_{arom.}$). IR (CDCl$_3$), cm^{-1}: 3064.65; 3030.17 (w, CH$_{arom}$ stretch.); 2926.72 (s, CH$_{aliph.}$ stretch.); 1791.39 (s, C=O$_{acid}$ stretch.).

Synthesis of (13S,17S)-3-(benzyloxy)-13-methyl-7,8,9,11,12,13,14,15,16,17-decahydro-6H-cyclopenta[a]phenanthren-17-yl 11-(benzylthio)undecanoate (48)
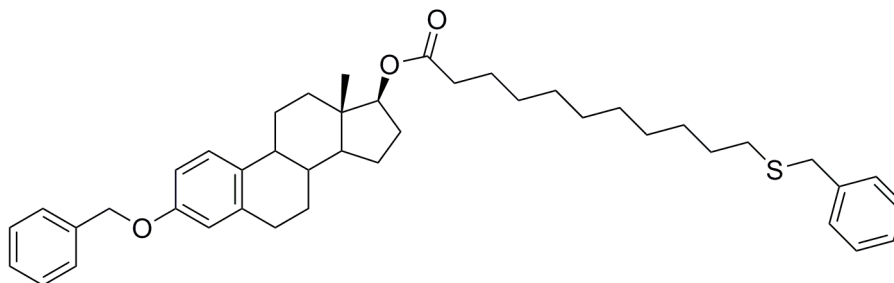
48

To a solution of 3-benzyloxyestra-1,3,3(10).trien-β-ol (**47**) (0.21g, 0.58 mmol) in dry DCM, TEA (160μL, 1.15 mmol) was added, under a N_2 atmosphere. The reaction mixture was cooled at 0°C, a solution of 11-(benzylthio)undecanoyl chloride (0.19 g, 0.58 mmol) was added drop wise, then the obtained yellow solution was stirred at r.t overnight. TLC analysis showed that only a little amount of final compound was formed, so DMAP was added (0.21 g,1.72 mmol) and the reaction mixture was stirred at reflux for 1 day, under a N_2 atmosphere, then diluted with 20 mL of DCM and 20 mL of water. The two phases were separated and the organic layer was washed with a saturated solution of NH_4Cl (3 x 30 mL), dried over Na_2SO_4, filtered and evaporated to obtain a yellowish oil. The crude was purified by flash chromatography using EtP : AcoEt 4 : 1 as eluent to obtain the final pure product (**48**) as colourless oil in 36% yield. IR (CDCl$_3$), cm^{-1}: 3086.20; 3060.34; 3025.86 (w, CH$_{arom}$ stretch.); 2922.41 (s, CH$_{aliph.}$ stretch.); 1720.43 (s, C=O$_{ester}$ stretch.).

Synthesis of 3-hydroxy-13-methyl-7,8,9,11,12,13,14,15,16,17-decahydro-6H cyclopenta[a]phenanthren-17-yl 4-((2-mercaptoethyl)amino)-4-oxobutanoate (51)
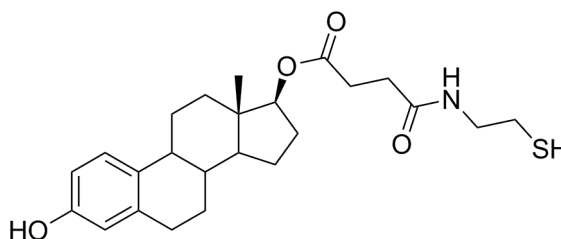

51

To a solution of Estradiol-17-β-O-carbonylpropionic acid (**16**) (0.1 g, 0.274 mmol) in 5 mL of anhydrous THF, HOBt (0.037, 0.274 mmol) and DIC (0.035, 0.274 mmol) were added at 0°C and stirred at this temperature for 0.5 h to provide solution. At 0°C, a solution of cysteamine hydrochloride (0.031 g, 0.274 mmol) in 5 mL of dry THF is added, the pH was adjusted to 8 with TEA (40μL) and the reaction mixture was stirred at r.t for 21 h. The white suspension was filtered and evaporated to obtain a colourless oil that was solubilised in DCM (20mL) and washed with a saturated solution of NH_4Cl (3x40 mL), then a saturated solution of $NaHCO_3$ (2x40 mL) followed by a saturated solution of NH_4Cl (5x40 mL). The recollected organic layer was dried over Na_2SO_4, filtered and evaporated to obtain a colourless oil (80 mg). The crude was purified by flash chromatography using AcOEt : DCM 8 : 1 as eluent to obtain the final pure product (**51**) (35 mg) as colourless oil in 30% yield. ^{1}H NMR, 400MHz, CDCl$_3$, δ: 0.80 (s, 3H, CH$_3$); 1.20-1.95 (m, 9H); 2.15-2.25 (m, 4H);2.43-2.58 (m, 2H), 2.61-2.68 (m, 4H, 2CH$_2$); 2.79-2.82 (m, 2H, CH$_2$SH); 3.44 (aq, *J*= 6.4 Hz, 2H, CH$_2$NH); 4.70 (t, *J*= 6.4 Hz, 1H, H-17); 5.80 (bs, 1H, OH$_{phenolic}$); 6.21 (bs, 1H, NH); 6.57 (d, *J*=2.6 Hz, 1H$_{arom}$); 6.57 (dd, *J$_1$*= 8.4 Hz, *J$_2$*= 1.3 Hz, 1H$_{arom}$); 7.12 (d, *J*=8.4 Hz, 1H$_{arom}$). ^{13}C NMR, 100 MHz, CDCl$_3$, δ: 12.01; 23.18; 24.49; 26.16; 27.12; 27.45; 29.51; 29.67; 31.09; 36.85; 38.49; 42.44; 42.97; 43.69; 49.67 (15C, C$_{aliph}$); 83.17 (1C, C-17); 112.68; 115.24; 126.38; 132.08; 138.00; 153.69 (6C, C$_{arom}$); 171.92 (1C, C=O$_{amide}$); 173.06 (1C, C=O$_{ester}$). IR (CDCl$_3$), cm^{-1}: 3594.82 (m, OH$_{phenol}$ stretch.); 3439.65, 3336.20 (m, NH

stretch. Free and bonded); 3060.34, 3017.24 (w, CH_{arom} stretch.); 2931.03, 2870.68 (w, $CH_{aliph.}$ stretch.); 1720.43 (s, $C=O_{ester}$ stretch.); 1668.81 (s, $C=O_{amide}$ stetch.). ESI -MS: m/z = 454.33 $[M+Na]^+$; 885.17 $[2M+Na]^+$; 861.06 $[2M-H]^-$.

Synthesis of Taxol-2'-hemisuccinate (25)
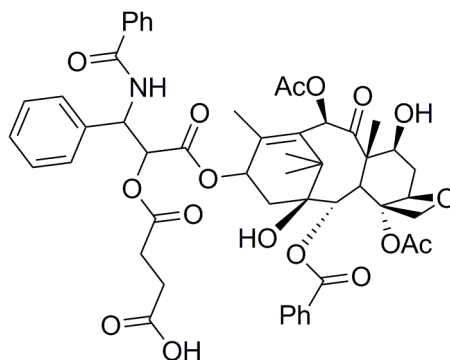
25

To a solution of taxol (**24**) (0.1 g, 0.12 mmol) in 4 mL of dry pyridine, succinic anhydride (0.014 g, 0.14 mmol) and DMAP (0.003 g, 0.02 mmol) WEre added. The obtained solution was stirred for 3 h, at r.t, under a N_2 atmosphere, then the solvent was evaporated under vacuum to obtain a colourless oil. The crude was dissolved in 20 mL of DCM and washed with a saturated solution of NH_4Cl (3 x 40 mL), followed by water (3 x 40 mL), to get rid of residual pyridine. The organic layer was dried over Na_2SO_4, filtered and evaporated to obtain a white solid as pure final compound (**25**) in 38% yield. ^1H NMR and ^{13}C NMR spectra are described in literature.[246] ESI-MS: m/z = 852.17 $[M-succ]^-$, 952.17 $[M-H]^-$, 1906.00 $[2M-H]^-$; 976.17 $[M+Na]^+$.
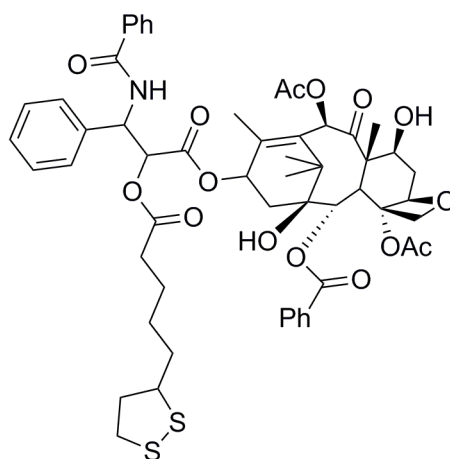
Synthesis of Taxol-2'-5-hexynoate (52)
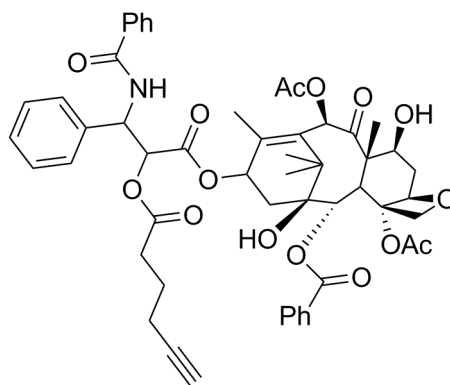
52

To a solution of Paclitaxel (**24**) (0.050g, 0.06 mmol) in 8 mL of dry DCM, DMAP (0.0007 g, 0.006 mmol) was added, in a N$_2$ atmosphere. The colourless solution was cooled at 0°C, then 5-hexynoic acid (0.006 g, 0.06 mmol) was added, followed by DIC (9 μL, 0.06 mmol). The reaction mixture was stirred for 18 h. at r.t., then poured onto 20 mL of DCM and washed with a saturated solution of NH$_4$Cl (3x40 mL), then a saturated solution of NaHCO$_3$ (2x40 mL) followed by a saturated solution of NH$_4$Cl (5x40 mL). The recollected organic layer was dried over Na$_2$SO$_4$, filtered and evaporated to obtain a colourless oil (35 mg). The crude was purified by flash chromatography using EtP : AcOEt 2 : 3 as eluent to obtain the final pure product (**52**) as white powder in 46% yield. ^{1}H NMR, 400MHz, CDCl$_3$, δ: 8.13 (d, J = 8.4 Hz, 2H); 7.74 (d, J = 8.4 Hz, 2H); 7.62-7.38 (m, 11H$_{arom}$); 6.89 (d, J = 9.2 Hz, 1H, NH); 6.30 (s, 1H, H-10); 6.26 (t, J = 9.2 Hz, 1H, H-13); 5.97 (dd, J_1 = 9.2 Hz, J_2= 2.8 Hz, 1H, H-3'); 5.69 (d, J =6.8 Hz, 1H, CH-2); 5.51 (d, J = 3.2 Hz, 1H, H-2'); 4.97 (d, J = 7.36 Hz, 1H, H-5); 4.49-4.41 (m, 1H, H-7); 4.31 (d, J = 8.2 Hz, 1H, H-20); 4.20 (d, J = 8.2 Hz, 1H, H-20); 3.82 (d, J = 7.2 Hz, 1H, H-3); 2.70-2.50 (m, 7H); 2.46 (s, 3H, CH$_3$); 2.34-2.31 (m, 1H); 2.22 (s, 3H, CH$_3$); 2.17 (s, 1H); 1.97 (t, J= 2.4Hz, 1H, H$_{vinyl}$); 1.94 (s, 3H, CH$_3$); 1.82-1.93 (m, 2H, CH$_2$); 1.68 (s, 3H); 1.23 (s, 3H, CH$_3$); 1.14 (s, 3H, CH$_3$). ^{13}C-NMR, 100 MHz, CDCl$_3$, δ: 203.78 (1C, C=O$_{ketone}$); 172.04; 171.21; 169.76; 168.03; 167.03 (6C, C=O); 142.75; 136.95; 133.65; 133.60; 132.78; 132.00; 130.20; 129.17; 129.06; 128.71; 128.46; 127.07; 126.47 (20C, C$_{arom}$+ C=C); 84.42; 82.93; 81.06; 79.15; 75.57; 75.09; 74.00; 72.10; 69.47; 58.51; 52.72; 45.55; 43.15; 35.55; 32.25; 26.79; 23.36; 22.67; 22.57; 22.11; 20.78; 17.49; 14.78; 9.57 (27C, C$_{aliph.}$). IR (CDCl$_3$), cm^{-1}: 3607.75, 3573.27 (m, OH free and bonded stretch.); 3512.93, 3443.96 (m, NH free and bonded stretch.); 3306.03 (m, CH$_{alkyne}$ stretch.); 3060.34 (w, CH$_{arom}$ stretch.); 2961.20, 2918.10, 2857.75 (w, CH$_{aliph.}$ stretch.); 1739.78 (s, C=O$_{ester}$ stretch.); 1718.27 (s, C=O$_{ketone}$ stretch.); 1670.96 (s, C=O$_{amide}$ stretch.). ESI -MS: m/z = 970.33 [M+Na]$^+$.

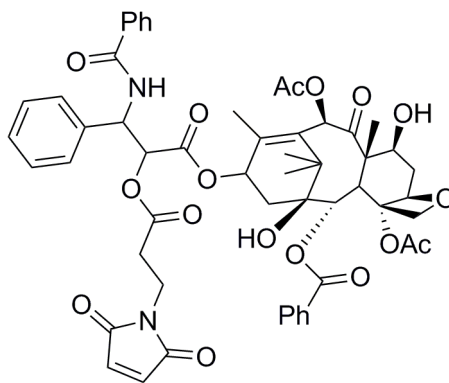**Synthesis of Taxol-2'- DL-α-lipoic ester (53)**

53

To a solution of Paclitaxel (**24**) (0.050g, 0.06 mmol) in 8 mL of dry DCM, DMAP (0.0007 g, 0.006 mmol) was added, in a N$_2$ atmosphere. The colourless solution was cooled at 0°C, then DL-α-lipoic acid (0.012 g, 0.06 mmol) was added, followed by DIC (9 μL, 0.06 mmol). The reaction mixture was stirred for 22 h at r.t., then poured onto 20 mL of DCM and washed with a saturated solution of NH$_4$Cl (3x40 mL), then a saturated solution of NaHCO$_3$ (2x40 mL) followed by a saturated solution of NH$_4$Cl

(5x40 mL). The recollected organic layer was dried over Na$_2$SO$_4$, filtered and evaporated to obtain a colourless oil (35 mg). The crude was purified by flash chromatography using EtP : AcoEt 2 : 3 as eluent to obtain the final pure product as colourless oil in (**53**) in 25% yield. ^{1}H NMR and ^{13}C NMR spectra are reported in literature.[203] ESI -MS: *m/z* = 1064.42 [M+Na]$^+$; 1077.39 [M+Cl]$^-$.
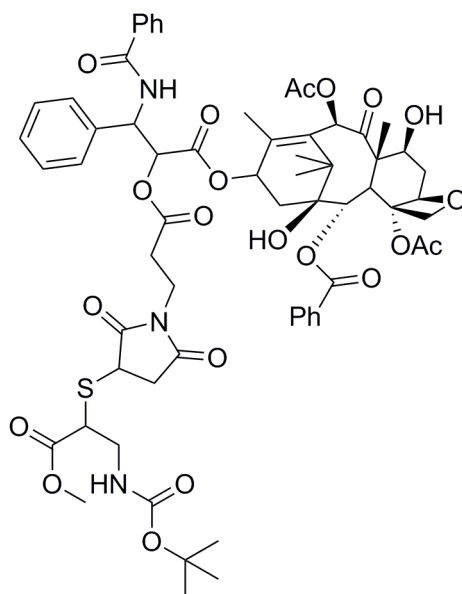
Synthesis of 2'-maleimido-paclitaxel (54)

54

To a solution of Paclitaxel (**24**) (0.050g, 0.06 mmol) in 8 mL of dry DCM, DMAP (0.0007 g, 0.006 mmol) was added, under a N$_2$ atmosphere. The colourless solution was cooled at 0°C, then 3-maleimidopropionic acid (0.01 g, 0.06 mmol) was added, followed by DIC (9 µL, 0.06 mmol). The reaction mixture was stirred for 18 h at r.t. to give a reddish solution, then poured onto 20 mL of DCM and washed with a saturated solution of NH$_4$Cl (3x40 mL), then a saturated solution of NaHCO$_3$ (2x40 mL) followed by a saturated solution of NH$_4$Cl (5x40 mL). The recollected organic layer was dried over Na$_2$SO$_4$, filtered and evaporated to obtain a reddish oil (48 mg). The crude was purified by flash chromatography using EtP : AcoEt 2 : 3 as eluent to obtain the final pure product (**54**) as white powder in 52% yield. ^{1}H NMR, 400MHz, CDCl$_3$ reported in literature.[206] ^{13}C-NMR, 100 MHz, CDCl$_3$, δ: 9.59; 14.77; 20.80; 22.14; 22.67; 26.77; 32.47; 33.29; 35.48; 43.13; 45.54; 52.36; 58.49; 71.74; 72.09; 74.47; 75.12; 75.60; 79.14; 81.02; 84.45 (24C, C$_{aliph.}$) 126.52; 127.43; 128.27; 128.50; 128.72; 129.01; 129.22; 130.26; 131.87; 132.67; 133.64; 134.03; 136.87; 142.86 (22C, C$_{arom}$+ 2C=C); 167.04; 167.24; 167.68; 169.36; 169.88; 171.24 (7C, C=O); 203.83 (1C, C=O$_{ketone}$). IR (CDCl$_3$), cm^{-1}: 3607.75, 3517.24 (m, OH stretch. free and bonded); 3387.93 (m, NH stretch. bonded); 3060.96 (w, CH$_{arom}$ stretch.); 2948.27, 2896.55 (w, CH$_{aliph.}$ stretch.); 1737.63 (s, C=O$_{ester}$ stretch.); 1711.82 (s, C=O$_{ketone}$ stretch.); 1664.51 (s, C=O$_{amide}$ stretch.). ESI -MS: *m/z* = 1027.33 [M+Na]$^+$; 1039.67 [M+Cl]$^-$.

Synthesis of (2aR,4S,4aS,6R,11S,12S,12bS)-9-((3-benzamido-2-((3-(3-((3-((tert-butoxycarbonyl)amino)-1-methoxy-1-oxopropan-2-yl)thio)-2,5-dioxopyrrolidin-1-yl)propanoyl)oxy)-3-phenylpropanoyl)oxy)-12-(benzoyloxy)-4,11-dihydroxy-4a,8,13,13-tetramethyl-5-oxo-2a,3,4,4a,5,6,9,10,11,12,12a,12b-dodecahydro-1H-7,11-methanocyclodeca[3,4]benzo[1,2-b]oxete-6,12b-diyl diacetate (55)


55

To a solution of 2'-maleimido-paclitaxel (**54**) (0.009 g, 0.0093 mmol) in 2 mL of dry DMF, a solution of N-Boc cysteine methylester (0.0022 g, 0.0093 mmol) in 1 mL of dry DMF and TEA (13µL, 0.0093 mmol) were added and stirred at r.t for 1 h. The reaction mixture was diluted with 10 mL of water and extracted with DCM (3 x 20 mL). The recollected organic phase was washed with water (3 x 20 mL), followed by a saturated solution of NH_4Cl (2 x 50 mL), then dried over Na_2SO_4, filtered and evaporated to obtain a colourless oil (9 mg). The crude was purified by flash chromatography using EtP : AcOEt 1 : 3 as eluent to obtain the final pure product (**55**) as colourless oil in 37% yield. The ^{1}H NMR spectrum was pretty complicated due to the presence of two diasteroisomers. Anyway, the disappearing of the signal related to the double bond of maleimido acid and the shift of the signals related to cysteine were clear evidences of the successful coupling. ^{1}H NMR, 400MHz, $CDCl_3$, δ: 8.17 (d, J = 7.8 Hz, 2H); 7.74 (d, J = 8.4 Hz, 2H); 7.63-7.31 (m, 11H$_{arom}$); 6.29 (s, 1H, H-10); 6.18-6.25 (m, 1H, H-13); 6.01 (dd, J_1 = 9.2 Hz, J_2= 2.8 Hz, 1H, H-3'); 5.69 (d, J =7.8 Hz, 1H, CH-2); 5.46-5.50 (m, 1H, H-2'); 5.23-5.30 (m, 1H, NH); 4.99 (d, J = 9.0 Hz, 1H, H-5); 4.51-4.58 (m, 1H, H-7); 4.41-4.90 (m, 1H, C*H*NH); 4.32 (d, J = 8.8 Hz, 1H, H-20); 4.20-4.25 (m, 1H, H-20); 3.93-4.01 (m,1H, C*H*S); 3.82 (d, J = 7.2 Hz, 1H, H-3); 3.73 and 3.70 (s, 6H, 2OCH$_{3\text{diasteroisomers}}$); 3.31-3.44 (m, 2H);2.84-2.99 (m, 2H, CH$_2$S); 2.70-2.50 (m, 6H); 2.51 (s, 3H, CH$_3$); 2.34-2.31 (m, 1H); 2.25 (s, 3H, CH$_3$); 2.17 (s,

1H); 1.92 (s, 3H, CH$_3$); 1.69 (s, 3H); 1.41 (s, 9H, *t*-butyl); 1.23 (s, 3H, CH$_3$); 1.14 (s, 3H, CH$_3$). ESI - MS: *m/z* = 1262.50 [M+Na]$^+$; 1274.58 [M+Cl]$^-$.

Synthesis of (3,4,5-trimethoxyphenyl)methanol (27)
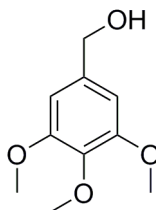
27

A solution of 3,4,5-trimethoxybenzaldehyde (**26**) (4.00 g, 20.41 mmol) in 40 mL of dry MeOH was chilled to 0 °C and NaBH$_4$ (0.94 g, 24.70 mmol) was added in small portions over 1 h. The resulting mixture was stirred overnight at r.t. and concentrated. The crude product was partitioned between Et$_2$O and water. The aqueous layer was extracted with Et$_2$O (3x100 mL) and combined organic phases dried and evaporated to obtain the final product (**27**) in 88% yield. ^{1}H NMR, 200 MHz, CDCl$_3$, δ: 3.81 (s, 3H, OCH$_3$); 3.83 (s, 6H, OCH$_3$); 4.60 (s, 2H, CH$_2$); 6.57 (s, 2H, H$_{arom}$).

Synthesis of 5-(bromomethyl)-1,2,3-trimethoxybenzene (28)
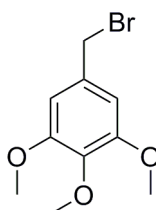
28

To a solution of **27** (3.02 g, 15.25 mmol) in 20 mL of dry CH$_2$Cl$_2$, cooled to -5 °C, a solution of PBr$_3$ (3.05 g, 11.29 mmol) in 10 mL of dry CH$_2$Cl$_2$ was added dropwise. The reaction mixture was stirred at the same temperature for 45 minutes, poured onto ice, neutralized with NaHCO$_3$ and stirred for 1h. The water phase was extracted with CH$_2$Cl$_2$ (5x100mL) and the recollected organic layers were washed with brine (2x150mL) and dried to obtain compound 28 in 96% yield. ^{1}H NMR, 200 MHz, CDCl$_3$, δ: 3.81 (s, 3H, OCH$_3$); 3.83 (s, 6H, OCH$_3$); 4.60 (s, 2H, CH$_2$); 6.57 (s, 2H, H$_{arom}$).

Synthesis of triphenyl(3,4,5-trimethoxybenzyl)phsphonium bromide (29)
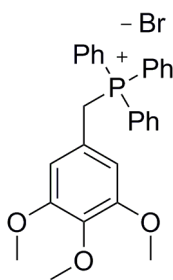
29

A solution of triphenylphosphine (3.94 g, 14.17 mmol) in 11 mL of toluene was added to a solution of **28** (3.75 g, 14.42 mmol) in 16 mL of toluene. The reaction mixture was stirred for 24 h at r.t. and the white precipitate formed filtered and dried to give the phosphonium salt (**29**) in 66% yield. ^{1}H NMR, 200 MHz, D$_2$O, δ: 3.27 (s, 6H, OCH$_3$);3.54 (s, 3H, OCH$_3$); 4.46 (d, J = 14.2 Hz, 2H, P-CH$_2$); 6.03 (d, J = 2.6 Hz 2H, H$_{arom}$);7.38-7.50 (m, 12H, H$_{arom}$); 7.60-7.76 (m, 3H, H$_{arom}$).

Synthesis of (Z)-5-(2-methoxy-5-(3,4,5-trimethoxystyryl)phenoxy)-5-oxopentanoic acid (31)
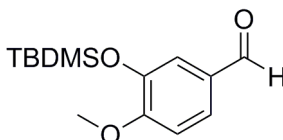
31

To a solution of isovanillin (**30**) (4.00 g, 26.31 mmol) in 30 mL of dry DMF, imidazol (2.68 g, 39.46 mmol) and a solution of TBDMSCl (4.76 g, 31.58 mmol) in 10 mL of dry DMF were added. The solution was stirred at r.t for 2 h, then diluted with 100 mL of water and extracted with EtP (2x50 mL). The combined organic phases were washed with a saturated solution of NaHCO$_3$ (1x100mL) and water (6x100mL), then dried over Na$_2$SO$_4$, filtered and concentrated under vacuum.The crude product was purified by flash chromatography with 80 : 1 CH$_2$Cl$_2$: EtP to give **31** in 99% yield. ^{1}H NMR, 200 MHz, CDCl$_3$, δ: 0.17 (s, 6H, CH$_3$); 1.00 (s, 9H, tBu); 3.89 (s, 3H, OCH$_3$); 6.95 (d, J=8.3 Hz, 1H, H$_{arom}$); 7.37 (d, J=2 Hz, 1H, H$_{arom}$); 7 .48(dd, J_1=8 Hz, J_2=2 Hz, 1H, H$_{arom}$); 9.82 (s, 1H, CHO).
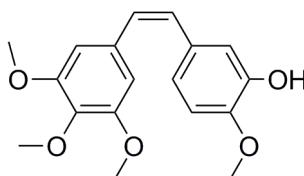
Synthesis of (z)-tert-butyl(2-methoxy-5-(3,4,5 trimethoxystyryl)phenoxy)dimethylsilane (32)
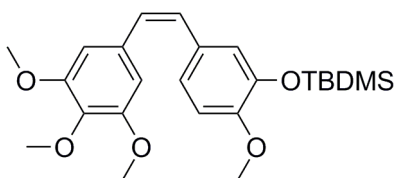
32

After application of two cycles using vacuum/nitrogen Schlenk line, a suspension of triphenylphosfonium bromide (**29**) (1.00 g, 1.91 mmol) in 50 mL of dry THF is put in the Schlenk and cooled at -23°C. Butyl lithium 1,3 M in hexane (1.24 mL, 1,98 mmol) was added drop wise and the orange suspension was stirred for 1 h. Then aldehyde **31** (0.53 g, 1.99 mmol) was added drop wise, the colour of the suspension turned to white and was stirred for 4 h. Finally, iced water and Brine solution were added and the mixture product was extracted with Et_2O (3x70mL). The organic phased was washed with water (2x100 mL), dried over Na_2SO_4, filtered and evaporated. The crude product was purified by flash chromatography with EtP : AcOEt 10 : 1 to isolate Z-stilbene (**33**) in 37% yield. ^{1}H NMR, 400 MHz, $CDCl_3$, δ: 0.06 (s, 6H, CH_3); 0.93 (s, 9H, CH_3); 3.70 (s, 6H, OCH_3); 3.77 (s, 3H, OCH_3); 3.83(s, 3H, OCH_3); 6.44 (d, J=2.2 Hz, 2H, H_{arom}); 6.49 (s, 2H, H_{arom}); 6.71-6.90 (m, 3H, H_{arom}). ^{13}C NMR, 100 MHz, $CDCl_3$, δ:18.3 (1C, $C(CH_3)_3$); 25.6 (3C, C_{tert}); 55.9 (1C, OCH_3); 105.9 (2C,C_{arom}); 111.6 (1C, C_{arom}); 121.3 (2C, C_{arom}); 122.8 (2C, CH=CH) 129.7; 130.0; 131.1 (3C, C_{arom}); 150.3(2C, C_{arom}); 152.9 (1C, C_{arom}).
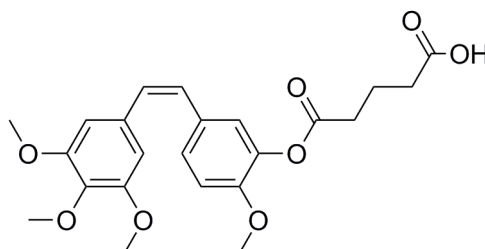
Synthesis of Combretastatin A4 (33)

33

To a solution of (z)-tert-butyl(2-methoxy-5-(3,4,5-trimethoxystyryl)phenoxy)dimethylsilane (**33**) (0.018 g, 0.04 mmol) in 1mL of dry THF, cooled at 0°C, was added drop wise a solution of

TBAF$_3$H$_2$O (0.014 g, 0.005 mmol) dissolved in 0.5 mL of dry THF, under a N$_2$ atmosphere. The solution was stirred at r.t for 3 h, then 0.9 equiv. of TBAF$_3$H$_2$O in o.4mL were added at 0°C because the TLC analysis still showed starting product's spot. After 1 h the reaction mixture was poured onto 5mL of a satureted aqueous solution of NH$_4$Cl and extracted with AcOEt(3X10mL). The recollected organic layer was washed with Brine (2X25mL), dried over Na$_2$SO$_4$, filtered and evaporated to obtain a yellow oil. The crude product was purify by flash chromatography using EtP : AcOEt 3 : 2 as eluent, to give Combratastatin A-4 (**33**) in 87% yield. ^{1}H NMR, 300 MHz, CDCl$_3$, δ: 3.69 (s, 6H, OCH$_3$); 3.84 (s, 3H, OCH$_3$); 3.87 (s, 3H, OCH$_3$); 5.51 (s, 1H, OH); 6.43 (AB system, J=12.3 Hz, 2H, H$_{arom}$); 6.53 (s, 2H, H$_{arom}$); 6.70-6.82 (m, 2H, H$_{arom}$); 6.92 (d, J=1.8 Hz, 1H, H$_{arom}$).

Synthesis of (Z)-5-(2-methoxy-5-(3,4,5-trimethoxystyryl)phenol)-5-oxopentanoic acid (35)

35

To a solution of Combretastatin A-4 (**33**) (0.011 g, 0.035 mmol) in 1mL of dry DCM, glutaric anhydride (0.094 g, 0.08 mmol) and DMAP (0.034g, 0.21mmol) were added and the resulting mixture stirred at r.t. for 16 h then refluxed for 24 h, under a N$_2$ atmosphere. The yellow solution was poured onto ice/water/NaHCO$_3$ (5%). The suspension was acidified to pH 5 using HCl (20%) and extracted with DCM (3x50mL). The recollected organic phases was washed with a saturated solution of NaHCO$_3$ (1x50mL) and water (1x50mL), then dried to give the final product as colourless oil (**35**) in 50% yield without further purification. ^{1}H NMR, 200 MHz, CDCl$_3$, δ: 2.05 (q, 2H, J=7.1 Hz, CH$_2$); 2.51 (t, 2H, J=7.1 H, CH$_2$); 2.59 (t, 2H, J=7.1 Hz, CH$_2$); 3.70 (s, 6H, OCH$_3$); 3.80 (s, 3H, OCH$_3$); 3.83 (s, 3H, OCH$_3$); 6.45 (s, 2H, H$_{arom}$); 6.50 (s, 2H, H$_{arom}$); 6.76 (d, J=8.4 Hz, 1H, H$_{arom}$); 6.99 (d, J=1.8 Hz, 1H, H$_{arom}$); 7.12 (dd, J_1=8.4 Hz, J_2=1.8 Hz, 1H, H$_{arom}$). ^{13}C NMR, 50 MHz, CDCl$_3$, δ: 20.0, 32.7, 32.9 (1C, CH$_2$); 55.9 (1C, OCH$_3$), 56.0 (2C, OCH$_3$); 60.9 (1C, OCH$_3$); 105.7 (2C, CH$_{arom}$); 111.8 (1C, C$_{arom}$); 122.9, 127.7 (1C, CH$_{arom}$); 128.4, 129.3 (1C, CH$_{vinyl}$); 129.9 (1C, CH$_{arom}$); 132.4, 136.9, 139.1, 150.0 (1C, C$_{arom}$); 152.8 (2C, C$_{arom}$); 170.6, 177.8 (1C, C=O).

Synthesis of (Z)-5-(2-methoxy-5-(3,4,5 trimethoxy styryl) fenyl)-11-mercapto-undecanoate (56)
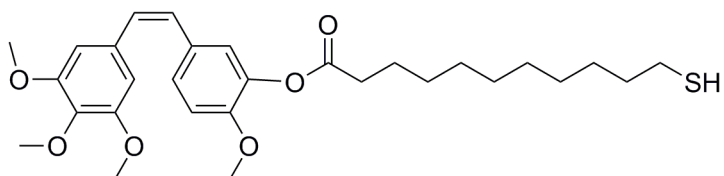
56

To a solution of combretastatin A-4 (**33**) (0.070 g, 0.221 mmol) in 8 mL of dry DCM, DMAP (0.003 g, 0.022 mmol) and 11-mercaptoundecanoic acid (0.050 g, 0.022 mmol) were added, under a N$_2$ atmosphere. After 5', the reaction mixture was cooled to 0°C and DIC (38 µL, 0.243 mmol) was added dropwise, then stirred at r.t. for 19 h. After that, DIC (75 µL, 0.486 mmol) and DMAP (3 mg, 0.022 mmol) were added and the thus obtained solution is allowed to stir at r.t. for another h. The reaction mixture was then diluted with 20 mL Et$_2$O and washed with a saturated solution of NH$_4$Cl (6x20 mL), then a saturated solution of NaHCO$_3$ (3x20 mL). The recollected organic layer was dried on Na$_2$SO$_4$, filtered and evaporated. The crude product was purified by flash chromatography with EP : AcOEt 7 : 1 to give ester **56** as colorless oil in 67% yield. ^{1}H NMR, 400 MHz, C$_6$D$_6$, δ: 1.13-1.23 (bs, 12H, 6CH$_2$); 1.35-1.43 (m, 2H, 1CH$_2$); 1.61-1.65 (m, 2H, 1CH$_{2\beta}$); 2.21 (apparent quartet, 2H, 1CH$_{2\omega}$); 2.32 (t, 2H, J=7.4 Hz, 1CH$_{2\alpha}$); 2.55 (t, 1H, SH); 3.23 (s, 3H, OCH$_3$); 3.38 (s, 6H, 2OCH$_3$); 3.83 (s, 3H, OCH$_3$); 6.42 (d, 1H, J$_1$=8.5 Hz, H$_{arom}$); 6.46 (as, 1H, H$_{olefinic}$); 6.47 (as, 1H, H$_{olefinic}$); 6.62 (s, 2H, H$_{arom}$); 7.11 (dd, J$_1$=8.5 Hz, J$_2$=2.1 Hz, H$_{arom}$); 7.30 (d, 1H, J$_2$=2.1 Hz, H$_{arom}$). ^{13}C NMR, 100 MHz, C$_6$D$_6$, δ: 23.15; 25.24; 25.81; 29.82; 29.94; 30.32; 30.37; 34.6; 34.92 (10C, C$_{aliphatic}$); 55.92; 56.32 (2C, 2OCH$_3$); 61.13 (2C, 2OCH$_3$); 107.36; 112.86; 124.45(5C, C$_{arom}$); 128.36 (2C, C$_{olefinic}$); 130.86; 131.16; 133.12; 139.44; 141.07; 151.64; 154.67 (7C, C$_{arom}$), 171.71 (1C, C=O). IR (C$_6$D$_6$), cm^{-1}: 2950; 2927; 2851(s, CH$_{aliph}$ stretch); 1765 (s, C=O stretch)

**Synthesis of 5-(3,4,5-trimethoxystyryl)-2-methoxyphenyl hex-5-ynoate (57)**
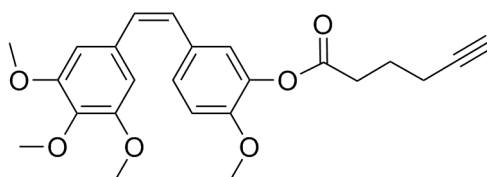
57

To a solution of Combretastatin A4 (**33**) (0.045 g, 0.14 mmol) in 2 mL of dry DCM, DMAP (0.002 g, 0.014 mmol) was added. The orange solution was cooled at 0°C, then 5-hexanoic acid (33 µL, 0.156 mmol) and DIC (24 µL, 0156. mmol) were added. The reaction mixture was stirred for 3 h at r.t., then poured onto 20 mL of diethyl ether and washed with a saturated solution of NH$_4$Cl (3x40 mL), then a saturated solution of NaHCO$_3$ (2x40 mL) followed by a saturated solution of NH$_4$Cl (5x40 mL). The recollected organic layer was dried over Na$_2$SO$_4$, filtered and evaporated to obtain the final product (**57**) as colourless oil (33 mg) in 38% yield. ^{1}H NMR, 400MHz, CDCl$_3$, δ: 1.95 (quintet, 2H, CH$_{2\beta}$); 1.98 (t, 1H, *J* = 2.8Hz, H$_{vinyl}$); 2.33 (td, 2H, J$_1$= 7.2Hz, J$_2$=2.8Hz, CH$_{2\gamma}$); 2.68 (at, 2H, *J*= 7.2Hz, CH$_{2\alpha}$);

3.70 (s, 6H, 2OCH$_3$); 3.80 (s, 3H, OCH$_3$); 3.83 (s, 3H, OCH$_3$); 6.45 (as, 2H, H$_{olefinic}$); 6.50 (as, 2H, H$_{arom}$); 6.84 (d, 1H, J= 8.4Hz, H$_{arom}$); 7.00 (d, 1H, J= 2.4Hz, H$_{arom}$); 7.11 (dd, 1H, J_1= 8.4Hz, J_2= 2Hz, H$_{arom}$). ^{13}C NMR, 100MHz, CDCl$_3$, δ: 17.69 (1C, CH$_{2\beta}$); 23.74 (1C, CH$_{2\gamma}$); 32.58 (1C, CH$_{2\alpha}$); 55.91 (1C, OCH$_3$); 55.93 (2C, 2OCH$_3$); 60.88 (1C, OCH$_3$); 69.18 (1C, C$_{vinyl}$); 83.18 (1C, C$_{vinyl}$); 105.88; 111.98; 123.08; 127.69 (5C, C$_{arom}$); 128.55; 129.52 (2H, H$_{olefinic}$); 130.10; 132.42; 137.22; 139.44, 150.18; 152.98 (8C, C$_{arom}$); 170.96 (1C, C=O$_{est}$). IR (KBr), cm^{-1}: 3306.03 (m, H-C$_{vinyl}$ stretch.); 1756.98 (s, C=O$_{est}$).

Synthesis of (Z)-2,5-dioxopyrrolidin-1-yl (2-methoxy-5-(3,4,5-trimethoxystyryl)phenyl) glutarate (57b)
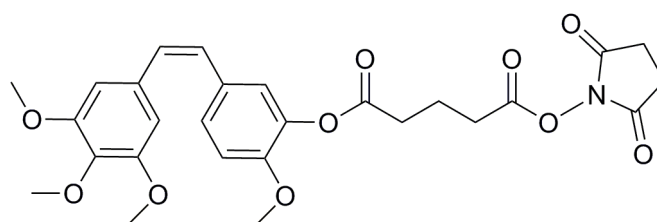
57b

To a solution of (Z)-5-(2-methoxy-5-(3,4,5-trimethoxystyryl)phenol)-5-oxopentanoic acid (**35**) (0.13g, 0.3 mmol) in 20 mL of dry DCM, DMAP (0.004 g, 0.03 mmol) was added, under a N$_2$ atmosphere. The colourless solution was cooled at 0°C, then N-hydroxysuccinimide(0.04 g, 0.33 mmol) was added, followed by DIC (52 µL, 0.33 mmol). The reaction mixture was stirred for 2 h at r.t. to give a yellowish solution, then poured onto 20 mL of DCM and washed with a saturated solution of NH$_4$Cl (3x40 mL), then a saturated solution of NaHCO$_3$ (2x40 mL) followed by a saturated solution of NH$_4$Cl (5x40 mL). The recollected organic layer was dried over Na$_2$SO$_4$, filtered and evaporated to obtain a yellow oil as final pure product (**57b**) in 60% yield. ^{1}H NMR, 400 MHz, CDCl$_3$, δ: 2.17 (q, 2H, J=7.2 Hz, CH$_2$); 2.70 (t, 2H, J=7.2 H, CH$_2$); 2.81 (t, 2H, J=7.2 Hz, CH$_2$); 2.85 (bs, 4H, 2CH$_{2succ}$); 3.71 (s, 6H, OCH$_3$); 3.81 (s, 3H, OCH$_3$); 3.84 (s, 3H, OCH$_3$); 6.46 (s, 2H, H$_{arom}$); 6.51 (s, 2H, H$_{arom}$); 6.85 (d, J=8.4 Hz, 1H, H$_{arom}$); 7.01 (d, J=2.0 Hz, 1H, H$_{arom}$); 7.12 (dd, J_1=8.4 Hz, J_2=2.0 Hz, 1H, H$_{arom}$). ^{13}C NMR, 100 MHz, CDCl$_3$, δ: 19.94; 25.55; 29:76; 32.40; 55:89; 60.87 (11C, C$_{aliph.}$); 105.77; 111.87; 123.02, 127.73 (4C, C$_{arom}$); 128.50; 129.50 (2C, C=C); 130.04; 132.39; 137.09; 139.26; 150.03; 152.93 (6C, C$_{arom}$); 168.06 (1C, C=OON); 169.00 (2C, NC=O); 170.42 (1C, C=O$_{ester}$). IR (CDCl$_3$), cm^{-1}: 3004.31 (w, CH$_{arom}$ stretch.); 2969.82 (w, CH$_{aliph.}$ stretch.); 1739.78 (s, C=O$_{ester}$ stretch.). ESI -MS: m/z = 550.50 [M+Na]$^+$, 1076 [2M+Na]$^+$.

Synthesis of bis(2-methoxy-5-((Z)-3,4,5-trimethoxystyryl)phenyl) 4,4'-disulfanediyldibutanoate (58)
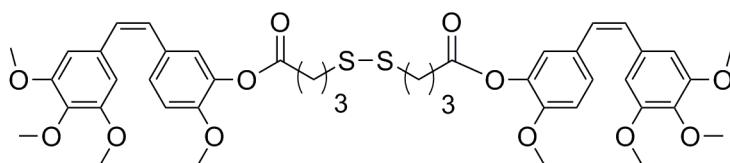
58

To a solution of (Z)-2-methoxy-5-(3,4,5-trimethoxystyryl)phenol (**33**) (0.065 g, 0.20 mmol) in 3 mL of dry DCM, DMAP (0.0012 g, 0.01 mmol) was added. The orange solution was cooled at 0°C, then 4,4′-dithiodibutyric acid (0.024 g, 0.1 mmol) was added; the obtained suspension was stirred for 30 minutes, then DIC (32 μL, 0.02 mmol) was added. During the adding of DIC the suspension became a solution. The reaction mixture was stirred for 3 days at r.t. then poured onto 20 mL of diethyl ether and washed with a saturated solution of NH$_4$Cl (3x40 mL), then a saturated solution of NaHCO$_3$ (2x40 mL) followed by a saturated solution of NH$_4$Cl (5x40 mL). The recollected organic layer was dried over Na$_2$SO$_4$, filtered and evaporated to obtain a yellowish oil (90 mg). The crude was purified by flash chromatography using EtP : AcOEt 3 : 2 as eluent to obtain the final pure product (**58**) as colourless oil in 45% yield. ^{1}H NMR, 400MHz, CDCl$_3$, δ: 2.13 (quintet, 4H, 2CH$_2$); 2.67 (t, 4H, J = 6.8Hz, 2CH$_2$); 2.80 (t, 4H, J_1= 6.8Hz, 2CH$_2$); 3.70 (s, 12H, 4OCH$_3$); 3.80 (s, 6H, 2OCH$_3$); 3.83 (s, 6H, 2OCH$_3$); 6.45 (as, 4H, H$_{olefinic}$); 6.50 (as, 4H, H$_{arom}$); 6.83 (d, 2H, J= 8.4Hz, H$_{arom}$); 7.00 (d, 2H, J= 2.0Hz, H$_{arom}$); 7.11 (dd, 2H, J_1= 8.4Hz, J_2= 2Hz, H$_{arom}$). ^{13}C NMR, 100MHz, CDCl$_3$, δ: 24.29 (1C, CH$_2$); 32.28 (1C, CH$_2$); 37.50 (1C, CH$_2$); 55.90 (2C, 2OCH$_3$); 55.93 (4C, 4OCH$_3$); 60.89 (2C, 2OCH$_3$); 105.88; 111.98; 123.11; 127.69 (10C, C$_{arom}$); 128.54; 129.54 (4H, H$_{olefinic}$); 130.11; 132.42; 137.22; 139.41, 150.15; 152.98 (16C, C$_{arom}$); 170.85 (2C, C=O$_{est}$). ESI-MS: m/z = 852.42 [M+NH$_4$]$^+$, 857.43 [M+Na]$^+$.

Synthesis of 11-11' dithiodiundecanoic acid (60)
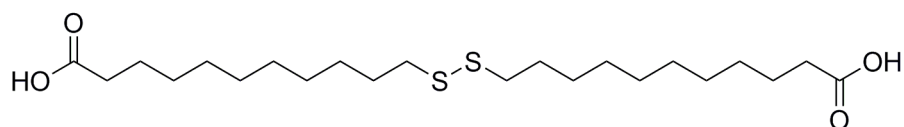

60

11-mercaptoundecanoic acid (**59**) (0.15 g, 0.69 mmol) was suspended in a 1 : 1 mixture of NaOH 0.1 M : DCM (6 mL). A solution of I$_2$ (0.096 g, 0.41 mmol) in 5 mL of DCM was added dropwise , in the end of the addiction the organic layer of the suspension turned from white to red. The reaction mixture was stirred at r.t for 30 minutes then diluted with 20 mL of AcOEt. The pH of the aqueous layer was adjusted to 5 with a saturated solution of NH$_4$Cl and the two phases were separated. The red organic layer was washed with a solution of Na thiosulfate (0.15 g in 100 mL of water) turning to yellow, then washed with Brine (3 x 50 mL). The recollected organic phase was dried over Na$_2$SO$_4$, filtered and evaporated to obtain a yellowish powder (**60**) (115 mg) as final pure product in 38% yield. ^{1}H NMR, 400MHz, DMSO-d, δ: 1.25 (bs, 20H, 10 CH$_2$); 1.35-1.39 (m, 4H, 2 CH$_2$); 1.41-1.52 (m, 4H, 2 CH_2CH$_2$SH); 1.53-1.62 (m, 4H, 2 CH_2CH$_2$COOH); 2.18 (t, 4H, J= 7.6 Hz, 2 CH_2SH); 2.68 (t, 4H, J=

7.2 Hz, 2 CH_2COOH); 11.90 (bs, 2H, 2 COOH). ^{13}C NMR, 100MHz, DMSO-d, δ: 24.94; 28.16; 28.97; 29.00; 29.16; 29.28; 29.301; 34.11; 39.37 (20C, C$_{aliphatic}$); 174.91 (2C, 2 COOH).

Synthesis of 5-(3,4,5-trimethoxystyryl)-2-methoxyphenyl 12-(2-(10-((5-(3,4,5-trimethoxystyryl)-2-methoxyphenoxy)carbonyl)decyl)disulfanyl)dodecanoate (61)
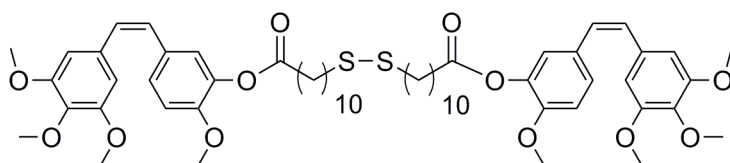
61

To a solution of (Z)-2-methoxy-5-(3,4,5-trimethoxystyryl)phenol (0.043g, 0.14 mmol) in 2 mL of dry DCM, DMAP (0.001 g, 0.01 mmol) was added. The yellow solution was cooled at 0°C, then 11-11' dithiodiundecanoic acid (0.028 g, 0.06 mmol) was added. The obtained suspension was stirred for 30 minutes, then DIC (21 µL, 0.14 mmol) was added. After 1 h of stirring, the suspension became a solution. The reaction mixture was stirred for 3 days at r.t., then poured onto 20 mL of diethyl ether and washed with a saturated solution of NH$_4$Cl (3x40 mL), then a saturated solution of NaHCO$_3$ (2x40 mL) followed by a saturated solution of NH$_4$Cl (5x40 mL). The recollected organic layer was dried over Na$_2$SO$_4$, filtered and evaporated to obtain a colourless oil (65 mg). The crude was purified by flash chromatography using EtP : AcOEt 3 : 2 as eluent to obtain the final pure product (**61**) as colourless oil in 40% yield. ^{1}H NMR, 400MHz, CDCl$_3$, δ: 1.2-1.42 (m, 28H, 14CH$_2$); 1.62-1.79 (m, 8H, 4CH$_2$); 2.52 (t, 4H, J= 7.6 Hz, 2CH$_2$S); 2.68 (t, 4H, J= 7.6 Hz, 2CH$_2$COO); 3.70; 3.80; 3.83 (s, 18H, 6OCH$_3$); 6.45 (as, 4H, H$_{olefinic}$); 6.50 (as, 4H, H$_{arom}$); 6.84 (d, 2H, J= 8.4Hz, H$_{arom}$); 7.00 (d, 2H, J= 2.0Hz, H$_{arom}$); 7.11 (dd, 1H, J_1= 8.4Hz, J_2= 2.0Hz, H$_{arom}$). ^{13}C NMR, 100MHz, CDCl$_3$, δ: 24.97; 28.37; 28.52; 29.01; 29.22; 29.23; 29.40; 29.45; 33.94; 37.51; 38.54; 39.16 (20C, C$_{aliph}$); 55.93 (2C, 2OCH$_3$); 60.87 (6C, 6OCH$_3$); 105.88; 111.98; 123.17; 127.58; 128.60; 129.46; 130.18; 132.44; 137.21; 139.55; 140.13 152.97; 167.42(36C, C$_{arom}$); 171.67 (2C, C=O$_{est}$). IR (CDCl$_3$), cm^{-1}: 3009.47 (w, CH$_{arom}$ stretch.); 2933.64 (m, CH$_{aliph}$ stretch.); 1756,21 (m, C=O$_{est}$).

Synthesis of CPA-SA
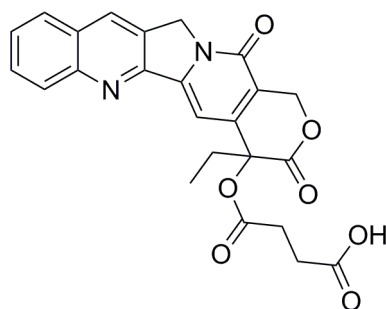
37

To a suspension of Camptothecin (**36**) (0.15 g, 1.43 mmol) in 3 mL of pyridine dry, succinic anhydride (1.21 g, 12.1 mmol) and DMAP (0.005 g, 0.043 mmol) were added, under a N_2 atmosphere. The mixture was stirred at 50°C for 2 days then 50 mL of HCl 1M were added. The solid obtained was crystallised by MeOH to give a mixture of starting material and desired product. The crude was then purified by flash chromatography using DCM : MeOH 20 : 1 as eluent to obtain the final product as white powder (**37**) (35 mg) in 18% yield. IR (KBr), cm^{-1}: 3700-3200 (vs, COOH stretch.); 1746 (s, C=O$_{acid}$ stretch.); 1720 (m, C=O$_{ester}$ stretch.); 1655 (m, NC=O$_{amide}$). ESI -MS: *m/z* = 894.92 [2M-H]$^-$. Further data are reported in literature.[195]

Synthesis of SPIONS-sulphonyl chloride (62)
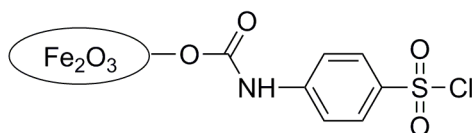
62

SPIONs (0.07 g) were suspended in 3 mL of dry toluene and sonicated for 10 minutes, under a N_2 atmosphere. Toluene was removed and the procedure was repeated 3 times. To a suspension of SPIONs in 7 mL of dry toluene, 4-chlorosulphenyl isocyanate (0.07 g) and DMAP (0.007 g) were added and the mixture was stirred for 4 h under N_2, then washed with toluene (3 x 7 mL). The procedure was repeated another time, finally SPIONs were dried under vacuum to obtaine the desired adduct (**62**). IR (KBr), cm^{-1}: 3182 (m, NH$_{carbamate}$ stretch.); 3092; 3047 (m, CH$_{arom}$ stretch.); 2913; 2845 (m, CH$_{aliph.}$ stretch.); 1717 (m, C=O$_{carbamate}$ stretch.); 1633 (s, C=C$_{arom}$ stretch.); 1583 (s, NH bend.); 1314; 1163 (s, SO$_2$Cl stretch.); 632; 581 (vs, Fe-O stretch.).

Synthesis of N-maleoyl-β-alanine (63)
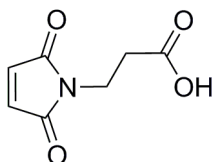
63

A suspension of maleic anhydride (1.50 g, 16.84 mmol) and β-alanine (1.65 g, 16.84 mmol) in 45 mL of acetic acid was heated at reflux (bath temperature: 140 °C) for 90 min., then stirred at r.t. for 16 h. The solution was refluxed again for 4h. The solution was then evaporated under vacuum and residual AcOH was removed by azeotroping with toluene (2 x 50 mL). The yellowish oil was dissolved in 50 mL of water and extracted with AcOEt (4 x 50 mL). The combined organic layers were dried over Na_2SO_4, filtered and evaporated to obtain a yellow powder. The crude residue was crystallized (AcOEt, 50 mL, 7° C) and washed with cold AcOEt (2 x 5 mL) to give desired compound (**63**) as white solid in 50 % yield. ^{1}H NMR and ^{13}C NMR spectra are reported in literature.[247]

**Synthesis of N-(6-aminohexyl)-3-(2,5-dioxo-2,5-dihydro-1H-pyrrol-1-yl)propanamide (64)**
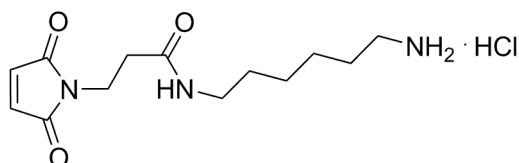
64

i) To a solution of N-Boc hexametylenediamine (0.29 g, 1.35 mmol) in 9 mL of dry DCM, DMAP (0.016 g, 0.135 mmol) was added, under a N_2 atmosphere. The obtained suspension was cooled at 0°C, then N-maleoyl-β-alanine (**63**) (0.25 g, 1.49 mmol) was added, followed by DIC (232 µL, 1.49 mmol). The reaction mixture was stirred overnight at r.t. to give a white suspension, then poured onto 30 mL of DCM and washed with a saturated solution of NH_4Cl (3x40 mL), then a saturated solution of $NaHCO_3$ (2x40 mL) followed by a saturated solution of NH_4Cl (5x40 mL). The recollected organic layer was dried over Na_2SO_4, filtered and evaporated to obtain a white solid as pure final compound without further purifications in 44% yield. This carbamate was not isolated, we directly proceeded with its deprotection.

ii) To a solution of the obtained carbamate (0.15 g, 0.42 mmol) in 5 mL of dry DCM, HCl 4M in dioxane (1.42 mL, 5.68 mmol) was added at 0°C, under a N_2 atmosphere. The reaction mixture was stirred at r.t for 3h then evaporated in vacuum to obtain the final pure product (**64**) as a yellow oil (110 mg) in quantitative yield. ^{1}H NMR, 400MHz, D_2O, δ: 1.14-1.36 (m, 4H, 2CH$_2$); 1.50-1.57 (m, 2H, CH$_2$); 2.38 (t, 2H, *J*= 6.4 Hz, CH$_2$); 2.88 (t, 2H, *J*= 6.8 Hz, CH$_2$); 2.99 (t, 2H, *J*= 6.8 Hz, CH$_2$); 3.67 (t, 2H, *J*= 6.8 Hz, CH$_2$); 6.76 (s, 2H, C=C). ESI-MS: *m/z* = 368.30 [M+H][+].

Synthesis of 3-(2,5-dioxo-2,5-dihydro-1H-pyrrol-1-yl)propanoyl chloride (65)

65
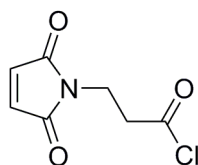
N-Maleoyl-β-alanine (**63**) (0.18 g, 1.06 mmol) was suspended in 4 mL of toluene dry, in a vial and stirred at r.t for 15 min. Then 355 µL of thionyl chloride dry (0.58 g, 4.9 mmol) was added, drop wise. The vial was stopped and the reaction mixture was stirred at 90°C for 4 h, then evaporated to obtain a yellowish oil as final pure product in 79% yield. ^{1}H NMR, 400MHz, CDCl$_3$ δ: 3.23 (t, 2H, J= 6.9 Hz, CH$_2$Cl); 3.83 (t, 2H, J= 6.9 Hz, CH$_2$N); 6.72 (s, 2H, H$_{olephinic}$). ^{13}C NMR, 50MHz, CDCl$_3$, δ: 32.8; 44.5 (2C, C$_{aliph}$); 133.9; 169.7 (2C, NC=O); 171.0 (C=O$_{chloride}$). IR (CDCl$_3$), cm^{-1}: 1791 (s, C=O$_{chloride}$ stretch.); 1712 (s, C=O$_{amide}$ stretch.).

Synthesis of 3-(2,5-dioxo-2,5-dihydro-1H-pyrrol-1-yl) propanoyl azide (66)
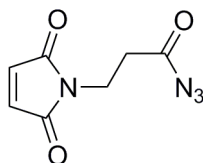
66

To a solution of propanoyl chloride (**65**) (1.05 g, 5.611 mmol) in 35 mL of dry acetone, 6.2 mL of a saturated aqueous solution of NaN$_3$ were added dropwise, at 0°C, under a N$_2$ atmosphere. As sodium azide was added, the sudden formation of an incarnadine precipitate was observed. The thus obtained suspension was allowed to stir at 0°C for 10 minutes, then at r.t for 2 minutes. Afterwards, the suspension wass poured onto 60 mL of water and extracted with DCM (4 x 50 mL). The recollected organic layer was dried on Na$_2$SO$_4$, filtered and evaporated to afford acylazide **66** as brown oil in 87% yield (1.00 g). The crude product is used without further purification. ^{1}H NMR, 300MHz, CDCl$_3$ δ: 2.66 (t, 2H, J=6.9 Hz, CH$_2$); 3.81 (t, 2H, N-CH$_2$); 6.70 (s, 2H, H$_{maleimide}$). IR (CDCl$_3$), cm^{-1}: 3172, 3103 (w, CH$_{oleph.}$ stretch.); 2948,2922 (w, CH$_{aliph}$ stretch.); 2146 (vs, O=C-N$_3$ stretch.); 1716 (vs, N-C=O stretch.).

Synthesis of 3-(2,5-dioxo-2,5-dihydro-1H-pyrrol-1-yl) propanoyl isocyanate (67)
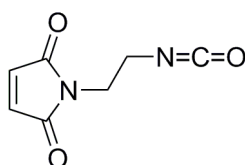
67

A solution of acylazide (**66)** (1.00 g) in 80 mL of dry toluene was heated at reflux and allowed to stir at 110°C, under a N atmosphere, for 1h, then left under magnetic stirring at r.t. over the weekend. The reaction mixture was then evaporated under vacuum to afford isocyanate **67** as brown oil in quantitative yield (0.85 g). The crude product is used without further purification. ^{1}H NMR, 400 MHz, CDCl$_3$, δ: 3.54 (t, *J*= 6 Hz, 2H, CH$_2$); 3.73 (t, *J*= 6 Hz, 2H, CH$_2$); 6.76 (as, 2H, C=C). ^{13}C NMR, 100 MHz, CDCl$_3$, δ: 38.27; 41.17 (2C, C$_{aliph}$); 122.89 (1C, N=C=O); 134.30 (2C, C=C), 170.29 (2C, 2NC=O). IR (CDCl$_3$), cm^{-1}: 2952; 2926;2857 (w, CH$_{aliph.}$ stretch.); 2280 (s, N=C=O stretch.); 1713 (vs, NC=O stretch.).

Synthesis of SPIONs-maleimidic linker conjugate (68)
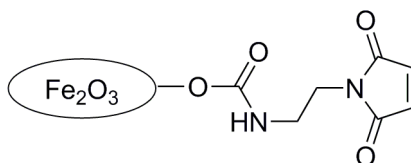
68

50 mg of SPIONs were suspended in 4 mL of dry toluene under a N$_2$ atmosphere and sonicated for 5 min. Then toluene was removed and the procedure was repeated two times. Thus washed, SPIONs were suspended in 10 mL of dry toluene, and to this suspension 5 mg DMAP and 50 mg of isocyanate **67** were and the reaction mixture was stirred for 14 h. Solvent was then removed and SPIONs were washed with dry toluene (4 x 6 mL). Residual solvent was eliminated in vacuo to afford final product (**68**). IR (KBr), cm^{-1}: 3406 (m, N-H$_{carbamate}$ stretch.), 3103 (m, C-H $_{olefinic}$ stretch.), 2946, 2845 (m, C-H $_{aliph}$ stretch.), 1703 (s, C=O$_{carbamate}$ stretch.), 1644 (m, C=C$_{olefinic}$ stretch), 632, 581 (s, Fe-O stretch.). Elemental analysis: C=19.74%, H=1.97%, N=7.12%. TGA: ΔW= -48.73% (30-700°C, nitrogen atmosphere); -3.49% (700-800°C, oxygen atmosphere)

Synthesis of Combretastatin A-4 –functionalised SPIONs (69)
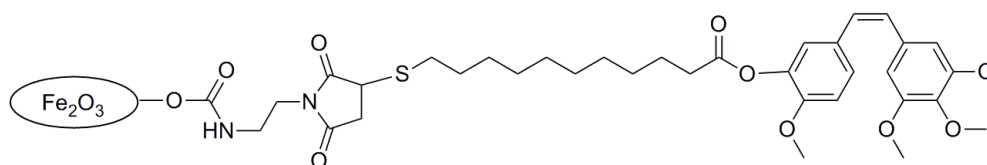
69

0.030 g of SPIONs-maleimmide (**68**) were put in a Schlenk in which 3 vacuum/nitrogen cycles had previously been applied. Afterwards, a solution of thiol **56** (0.030 g in 5 mL of deoxygenated, dry DCM, 0.058 mmol) and 14 µL TEA (0.099 mmol) were added to the nanoparticles. The suspension was sonicated at r.t. under a N_2 atmosphere for 4 h and then allowed to stir at same temperature overnight. The solvent was then eliminated and the nanoparticles were washed with dry DCM (3 x 10 mL). Residual solvent was later eliminated by evaporation in vacuo to afford **69** as final product. IR (KBr), cm^{-1}: 2946, 2917, 2851 (m, C-H $_{aliph}$ stretch.), 1770 (s, C=O$_{ester}$ stretch.), 1647 (m, C=C$_{olefinic}$ stretch), 1244, 1210, 1154 (s, succinidimyl-thioether signals), 632, 581 (s, Fe-O stretch.) Elemental analysis: C=6.84%, H=0.84%, N=1.86% TGA: ΔW= -25.55% (30-700°C, nitrogen atmosphere); +7.48% (700-800°C, oxygen atmosphere).

Synthesis of Combretastatin -1-hexynoate functionalized Co-NPs (70)
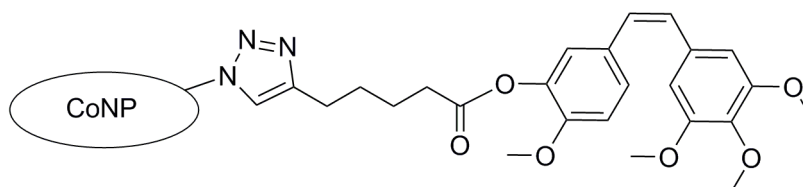
70

50 mg of commercial azide-coated *Turbobeads* © Co-NPs (0.1 mmol/g) were suspended in 5 mL of dry toluene under a N_2 atmosphere and sonicated for 10 min. at r.t. Toluene was removed and the procedure was repeated 3 times. Thus washed, Co-NPs were suspended again in 10 mL of dry toluene, and to this suspension 20 mg of combretastatin-1-hexynoate (**57**) (0.05 mmol), 1 mg CuI (0.5 eq) and 7 µL triethylamine (1.0 eq) were added. The suspension was sonicated for 16 h at r.t., then solvent was removed and the nanoparticles were washed with dry toluene (3 x 7 mL). Residual solvent was eliminated under vacuum to afford product **70**. IR (KBr): 2909, 2840 (w, CH$_{aliph}$ stretch.); 1572 (w, C=C$_{triazole}$ stretch.). TGA: ΔW= -5.89% (30-700°C, nitrogen atmosphere); +22.80% (700-800°C, oxygen atmosphere).

Synthesis of Combretastatin -1-NHS functionalized Co-NPs (70b)
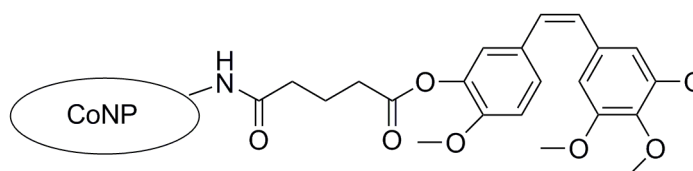
70b

For the fully separation of the Amine coated TurboBeads, the particles needed to be washed twice with 0.1 M Tris buffer. Tris buffer was prepared dissolving 1.21 g Tris in 90 mL of deionized water, pH was adjusted to 8.5 and filled with H_2O to 100 mL. 20 mg of Amine coated TurboBeads (0.1 mmol/g) are suspended in 30 mL of freshly prepared Tris buffer and sonicated for 10 min. at r.t. Tris buffer was removed and the procedure was repeated three times. Meanwhile, PBS buffer was prepared dissolving 0.13 g NaH_2PO_4 H_2O (Sodium phosphate monobasic monohydrate), 0.72 g Na_2HPO_4 $2H_2O$ (sodium phosphate dibasic dehydrate) and 4.4 g NaCl and adjusting the pH to 7.5 with HCl. Co-NPs were washed twice with 20 mL of PBS buffer and then resuspended in 12 mL of the same buffer. The such prepared suspension was added to a suspension of (Z)-2,5-dioxopyrrolidin-1-yl (2-methoxy-5-(3,4,5-trimethoxystyryl)phenyl) glutarate (**57b**) in 60 mL of PBS buffer, in a Schlenk tube. The reaction mixture was sonicated for 2 h, then washed several times with PBS and DCM and finally dried under vacuum to obtain a black powder. IR (KBr): 2956; 2913; 2844 (w, CH_{aliph} stretch.); 1738 (w, $C=O_{ester}$ stretch.); 1626 (w, $C=O_{amide}$ stretch.).

Synthesis of AuNPs-Combretastatin (71)
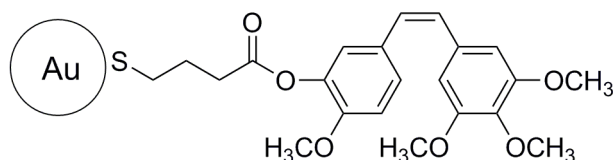
71

To a golden solution of $HAuCl_4$ (0.019 g, 0.057 mmol) in 2 mL of water, a suspension of n-tetrabutylammonium bromide (0.027 g, 0.085 mmol) in 2 mL of toluene was added. The biphasic system was stirred at r.t for 10 min. A solution of bis(2-methoxy-5-((Z)-3,4,5-trimethoxystyryl)phenyl) 4,4'-disulfanediyldibutanoate (**54**) (0.033 g, 0.039 mmol) in 1 mL of toluene was added and stirred 10 min at r.t then cooled at 0°C. A freshly prepared solution of $NaBH_4$ (0.043 g, 1.14 mmol) was added dropwise, after a few drops the aqueous layer turned to black and bubbles were observed. The mixture was stirred at r.t for 24 h to give a biphasic system with black organic layer and colourless aqueous layer. The two phases were separated, the organic layer was evaporated in vacuum, below 30°C, then washed with diethyl ether to finally give a black oil with purple glare (38 mg). ^1H NMR ($CDCl_3$): a clear characterisation of the adduct's signals was impossible. IR ($CDCl_3$), cm^{-1}: 3004 (w, $C-H_{arom}$ stretch.); 2961; 2935; 2840 (m, $C-H_{alifph}$ stretch.); 1756 (s, $C=O_{ester}$ stretch.). Theoric

loading from ^{1}H NMR spectrum (reference: DCM signal at 5.25 ppm in CDCl$_3$)**:** Au-NPs 38mg + 20 mg DCM: 32.7 mg organic moiety loaded on AuNPs. TGA: ΔW= -86.76% (30-700°C, nitrogen atmosphere); -7.718% (700-800°C, oxygen atmosphere).

1.6 References

References Introduction

1. DeVita, V., Chu, E. *Cancer Res,* **2008**, *68*, 8643.

2. Gibaud, S., Jaouen, G. *Topics in Organometallic Chemistry*, **2010**, *32*, 1-20.

3. Chabner, B.A., Roberts, T.G. *Nature reviews*, **2005**, *5*, 65-72.

4. http://www.opcw.org/about-chemical-weapons/types-of-chemical-agent/mustard-agents/

5. Bos, J.L., *Reviews in Genetic Toxicology*, **1988**, *195*(3), 255-271.

6. Nigro, J., Baker, S., Vogelstein, B. *et al.*, *Nature*, **1989**, *342*, 705-708.

7. Joseph, E.K., Levine, J.D. *The Journal of Pain*, **2009**, *10*(5), 534-541.

8. *Report on Carcinogens*, **2011**, Twelfth Edition

9. Nardi, V., Azam, M., Daley, G. *Current opinion in hematology,* **2004**, *11*(1), 35-43.

10 Druker, B.J. *et al.*, *N. Engl. J. Med.*, **2006**, *355*(23), 2408-2417.

11. Stix, G. *Scientific American*, **2006**, *294*(4), 81-83

12. Yildirimer, L., Thanh, N., Loizidou, M. *et al.*, *Nano Today,* **2011**, *6*, 585-607.

13. DiJoseph, J.F., Khandke, K., Dougher, M.M, Evans, D.Y., Damle, N.K. *Hematology Meeting Reports*, **2008**, *5*(6), 74-77.

14. Sugiura, Y. *et al.*,*Proc. Nati. Acad. Sci.*, USA, **1989**, *86*, 7672-7676.

15. http://www.hopkinsmedicine.org/vascular/procedures/chemoembolization/

16. Shin, S.W. *Korean Journal of Radiology,* **2009**, *10*(5), 425-434.

17. Torchilin, V.P. *Nat Rev Drug Discov.*, **2005**, *4*(2),145-60.

18. Zhang, J.N., Hsieh, T.H. *Cancer Genomics and Proteomics*, **2006,** *3*(34), 147-157.

19. Rehlaender, B.N, Cho, M. *J. Pharm Res.*, **1998**, *15*(11), 1652-6.

20. Carter, P. *Nature Reviews Cancer*, **2001**, *1*, 118-129.

21. Drews, J. *Science*, **2000**, *287*(5460), 1960-1964.

22. Reichert, J.M. and Valge-Archer, V.E. *Nature Reviews*, **2007**, *6*, 349-356.

23. Ding, B.S., Dziubla, T., Muzykantov, V.R. *et al.*, *Molecular interventions*, **2006**, *6*(2), 98.

24. Chames, P., Van Regenmortel, M., Baty, D. *Br. J. Pharmacol.*, **2009**, *157*(2), 220-233.

25. Reubi, J.C. *Endocrine Reviews*, **2003**, *24*(4), 389-427.

26. Reubi, J.C., Maecke, H., Krenning, E. *Journal of Nuclear Medicine*, **2005**, *46*, 67-75.

27. Van der Lely, A.J., De Herder, W.W., Krenning, E.P. *Endocrine*, **2003**, *3*, 307-311.

28. Falciani, C., Fabbrini, M., Bracci, L. *et al.*, *Molecular Cancer Therapeutics*, **2007**, *6*, 2441.

29. Carraway, R., Leeman, S. *The Journal of Biological Chemistry*, **1973**, *248*, 6854-6861.

30. Binder, E., Kinkead, B., Owens, M. *et al.*, *Pharmacological Review*, **2001**, *53*, 453-486.

31. Bourcier, T., Rondeau, N., Laroche, L. *et al.*, *Investigative Ophtalmology and Visual Science*, **2002**, *43(6),*1765-1771.

32. Nemeroff, C. B., Bissette, G., Lipton, M. A. *et al.*, *Brain Research*, **1977**, *128*, 485-496.

33. Drewe, J., Mihailovic, S., D'Amato, M. *The Journal of Clinical Endocrinology & Metabolism,* **2008**, *93*(5), 1964-1970

34. White, J. F., Noinaj, N., Shibata, Y. *Nature*, **2012**, *490*(7421), 508-13

35. Langer, M., Beck-Sickinger, A. G. *Current Medicinal Chemistry -Anti-Cancer Agents,* **2001**, *1*, 71-93.

36. Reubi, J. C., Waser, B., Friess, H. *et al.*, *Gut*, **1998**, *42*, 546-550.

37. Gui, G. P. H. *Journal of Cancer Therapy*, **2013**, *4*, 12-17.

38. Hong, F., Zaidi, J., Cusack, B. *et al.*, *Bioorganic & Medicinal Chemistry*, **2002**, *10*, 3849-58.

39. Bracci, L., Falciani, C., Lelli, B. *J Biol Chem*, **2003**, *278*, 46590-5.

40. Marquez, A.F. *et al.*, *Antimicrob. Agents Chemother.*, **2006**, 50(8), 2814-2819.

41. Tam, J., Zavala, F., *Journal of Immunological Methods*, **1989**,*124*(1), 53-61.

42. Bracci, L., Falciani, C., Lelli, B. et al., *Journal of Biological Chemistry*, **2003**, *278*, 46590-5,

43. Garcia-Garayoa, E., Conrath, P., Schubiger, P.A. *et al.*, *Nuclear Medicine and Biology*, **2001**, *28*, 75-84.

44. Kent Brown, C., Madauss, K., Rodgersi, D. *et al*, *Proceedings of the National Academy of Sciences*, **2001,** *98* (6), 3127-3132.

45. Ettmayer, P., Amidono, G.L., Clement, B., Testa, B. *J. Med. Chem.*, **2004**, *47*, 2393-2404.

46. Rooseboom, M., Commandeur, J.N.M. and Vermeulen, N.P.E. *Pharmacological Reviews*, **2004**, *56*, 53-102.

47. Brannon-Peppas, L., Blanchette, J.O *Advanced drug delivery reviews*, **2012**, *64*, 206-212.

48. Vithiya, K. and Sen, S. *IJPSR*, **2011**, *2*(11), 2781-2785.

49. Faraday, M. *Philosophical Transactions of the Royal Society of London*, **1957**, *147*, 145-181.

50. http://www.malvern.com/labeng/industry/nanotechnology/nanoparticles_definition.htm

51. Cheng, R., Feng, F., Meng, F.*et al.*, *Journal of Controlled Release*, **2011**, *152*, 2-12.

52. Talelli, M., Rijcken, C.J.F., Lammers, T. *et al.*, *Langmuir,* **2009***, 25* (4), 2060-2067.

53. Zhang, L., Gu, F.X., Chan, J.M. *Clinical Pharmacology & Therapeutics*, **2008**, *83*(5), 761-769.

54. Hussain, S.M., Hess, K.L., Geiss, K.T *et al.*, *Toxicology in vitro*, **2005**, *19*, 975-983.

55. Matsumura, Y., Maeda, H. *Cancer Research,* **1986**, *46* (12), 6387-92.

56. Mahmoudi, M., Sant, S., Sen, T. *Advanced Drug Delivery Reviews*, **2011**, *63* (1-2), 24-42.

57. Chatterjee, D.K., Diagaradjane, P., Krishnan, S. *et al.*, *Therapeutic Delivery*, **2011**, *2*(8), 1001–1014.

58. http://www.cancer.gov/cancertopics/factsheet/Therapy/hyperthermia.

References Results and Discussion

59. http://www.wisegeek.com/what-is-a-cytotoxin.htm

60. Gibbs, J.B *Science,* **2000**, *287*, 1969-1973.

61. Scagliotti, G.V, Novello, S. *Lung Cancer*, **2002**, *38*, 13-19.

62. Smith, A. L. *Oxford dictionary of biochemistry and molecular biology*, Oxford University Press, **1997**, 43.

63. http://www.pharmacology2000.com/Anticancer/classes2.htm

64. Denny, A. *Aust. J. Chem.*, **2004**, *57*, 821-828.

65. Gerben, A., Koning, J., Kamps, A.A.M., Gerrit, L., Scherphof, A. *Cancer Detection and Prevention*, **2002**, *26*, 299-307.

66. Uchikubo, Y., Hasegawa, T., Mitani, S., Kim, H.S., Wataya, Y. *Nucleic Acids Res Suppl*. 2002, 2, 245-6.

67. Sivridis, E. *et al.*, *British Journal of Cancer*, **2002**, 86*,* 1465-1471.

68. Malet-Martino, M., Jolimaitre, P. and Martino, R. *Curr. Med. Chem.-Anti-Cancer Agents,* **2002***, 2,* 267-310.

69. Fisher, J.A., Muller-Weeks, S., Caradonna, S.J. *Cancer Research*, **2006**, *66*, 8829-8837.

158

70. Meropol, N.J. *European Journal of Cancer*, **1998**,*34*, 1509-1513.

71. Goerlac, A., Krauer Kenia, G., Mckenzie, I.F.C., Pietersz, A.G. *Bioconjugate Chem.*, **1991**, *2*, 96-101.

72. Burris, H.A. *et al*. *J Clin Oncol*., **1997**, *15*(6), 2403-13.

73. Ahn, G., Brown, M. *Frontiers in Bioscience*, **2007**, *12*, 3483-3501.

74. Oettle, H. S. *et al*., *JAMA*, **2007**, *297*, 267-277.

75. Plunkett, W., Huang, P. *PubMed,* **1995** , *22*(4 Suppl 11), 3-10.

76. Valle, J. *N. engl j med*, **2010**, *362*(14), 1273-1281.

77. Reck, M., von Pawel, J. *JCO*, **2009**, 27(8), 1227-1234.

78. Kindler, H.L. *et al*., *JCO*, **2010**, 28(22), 3617-3622.

79. Anderson, R.F., Shinde, S.S., Hay, M.P., Denny, W.A. *JACS.*, **2006**, *128*, 245-249.

80. Brown, J.M. *Br. J. Cancer*, **1993**, *67*, 1163-1170.

81. da Consolacao, M., Linardi, F., de Oliveira, M.M, Sampaio, M.R.P. *Expert Opin Investig Drugs*, **1998**, *7*(6), 905-28.

82. Helleday, T., Petermann, E., Lundin, C., Hodgson, B., Sharma, R.A. *Nature Rev. Cancer*, **2008**, *8*, 193 204.

83. Wilson, W.R. and Hay, M.P. *Nature Reviews*, **2011**, 11, 393-410.

84. Castellanos, G., Rubén, J., Heinrich, M. *Journal of Ethnopharmacology*, **2009**, *121*(1), 1-13.

85. Sacau, E.P., Estévez-Braun, A., Ravelo, G.A. *et al*., *Bioorganic & Medicinal Chemistry*, **2007**, *11*, 483-488.

86. "Pau d'arco", *American Cancer Society*, **2013**.

87. da Consolacao, M., Linardi, F., de Oliveira, M.M., Sampaio, M.R.P. *Journal of Medicinal Chemistry,* **1975**, *18*, 11.

88. D'Anneo, A., *et al*. *Journal of Cellular Physiology*, **2010**, *222* (2), 433-443.

89. Li, C.J., Averboukh, L., Pardee, A.B. *The Journal of Biological Chemistry*, **1993**, *268*, 22463-22468.

90. Ahn, K.J., Lee, H.S., Bai, S.K., Song, C.W. *Radiat Oncol J.*,**2013**, *31*(2), 57-65.

91. Bellon, S.F., Coleman, J.H., Lippard, S.J. *Biochemistry*, **1991**, *30* (32), 8026-8035.

92. Donahue, B.A., Lippard, S.J. *Biochemistry*, **1990**, *29*(24), 5872-5880.

93. Reardon, J.T., Vaisman, A., Chaney, S.G., Sancar, A. *Cancer Res*, **1999**, *59*, 3968.

94. He, Q., Liang, C.H., Lippard, S.J. *PNAS*, **2000**,97(11), 5768-5772.

95. Siddik, Z.H. *Oncogene*, **2003**, *22*, 7265-7279.

96. Florea, A-M., Büsselberg, D. *Cancers*, **2011**, *3*, 1351-1371.

97. Splettstoesser, F., Florea, A.M., Büsselberg, D. *Br. J. Pharmacol.* **2007**, *151*, 1176-1186.

98. Shamimi-Noori, S., Yeow, W.S., Ziauddin, M.F., Xin, H.; Tran, T.L., Xie, J., Loehfelm, A., Patel, P., Yang, J., Schrump, D.S., Fang, B.L., Nguyen, D.M *Cancer Gene Ther.* **2008**, *15*, 356-370.

99. Muscella, A., Calabriso, N., Fanizzi, F.P., De Pascali, S.A., Urso, L., Ciccarese, A., Migoni, D., Marsigliante, S. *Br. J. Pharmacol.* **2008**, *153*, 34-49

100. Wisnovsky, S.P., Wilson, J.J., Radford, R.J., Pereira, M.P., Chan, M., Laposa, R., Lippard, S.J., Kelley, S.O., *Chemistry and Biology*, **2013**, *20*, 1323-1328.

101. Desoize, B., Madoulet, C. *Crit. Rev. Oncol. Hematol.*, **2002**, *42*, 317-325.

102. Rosenberg, B. *Nucleic Acid-Metal Ion Interactions*, Spiro, T.G., Ed., USA, **1980**, *1*, 1-29.

103. Lebwohl, D., Canetta, R. *Eur. J. Cancer.*, **1998**, *34*, 1522-1534.

104. Olszewski, U., Hamilton G. *Anticancer Agents Med. Chem.*, **2010**, *10*, 293-301.

105. Okusaka, T., *et al*. *British Journal of Cancer*, **2010**,*103*, 469-474.

106. Sato, Y., *et al*. *Cancer Chemotherapy and Pharmacology*, **2010**, 66(4),721-728.

107. Takano, M., *et al*. *Oncology*, **2009**, *76*,315-321.

108. Posner, M.R. *Ann Oncol*, **2010**, *21*(7), 246-251.

109. Brozovic, A., Ambriović-Ristov, A., Osmak, M. *Critical Reviews in Toxicology*, **2010**, *40*(4), 347-359.

110. Halla, M.D., Martinb, C., *et al*. *Biochemical Pharmacology*, **2004**, *67* ,17-30.

111. Tsang, R.Y., Al-Fayea, T., Au, H.J. *Drug Saf*, **2009**, *32*, 1109-1122.

112. Feazell, P.R., Nakayama-Ratchford, N., Hongjie, D., Lippard, S.J., *J. Am. Chem. Soc.*, **2007**, *129*, 8438-8439.

113. Dhar, S., Daniel, W.L, Gilijohann, D.A., Mirkin, C.A., Lippard, S.J. *J.Am.Chem.Soc.*, **2009**, *131,* 14652-14653.

114. Legha, S.S. *Ann Intern Med.*, **1988**, *109*(3), 219-228.

115. Davis, C., *et al*., *Lancet*, **2011**, *378*(9793),771-84.

116. Horwitz, K.B,, McGuire, W.L. *Endocrinology*, 1978**,** 103(5), 1742-1751.

117. Munster, P.N., Carpenter, J.T. *JAMA*, **2009**, *302*(7),797-798.

118. http://www.nlm.nih.gov/medlineplus/ency/article/003711.htm

119. Ellis, M.J., Gao, F., Dehdashti, F. *JAMA*, **2009**, *302*(7), 774-780.

120. Lux, M.P., Fasching, P.A., Beckmann, M.W. *Journal of Molecular Medicine*, **2006**, *84*(1), 16-28.

121. Brueggemeier, R.W., Bhat, A.S, *et al*. *The Journal of Steroid Biochemistry and Molecular Biology*, **2001**, *78*(2), 145-146.

122. Pribluda, V.S., Gubish, E.R., LaVallee, M.T., Treston, A., Swartz, G.M., Green, S.J. *Cancer and Metastasis Reviews*, **2000**, *19* (1-2), 173-179.

123. Fotsis, T., Zhang, Y., Pepper, M.S., Adlercreutz, H., Montesano, R., Nawroth, P.P. *Nature*, **1994**, *368*, 237-239.

124. D'amato, R.J., Lint, C.M., Flynn, E., Folkman, J., Hamelt, E. *Proc. Nati. Acad. Sci.*, **1994** , *91*, 3964-3968.

125. Epe, B., Hegler, J. Metzler, M. *Carcinogenesis*, **1987**,*8*, 1271-1275.

126. Degen, G.H., Blaich, G., Metzler, M. *J. Biochem. Toxicol.*,**1990**, *5*, 91-97.

127. Attalla, H., Knuutila, S., Makela, T.P., Andersson, L.C. Aldercreutz, H. *Cancer Genet. Cytogenet.*, **1998**, *102*, 139-141.

128. Mukhopadhyay, T. Roth, J.A. *Oncogene*, **1997**, *14*, 379-384.

129. Attalla, H., Westberg, J.A., Andersson, L.C., Aldercreutz, H., Makela, T.P. *Biochem. Biophys. Res. Commun.*, **1998**, *247*, 616-619.

130. Tsukamoto, A., Kaneko, Y., Yoshida, T., Han, K., Ichinose, M., Kimura, S. *Biochem. Biophys. Res. Commun.*, **1998**, *248*, 9-12.

131. Wang, Y., *et al*. *Biomaterials*, **2011**, *32*(12), 3322-3329.

132. Kulke, M.H. *Cancer Chemotherapy and Pharmacology*, **2011**, *68* (2), 293-300.

133. Schmidt, M. Bastians, H. *Drug Resistace Updates*, **2007**, *10*,162-181.

134. Brito, D.A., Rieder, C.L. *Curr. Biol.*, **2006**, *16*, 1194-1200.

135. Trudeau, M.E. *Can. J. Oncol.*, **1996**, *6*, 443-457.

136. Hooper, A.T., Loganzo, F., May, C., Gerber, H.P. *Cancer Drug Discovery and Development,* **2013**, 17-38.

137. Patterson, D.M, Rustin, G.J. *Clin Onco,* **2007**, *119*(6), 443-456.

138. Kingston, D.G.I. *Journal of Natural Products*, **2009**, *72*(3).

139. Rowinsky, E.K., Onetto, N.,Canetta, R.M., Arbuck, S.G. *Semin Oncol.*, **1992**, *19*(6),646-62.

140. Rowinsky, E.K. *Annu. Rev. Med.*, **1997**, *48*(353), 74.

141. Wani, M., Taylor, H., Wall, M., Coggon, P., McPhail, A. *J Am Chem Soc*, **1971**, *93*(9), 2325-7.

142. Wall, M.E., Wani, M,C. *Cancer Research*, **1995**, *55*(4), 753-60.

143. Schiff, P.B., Fant, J., Horwitz, S.B. *Nature*, **1979**, *277*,665-7.

144. Pazdur, R. *JCO*, **2012**, 30(14), 1705-1711.

145. Nilufer, J., Selimah, F. *et al*, *Asian Pacific Journal of Cancer Prevention,* **2011**, *12*, 837-850.

146. Jordan, M.A., Wendell, K., Gardiner, S. et all., *Cancer Res*, **1996**, *56*, 816-25.

147. Giannakakou, P., Robey, R., Fojo, T. *et al.*, *Oncogene*, **2001**, *20*, 3806-13.

148. Klauber, N., Parangi, S., Flynn, E. *et al.*, *Cancer Res*, **1997**, *57*, 81-6.

149. Fujita, K., Sano, D., Kimura, M. *et al.*, *Oncology Rep*, **2007**, *18*, 47-51.

150. Singla, A.K., Garg, A., Aggarwal, D. *International Journal of Pharmaceutics*, **2002**, *235*, 179-192.

151. Du Bois, A., Luck, H.J., Meier, W., *et al*. *J NatlCancer Inst*, **2003**, *95*, 1320-30.

152. Piccart-Gebhart, M.J., Burzykowski, T., Buyse, M., *et al.*, *J Clin Oncol*, **2008**, *26*, 1980-6.

153. Si-Shen, F., Guofeng, H., J. *Controlled Release*, **2001**, *71*, 53-69.

154. Lilley, L.L., Scott, H.B., *Am. J. Nurs.*, **1993**, *93*, 46-50.

155. Sampath, D., Discafani, C.M., Loganzo, F., et *al.*, *Mol Cancer Ther*, **2003**, *2*, 873-88.

156. Bissery, M.C., Guenard, D., Guerrite-Voegelein, F., Lavelle, F. *Cancer Res.*, **1991**, *51*, 4845.

157. Sharma, U.S., Balasubramanian, S.V., Straubinger, R.M. *J. Pharm. Sci.*, **1995**, *84*, 781-791.

158. Straubinger, R.M. *Science and Applications. CRC press*, **1995**, 237-254.

159. Wang, Y.M., Sato, H., Adachi, I., Horikoshi, I. *Chem. Pharm. Bull.*, **1996**, *44*, 1935-1940.

160. Si-Shen, F., Guofeng, H. J. *Controlled Release*, **2001**, *71*, 53-69.

161. Williams, H.J., Scott, A.I., Dieden, R.A., Swindell, C.S., Chirlian, L.E., Francl, M.M., Heerding, J.M., Krauss, N.E. *Tetrahedron*, **1993**, *49*, 6545.

162. Kingston, I. *J. Nat. Prod.* **2000**, *63*, 726-734.

163. Greenwald, R.B., Gilbert, C.W., Pendri, A., Conover, C.D., Xia, J., Martinez, A. *J. Med. Chem.*, **1996**, *39*, 424-431.

164. Liu, D., Sinchaikul, S., Reddy, P.V., Changd, M., and Chenb, S. *Bioorganic & Medicinal Chemistry Letters*, 2007, 17, 617-620.

165. Pettit, G.R., Singh, S.B., Schmidt, J.M. *et al.*, *Journal of Medicinal Chemistry*, **1995**, *38*, 1666-1672.

166. Queiroz, S.C.N., Assalin, M.R., Cerdeira, A.L. *et al.*, *Planta Medica*, **2010**, *76*, 53.

167. Dowlati, A., Robertson, K., Cooney, M. *et al.*, *Cancer Research*, **2002**, *62*, 3408-3416.

168. Pettit, G.R. *Can. J. Chem.*, **1982**, *610*, 1374.

169. Griggs, J., Hesketh, R., Smith, G.A., Brindle, K.M., Metcalfe, J.C., Williams, E.D. *British Journal of Cancer*, **2001**, *84*(6), 832-835.

170. Boyland, E., Boyland, M., Greville, G. *Biochemical Journal*, **1937**, *31*, 461-470.

171. Woo, M., Hakem, R., Mak, T.W. *et al.*, *Genes & Development*, **1998**, *12* (6),806-19.

172. Iyer, S., Chaplin, D.J., Rosenthal, D.S., *et al.*, *Cancer Research*, **1998**, *58*, 4510- 4514.

173. Nabha, S., Wall, N., Mohammad, R. *et al.*, *Anti-Cancer Drugs*, **2000**, *11*,385-392.

174. Castedo *et al.*, *Oncogene*, **2004**, *23* (16), 2825-37.

175. Dark, G.G., Hill, S.A., Prise, V.E., Tozer, G.M., Pettit, G.R., Chaplin, D.J. *Cancer Res* **1997**, *57*, 1829-1834.

176. Sengupta, S., Eavarone, D., Capila, I., Zhao, G., Watson, N., Kiziltepe, T. *Nature*, **2005**, *436*(28), 572.

177. Nabha, S.M., Wall, N.R., Mohammad, R.M., Pettit, G.R., Al-Katib, A.M. *Anticancer Drugs*. **2000**, *11(5),* 385-392.

178. Rustin. G.J., Galbraith, S.M., Anderson, H. *et al.*, *Int J Clin Oncol.*, **2003**, *21*(15), 2815-2822.

179. Patterson, D.M., Rustin, G.J. *Clin Onco,* **2007**, *119*(6), 443-456.

180. Rustin, G.J., Shreeves, G., Nathan, P.D. *et al.*, *British Journal of Cancer*, **2010**, *102*, 1355-1360.

181. Leach, M.O., Judson, I., Nathan, P. *Eur Radiol*, **2009**, *19*, 2728-2738.

182. Nathan, P., Zweifel, M., Padhani, A.R., *et al.*, *Clin Cancer Res*, **2012**, *18*(12), 3428-3439.

183. Zweifel, M., Jayson, G.C., Reed, N.S., Osborne, R., Hassan, B., Ledermann, J., *et al.*, *Ann Oncol*, **2011**, *22*, 2036-41.

184. Stevenson, J.P., Rosen, M., Sun, W. *Journal of Clinical Oncology*, **2003**, *21*(23), 4428-4438.

185. Young, S.L., Chaplin, D.J. *Expert Opinion on Investigational Drugs*, **2004**, *13*(9), 1171-1182.

186. Sherman, S.I. *Biochemical Pharmacology*, **2010***, 80*, 592-601.

187. http://www.cancer.gov/dictionary; "Definition of topoisomerase inhibitor - NCI Dictionary of Cancer Terms"

188. Rothenberg, M.L. *Annals of Oncology*, **1997**, *8*, 837-855.

189. Kejie, D., Yi, W., Jiewen, L., Liangnian, J., Hui, C. *Progress in chemistry*, **2013**, *25*(4), 545-554.

190. Hino, M., Niitani, H. *Nihon Rinsho*, **1993**, *51*(12),3291-300.

191. Pommier, Y. *Nature Reviews*, **2006**, *6*, 709-802.

192. Nitiss, J., Wang, J.C. *Proc. Natl Acad. Sci. USA*, **1988**, *85*, 7501-7505.

193. Eng, W.K., Faucette, L., Johnson, R.K., Sternglanz, R. *Mol. Pharmacol.,***1988**, *34*, 755-760.

194. Ulukan, H., Swaan, P.W. *Drugs*, **2002**, *62*(2), 2039-2057.

195. Tongand, R., Cheng, J. *Bioconjugate Chem.*, **2010**, *21*(1), 111-121.

196. http://www.organic-chemistry.org/namedreactions/click-chemistry.shtm

197. Kolb, H.C., Finn, M.G., and Sharpless, K.B. *Angewandte Chemie International Edition*, **2001**, *40*(11), 2004-2021.

198. Spiteri, C.M., John, E. *Angewandte Chemie International Edition*, **2010**, *49*(1), 31-33.

199. Hoogenboom, R., *Angewandte Chemie International Edition*, **2010**, *49*(20), 3415-7.

200. Diels, O., Alder, K. *Justus Liebig's Annalen der Chemie*, **1928**, *460*,98-122.

201. Prokai, L., Oon, S., Prokai-Tatrai, K., Abboud, K.A. Simpkins, J.W. *Journal of Medicinal Chemistry*, **2001**, *44* (1), 110-114.

202. Kassam, A., Bremner, G., Clark, B., Ulibarri, G., Lennox, R.B. *J. Am. Chem. Soc.*, **2006**, *128*(11), 3476-3477.

203. Kingston, D.G.I. PCT/2008/082956 WO 2009/062138, **2008.**

204. Ryppa, C., Mann-Steinberg, H., Biniossek, M.L., Satchi-Fainaro, R., Kratz, F. *Int J Pharm.*, **2009**, *368*, 89.

205. Le Sann, C. *Nat. Prod. Rep.*, **2006**, *23*, 357-367.

206. Li, S., Gray, B.P., McGuire, M.J., and Brown, K.C. *Bioorg Med Chem.*, **2011**, *19*(18), 5480-5489.

207. Seifert, B., Karst, U. *Analytical Chemistry,* **2007**, *79* (18), 7131-7138.

208. http://www.turbobeads.com

209. Lutz, J.F., Zarafshani, Z. *Advanced Drug Delivery Reviews*, **2008**, *60*, 958-970.

210. Spaldin, M. *Magnetic Materials: Fundamentals and Device Applications*, **2003**, Cambridge University Press.

211. Leuba, K.D., Durmus, N., Taylor, E. *International Journal of Nanomedicine*, **2013**, *8*, 731-736.

212. Wang, Y.X. *Quantitative Imaging in Medicine and Surgery*, **2011**, *1*, 35-40.

213. Mahmoudi, M. *Advanced Drug Delivery Reviews,* **2011**, *63*, 24-46.

214. Yen, S.K., Parasuraman, P., Tamil, S., *Theranostic*, **2013**, just accepted, doi:10.7150/thno.4827.

215. Kievit, F.M., Wang, F.Y., Zhang, M. *Journal of controlled release,* **2011**, *152*, 76-83.

216. Kaaki, K. *et al.*, *Langmuir*, **2012**, *28*(2), 1496-1505.

217. Hafeli, U., Riffle, J.S., Bardenstein, D. *Molecular Pharmaceutics*, **2009**, *6*, 1417-1428.

218. Weissleder, R., *et al.*, *American Journal of Roentgenology*, **1989**, *12*(1), 167-173.

219. Carrara, C., Licandro, E., S. Maiorana, "*Design and synthesis of new heterobifunctional linkers for the covalent binding of biomolecules onto superparamagnetic iron oxide nanoparticles(SPIONs)*", Conference Object, presented at "Attilio Corbella Summer School on Organic Synthesis" conference, Gargnano, **2012**.

220. Matsuo, J., Okano, M., Ishibashi, H., et al., *Tetrahedron: Asymmetry*, **2007**, *18*, 1906-1910.

221. Nara, K., Tsujimura, K. *Agricultural and Biological Chemistry*, **1978**, *42*(4), 793-798.

222. Kim, J.G., Jang, D.O. *Synlett*, **2008**, *13*, 2072-2074.

223. Schaetz, A., Grass, R., Kainz, Q., *et al.*, *Chemistry of Materials*, **2010**, *22*(2), 305-310.

224. Weber, W., Lienhart, C., Fussenegger, M. *et al.*, *Journal of Biotechnology*, **2009**, *141*, 118-122.

225. Dobson, J. *Drug Development Research*, **2006**, *67*(1), 55-60.

226. Buschow, K.H.J *Encyclopedia of materials: science and technology*, **2001**, Elsevier.

227. Jiang, H., Liu, F., Yang, H., Li, Y. *Biological Trace Element Research*, **2012**, *146,* 23-29.

228. Papis, E., Rossi, F., Gornati, R. *Toxicology Letters*, **2009**, *189*, 253-259.

229. Sekhan, B., Kamboj, S. *Nanomedicine*, **2010**, *6*(5), 612-618.

230. Grass, R.N., Athanassiou, E.K., Stark, W.J. *Angewandte Chemie International Edition*, **2007**, *46*, 4909-4912.

231. Reddy, V. R. *Synlett*, **2006**, *11*, 1791-1792.

232. Brust, M., Walker, M., Whyman, R. *Journal of the Chemical Society, Chemical Communications*, **1994**, 801-802.

233. http://www.nlm.nih.gov/medlineplus/druginfo/meds/a685038.html.

234. Pissuwan, D., Valenzuela, S.M., Cortle, M.B *Trends in Biotechnology*, **2006**, *24*(2),62-67.

235. Chen, Y.S., Hung, Y.C., Huang, G.S. *Nanoscale Research Letters*, **2009**, *4*, 858-864.

236. Qian, X. *Nature Biotechnology*, **2008**, *26* (1).

237. Conde, J., Ibarra, M.R., Tortiglione, C. *ACS Nano*, **2012**, *6*(9), 8316-8324.

238. Gibson, J.D., Khanal, B.P., Zubarev, E.R. *Journal of American Chemical Society*, **2007**, *129*, 11653-11661.

239. Jain, S., Hirst, D.G, O'Sullivan, J.M. *British Journal of Radiology*, **2012**, *85*(1010), 101-113.

240. Aillon, K.L. *et al*., *Advanced Drug Delivery Reviews*, **2009**, *61*, 457-466.

241. Schmid, G. *Chem. Soc. Rev*., **2008**, *337*, 1909-1930.

242. Pan, Y.*et al*., *Small*, **2007**, *3*, 1941-1949.

243. Chithrani, B.D., Ghazani, A.A., Chan, C.W. *Nano Lett.*, **2006**, *6*(4), 662-668.

244. Falciani, C., Fabbrini, M., Pini, A., Lozzi, L. *et al*., *Mol Cancer Ther*, **2007**, *6*(9),OF1-8.

245. Falciani, C., Lelli, B., Brunetti, J. *et al*., *Current Cancer Drug Targets*, **2010**, *10*(7), 695-704.

246. Liu, D.Z., *et. Al*., *Bioorg. Med. Chem.*, **2007**, *17*, 617-620-SI.

247. B. Allen, V.C., Robertson, C.G., Turega, S.M., Philp, D. *Organic Letters*, **2010**, *12*(9), 1920-1923-SI.

References Conclusion

248. Falciani, C., Brunetti, J., Lelli, B., Ravenni, N., Lozzi, L., Depau, L., Scali, S., Bernini, A., Pini, A., Bracci, L. *J. Med. Chem.*, **2013**, *56*, 5009-5018.

249. Mustain, W.C., Rychahou, P.G., Evers, B.M. *Curr. Opin. Endocrinol., Diabetes Obes.*, **2011**, *18*, 75-82.

250. Go, G.W., Mani, A. *J. Biol. Med*., **2012**, *85*, 19-28.

251. Gettins, P.G., Dolmer, K. *Biochem. J.*, **2012**, *443*, 65-73.

2. Protein inspired tumor targeted therapy: Synthesis of Pt(II) complexes tethered to nuclear targeting peptides

2.1 Platinum(II)-RrRK peptide conjugates

2.1.1. Introduction

Currently available platinum-containing drugs lack optimal selectivity for tumors and have narrow therapeutic indices. Very extensive efforts to identify analogues with a broader spectrum of antitumor activity and reduced toxicity have been carried out[1] but only cisplatin, carboplatin and oxaliplatin are currently FDA approved. An aim of recent studies in this field is to increase the therapeutic index by targeting drugs to the tumor and limiting their access to normal tissues.[2]

The biological target of the widely used anticancer drug cisplatin is nuclear DNA.[3] There is ample evidence to support this hypothesis, the most convincing of which is the observation that cells with decreased nuclear DNA repair capacities are hypersensitive to cisplatin.[4] Nevertheless, the electrophilic properties of cisplatin and its aquated analogues enable this and related platinum-based drugs to bind to a wide range of intracellular nucleophiles, such as proteins, RNA, and phospholipids.

Biological barriers are of fundamental importance in understanding evolution, systems biology, and the prevention, detection, and treatment of disease. Methods to enhance or control selective passage of therapeutics into or through such barriers are key to the future of drug therapy and many fundamental advances in science. Research in this area offers the possibility of improving the bioavailability of existing drugs, enabling the delivery of new cargo and drug candidates (e.g., RNAi, shRNA, DNA, proteins, imaging agents, and sensors)[5] and accessing difficult sites (e.g., the blood–brain barrier and eye). Other techniques allow tissue- or cell-selective entry, modulate the activity of agents by controlling their release, and avoid or minimize toxicity and metabolism.[6-7] All of them could dramatically enhance human therapy and our fundamental understanding of living systems.

Several physical and molecular techniques have been developed over the years to enable small molecule (diagnostic or therapeutic) uptake into cells and tissue. Peptide conjugation is a widely used and effective method for improving both cellular and nuclear entry of a variety of cargo molecules.[8] Much emphasis in recent years has been placed on peptide transporters, often referred to as cell-penetrating peptides (CPPs). CPPs are short peptides with fewer than 30 residues and a net positive charge and act in a receptor- and energy-independent manner. Other protein and peptide-inspired transporters, including non-natural peptides and peptoids have also been investigated.[9] Organelle-specific CPPs been generated, providing a means to target specific subcellular sites.[10] Cellular internalization of large hydrophilic therapeutic agents such as proteins or nucleic acids is still a challenging task because of the presence of the plasma membrane, which constitutes an impermeable barrier to such molecules. In order to circumvent this problem, many CPPs were designed from sequences of membrane interacting proteins, such as fusion proteins, signal peptides, transmembrane domains and antimicrobial peptides.[10]

Among others, the transcription-transactivating (Tat, RKKRRQRRR) protein of HIV-1 has the ability to cross the plasma membrane of neighboring cells and can also form complexes which are rapidly

internalized.[11] These complexes are stabilized by electrostatic interactions occurring between the positive charges of the peptide and the negative charges of the plasma membrane and the phosphate groups in nucleic acids.[11] Here the synthesis and characterization of platinum(II) complexes tethered to a nuclear targeting peptide is reported. The RrRK-amide peptide was explored as a targeting peptide. $[PtCl(DMF)(NH_3)_2](NO_3)$ (**1**), $[Pt(DAP)(Cl_2)]$ (**2**) and $[Pt(succac)(NH_3)_2](NO_3)$ (**3**), where DAP = 2,3-diaminopropionic acid and succac = succinylacetonate were selected to investigate the effect of different chemical-physical properties of the cargo on the passage of the complexes through the plasma membrane (Figure 2.1).
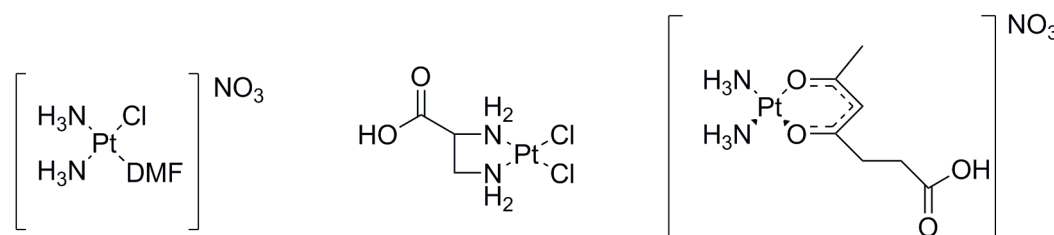
Figure 2.1. Chemical structures of $[PtCl(DMF)(NH_3)_2](NO_3)$ (**1**), $[Pt(DAP)(Cl_2)]$ (**2**) and $[Pt(succac)(NH_3)_2](NO_3)$ (**3**)

Studies by *Kelley* and co-workers have demonstrated the feasibility of using very short peptides, Tat derivatives, to target small molecules to the nucleus or mitochondria. Previous studies of arginine-based peptide oligomers indicated that high levels of cellular uptake can be achieved through the inclusion of cationic residues. While many CPPs, including Tat, have been shown to enter cells by endocytosis[12], some artificial sequences have been shown to traverse the plasma membrane by direct potential-driven diffusion.[13-14] Indeed, while treatment with endocytosis inhibitors does not decrease the uptake of the CPPs, treating with gramicidin or valinomycin valinomycin, two agents that alter the plasma membrane potential, results in a pronounced decrease in the uptake of the peptides, due to the depolarization of the plasma membrane.[15] The positive molecular charge of CPPs facilitates charge-driven uptake through the plasma membrane ,which exhibits a potential gradient that will electrophorese cationic species from the extracellular space into the cell.[16] Kelley et al. demonstrated that the antioxidant thiazole orange (TO) conjugated to the tetrapeptide RrRK (r = D-arginine and R= L-arginine) accumulates primarily in the nucleus of HeLa cells, whereas TO-FrFK (F = phenylalanine) localizes mainly in the mitochondria. Both conjugates were reported to cross the plasma membrane with efficiencies approaching that of the longer Tat peptide (RKKRRQRRR). Nevertheless, the inner membrane of mitochondria is much more hydrophobic than the plasma membrane, which necessitates preservation of a high degree of lipophilicity in order to allow partitioning of the peptides through the lipid bilayer. Using short peptides as the nuclear targeting signal for metal complexes reduces the positive charge added by the peptide as compared to the longer octaarginine, and thus should reduce the amount of nonspecific DNA binding. [17] Moreover, it has been proved that peptides containing D-amino acids (in this case,r = D-Arg) are generally much more resistant to proteolysis, which is critical for effective cancer therapeutics.[18] The synthesis, purification and preliminary characterization of four different platinum(II) amide-peptide-functionalized complexes is reported. A fluorophore-labeled analogue (**7**), was also prepared featuring attachment of Coumarin343 on the amino side-chain of a *C*-terminal lysine. The complex was used to facilitate cellular imaging studies and its cytotoxicity in cancer cells was tested.

2.1.2. Experimental Section

Materials and methods.

NMR measurements were recorded on a Bruker DPX-400 spectrometer in the MIT Department of Chemistry Instrumentation Facility at 20 °C. ^{1}H and ^{13}C NMR spectra were referenced internally to residual solvent peaks and chemical shifts are expressed relative to tetramethylsilane, $SiMe_4$ (δ = 0 ppm). Reverse-phase HPLC purifications were carried out on an Agilent Technologies 1200 Series HPLC system. Electrospray ionization mass spectrometry (ESI-MS) measurements were acquired on an 1100-series Agilent LC/MSD ion trap. For FTIR spectra, samples were prepared as KBr disks, and data were recorded with a ThermoNicolet Avatar 360 spectrophotometer running the OMNIC software. Solutions used for biological studies were dissolved in MilliQ water (or PBS for cisplatin) and sterile filtered. The platinum concentrations of the solutions were determined by graphite-furnace atomic absorption spectroscopy (GFAAS) using a Perkin-Elmer AAnalyst600 spectrometer. All solvents were reagent grade unless otherwise specified and commercially available reagents were used as received. HPLC grade acetonitrile, anhydrous *N,N*-dimethylformamide (DMF), dichloromethane, 4-methylpiperidine, *N,N*-diisopropylethylamine (DIPEA), Rink amine resin (0.61 mmol/g loading, 100-200 mesh), Coumarin 343 and trifluoroacetic acid (TFA) were purchased from Sigma-Aldrich. The amino acids: FMOC-L-Arg(Pfb)-OH, FMOC-D-Arg(Pfb)-OH, FMOC-Lys(Mtt)-OH and FMOC-Lys(Boc)-Wang resin (0.50 mmol/g loading, 100-200 mesh) were purchased from Aapptec. 2-(7-Aza-1H-benzotriazole-1-yl)-1,1,3,3-tetramethyluronium hexafluorophosphate (HATU) was procured from Oakwood Chemicals. Disposable 2.5-mL reaction vessels were ordered from Torviq.

Synthesis of [PtCl(DMF)(NH$_3$)$_2$](NO$_3$) (1)

1
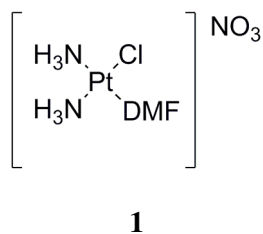
To a suspension of cisplatin (75.3 mg; 0,25 mmol) in 1.5 mL of anhydrous DMF, AgNO$_3$ (40.77 mg; 0.24 mmol, 0.9 equiv.) was added as solid and stirred in the dark, at r.t, overnight. The white suspension was filtered through Celite and the the light yellow filtrate was used for the coupling to the peptide without further purifications.

Synthesis of [Pt(DAP)(Cl₂)] (2)
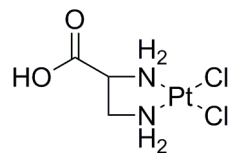
2

To a red solution of K_2PtCl_4 (0.20 g, 0.48 mmol) in 4 mL of water, DL- 2,3 diaminopropionic acid hydrochloride (0.068 g, 0.48 mmol) was added, in the dark. The mixture was stirred at reflux, in the dark, overnight, and a yellow precipitate was observed. The reaction solvent was removed under vacuum to obtain a yellow powder in quantitative yield. ESI -MS: m/z = 368.8 [M-H]⁻. Further data are reported in literature.[19]

Synthesis of succinylacetone
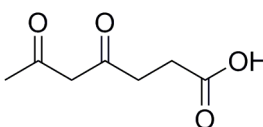
A round bottom flask was purged with Argon and NaH (60% in oil; 6.0 g; 250 mmol) was suspended in ethyl acetate (65 mL). Levulinic acid (5.8 g; 50.0 mmol) was added over a period of 10 min at r.t, after the allotted time the mixture was refluxed for 20 min and cooled at r.t and poured onto 50 mL of water. The suspension was acidify to pH=2 with concentrated H_2SO_4 (3.5 mL), the layers were separated. The aqueous phase was saturated with NaCl and extracted with AcOEt (2 × 50 mL). The combined organic phase were dried over Na_2SO_4, filtered and evaporated *in vacuo*. The crude product was co-evaporated with toluene (2× 50 mL), diluted with diethyl ether (100 mL) and precipitated with hexane (50 mL). The suspension was kept at -40°C for 4 h and the white precipitate was isolated by vacuum filtration as pure final product in 60 % yield. NMR and IR data reported in literature.[20]

Synthesis of [Pt(succac)(NH₃)₂](NO₃) (3)

3
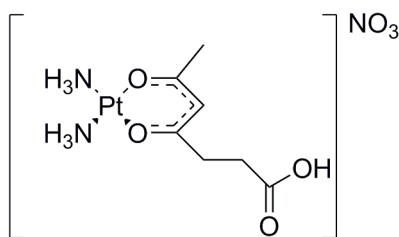
To a suspension of cisplatin (200 mg; 0.66 mmol) in 5 mL of water, AgNO$_3$ (214 mg; 1.26 mmol; 1.9 eqiv.) was added and the mixture was stirred in the dark, at r.t, overnight. The white suspension was filtered through celite to remove the AgCl. To the filtrate, a 70°C solution of NaOH (27 mg; 0.664 mmol) and succinylacetone (106.3 mg; 0.67 mmol) in 4 mL of water was added in a dropwise manner. The yellow solution was stirred at r.t for 5 h then freeze-dried overnight. The resulting pale powder was dissolved in 5 mL of water and 2 drops of 25% HNO$_3$ were added. Subsequently, acetone (25 mL) was added to afford a clear orange solution. The orange solution was added to 100 mL of diethyl ether in a dropwise manner and the turbid white suspension was stirred for approximately 3 min, resulting in the deposition of an oily orange-brown residue. The turbid supernatant was decanted and added to 100 mL of ether. The mixture was stored at -40 °C for 1.5 h and filtered to collect a white solid. The white solid was washed with diethyl ether (2 x 10 mL) and then dried in vacuo to obtain a white power (95 mg) in 37 % yield. Mp 159–164 °C (dec.). ^{1}H NMR (400 MHz, MeOD-d_4): δ 5.65 (s, 1H), 4.44 (br s, 6H), 2.58 (t, 2H), 2.44 (t, 2H), 1.88 (s, 3H). ^{13}C NMR (100 MHz, MeOD-d_4): δ 186.5, 186.3, 176.7, 102.7, 35.1, 31.0, 26.1. ^{195}Pt NMR (86 MHz, MeOD-d_4): δ -1570. IR (KBr, cm^{-1}): 3432 m, 3285 s, 1708 m, 1563 s, 1524 s, 1384 vs, 1356 s, 1309 s, 1202 w, 1175 m, 1039 w, 807 w, 645 w. ESI-MS (m/z) Calcd [M+H]$^+$ 386.1, Found [M+H]$^+$ 386.1.

Synthesis and characterization of peptides:

All the peptides described herein were prepared using standard FMOC solid-phase peptide synthesis (SPPS) protocol[21] on the Aapptec Focus Xi synthesizer.

General procedure SPPS for RrRK-COOH peptides:

FMOC-Lys(Boc)-Wang resin (0.5 mmol/g loading) was placed in a fritted reaction vessel and swelled with 7 mL of DCM for 20 min. *N*-terminal FMOC groups were removed by treating the resin with a solution of 20% 4-methylpiperidine in DMF (v/v) for a period of 15 min, followed by a 5 × 5 mL wash with DMF. For all coupling reactions, 4 equiv. of FMOC-protected amino acids and 4 equiv. of HATU were combined in the amino acid vial and dissolved *in-situ* with 3 mL of a 10% DIPEA/DMF (v/v) solution, added to the resin and allowed to react for 60 min. Between each FMOC-deprotection and amino acid addition, the resin was thoroughly washed with DMF (4 x 5 mL). After all amino acids have been added, the resin was washed with DMF 5 x 5 mL and 5 x 5 mL of DCM. The resin was dried overnight under vacuum. A few resin beads were taken, treated with TFA for 60 min to analyze the product by ESI-MS. Following confirmation that the desired product was formed, the last N-terminal FMOC group was removed by treating the resin with a solution of 20% 4-methylpiperidine in DMF (v/v) for a period of 15 min. Subsequently, the resin was washed with DMF (5 x 5 mL) and the resin beads containing the peptide were transfer to a 5 mL Torviq disposable syringe. The platinum(II) complexes were coupled directly on the resin using different conditions as described below. Subsequently the solution was pushed out from the reaction vessel and the resin was washed with DMF (5 x 5 mL), with DCM (5 x 5 mL) and dried under vacuum. The platinum(II)-peptide constructs were cleaved from the resin using a mixture of 95% TFA and 5% water (v/v). The cleavage proceeded for 120 min after which the cleaving solution was poured into water and lyophilized. The platinum(II)-peptide construct was purified using semi-preparative HPLC on a C18 reverse-phase column (Agilent Zorbax SB-C18, 9.4 mm × 250 mm, 5 µm). A two-solvent system (A = 0.1% (v/v) TFA in H$_2$O; B = 0.1% TFA in acetonitrile (v/v)) was employed for purification. All platinum(II) complexes were purified using the following protocol. Isocratic flow: 2% B, 0-8 min; gradient, 2-35% B, 8-20 min;

gradient, 35-95% B, 20-25 min, isocratic flow: 2% B, 25-36 min. The flow-rate was kept constant at 3 mL/min throughout the purification. Fractions from sequential runs containing the desired platinum(II) complex were combined and lyophilized. The purity of the final product was assessed via analytical HPLC (Agilent Zorbax SB-C18, 5 μm, 4.6 mm x 250 mm) using the same protocol described above with a constant flow rate of 1 mL/min. The yield for each platinum(II)-peptide construct was determined using the resin loading and the platinum content as determined by GFAAS.

[PtCl(NH$_3$)$_2$]-RrRK-COOH (4): The resin containing the RrRK peptide was placed in a fritted 2.5-mL Torviq disposable syringe and swelled with 2 mL of anhydrous DMF for 30 min, then dried in vacuum. A solution of [PtCl(DMF)(NH$_3$)$_2$](NO$_3$) (**1**) was added with TEA (49 μL in 500 μL of dry DMF) in the syringe and the reaction mixture was shaken in the dark, overnight. The final platinum(II)-peptide complex (**4**) was purified as described above with a retention time of = 2.9 min and it was judged to be ≥ 99% pure based on the integrated chromatogram (yield 3%). The isolated species (**4**) was characterized using ESI-MS (m/z) Calcd [M+H]$^+$ 878.4, Found [M+H]$^+$ 879.4.

[Pt(DAP)(Cl$_2$)]-RrRK-COOH (5): The resin containing the RrRK peptide was placed in a fritted 2.5-mL Torviq disposable syringe and swelled with 3 mL of anhydrous DCM for 30 min, then dried under vacuo. [Pt(DAP)(Cl$_2$)] (**2**) (92 mg; 0.25 mmol), DIC (39 μL, 0.25 mmol) and NHS (57.5 mg; 0.5 mmol) were combined in a glass vial. Immediately prior to coupling, the solids were dissolved in 3.0 mL of a freshly prepared 0.5 M DIPEA/DMF (v/v) solution, added to the peptide in the reaction vessel and shaken for overnight. After purification, the final platinum(II)-peptide (**5**) with a retention time of = 14.6 min, was judged to be ≥ 97% pure based on the integrated chromatogram (yield 5%). The isolated species (**5**) was characterized using ESI-MS (m/z) Calcd [M+H]$^+$ 966.8, Found [M+H]$^+$ 967.4.

[Pt(succac)(NH$_3$)$_2$]-RrRK-COOH (6): [Pt(succac)(NH$_3$)$_2$](NO$_3$) (**3**) (92 mg; 0.25 mmol) and HATU (93 mg, 0.25 mmol) were combined in a glass vial. Immediately prior to coupling to the peptide, the solids were dissolved in 3.0 mL of a freshly prepared 0.5 M DIPEA/DMF (v/v) solution, placed in the reaction vessel and shaken for 60 min. After purification, the final platinum(II)-peptide (**6**) with a retention time of = 21.6 min, was judged to be ≥ 96% pure based on the integrated chromatogram (yield 9%). The isolated species (**6**) was characterized using HR- ESI -MS: m/z = Calcd [M+2H]$^{2+}$ 491.7364, Found [M+2H]$^{2+}$ 491.7378; Calcd [M+H]$^+$ 982.4721, Found [M+H]$^+$ 983.4736.

[Pt(succac)(NH$_3$)$_2$]-RrRK-Coumarin343 (7): Rink amide resin (100 mg; 0.06 mmol) was placed in a fritted 5.0-mL Torviq disposable syringe and deprotected with a 20% solution of PIP in dry DMF for 20 min, then washed with DMF (5 × 1.5 mL) and swelled with DCM. The resin was loaded with FMOC-Lys(MTT)-OH (150 mg; 0.24 mmol) and HATU (93 mg; 0.24 mmol) in a freshly prepared 0.5 M DIPEA solution in dry DMF and shaken for 1 h at r.t. After the allotted time, the resulting solution was expelled from the syringe and the resin was washed with DMF (5 × 1.5 mL). The resin was subsequently washed with DCM (5 × 1.5 mL) and dried in vacuo for a period of ≥ 20 min. MTT group was removed with a 2% TFA solution in DCM (2 x 10 min). Several washings with DCM were performed and the resin was dried in vacuo. The resin was loaded with Coumarin 343 (65.8 mg; 0.24 mmol) and HATU (93 mg; 0.24 mmol) in a freshly prepared 0.5 M DIPEA solution in dry DMF and shaken for 1 h at r.t. After the allotted time, the resulting solution was expelled from the syringe and the resin was washed with DMF (5 × 1.5 mL). The resin was subsequently washed with DCM (5 × 1.5 mL) and dried in vacuo for a period of ≥ 20 min. A small amount of resin was cleaved with TFA to confirm the presence of the desired product by ESI-MS (ESI -MS: m/z = 882 [M+H]$^+$). The resin was placed in the automatic peptide synthesizer and the RrRK primary sequence was assembled using a synthesizer utilizing a single coupled 4 fold excess HATU/0.5M DIPEA solution in dry DMF

activation protocol using Fmoc-Arg(Pbf)-OH, Fmoc-D-Arg(Pbf)-OH and Fmoc-Arg(Pbf)-OH as building blocks. [Pt(succac)(NH$_3$)$_2$](NO$_3$) (**3**) was coupled with the resin for 1 h and the platinum complex (**7**) was cleaved and purified as above described with a retention time of= 22.2 min and was judged to be ≥ 97% pure based on the integrated chromatogram (yield 8%). HR- ESI -MS: m/z = Calcd [M+2H]$^{2+}$ 625.2913, Found [M+2H]$^{2+}$ 625.2933.; Calcd [M+H]$^{+}$1249.5790., Found [M+H]$^{+}$1249.5793.

Cytotoxicity assay

Cytotoxicity assays were performed in HeLa, A2780 and A2780CP70 cells. A trypsin (Promega, Madison, WI, USA) stock solution was obtained by dissolution in 1 mM acetic acid (1 µg/µL, pH 3.0). A2780 and A2780CP70 cells were cultured in RMPI medium containing L-glutamine, 10% FBS, 100 U/mL penicillin, and 100 µg/mL streptomycin (all from cellgro, Manassas, VA, USA) at 37 °C, in a humidified atmosphere at 5% CO$_2$. Hela cells were cultured in DMEM medium supplemented with 10% fetal bovine serum (FBS) and 1% penicillin/streptomycin. The cytotoxicity assay was preformed according to the following protocol. On the first day, 200 µL of trypsinized tumor cells (2000–2500 cells/well) were plated in 96-wells flat bottom microtiter plates. The plates were preincubated for 24 h at 37 °C, 5% CO$_2$ to allow the cells to adhere. On day 2, a threefold dilution sequence of eight concentrations in full medium was made, starting with stock solution of the compounds in PBS. The cell medium was removed carefully and 150 µL of fresh medium was added to each well. The compound was added at each concentration (50 µL) to the wells in triplicate. The cells were exposed to the compounds for 72 h at 37 °C and 5% CO$_2$ atmosphere. On day 5, the medium was carefully removed from the wells and 200 µL of MTT solution (0.8 mg/ml) was added to each well. The plates were stored at 37 °C for 3 h to obtain formazan crystals.[22] The supernatant was carefully removed from each well and the blue formazan crystals were dissolved in 100 µL DMSO. The absorbance of the resulting solution was read at 570 nm using an automatic microplate reader. The absorbance was normalized to the control (platinum-free wells) and the results were analyzed with GraphPad Prism™ analysis software package (Graph- Pad Software, San Diego, USA) using non-linear regression (sigmoidal dose response, variable slope). The pIC$_{50}$ values (IC$_{50}$ is the drug concentration that produces 50% of the maximum possible response) were determined.

Cell Imaging Studies. HeLa cells were seeded in poly-d-lysine coated MatTek petri dish (35 mm, 14 mm Microwell) in 2 mL of growth medium. At ≈ 60% confluency, the cells were imaged. The growth media was exchanged for premixed media containing 10 µM of the Pt-Coumarin343 construct (**7**) and the cells were allowed to incubate with the dye for either 2 h or overnight. At the end of the incubation period, the media was aspirated, and the cells were washed with 3 × 1 mL PBS and submerged in 2 mL of dye-free DMEM for imaging. The imaging experiments were performed using a Zeiss Axiovert 200M inverted epifluorescence microscope equipped with an EM-CCD digital camera (Hamamatsu) and a MS200 XY Piezo Z stage (Applied Scientific Instruments). The light source is an X-Cite 120 metal-halide lamp (EXFO) and the fluorescence images were obtained using an oil-immersion objective at 63× magnification. The microscope is operated using Volocity software (Perkin-Elmer).

For IR, ESI-MS and NMR spectra see Supporting Information.

2.1.3. Results and Discussion

RrRK peptide

In a recent paper by Barton and coworkers,[23] a series of nuclear targeting peptides, coupled to Ru(II) complexes, has been investigated to better understand the importance of the length of polyarginine CPPs in internalization. The results show that the tetrapeptide RrRK (r = D-arginine) accumulates primarily in the nucleus of HeLa cells and that there was an enhancement in cellular uptake for Ru– RrRK versus Ru-octaarginine, when incubated with HeLa at 20 µM for 24 h. No platinum-based-RrRK complexes have been synthesized so far. Thus, I decided to investigate the internalizing capability of RrRK peptide coupled to a Pt-cargo and the manner in which different platinum(II) ligands affect the internalization process.

[PtCl(NH$_3$)$_2$]-RrRK-COOH (4)

As described by *Reedijk et al.*[24] after the synthesis of the peptide on solid phase, the free terminal amine was platinated with a five fold-excess of activated *cis*-diamminedichloroplatinum (II) by overnight reaction with 0.9 eqiv. of AgNO$_3$, leading to the immobilized compound (4) in a 2% yield (Scheme 2.1)
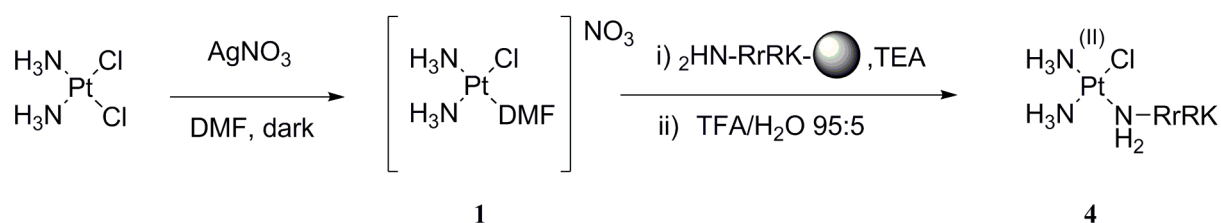
Scheme 2.1.

To overcome the poor yield obtained for complex (4), alternative strategies have been investigated, in particular avoiding the direct platination of the peptide on solid phase. For this purpose two platinum(II) ligands have been designed. The amide functionalization of platinum derivatives can provide access to a variety of new complexes. This approach was used in our lab and others to attach targeting peptides to platinum ligands[25] and has been used for the synthesis of all the compounds reported herein.

[Pt(DAP)(Cl$_2$)]-RrRK-COOH (5)

Platinum(II) complexes containing ethylene diamine or functionalized ethylene diamines have previousely been tested for in vitro and in vivo activity. Several studies on structure–activity relationships concern [PtAm$_n$X$_2$] species where Am=amine and X=halide.[26] The nature of the amine side chain and its length play an important role in the hydrolytic behavior of the complexes, influencing their solubility and thus affecting the membrane permeability and consequently influencing the platinum concentration inside the cell.[27] In particular, the platinum complex of 2,3-diaminopropionic acid, called [PtCl(DAP)(Cl$_2$)], has been shown to be able to form intrastrand adducts with DNA and to distort the double helix by changing the base stacking. Moreover, cell-survival assays indicate that [PtCl(DAP)(Cl$_2$)] shows cytotoxic activity, at high concentrations, against tumor cells in a dose- and time-dependent way, similar to that known for carboplatin.[28] [PtCl(DAP)(Cl$_2$)] (2) was synthesized from K$_2$PtCl$_4$, by reaction with AgNO$_3$ and subsequently DL- 2,3 diaminopropionic

acid hydrochloride. The compound was used for the coupling without further purification. In a first attempt, the RrRK was treated with a 4-fold excess of (**2**) and HATU for 1 h but the coupling was unsuccessful. Subsequently, the obtained platinum complex (**2**) was coupled to the free terminal amine of RrRK peptide on the resin using DIC and NHS as coupling agents overnight. The more harsh conditions allowed the desired platinum complex (**5**) to be isolated in 9 % yield (Scheme 2.2).
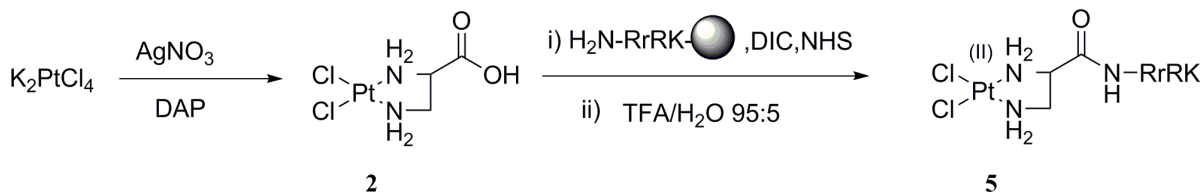
Scheme 2.2.

[Pt(succac)(NH$_3$)$_2$]-RrRK-COOH (6)

Since the introduction of cisplatin, thousands of platinum complexes have been synthesized and evaluated for their antitumor activity. The main aim of these intensive investigations was to obtain drugs with at least an equal activity but reduced toxicity compared to that found for cisplatin. The strategy to reduce toxicity involved increasing the solubility and stability of the complexes in water. This has been generally achieved by replacing the chloro ligands either with chelating carboxylate, oxalate, or glycolate. This kind of leaving group is the main feature of the second generation compounds. The amelioration of toxic side effects associated with the use of this drug has been an impetus for the development of the second-generation platinum chemotherapeutic agent, carboplatin. Cisplatin and carboplatin operate by the same mechanism. Labile ligands in the coordination sphere, chloride for cisplatin and 1,1-cyclobutanedicarboxylate (CBDCA) for carboplatin, are displaced by water or other biological nucleophiles, and the activated cis-diammineplatinum(II) moiety binds to purine bases in nuclear DNA.[29] The so-called leaving ligands of platinum anticancer agents influence not only the aquation rate but also the lipophilicity of the resulting complex. Both parameters, as exemplified by carboplatin, influence overall pharmacokinetic properties. In particular, exchange of the original halide leaving groups of platinum(II) compounds with carboxylates led to new complexes with improved aqueous solubility, hydrolytic stability, and cellular uptake. In recent time, *Wilson et al.* described how acetylacetonate (acac) and related β-diketonates ligands form a diverse class of complexes with many applications in inorganic chemistry. Moreover, complexes containing these ligands have a similar spectrum of activity as that of cisplatin.[30]
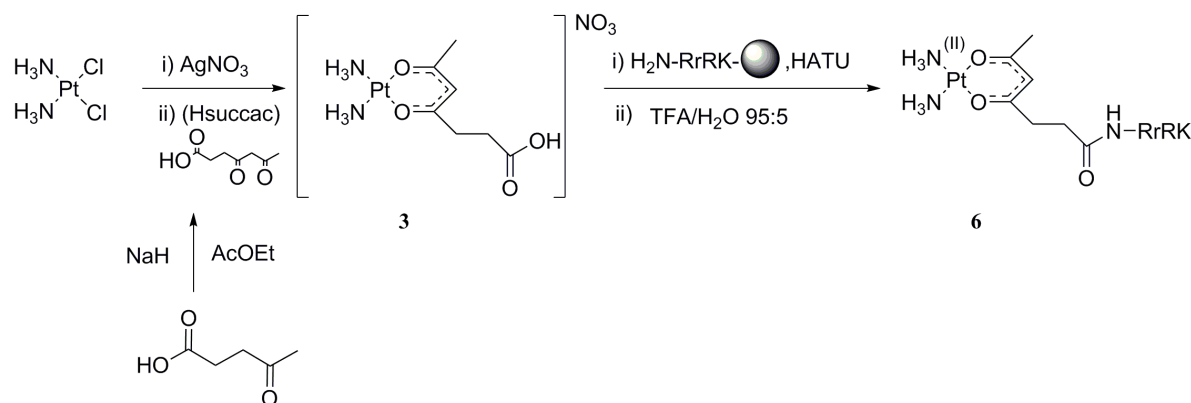
Scheme 2.3.

Succinylacetonate (succac) β-diketonate was used to realize a ligand with a free carboxylic acid, suitable for the coupling to the N-terminal amine of the targeting peptide RrRK. The platinum β-diketonate was synthesized from cisplatin. Cisplatin was first activated by treatment with AgNO₃ to remove the chloride ligands as insoluble AgCl and generate reactive solvated cisdiammineplatinum(II) cations. Subsequent treatment with the sodium salt of the β-diketonate ligand and purification by precipitation in diethyl ether affords compound (**3**) in 50 % yield. The obtained complex was treated as an amino acid and coupled, in 4-fold excess, to the free terminal amine of RrRK peptide, using HATU as coupling agent and a 0.5 M solution of DIPEA in dry DMF, for 1 h. Cleavage from the resin and purification by HPLC was performed as described above to obtain the desired platinum complex (**6**) in 12% yield (Scheme 2.3).

[Pt(succac)(NH₃)₂]-RrRK-Coumarin343-COOH (7)

The different physicochemical natures of fluorophores influence passage trough the membrane of the cell-permeable constructs. Analysis of the subcellular distribution of cell-permeable peptide/cargo constructs by fluorescence microscopy enables the identification of the cellular compartments targeted by a cell-permeable construct. [31]A fluorescein group, for example, carries negative charge and impaires nuclear internalization of the peptide complexes. As evidence, endosomal trapping of fluorescein-tag derivatives can be observed as punctuate cytoplasmatic staining.[31-32] Since no co-localization in endosomes was reported for Coumarin343, this fluorophore was selected among others. A fluorescent-tagged construct was prepared to facilitate cellular imaging studies. [Pt(succac)(NH₃)₂](NO₃) (**3**) was selected from among the other complexes prepared selected because it easily reacted with RrRK peptide to give the final complex in good yield.
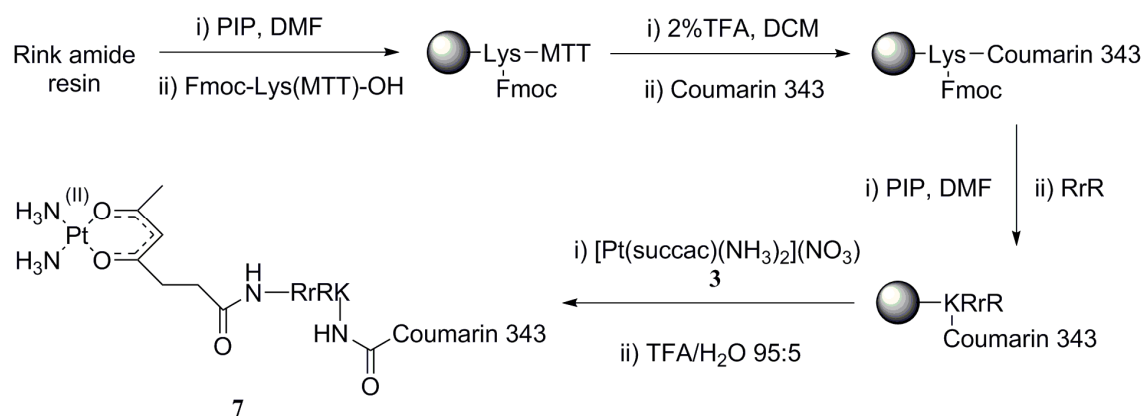
Scheme 2.4.

Coumarin 343 was attached to the ε- amino group of the lysine side chain through an amide bond, enabling the N-terminal modification of the RrRK peptide with [Pt(succac)(NH₃)₂](NO₃) (**3**). Conjugation of the fluorophore was carried out via incorporation of FMOC-Lys(MTT)-OH as a building block durimg peptide synthesis. In an initial attempt, the RrRK peptide was assembled on solid phase and the MTT group was selectively removed with a 2% TFA solution in DCM. Coumarin 343 and [Pt(succac)(NH₃)₂](NO₃) were attached following the same coupling protocol as the one for (**5**). No ESI-MS peak corresponding to the desired product was found. Since the steric hindrance of Coumarin 343 seemed to impair the reactivity of the N-terminus of the peptide, an alternative strategy was developed. In the first step FMOC-Lys(MTT)-OH was attached to the Rink amide resin, MTT was removed and Coumarin 343 was coupled. In subsequent steps, the construction of the primary sequence of the peptide and the coupling with (**3**) was performed to provide (**7**) in 7% yield (Scheme 2.4).

Cytotoxicity determination of platinum(II) complexes

MTT assays were carried out in two or three independent experiments in duplicate as described above. A series of eight concentrations of cisplatin and platinum(II)-peptide conjugates were prepared to perform a dose-response study. The IC_{50} values from the cytotoxicity assays are summarized in Table 2.1.

Considering the ligands coordinated to the platinum, [Pt(DAP)(Cl₂)] (**2**) was ineffective in all the cancer cell lines, likely because its negative charge at physiological pH impaired passage through the plasma membrane.

Compound	HeLA cells IC$_{50}$ (µM)	A2780 cells IC$_{50}$ (µM)	A2780CP70 cells IC$_{50}$ (µM)
Cisplatin	3.5±0.34	5±0.31	10±0.15
[Pt(DAP)(Cl$_2$)] (**2**)	> 200	> 200	> 200
[Pt(succac)(NH$_3$)$_2$](NO$_3$) (**3**)	110±0.30	> 200	> 200
[PtCl(NH$_3$)$_2$]-RrRK (**4**)	10-30	/	/
[Pt(DAP)(Cl$_2$)]-RrRK (**5**)	15±0.40	40±0.24	> 200
[Pt(succac)(NH$_3$)$_2$]-RrRK (**6**)	60±0.23	>200	>200
[Pt(succac)(NH$_3$)$_2$]-RrRK-Coumarin343 (**7**)	5.5±0.07	/	/

± is referred to standard deviation

Table 2.1. IC$_{50}$ valus and standard deviation of platinum ligands and complexes in HeLa, A2780 and A2780CP70 cells.

The IC$_{50}$ values of [Pt(DAP)(Cl$_2$)]-RrRK-COOH (**5**) in HeLa and A2780 cells confirmed this hypothesis since the presence of two positive charges increased the uptake and the toxicity of the construct. [Pt(succac)(NH$_3$)$_2$](NO$_3$) (**3**) revealed a moderate activity in HeLa, but not in A2780 or A2780CP70 (as previously shown)[30]. In general, the results revealed a higher activity of all the tested platinum-peptide complexes than the unconjugated ones in cancer cell. [PtCl(NH$_3$)$_2$]-RrRK-COOH (**4**) showed high cytotoxicity in HeLa cells, mirroring the behavior of cisplatin in this cell line. This is likely because inside the cells (**4**) releases cisplatin. [Pt(succac)(NH$_3$)$_2$]-RrRK-COOH (**6**) followed the same trend of (**3**) but the conjugation with the peptide decreased the IC$_{50}$ value, demonstrating the effective targeting activity of RrRK. Finally, the fluorescent-tagged complex (**7**) showed cytotoxicity in HeLa cells, comparable to the one of cisplatin, confirming the idea that increasing the lipophilicity of constructs ameliorates the internalization process. Further studies of (**7**) in A2780 cells need to be performed

Cell Imaging Studies. Imaging studies of the Pt[(succac)(NH$_3$)$_2$]-RrRK-Coumarin343 (**7**) were carried out in HeLa cell line. 10 µM incubation concentration was used for these studies. Representative images are shown in Figure 2.2.
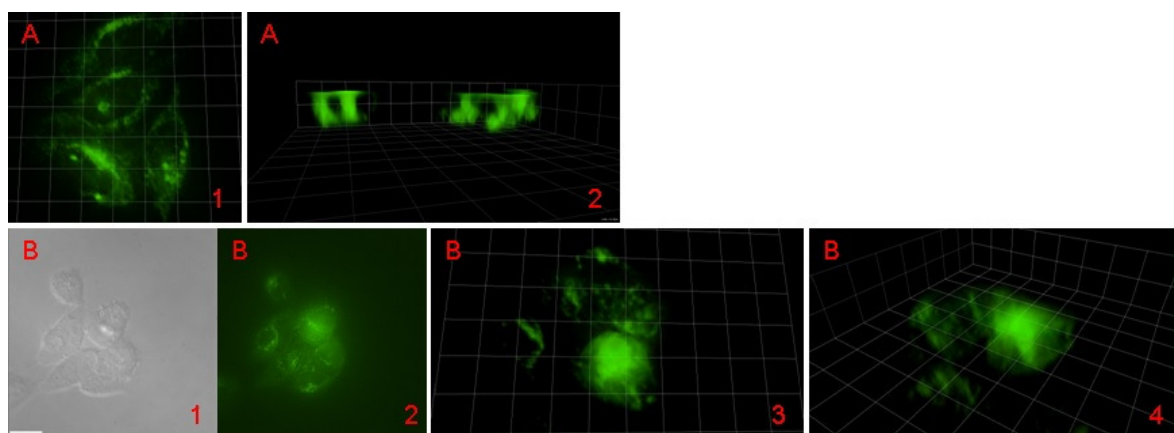
Figure 2.2. 2D images of HeLa cells treated with 10 μM Pt[(succac)(NH$_3$)$_2$]-RrRK- Coumarin343 (**7**) for 2 h (A1) and overnight (B1-B2) visualized by green channel(Mito-tracker green). 3D images of A1, side view (A2). 3D images of B1, overnight: top view (B3) and side view (B4).

Considering the IC$_{50}$ value of Pt[(succac)(NH$_3$)$_2$]-RrRK for this cell line, in the first attempt, HeLa cells were incubated with a 50 μM solution of (**7**). After 2 h of incubation cells were all dead. Cytotoxicity tests of [Pt(succac)(NH$_3$)$_2$]-RrRK- Coumarin343 was performed and showed the higher toxicity of the fluorescent-tagged construct as compared to the construct without the fluorophore. . Imaging studies were repeated, using a 10 μM solution of (**7**). Some punctate staining was observed after 2 hours of incubation (A1), indicating that the complex localized outside the nuclei. The 3D side view clearly show the lack of fluorescence in the nuclear area. Overnight, nuclear internalization was observed since the fluorescence was diffused and no punctuate staining was visible (B1-B4). These results clearly showed that the uptake through the plasma membrane is fast while the passage of the constructs through the nuclear membrane requires longer time.

2.1.4. Conclusions and future directions

In conclusion a series of platinum(II)-peptides complexes has been synthesized. All the compounds tested showed a better cytotoxic profile than the unconjugated ones, confirming that RrRK sequence is a valid nuclear internalizing peptide. The chemo-physical nature of the Pt precursors affects the internalization process since an increased lipophilicity of the constructs ameliorates the passage through the nuclear membrane. Further studies of DNA platination to confirm these hypotheses are required.

2.2 [Pt(succac)(NH$_3$)$_2$]-(Yr)$_3$-CONH$_2$ peptide complex

2.2.1. Introduction

The relationship between chemical structure and cellular localization of Tat derivatives peptides has been thoroughly investigated by Kelley and co-workers.[17] Peptide conjugates with a +3 charge showed

a striking trend between the lipophilicity and subcellular localization. The inner membrane of mitochondria is much more hydrophobic than the plasma membrane, which necessitates preservation of a high degree of lipophilicity in the primary sequence of the peptides in order to allow them to partition through this lipid bilayer. Tat derivatives with partition a coefficient (logP value) lower than -2.0 were essentially excluded from mitochondria, and instead appeared in the nuclei and cytoplasm of HeLa cells. In a recent submitted paper,[33] *Wisnovsky et al*. described a mitochondria penetrating peptide (MPP), $r(F_x r)_3$, coupled to platinum(II) complex (**3**). This study is the first to probe the consequences of platinum directed specifically to the mitochondria of cancer cells. In this work, phenylalanine (F) and cyclohexylalanine (F_x) were used to impart lipophilicity to the peptide. Replacing F_x with tyrosine (Y) is known to allow drug-peptide conjugates to be directed and to accumulate within the nucleus and the cytoplasm of cells rather than the mitochondrion.[34] Thus, $[Pt(succac)(NH_3)_2]$-$(Yr)_3$-$CONH_2$ conjugate (**8**), so called nucP, was synthesized to verify the effective nuclear targeting capability of the peptide on this complex as compared to the $r(F_x r)$ peptide. Synthesis and citotoxicity of (**8**) are reported here.

2.2.2. Experimental

Materials and methods

NMR measurements were recorded on a Bruker DPX-400 spectrometer in the MIT Department of Chemistry Instrumentation Facility at 20 °C. ^{195}Pt NMR spectra were referenced externally using a standard of K_2PtCl_4 in D_2O (δ = -1628 ppm). Reverse-phase HPLC purifications were carried out on an Agilent Technologies 1200 Series HPLC system. Electrospray ionization mass spectrometry (ESI-MS) measurements were acquired on an 1100-series Agilent LC/MSD ion trap. The platinum concentrations of the solutions were determined by graphite-furnace atomic absorption spectroscopy (GFAAS) using a Perkin-Elmer AAnalyst600 spectrometer. All solvents were reagent grade unless otherwise specified and commercially available reagents were used as received. HPLC grade acetonitrile, anhydrous *N,N*-dimethylformamide (DMF), dichloromethane, 4-methylpiperidine, *N,N*-diisopropylethylamine (DIPEA), Rink amine resin (0.61 mmol/g, 100-200 mesh), and trifluoroacetic acid (TFA) were purchased from Sigma-Aldrich. The amino acids: FMOC-D-Arg(Pfb)-OH and FMOC-L-Tyr(tBu)-OH were purchased from Aapptec. 2-(7-Aza-1H-benzotriazol-1-yl)-1,1,3,3-tetramethyluronium hexafluorophosphate (HATU) was procured from Oakwood Chemicals. Disposable 2.5-mL reaction vessels were ordered from Torviq.

General procedure SPPS for $(Yr)_3$ peptide:

Rink amide resin (0.61 mmol/g, 100-200 mesh) was placed in a fritted reaction vessel and swelled with 7 mL of DCM for 20 min. *N*-terminal FMOC groups were removed by treating the resin with a solution of 20% 4-methylpiperidine in DMF (v/v) for a period of 15 min, followed by 5 × 5 mL washes with DMF. For all coupling reactions, 4 equiv. of FMOC-protected amino acids and 4 equiv. of HATU were used. The peptide was assembled according to the procedure reported above for RrRK peptides and purified using the following protocol: isocratic flow: 2% B, 0-16 min; gradient, 2-20% B, 16-18 min; gradient, 20-95% B, 18-30 min, isocratic flow: 2% B, 30-36 min.

Neurotoxicity Studies. Dorsal root ganglion (DRG) tissue was extracted from an embryonic day 18 Sprague-Dawley rat. Microdissection was performed at Neuromics Inc. Connective tissue was digested with 1 mg/mL Collagenase/Dispase and cells were disassociated by trituration. Cells were

plated at 50,000 cells/well in 8 well Ibidi μ-slides coated with Poly-D-Lysine (30 μg/mL) and cultured for 4 days in NbActive media containing 25 ng/mL NGF. Following differentiation cells were treated for 48 hours with mtPt ([Pt(succac)(NH$_3$)$_2$]-r(F$_x$r)-CONH$_2$ complex), cisplatin and nucPt **8** and fixed in 4% PFA. Cells were permeabilized and stained using the *In Situ* Cell Death Detection Kit (Fluorescein) from Roche according to manufacturer's protocol. Cells were counterstained with Tubulin III (Primary mouse anti-Tubulin III (1:1000), Secondary AlexaFluor568 goat anti-mouse (1:1000)) and DAPI and visualized in Ibidi mounting media using a Inverted Zeiss LSM 510 microscope. TUNEL+ neurons were counted and divided by the total number of DAPI+ neurons to quantitatively assess toxicity. At least 10 microscope fields at 10x magnification were sampled for each experimental condition. Cell counting was performed using Metamorph software.

DNA platination. 1 million cells were seeded in sterile tissue culture dishes and allowed to attach overnight at 37 ºC at 5% CO$_2$. Cellular accumulation was determined in A2780CP70 cells exposed to cisplatin (10 μM in complete medium), [Pt(succac)(NH$_3$)$_2$](NO)$_3$ (**3**) or nucPt (**8**) at a final concentration of 100 μM in complete medium. After 4 h of drug exposure, the medium was removed and the cells were washed twice with cold PBS buffer. The cells were collected and incubated with a INVITOGEN DNAzol Reagent solution (1 mL) for 1 h. After the allotted time the isolated DNA was washed with cold PBS and dissolved in 1 mL of water. The DNA concentrations were measured by Eppendorf Biophotometer plus. The intracellular platinum concentrations were measured by flameless atomic absorption spectrometry (FAAS). The results were related to DNA concentrations.

[Pt(succac)(NH$_3$)$_2$](NO$_3$)-(Yr)$_3$-CONH$_2$ (8)

The synthesis of derivative **8** was straightforward and illustrated in Scheme 2.5.
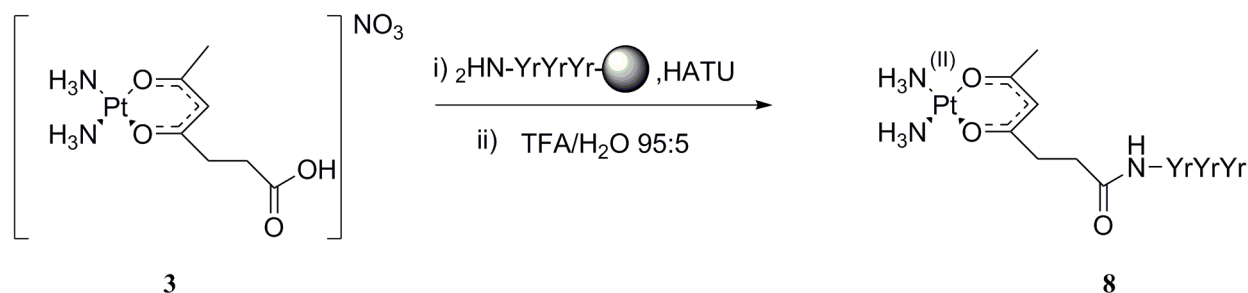
Scheme 2.5.

[Pt(succac)(NH$_3$)$_2$](NO$_3$) (**3**) was synthesized as above described. [Pt(NH$_3$)$_2$(succac)](NO$_3$) (92 mg, 0.2 mmol) was combined with HATU (93 mg, 0.2 mmol). Immediately prior to coupling, the solids were dissolved in 1.5 mL of a freshly prepared 0.5M DIPEA solution in dry DMF, placed in the syringe and shaken for 60 min. After purification, the final platinum(II)-peptide (**8**) with a retention time of = 22.7 min, was judged to be ≥ 99% pure based on the integrated chromatogram (yield 20%). The isolated specie was characterized by HR- ESI -MS: *m/z* = Calcd 672.2959 [M+2H]$^{2+}$, Found 672.2933 [M+2H]$^{2+}$. ^{195}Pt NMR data (D$_2$O) -1605.6 ppm.

2.2.3. Results and discussion

Cytotoxicity determination

MTT assays were carried out in two or three independent experiments in duplicate as described above. The IC_{50} values data for the cytotoxicity are summarized in Table 2.2.

Compound	HeLA cells IC$_{50}$ (µM)	A2780 cells IC$_{50}$ (µM)	A2780CP70 cells IC$_{50}$ (µM)
Cisplatin	3.5±0.34	6±0.52	10±0.45
[Pt(succac)(NH$_3$)$_2$](NO$_3$) (**3**)	> 200	110±0.30	> 200
[Pt(succac)(NH$_3$)$_2$]-(Yr)$_3$-CONH$_2$ (**8**)	> 200	>41*	75±0.06

*This IC_{50} value is related to A2780 WT cancer cells. Assay performed at the University of Toronto, Kelley's Lab.

Table 2.2. IC_{50} values and standard deviations of nucPt (**8**) in HeLa, A2780 and A2780CP70 cancer cells.

NucPt (**8**) showed selective cytotoxicity in A2780 WT cells (data from A2780 WT were obtained from the University of Toronto) and A2780CP70. The cytotoxic activity of (**8**) in A2780CP70, even if lower than the one in WT cells, is particularly remarkable since overcoming resistance of platinum compound is one the major aim of current studies in this field.

Neurotoxicity Studies

The dose limiting side effect of cisplatin is peripheral neuropathy, which reduces the quality of life for many long-term cancer survivors. Cisplatin-induced peripheral neuropathy occurs in about 30% of patients with 20% being forced to discontinue treatment.[35-36] Several studies reveal that cisplatin induces nuclear DNA (nDNA) damage and apoptosis in dorsal root ganglion (DRG), binds to mtDNA, inhibits mtRNA transcription, and induces mitochondrial degradation in primary neuronal cell lines.[37] Peripheral neurotoxicity of nucPt (**8**) has been investigated at the University of Toronto.
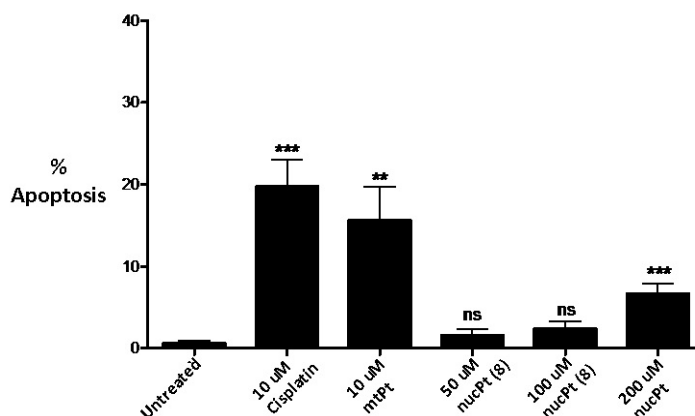
Figure 2.3. Toxicity of nucPt (**8**) to neuronal cells

Kelley and co-worker investigated whether [Pt(succac)(NH₃)₂]-(Yr)₃-CONH₂ (**8**), would exhibit activity against primary neurons in addition to cancer cells. A comparison with mtPt, a mitochondrially-localized compound with DNA damaging activity, has been also evaluated. Dorsal root ganglion (DRG) cells from 18-day-old Sprague-Dawley rat embryos were exposed in culture to a 10μM solution of cisplatin, a 10μM solution of mtPt or a 50 to 200 μM solution of nucPt (**8**) for 48-h time period. Late apoptotic cells were stained using terminal deoxynucleotidyl transferase dUTP nick end labeling (TUNEL assay) and quantitated by fluorescence microscopy. As shown in Fig. 2.3, mtPt and cisplatin induced similar levels of apoptosis in DRGs while nucPt showed a fairly lower neurotoxicity even at high concentrations. These data therefore provide strong evidence that cisplatin neurotoxicity is mediated specifically by damage to mtDNA, and that the nuclear DNA damaging activity of the drug is not the main causative agent of death in these cells. In conclusion, nucPt (**8**) has lower peripheral neurotoxicity than cisplatin, while maintaining its cytotoxic effect against A2780 cisplatin-resistant cells.
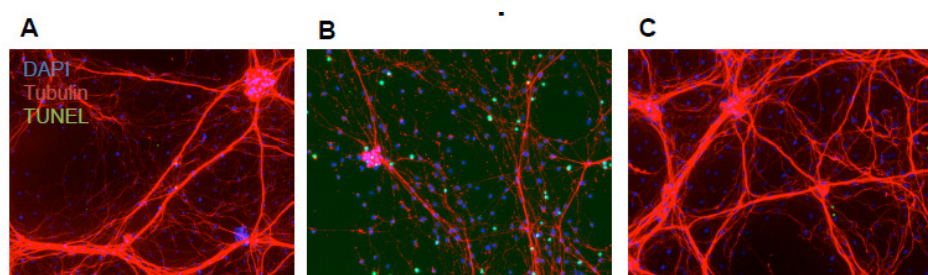
Figure 2.4. Dorsal root ganglion neurons (DRG's) treated for 48 h and assayed for induction of apoptosis using TUNEL staining. **A**. Untretated; **B**.10 μM mtPt; **C**. μM ntPt

In conclusion, mtPt is highly cytotoxic to cultured primary neurons at doses similar to its cytotoxic dose in cancer cells, thus neurons die by apoptosis in response to mtPt treatment. Nuclear-targeted platinum (ntPt), on the other hand, is not significantly toxic to neurons at concentrations equivalent to its anticancer cytotoxic dose, as highlighted from apoptosis induction assays performed on DRG's, upon incubation with the two complexes (Figure 2.4).

DNA platination

Measuring Pt concentration in DNA of cancer cells, after exposure to the platinum-peptide complexes, is a strong proof of the effective nuclear targeting capability of the peptide. DNA platination was performed in A2780CP70 cells. Cisplatin and $[Pt(succac)(NH_3)_2](NO)_3$ (**3**) were used as controls. The results are reported in Fig 2.5.
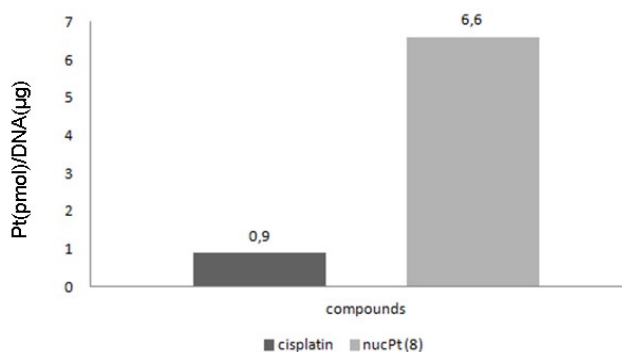
Figure 2.5. Pt concentration in DNA of A2780CP70 cells, treated with cisplatin and nucPt (**8**)

The DNA platination study in A2780CP70 cells clearly showed that nucPt (**8**) has an improved nuclear internalization as compared to the controls. Indeed, no detectable concentration of Pt was found in DNA of cells exposed to (**3**) and low concentration in those exposed to cisplatin (0.9pmol/μgDNA). NucPt (**8**), on the other end, showed a DNA platination 7-fold higher (6.6pmol/μgDNA)

2.2.4. Conclusions

NucPt (**8**) has been synthesized and fully characterized. This complex showed higher nuclear internalization and higher cytotoxicity than the unconjugated one (**3**). Despite its strong cytotoxic effect in A2780CP70 cells, the *in vitro* cytotoxicity is not associated with neurotoxicity in primary neuronal cell lines. In conclusion, complex (**8**) is particularly effective in cisplatin resistant cancer cells and has lower peripheral neurotoxicity than cisplatin.

2.2.5. References

1. Kelland, L. R. *Drugs*, **2000**, *59*, 1-8.

2. Lina, X., Stewartb, D.R., Nowotnikb, D.P., Howella, S.B *European Journal of Cancer*, **2004**, *40*, 291-297.

3. Roberts, J. J., Thomson, A. J. *Prog. Nucleic Acid Res. Mol. Biol*, **1979**, *22*, 71-133.

4. Speelmans, Staffhorst, R.W., de Kruijff, B., Versluis, K., Reedijk, J. *Biochemistry*, **1997**, *36*, 10545-10550.

5. Veldhoen, S., Trampe, A., Restle, T. *Nucl. Acids Re*, **2006**, *34*, 6561-6573.

6. Desai, S. *Pharmaceutical Research*, **1993**, *10*, 1321-1325.

7. Trewyn, B.G., Slowing, I.I., Lin, V.S-J *Chem. Commun*, **2007**, 326-3245.

8. Goun E.A., Jones, L.R., Rothbard, J.B., Wender, P.A. *Chem Bio Chem*, **2006**, *7*, 1497-1515.

9. Wender P.A, Geihe, E.I. *Drug Discovery Today: Technologies*, **2012**, *9*, 49-55.

10. Stewart K.M., Horton, K.L., Kelley, S.O. *Org. Biomol. Chem*, **2008**, *6*, 2242-2255.

11. Deshayes S., Divita, M. Heitz, F. *CMLS, Cell. Mol. Life Sci*, **2005**, *62*.

12. Fotin-Mleczek, M., Fischer, R., Brock, R. *Curr. Pharm.Des*, **2005**, *11*, 3613-3628.

13. Henriques, S.T., Costa, J., Castanho, M.A. *FEBS Lett.*, **2005**, *579*, 4498-4502.

14. Terrone, D., Sang, S.L., Roudaia, L., Silvius, J.R. *Biochemistry*, **2003**, *42*, 13787-13799.

15. Horton, K.L., Fonseca, S.B., Guo, Q., Kelley, S.O. *Chemistry & Biology*, **2008**, *15*, 375-382.

16. Rothbard, J. B., Jessop, T.C., Lewis, R.S., Murray, B.A., Wender, P.A. *J. Am. Chem. Soc.*, **2004**, *126*, 9506-9507.

17. Kelley, S.O. *et al.*, *Chem. Biol*, **2007**, *14*, 923.

18. Aina, O.H, Liu, R., Lau, D.H., Lam, K.S. *Mol Cancer Ther*, **2005**, *4*.

19. Altman, J., Wilchek, M. *Inorganic Chimica Acta,* **1985**, *101*, 171-173.

20. Bal, D., Gryff-Keller, A. *J. Org. Chem*, **2009**, *74*, 8604-8609.

21. Kirin, S.I., Metzler-Nolte, N., Mier, W. *Chem. Educ.*, **2007**, *84*, 108-111.

22. Mosmann, T. *J. Immunol. Methods* ,**1983**, *65*, 55-63.

23. Puckett, C.A., Barton, J. K. *Bioorg. Med. Chem.*, **2010**, *18*, 3564-3569.

24. Van Zutphen, S., Van der Marel, G.A., Overkleeft, H.S., Reedijk, J. *Chem.Commun.*, **2003**, 634-635.

25. Graf, N., Lippard, S.J. *Journal of Inorganic Biochemistry*, **2012**, *110*, 58-63.

26. Kageyama, Y., Okuno, H. *Journal of Inorganic Biochemistry*, **1998**, *70*, 25-32.

27. Cherchi, V., Sindellari, L., Voltarel, G., Sitran, S., Furlani, A., Ravalico, L., Scarcia, V., Niconi, M. *Platinum and Other Metal Coordination Compounds in Cancer Chemotherapy*, **1988**.

28. Moradella S., Rovirab, A., Robillardc, M.S, Reedijkc, J. *Journal of Inorganic Biochemistry*, **2003**, *96*, 493-502.

29. Jamieson, E.R., Lippard, S. J. *Chem. Rev.*, **1999**, *99*, 2467-2498.

30. Wilson, J.J, Lippard, S.J *J. Med. Chem.*, **2012**, *55*, 5326-5336.

31. Fischer R., Kohler, K., Brock, R. *Biochimica et Biophysica Acta*, **2002**, *1564*, 365-374.

32. Puckett, C.A. Barton, J.K *J. Am. Chem. Soc.*, **2009**, *131*, 8738-8739.

33. Wisnovsky S.P., W. J. J., Radford R.J., Pereira M.P., Chan M.R., Laposa R.R., Lippard S.J. and Kelley S.O. *Chemistry & Biology*, **2013**, *20*, 1323-1328.

34. Mourtada R., Kelley, S.O. *PLOS ONE*, **2013**, *4*, E60253.

35. Windebank, A. J., Grisold, W.J. *Peripher. Nerv. Syst.*, **2008**, *13*, 27-46.

36. Podratz, J. *Neurobiol. Dis*, **2011**, *41*, 661-668.

37. Melli, G. *et al.*, *Exp. Neurol*, **2008**, *241*, 276-284.

3. ELTEx A multidisciplinary approach for the synthesis of a new family of potent FKBP12 inhibitors

3.1 Introduction

Immunophilins comprise a family of proteins that were identified on the basis of their ability to bind the immunosuppressant drugs cyclosporin A (CsA), FK506, and sirolimus (rapamycin). Cyclophilins bind CsA, and FK506 binding proteins (FKBPs) bind FK506 and rapamycin.[1] The majority of research on the immunophilins and their ligands has focused on cells of the immune system, especially lymphocytes, but the finding that the immunophilins are much more abundant in the nervous system than in the immune system led to research that reveals important roles for the immunophilins in multiple areas of neural function. These include regulation of nitric oxide (NO) neurotoxicity, neurotransmitter release, intracellular Ca^{2+} flux via the ryanodine and the inositol (1,4,5) trisphosphate (IP3) receptors, as well as neurotrophic influences with therapeutic potential.[2]

The family of FKBPs includes at least five members with molecular masses ranging from 12 to 57 kDa,[1] all sharing at least one common peptidylprolyl isomerase (PPI) domain (Figure 3.1).[3] FKBP proteins are ubiquitous in the body of mammalians and are highly enriched in the central and peripheral nervous system.[4,5]
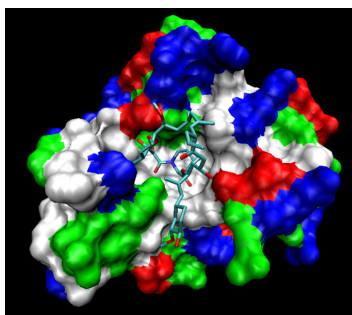
Figure 3.1. FKBP protein with a generical inhibitor bound in its deep cleft

FKBPs have regulatory and/or chaperone function, possibly related to PPI mediated protein folding/unfolding assistance and are involved in several biochemical processes including receptor signaling, protein trafficking and transcription.[3,6,7] In particular, *cis-trans* interconversion of Xaa-Pro peptide bond occurs through binding of a peptide substrate in the hydrophobic binding pocket of the PPIase (rotamase activity). The isomerization is facilitated by out-of-plane conformational change of amide bond, which is stabilized through a hydrogen bonding to the amino acid located in the hydrophobic binding cleft, resulting in stabilizing the transition state during the isomerization process.[8] Since the late 1980s, some members of the PPIase superfamily of proteins have been extensively studied because they bind to several immunosuppressive macrolides of fungal origin that can effectively suppress the immune system of patients with transplanted organs, namely cyclosporin A (CsA), FK506 (known also as Tarcolimus), and Rapamycin (known as Sirolimus). Small size FKBP family members contain only FK506-binding domain, while FKBPs with large molecular weights possess extra domains such as tetratricopeptide repeat domains, calmodulin binding and transmembrane motifs.[9]

3.1.1 The emerging role of FKB12 and its medical implications

The archetypal FKBP12 protein, the smallest member of the family, contains just one PPI domain and is notable in humans for binding to the immunosuppressant molecules FK506 and Rapamycin (Figure 3.2).
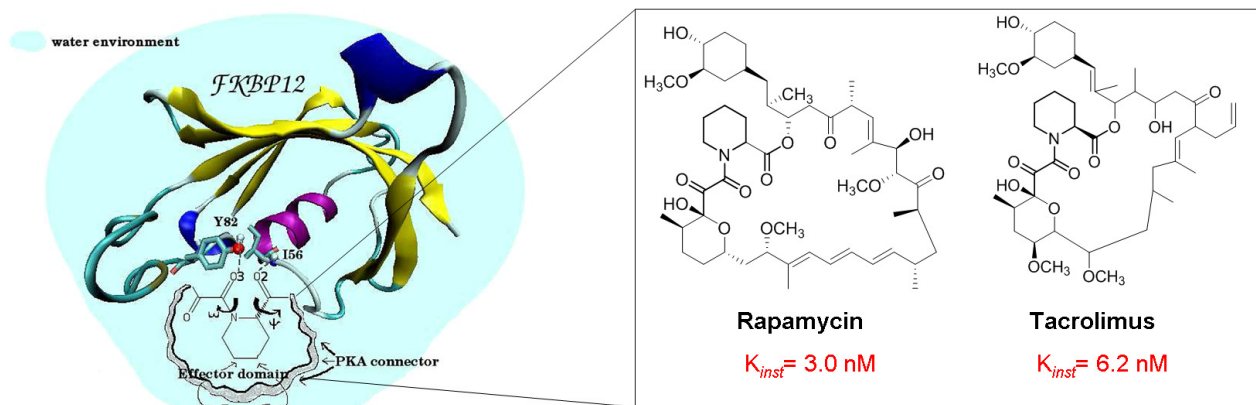
Figure 3.2. FKBP12 protein and the immunosuppressive macrolide Rapamycin and Tacrolimus.

FKBP12 is comprised of 108 amino acids that are 100% conserved between human and rabbit forms and 96% conserved with rat and murine forms. The structure of FKBP12 is characterized by an amphiphilic fivestranded β-sheet. The β-sheet has a right-handed twist and wraps around the helix, and forms a hydrophobic pocket in which the macrolides bind between the α-helix and β-sheet.[5] FKBP12 is thought to stabilize the twisted amide intermediate of the transition state during the *cis-trans* peptidyl-prolyl isomerization. Spectroscopic data demonstrate that FK506 interacts noncovalently with FKBP12. This finding suggested that the mechanism whereby FK506 inhibits the rotamase activity of FKBP12 involves the α-keto amide of FK506, which acts as a surrogate for the twisted amide of the peptide substrate.[10]

The molecular nature of the interaction between Rapamycin and FK506 is now known in considerable detail. Although FKBP12 is a *cis-trans* peptidyl-prolyl isomerase that binds these immunosuppressant macrolides, the prolyl isomerase activity of FKBP12 is not involved in the immunosuppressant properties of the two drugs. Indeed, immunosuppressant drugs often act at low nanomolar concentrations, whereas tissue levels of some of the immunophilins are almost micromolar so that in intact tissues only a tiny percent of rotamase activity would be inhibited.

Despite differing chemical structures, FK506 has very similar mechanism of action of Cyclosporin A, another member of the immunophilin family, resulting in the inhibition of the protein phosphatase calcineurin.[1] FK506 possesses separate domains that bind FKBP-12 and calcineurin, respectively. FK506 is hydrophobic and is thought to diffuse across the plasma membrane. Once inside the cell, the formation of FKBP/FK506 complexes inhibits not only the PPIase activity of FKBP, but has also the phosphatase activity of the secondary target calcineurin (CaN), which is required to dephosphorylate and thereby promote the transport into the nucleus of the cytoplasmic moiety of the transcription factor NF-ATc.[9] NF-AT is required for the encoding interleukine IL-2 gene expression and T-cell activation (Figure 3.3).[11,12]
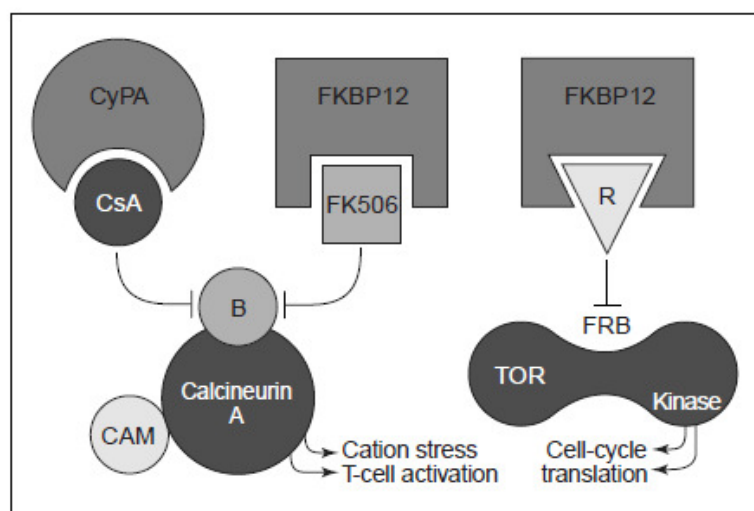
Figure 3.3. Mechanisms of action of FK506 and Rapamycin that involve Calcineurin and m-Tor, respectively.

On the other hand, rapamycin binds to FKBP12, but the FKBP/rapamycin complex interacts with mammalian target of rapamycin (mTOR), a kinase that has a regulatory function in cell growth, cell motility, and cell proliferation.[13] The immunosuppression or cell growth regulation power of FK506 or Rapamycin natural drugs is allosteric in nature as their binding ability versus calcineurin or mTOR requires the formation of the ligand-FKBP12 complex. Thus, the FKBP-FK506 and FKBP-rapamycin complexes apparently function as the modulators of signal transduction, each complex having a distinct biological mechanism, by interacting with distinct downstream targets associated with calcium dependent and calcium-independent pathways, respectively (Figure 3.3).

The centrality of the FKBP family, and notably of the archetypal FKBP12 PPI single domain, in the protein metabolism[9] and its involvement in many incurable diseases has been reported. In particular, cellular reduction and redistribution of FKBP12 may be involved in the aberrant phosphorylation or misfolding of the microtubule associated protein 'tau', which leads to the formation of NFT (neurofibrillary tangles), typical of Alzheimer's disease.[14] Neuroregenerative and neuroprotective properties have also been assigned to FKBP12 since its inhibition or endogenous downregulation reduces α-synuclein aggregation in Parkinson's disease.[15] Striking neurotrophic effects of FK506 were observed in PC12 cells and sensory ganglia with subnanomolar potencies, and these effects were also observed with rapamycin and CsA. Recently, it was shown that non-calcineurin binding analogues of FK506 and cyclosporine also promote neurite outgrowth. These immunosuppressive derivatives bind to the immunophilins with similar potencies as the parent drugs, but the drug-immunophilin complex fails to bind to and inhibit calcineurin and these derivatives are not immunosuppressants. As the non-immunosuppressant derivatives are just as neurotrophic as the parent drugs, the immunosuppressive properties of FK506 and cyclosporin could be functionally dissociated from their neurotrophic effects.[2] Furthermore, FKBPs seem to be involved in multiple sclerosis (MS)[16], amyotrophic lateral sclerosis (ALS)[17] and proliferation disorders.[18]

FK506 and FK506-related ligands are routinely used in treating patients after organ transplant and in patients suffering from autoimmune disorders.[19] In recent time, the neuroprotective and neuroregenerative activity of FK506 analogues, both in vitro and in vivo,[20] has stimulated the interest in the design and/or identification of novel FKBP12 ligands (Figure 3.4).[21]
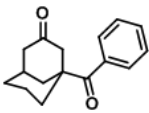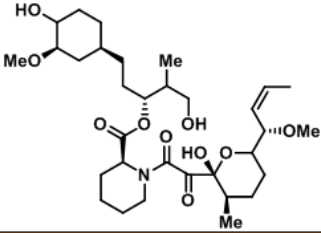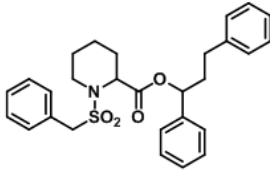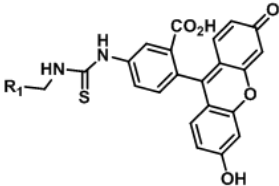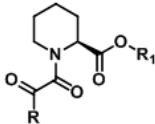
Figure 3.4. FKBP12 inhibitors with different chemical structures

The greatest number of designed FKBP ligands[22] arose from the so-called dual-domain concept whereby ligands bind FKBP12 through the α-keto amide binding domain and act, in the resulting complex, as an immunosuppressant agent via the complementary effector domain. These designs of FKBP inhibitors were based on the binding domain of the common structural elements of FK506 and Rapamycin that dock the FKBP protein in the primary site through two H-bonds in the pipecolyl α-keto amide region and two more H-bonds between hydroxy groups of the macrocycle in the secondary binding site.[23]

3.1.2 Towards the synthesis of a FKBP12 nanomolar inhibitor

In the last years, a large variety of synthetically different ligands (such as fluoresceinated[24], sulfonamide, urea-containing FKBP analogues,[25] pipecolyl amides,[25] steroids,[26] and seco-bridging FK506 analogues[27]) has been realized (Figure 3.4). Important synthetical efforts and micromolar affinity for the protein have been reported. Recently, *Roehring et al.*[28] analyzed the minimal binding domain of FK506-related drugs by individually evaluating the effect of each part on the potency of the FKBP inhibition. Pipecolyl-containing compounds (i.e. primary site binders) presented better inhibition than any acyclic amide or prolyl-containing compound, while efforts to synthesize nonmacrolide compounds that bind at both the primary and secondary site of FKBP12 went frustrated.[28] Despite new categories of FKBP12 inhibitors emerging every year, a lack of potent ligands, with nanomolar activity comparable to the ones of Rapamycin and FK506, is reported in literature. Following a multidisciplinary approach, we have set up a rational drug design based on preliminary costless simulations of potential binders in bulk solution (i.e. in absence of the protein) and on the analysis of their conformational behavior.[29]
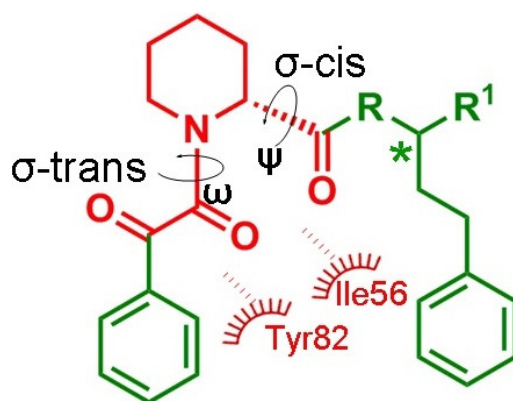
Figure 3.5. The essential ingredients of the PKA pharmacore for PPI domain of FKBP12 protein

From preliminary *in silico* studies, prolin-mimetic pipecoyl α-keto amide subunit (PKA) has been identified as the pharmacore of FKBP12 protein. Thus, a synthetic molecule has the potential to strongly bind the PPI domain of FKBP proteins when the following requirements are met:

- ➢ Optimal mutual exposure of the two carbonyls for binding to the highly conserved aminoacidic residues (Tyr82 and Ile56) of the active site;
- ➢ Former torsional angle ω in the σ-*trans* and angle ψ in the σ-*cis* configuration that allow the optimal exposure of the CO binding units (red portion, Figure 5);
- ➢ Intraligand hydrophobic interactions of the two groups on opposite sides of the PKA that impart to the ligand a quasi cyclic structure mimicking the rigidity of the macrolides FK506 or Rapamycin, while maintaining solvent-exposed the binding domain of the ligand (green portion, Figure 3.5);
- ➢ Low configurational entropy;
- ➢ Flexibility at R position. R can be C, N or O. Inserting a C atom at this position resulted to be challenging so this synthetical route was avoided. Inserting N and O atoms led to amide and ester derivatives, respectively.
- ➢ Not relevant stereochemical conformation at C-15 (for $R^1 \neq H$).

The best candidates meeting above described pharmacore criteria were then properly filtered, considering organic synthesis features, leading to a new family of nanomolar inhibitors of FKBP12, named Eltex (Figure 3.6).
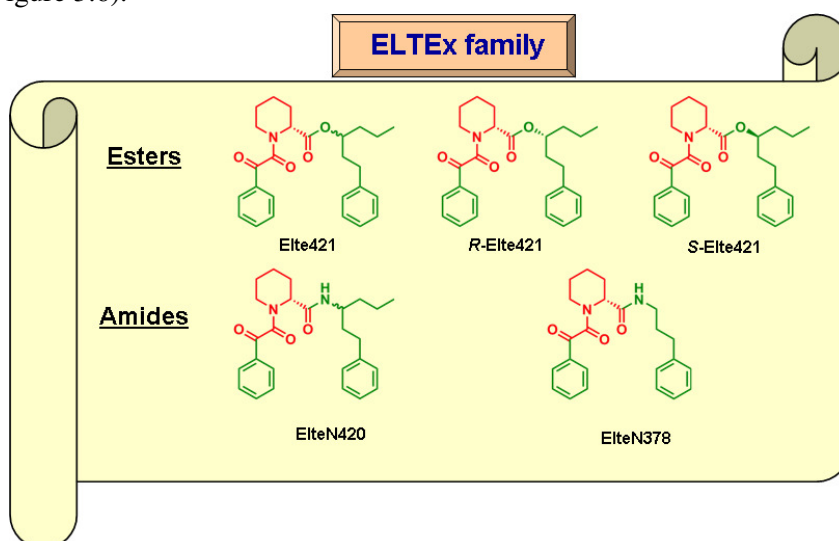
Figure 3.6. Eltex family

The structural features and resulting binding affinities versus FKBP of the selected compounds in bulk solution were finally measured and assessed using fluorescence spectroscopy. The experimental binding affinity K_{inst} versus FKBP12 was expressed as the ratio with respect to that of the FK506 compound measured in the same experimental conditions. The calculation, synthesis, purification and *in vitro* binding assays of all the member of Eltex family are below reported.

3.2 Results and Discussion

3.2.1 Calculation

In a recent work,[30] using solute tempering replica exchange (REM) molecular dynamics simulations, Procacci and all. have shown that the molecular recognition of known FKBP12 proline-mimetic drugs such as (1R)-1,3-diphenyl-1-propyl-(2S)-1-(3,3-dimethyl-1,2-dioxopenty1)-2-piperidinecarboxylate (**sb3**, Figure 3.7 left) resides in the correct 3D orientation and in the stability of the two binding carbonyls of the ligand acting like a sort of "pipecolic clamp" in bulk water solution.[31] Such a feature is favored by persistent through-space intraligand hydrophobic interactions that significantly reduce the entropy loss upon binding by imparting to the drug a pseudocyclic structure (like Rapamycin and FK506) with solvent exposure of the highly polar pipecolic clamp.
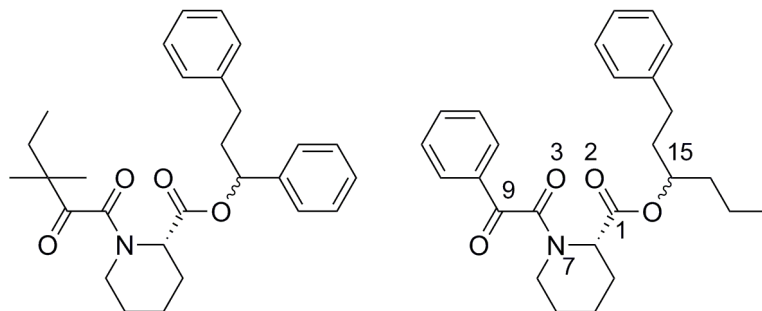
Figure 3.7. Left: sb3; right: Elte421

The activity of sb3 is related to the mean mutual orientation of the two carbonyl units (C1-O2 and C8-O3) in bulk solution that is in turn controlled by the mutual arrangement of the dihedral involving the C2 and N7 substituents, that is, angle ω (C9C8N7C2) and angle ψ (O1C1C2N7). When the former torsional angle is in the *trans* and the latter in the *cis* configuration, the orientation of the carbonyl units and the O2-O3 distance (around 4.5 Å) is optimal for binding in the active site with Tyr86 and Ile56, the two most conserved residues across the entire FKBP family.[3]

In this work, it was further shown that in the right-handed stereoisomer (15R)-sb3, this optimal *trans-cis* arrangement is stabilized in bulk solution by a stereospecific intraligand hydrophobic interaction of the 1,1-dimethyl propyl group of the N2 substituent with one phenyl ring of the C2 substituent. These hydrophobic interactions are not observed in the (15S)-sb3 epimer, consequently reducing the probability of potential binding conformation in bulk solution, with a remarkable impact on the observed potency of the compound (30-60 times less effective than the (15R) counterpart).

Using this guidance, starting from sb3, a new FKBP12 inhibitor, 1-phenylhexan-3-yl-1-(2-oxo-2-phenylacetyl)piperidine-2-carboxylate, a 1:1 disteroisomeric mixture named Elte421 (**1**) (Figure 3.7, right), was *in silico* designed, replacing the isopropyl moiety at carbon 9 of sb3 with a phenyl ring and the phenyl ring at the stereocenter C15 with a propyl chain (Figure 3.8).
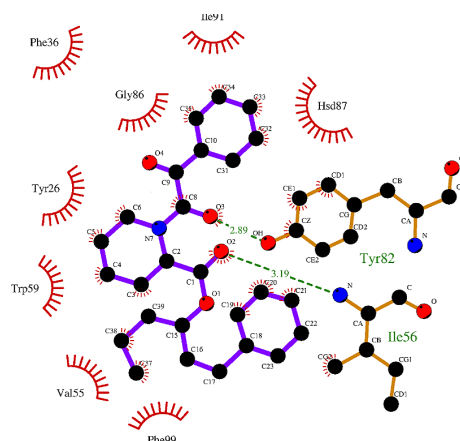
Figure 3.8. Schematic diagram of FKBP12−Elte421 interactions. The diagram has been obtained running the LigPLot program31 on a snapshot configuration taken from an MD trajectory of the ligand-protein complex at 300 K.

18 ns REM simulations with solute tempering[32] of (15R)-Elte and (15S)-Elte in water solution at T = 300 K and P = 1 atm, using the ORAC program,[33] were performed to evaluate at the atomistic level the free-energy surface (FES) with respect to ω and ψ angles, characterizing the conformation of the binding carbonyl groups. The results show that both the Elte421 diastereoisomers exhibit a significant conformational population in the FKBP12 binding ω-ψ (gridded quadrant, Figure 3.9) comparable to that of the potent (15R)-sb3 ligand, confirming the optimal redislocation of the hydrophobic groups in sb3 (phenyl and alkyl chains) so as to stabilize at the same time via π-π stacking interactions the 15R stereoisomer and, as in (15R)-sb3, via phenyl-alkyl hydrophobic interactions the 15S partner.[30] Starting from these promising data, Elte421 (**1**) was synthesized in our laboratory, confirming the prediction based on the above described FES analysis, the (15R)-Elte and (15S)-Elte 1:1 mixture therefore was three times as potent as (15R)-sb3.
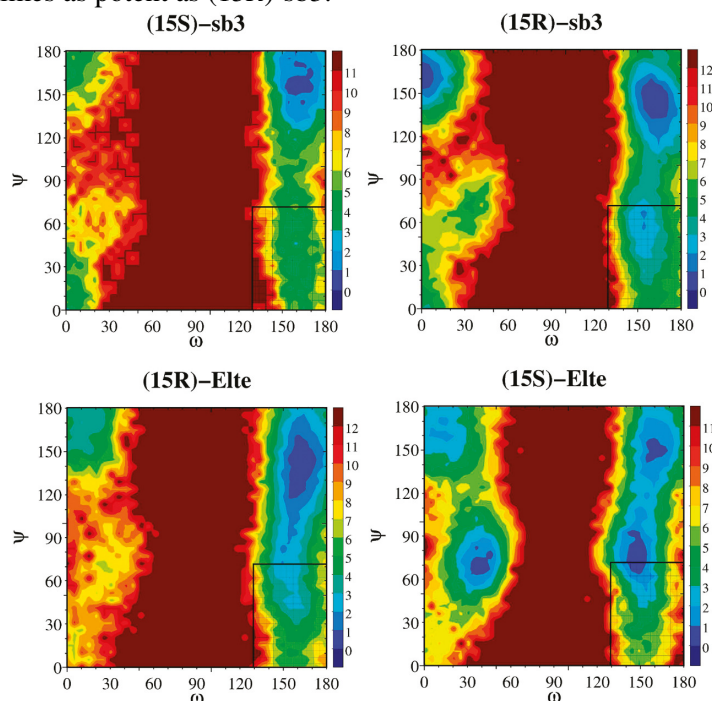
Figure 3.9. Free-energy surface with respect to the dihedral angles ω and ψ of Elte421 and sb3 in water at T = 300 K and P = 1 atm calculated via solute tempering REM.

Moreover, as correctly inferred from calculation, 15R-Elte421 and 15S-Elte421 have both K_d of nanomolar order with *S*-Elte having a slightly higher affinity. This behavior can be rationalized by assessing the exposure of the two carbonyls in the PKA as derived from the FES in the ω, ψ space calculated in a REM simulation of the drug in a water environment in standard conditions. The *S*-Elte421 compound is characterized by a deep minimum in the FES close to the optimal ω, ψ values. Such a minimum is less pronounced in the *R*-Elte compound and somewhat shifted toward the ω, ψ *trans−trans* rotameric state. Correspondingly, the measured binding affinity of *S*-Elte421 is larger than that of the *R*-compound. We also notice that the *R*-Elte421 epimer has a less populated ω-*cis* rotamer with respect to S-Elte. The incidence of ω-*cis* conformation in *R*-Elte421 has a negative impact on the FKBP affinity since only the ω-*trans* rotamer is able to form the two conserved H-bonds in the PPI domain. Therefore, the low population of the *cis* conformer at equilibrium in bulk water solution partly compensates, in *R*-Elte421, the nonoptimal exposure of the two binding carbonyls. As a consequence and in contrast to the sb3 parent compound where the *S* and *R* diastereoisomer affinities differ by 2 orders of magnitude, in Elte421 the stereocenter at C15 has a marginal role: the two Elte421 diastereoisomers have both nanomolar binding affinity versus FKBP12. The full confirmation derived from the enantioselective synthesis of the two diastereoisomers that, again, showed both nanomolar affinity for FKBP12.[34]

Encouraged by the promising results, the chemical-physical determinants of the peptidomimetic FKBP ligands was further characterized.[34] In order to stabilize *cis−trans* configuration of the ω, ψ dihedral angles, we tried to substitute the carboxylate group in Elte421 with an amide group, arriving at (15R/S,2S)-1-(2- oxo-2-phenylacetyl)-N-(1-phenylhexan-3-yl)piperidine-2-carboxamide, named ElteN420 (**4**). The N1-H moiety, by interacting via H-bond with O3 thus mimicking a tight turn of δ type, should force at the same time the *trans* conformation for ω dihedral and the *cis* conformation for ψ dihedral. The potency of the 1:1 diastereoisomeric mixture ElteN420 disgruntledly turned out to be lower than that of the Elte421 mixture (**1**). An accurate inspection of the highly populated binding cluster structures reported in the ω, ψ *trans-cis* region revealed that the propyl moiety points in both cases *outward*, in the same direction of the pipecolic clamp, possibly interfering, at least in one epimer, with FKBP binding. Hence we decided to eliminate altogether the propyl group along with the stereocenter C15, finally landing on the compound (2*S*)-1-(2-oxo-2-phenylacetyl)-N-(3-phenylpropyl)-piperidine-2-carboxamide, named ElteN378 (**5**). From REM configuration analysis showed that the population of the most populated binding clusters is characterized by a parallel displaced stacking of the two phenyl rings with one of these rings additionally stacked right above the planar α-keto amide moiety (Figure 3.10, left). More precisely, the extensive stacking system involving the two phenyl and the planar amide moiety is stabilized by solvophobic effects due to the free energy gain (notably of the intrasolvent enthalpy) promoted by the minimization of the solvent- ElteN378 interface upon intraligand stacking.
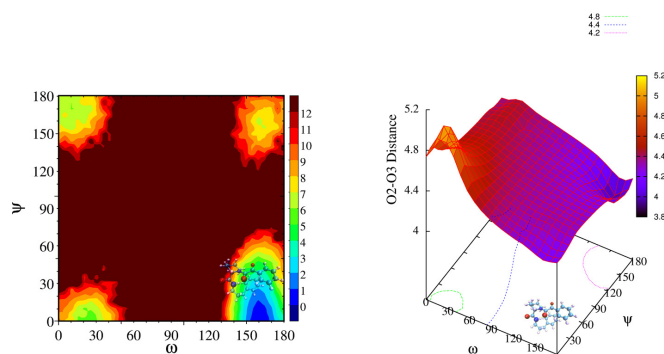
Figure 3.10. Left: Free energy surface (FES) with respect to the dihedral angles ω and ψ (in degrees) of ElteN378 calculated via solute tempering REM in water bulk solution. Right: Contour map of the O2−O3 distance (in Å) as a function of ω and ψ (in degrees) in ElteN378

A 3D interpolation of the resulting surface using the pm3d algorithm[35] revealed that basically the entire O2-O3 distance spread in the case of ElteN378 (**5**) is restricted to the binding range 4.2-5.0 found in the experimental structures of ligand-FKBP complexes (Figure 3.10, right), imparting to the molecule an extraordinary rigidity. In this case, *in silico* calculations have been so predictive that drove us to the synthesis of ElteN378 (**5**), the most powerful synthetic inhibitor of FKBP12 ever described in literature.

3.2.2. Organic synthesis

The organic synthesis of all the member of Eltex family exploited as pivotal compound the (R)-N-Boc pipecolic acid, enantiopure commercially available. Eltex compounds included esters and amides that were obtained using different alcohols or amines to functionalize the pipecolic acid, while the final coupling with phenylglyoxylic acid was the same for all the derivatives.
Synthesis of Elte421(**1**) and ElteN378 (**5**) were straightforward, since no stereochemical control was required, while a continuous monitoring of the stereochemistry at position 3 during the entire process of R-Elte421 and S-Elte421 made theirs synthesis more challenging.
Esters
The first inhibitor we synthesized was a 1:1 disteroisomeric mixture at carbon 3, named Elte421(**1**) (Scheme 3.1).
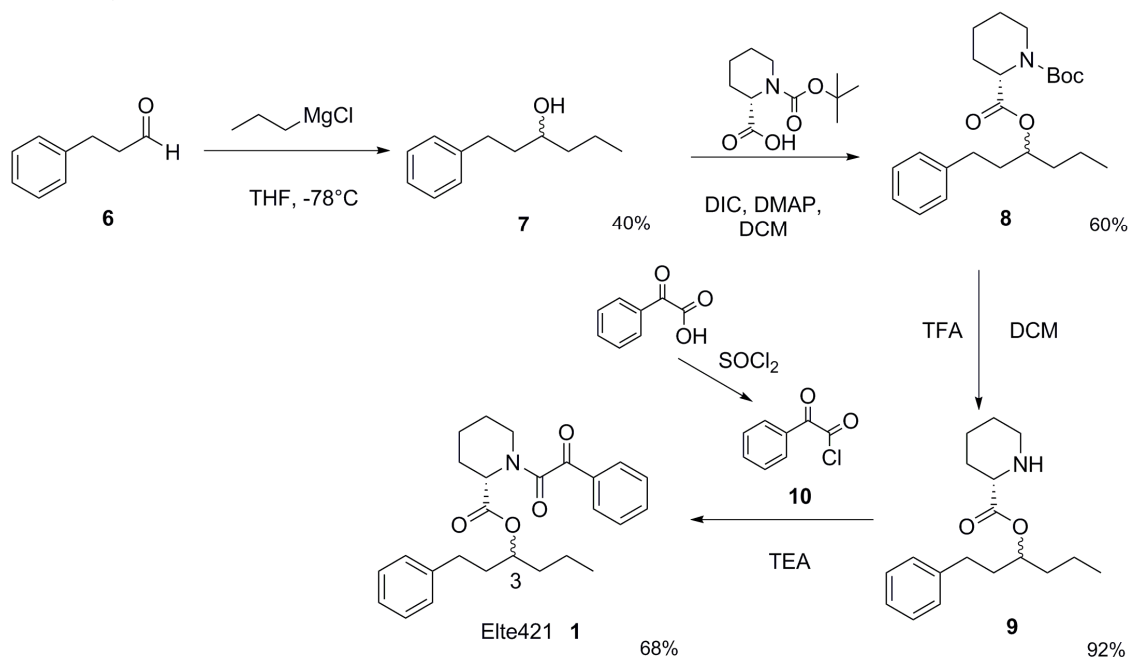
Scheme 3.1. Synthesis of Elte421 (**1**)

The first step of the procedure simultaneously introduced an alkyl chain on 3-phenylpropionaldheyde (**6**) and reduced it, after treatment with a stoichiometric amount of propylmagnesium chloride 2M in ether at -78°C to have (3*R/S*)-1-phenylhexan-3-ol (**7**). The obtained alcohol, racemic at position 3, underwent a first coupling with (*R*)-N-Boc pipecolic acid (2 equiv.), using diisopropylcarbodiimide

(DIC, 2 equiv.) as coupling agent and 4-dimethylaminopyridine (DMAP) in catalytic amount (0.1 equiv.). Besides flash chromatography on silica gel, the purification of (**8**) required several washing with a saturated solution of NH_4Cl to get rid of diisopropylurea (DCU), a water soluble side-product of DIC. After the removal of Boc protecting group with a 99% TFA solution in DCM, achieved in almost quantitative yield, the free amine of (**9**) underwent the final coupling with phenylglyoxylic acid. In the first attempt, DIC-DMAP protocol, above described, was exploited but the final compound was obtained in low yield since the presence of urea was detected and purification of (**1**) to get rid of that was not successful. Phenylglyoxylic acid was, thus, activated to the correspondent chloride (**10**) with an excess of thionyl chloride and coupled with (3*R/S*)-1-phenylhexan-3-yl piperidine-2-carboxylate (**9**) in the presence of TEA (2 equiv.) to give Elte421 (**1**) as pure final product in 68 % yield. The ^{1}H NMR spectrum showed the presence of two diatereoisomers in 1:1 ratio (d1 and d2) and two rotamers (r1 and r2, *trans*/*cis* ratio of the order of 4:1) with different patter of signals (Figure 3.11)
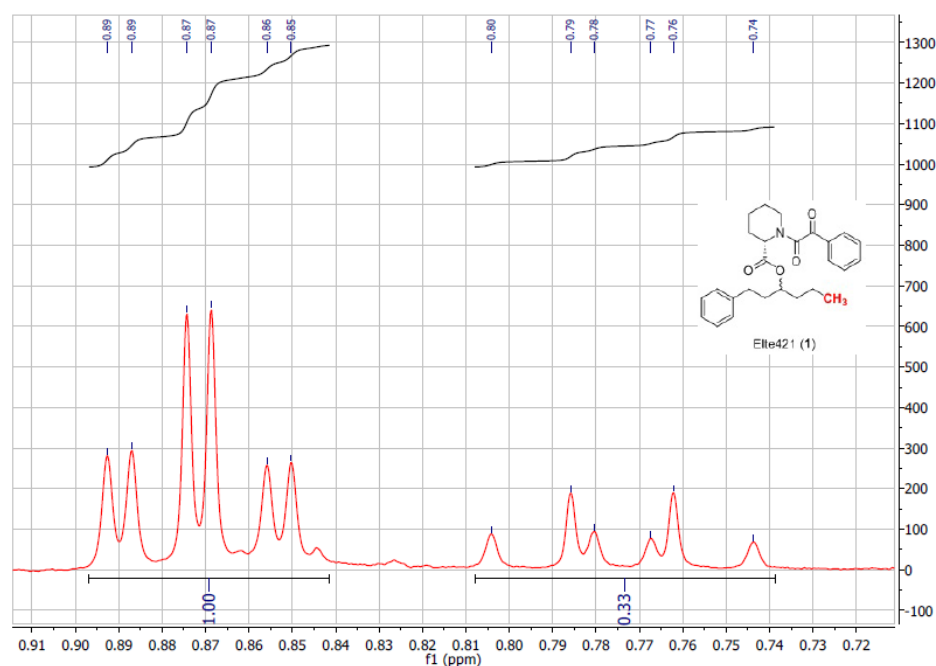
Figure 3.11. ^{1}H NMR, 400 MHz spectrum of the Elte421 (**1**) in DMSO at 27°C (region of CH_3 group)

In the region of CH_3 group, for instance, two doublets of triplets (corresponding to *trans* and *cis* ω rotamers of the mixture of the diastereoisomers) were observed, whose integrals yield the intensity ratio 3:1,indicating that the *trans-cis* ration in DMSO is identical for the diastereoisomers. Due to the high barriers, the *cis-trans* isomerization in Elte421 followed, in standard conditions, a kinetics that is similar to that of the *cis-trans* isomerization in proline (i.e. *cis-trans* swaps in the order of seconds per molecule). In order to test the intrasolute force field, the *cis-trans* equilibrium of *R*-Elte421 and *S*-Elte421 in DMSO has been also evaluated by REM simulations, yielding *trans*/*cis* ratio of the order of 4:1, in reasonable agreement with the 3:1 ratio of the experimental data (data not shown).
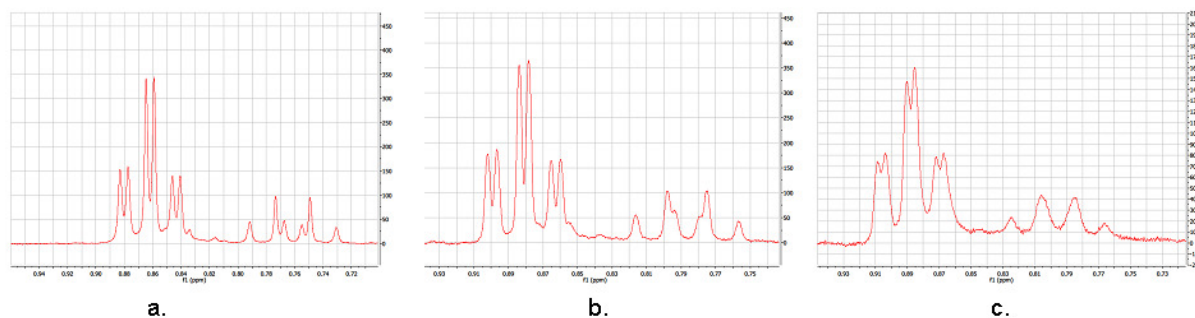
Figure 3.12. ^{1}H NMR, 400 MHz spectrum of the Elte421 (**1**) in DMSO at: a. 30°C, b. 70°C, c. 99°C.

A variable temperature NMR study has been conducted on Elte421. Increasing the temperature during the acquisition of ^{1}H spectra reduced the energy barrier between the rotamers, promoting the *cis-trans* interconversion. A clear evidence of this phenomenon was the overlapping of doublets of triplets of CH$_3$ terminal group at high temperature, ending in a loss of multiplicity (Figure 3.12). In the ^{13}C NMR spectrum the total number of signals was higher than expected, due the partial superimposition of the carbon chemical shifts of the two rotamers for each diastereoisomer.

To confirm the hypotheses derived from theoretical calculations and elucidate the contribute of the single diasteroisomer on binding affinity, we decided to undertake the enantioselective synthesis of *R*-Elte421 and *S*-Elte421. Using boranes with the appropriate absolute stereochemistry, we successfully synthesized alcohols (**S**)-**7** and (**R**)-**7** as enantiopure compounds, crucial intermediates to obtain diasteroisomers (**2**) and (**3**), separately (Scheme 3.2 and 3.3).
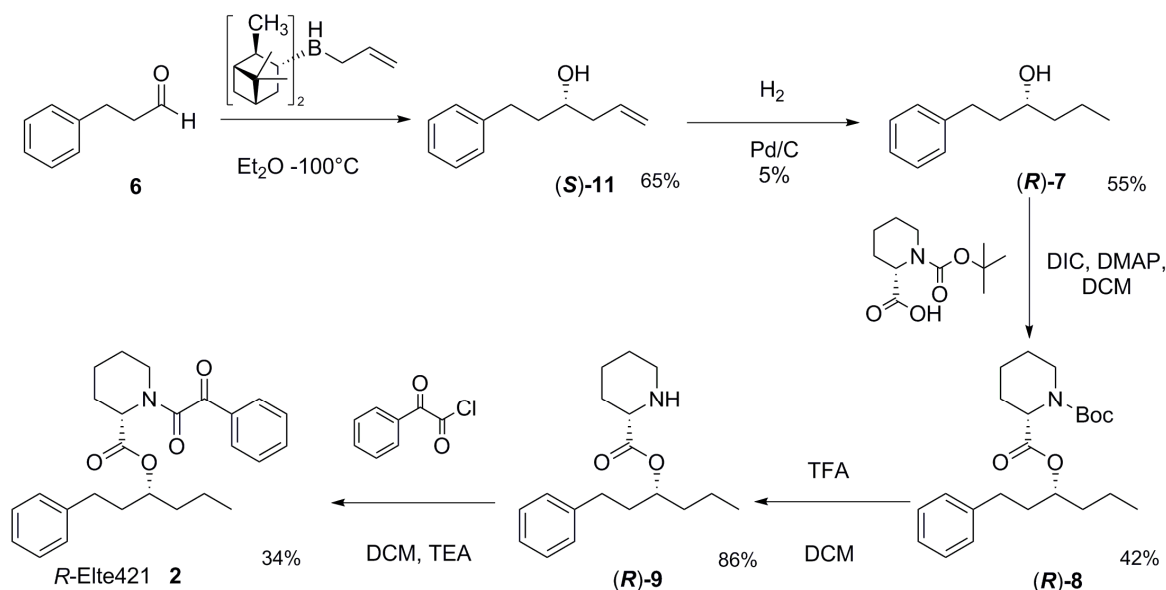
Scheme 3.2. Synthesis of R-Elte421 (**2**)

Allylboration of 3-phenylpropionaldehyde (**6**) with (+)-β-allyldiisopinocampheylborane in Et$_2$O-dioxane mixture was led at -100°C for 1 h in freshly distilled diethyl ether. The following oxidation with 10% H$_2$O$_2$ and a 3M NaOH solution at reflux provided (3*S*)-1-phenylhex-5-en-3-ol ((**S**)-**11**) as enantiopure compound, after purification by flash chromatography to get rid of isopinocampheol, side product from allylborane. In the next step a careful use of Pd/C catalyst had to be done. A catalytic amount was strongly suggested since the use of a stoichiometric quantity led to the oxidation of the

alcoholic moiety to ketone instead of reducing of the double bond on alkyl chain as desired. This side reaction was already described in literature.[36] The stereochemistry at position 3 of (**R**)**-7** was assigned by optical rotatory power in EtOH, comparing it with the value reported in literature.[37,38] While (**S**)**-11** has a *S* stereochemistry, an inversion of configuration at carbon 3 was observed after the reduction of the alkene. The *R* configuration was preserved during all the synthetical procedure. The last steps, including an initial coupling with N-Boc pipecolic acid, deprotection and final coupling with phenylglyoxylic acid, were the same reported for the synthesis of Elte421 and allowed to obtain *R*-Elte421 (**2**) in a good yield (Scheme 3.2).

Scheme 3.3. Synthesis of S-Elte421 (**3**)
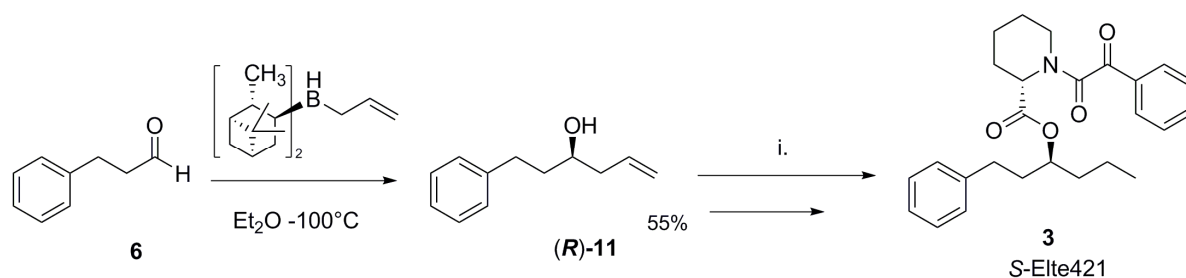
For the synthesis of S-Elte421 (**3**), we exploited the procedure described above (Scheme 2), excepted from using the (-)-β-allyldiisopinocamphenylborane instead of the (+)-β-allyldiisopinocamphenylborane to obtain (**R**)**-11** (Scheme 3.3). NMR and IR spectra are comparable to the ones of *R*-Elte421 (**2**).

Amides

In order to replace an ester group with an amide at position 3, we converted (3*R/S*)-1-phenylhexan-3-ol (**7**) in a primary amine (**14**), through an intermediate conversion in an azide derivative (**13**) (Scheme 3.4).

Scheme 3.4. Synthesis of ElteN420 (**4**)
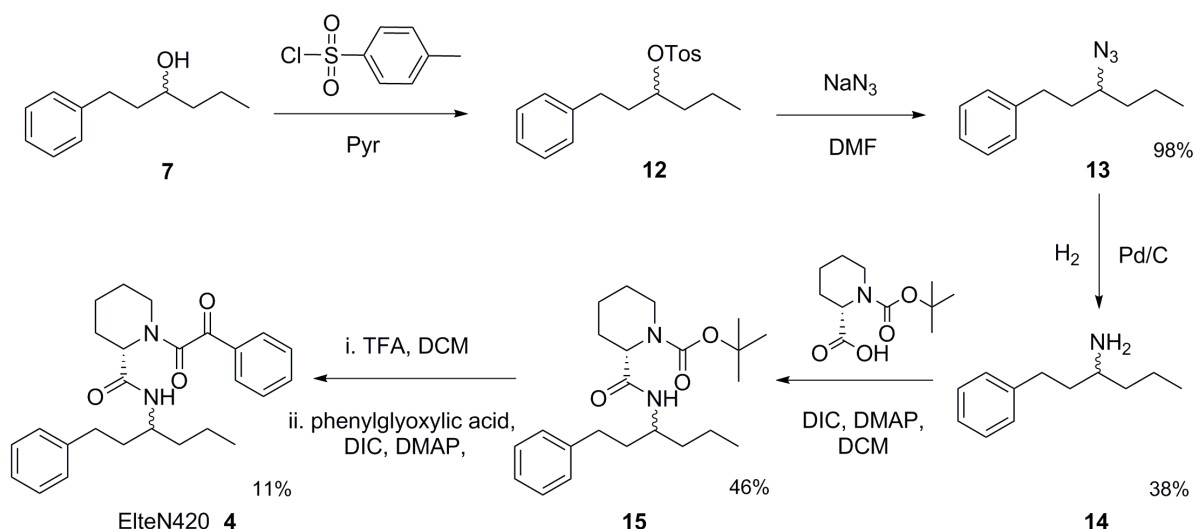
(3R/S)-1-phenylhexan-3-ol (**7**) was first activated to the correspondent tosylate (**12**), using p-tosyl chloride (2 equiv.) in 2 mL of dry pyridine. The ^{1}H-NMR spectrum of the crude showed the presence

of p-tosyl chloride as impurity, not removable by flash chromatography at this stage. The crude was used and the impurity was easily removed in the next step, that provided azide (**13**), by treatment of the tosylate with NaN$_3$ (8 equiv.) in dry DMF, overnight. The presence of (**13**) was confirmed from IR spectrum that showed a very strong signal at 2099 cm^{-1} corresponding to N$_3$ asymmetrical stretching. In the next step, all the attempts of reduction, using triphenylphosphine in a 30% THF solution in water, went frustrated.[39] Azide (**13**) was successfully reduced by a catalytic hydrogenation, providing (3R/S)-1-phenylhexan-3-amine (**14**). The above described procedure closely resembled the one used to obtain ester derivatives, except for the last in which we preferred to use a coupling agent as DIC to insert phenylglyoxylic acid, instead of activating it to the correspondent chloride. The procedure allowed us to obtain ElteN420 (**4**) as a 1:1 racemic mixture (Scheme 4). The ^{1}H-NMR spectrum of ElteN420 appeared quite complex due to the presence of two rotamers (1:1.3 ratio), each as 1:1 mixture of diastereoisomers.

Surprisingly, the synthesis of the most potent inhibitor (**5**) required the easiest syntetic procedure (Scheme 3.5). Once synthesized for the first time ElteN378, different coupling agents and reaction conditions have been tested in order to optimize the procedure, increasing the final yield and shortening the required times, as discussed above.
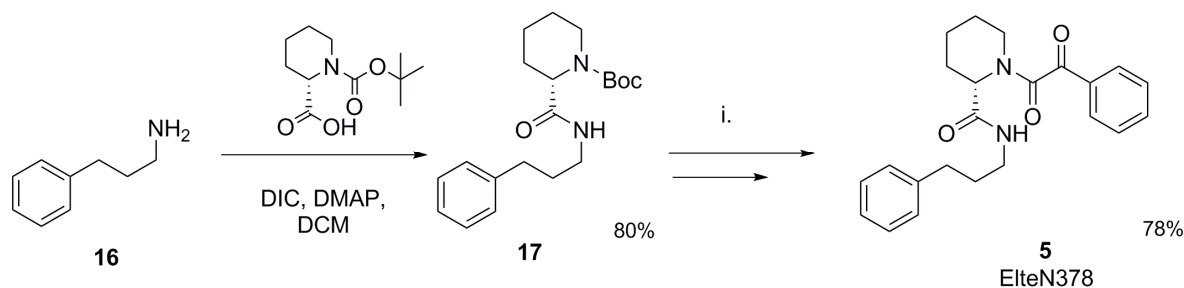
Scheme 3.5. Synthesis of ElteN378 (**5**)

First procedure: commercially available 3-phenylpropan-1-amine (**16**) was activated with 2 equiv. of DIC in dry DCM and reacted with N-Boc pipecolic acid (2 equiv.) and a catalytic amount of DMAP (0.1 equiv.). TLC analysis of the reaction mixture after 16 hours still showed the presence of the starting material (**16**), while a massive white precipitate of DCU appeared in the flask. The reaction was thus stopped and the crude was purified by flash chromatography and several acid washings to get rid of the DCU. The desired product (**17**) was isolated in 26% yield, also due to the challenging work-up. N-Boc protecting group of (2S)-*tert*-butyl 2-(3-phenylpropylcarbamoyl)piperidine-1-carboxylate (**17**) was carefully removed with an excess of a TFA solution in DCM (5 equiv.), added over a period of 4 hours at 0°C, due to the decomposition of the product caused by a strong acid environment. Intermediate (**18**) was directly used without further purification since the ^{1}H NMR spectrum showed an acceptable purity. The final coupling reaction was realized using the same DIC-DMAP in DCM protocol above described. Again the purification was not straightforward, requiring two flash chromatographes and ElteN378 (**5**) was obtained in 36% yield.

Optimized procedure: initial amidation was led using HATU, instead of DIC as coupling agent. Primary amine (**16**) was reacted with N-Boc pipecolic acid (1 equiv.), in a DIPEA solution in dry DMF. Pipecolic acid was activated with an excess of HATU (6 equiv.). Side products of HATU were easily removed from the crude by flash chromatography to obtain (**17**) in a very good yield (80%). The following step involving the removal of N-Boc protecting group was achieved as above described and allowed to obtain (**18**) in 72% yield. Regarding the final amidation, we decided to first activate in a

DIPEA in dry DMF solution phenylglyoxylic acid (1 equiv.) with an equimolar amount of HATU, prior to add the amine (**18**). Thanks to the good efficacy of HATU we avoided to use an excess of coupling agent, resulting in a easier purification process with a more satisfying yield (78%) of ElteN378.

3.2.3 Fluorescence-Based assay

Experimental details

FKBP12 (expressed in Escherichia coli, M.W. 11000) and FK506 (M.W. 804.02) were supplied by Sigma Aldrich (Italy). The purity of FKBP12 was greater than 90% determined by SDS electrophoresis; purity of FK506 was greater than 98% (obtained by HPLC). Absorption spectra were recorded on a Lambda900 spectrophotometer (Perkin Elmer, Italy) with cuvette cell holder connected to a thermostatic bath. Fluorescence spectra were recorded on a PerkinElmer LS 50B luminescence spectrometer, excitation and emission slits were set to 10 or 15 nm depending on the optical path length of cell employed. Emission measurements were performed using different excitation wavelengths in the range 270-310 nm, excitation spectra were run at λ_{em} = 310 nm, 350 and 380 nm. Stock FKBP12 concentration in PBS buffer (pH 7.4, 0.15 M NaCl) was determined by UV/Vis (ε 280=9970 $M^{-1}cm^{-1}$), aliquots of this solution were used to prepare adequate concentrations for quenching experiments by dilution with standard phosphate buffered saline. The molar extinction coefficient of Elte421 ligand in DMSO was obtained from a dilution series in the linear Lamber-Beer regime and resulted to be ε_{260}=16446 M^{-1} cm^{-1}. Regarding fluorescence, data points are the average of at least two separate experiments, emission spectra of the corresponding FKBP12-free samples were subtracted from each recording of fluorescence spectra. The apparent dissociation constant for ligands was calculated from the fluorescence intensity results.

Binding assay

In literature is reported that the PPIase assay used to measure the enzymatic activity of the FKBPs has some major technical limitations. Due to the high background rate of the uncatalyzed isomerization, the time window of the reaction is very short (<120 s) even if performed at low temperatures. Furthermore, water-free reagents are required to enrich the initial percentage of substrate in the *cis*-prolyl conformation. This makes this assay incompatible for high-throughput applications.[40] Alternatively, fluorescence quenching assays could be performed, measuring the decrease of intrinsic tryptophan (Trp59) fluorescence at 330 nm as a function of ligand (Elte derivative or natural macrolide) concentration. The tryptophan fluorescent residue (Trp59) in the active site lies just above the piperidinic ring of the ligand in a quasi-stacked configuration with interatomic Trp-piperidine distances as low as 3.7 Å (Figure 3.13), thus making FKBP12 amenable for intrinsic fluorescence quenching determination of binding affinities.
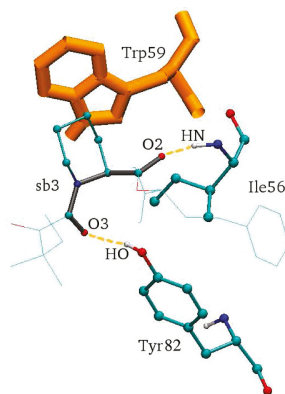
Figure 3.13. Binding pocket of the (15R)-sb3-FKBP12 complex, showing the tryptophan fluorescent residue (bonds representation, orange color) above the piperidinic ring of sb3 ligand.

We first started binding assay studies from Elte421. The final FKBP12 concentration used for measurements was 1.09 µM, the desired ligand concentration in the sample was obtained by appropriate dilution of ligand stock solution. Ligand concentrations in the range 10 nM to 400 nM were used, with a final DMSO concentration in the sample lower than 0.5%. A decrease in the intrinsic tryptophan fluorescence of FKBP12 protein was readily observed upon addition of Elte421 (Figure 3.14, solid line), indicating binding of the Elte421 ligand in the region of the Trp59 in FKBP12.
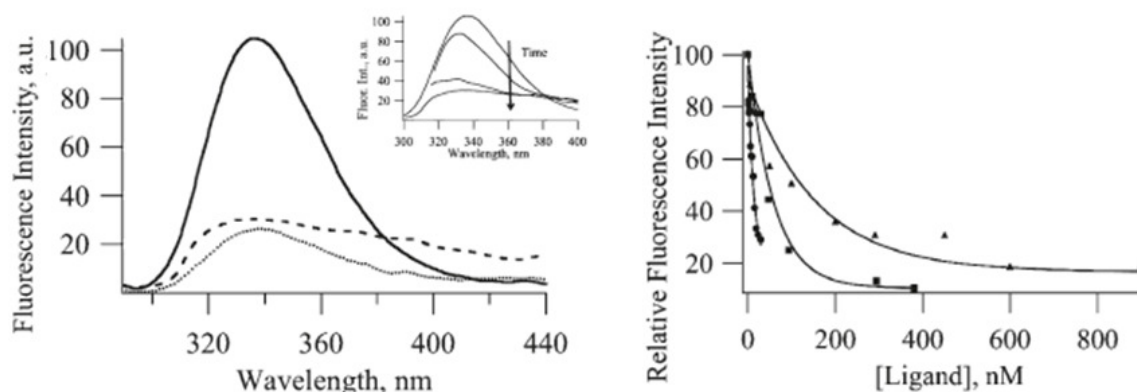
Figure 3.14. Left: Fluorescence spectra of FKBP12 in PBS (solid line), FKBP12 with FK506 in PBS (dotted line) and FKBP12 with Elte421 in PBS (dashed line) at 288 K. (Inset) Fluorescence emission spectra of FKBP12-Elte421 system as a function of time after ligand addition: 5 min, 20 min, 1 h, and 2 h. Right: Relative fluorescence intensity decrease of FKBP12 fluorescence with FK506 (squares), Elte421 (triangles), and Rapamycin (circles).[40]

The decrease in protein fluorescence for a similar concentration of FK506 was found to be of comparable extent. Closer inspection of the concentration dependence of the quenching data for Elte421, FK506, and Rapamycin (Figure 3.14, right) shows that all three ligands exhibit a similar binding behavior.

The data were fitted to extract the dissociation constant (K_d) for the three ligands. Due to the well-known dependence of K_d on experimental conditions and systematic concentration errors,[41] the binding activity of the Elte421 is reported with respect to that of the Tacrolimus natural drug. The experimentally determined dissociation constant of the Elte421-FKBP12 complex was found to be

only 3 times larger than that of Tacrolimus and 5 times larger than the K_d for Rapamycin calculated from data extracted from the literature.[40] Confirming the prediction based on the above free-energy conformational analysis, the (15R)-Elte and (15S)-Elte 1:1 mixture therefore is three times as potent as (15R)-sb3 (K_d[(15R)-sb3)]/K_d(FK506) = 10).[29,42] As stated above, only the *trans* rotamers bind FKBP12. Consequently, the *cis-trans* equilibrium of nonmacrolide FK506-related ligands progressively shifted toward the *trans* form upon binding to the protein FKBP12, with a kinetics that is typical of the *cis-trans* isomerization in proline. Such behavior was confirmed by the decrease of fluorescence of the FKBP12 as a function of time after Elte421 was added to the protein in solution (see the inset of Figure 3.14). In the natural drug Tacrolimus, which exhibits only the (ω) *trans* form, such kinetic behavior was not observed.

Moreover, in order to elucidate the reason why the results of the REM simulations assigned to Elte421 in water a much more compact structure than that in DMSO, fluorescent measurements on Elte421 dissolved in water and DMSO has been performed (Figure 3.15).
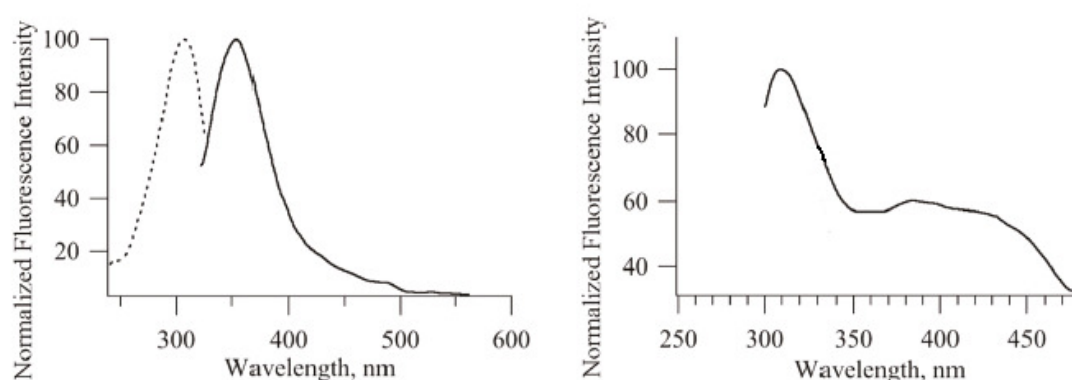
Figure 3.15. Left: normalized fluorescence emission (solid line) and excitation (dashed line) spectra of Elte421 in DMSO; concentration = 1.35 mM, λexc. = 300 nm, and λem. = 350 nm. Right: fluorescence emission spectrum of Elte421 in PBS; concentration = 8 μM and λexc. = 270 nm.

In DMSO, the clustering analysis done using the data from REM simulations showed that Elte421 overwhelmingly adopts open configurations, with the three hydrophobic groups pointing away from each other. Such behavior was due to the amphiphilic character of the DMSO molecule that can interact favorably with both hydrophobic and hydrophilic groups in Elte421. Consequently, in the fluorescence spectrum of Elte421 in DMSO, only one broad peak was observed at λ = 360 (Figure 3.15, left). In water solution, the Elte421 major fluorescence peak underwent a blue shift, while a broad secondary peak at larger wavelengths (λ = 380-430) appeared (Figure 3.15, right). This was reminiscent of formation of aggregates, a common behavior found in molecules containing aromatic moieties in water solution or confined environment.[43] In addition, an emission dependent behavior for the excitation spectra of Elte421 in water was found, suggesting the presence of a significant population of long-lived intraligand ground-state structures stabilized by π-π stacking and fully confirming the REM simulations.

Encouraged by the optimal capability of fluorescence assays to determinate the binding affinity of Elte421, we extended these tests to the other members of Eltex family. Doing this, we kept in mind that the ω-*trans-cis* ratio, due to the high barrier, could be one of the rate-determining step in the kinetics of the FKBP binding and hence on the kinetics of Trp59 quenching by Eltex ligands.
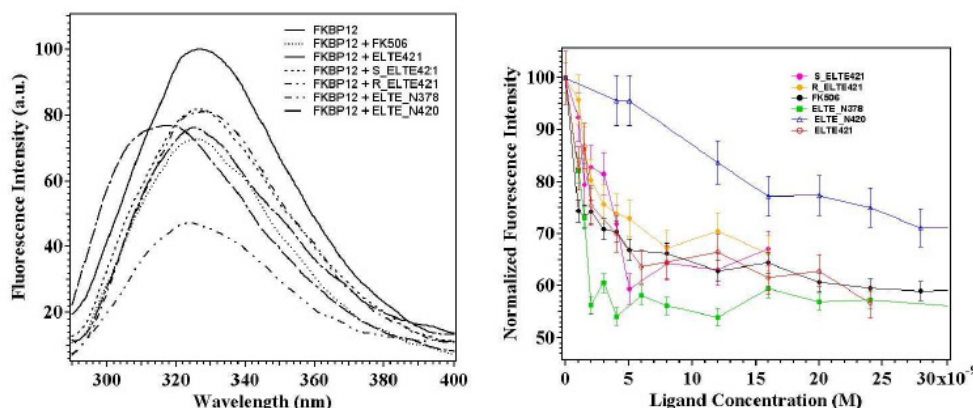
Figure 3.16. Left: fluorescence emission spectra of FKBP12 in PBS buffer solution compared to spectra obtained when a 4nM solution of the ligand is added to the protein. Right: relative fluorescence intensity decrease of FKBP12 fluorescence at 325 nm (excitation wavelength lexc = 265 nm) as a function of ligand concentration for the series of Eltex compounds and for FK506.

Indeed, we observed a faster decrease in fluorescence for the compounds that, according to the REM simulation, have a large *trans*/*cis* ratio, as the potent ElteN378 and the diastereoisomer *R*-ElteN420 (Figure 3.16). Among esters, Elte421 (**1**, purple circles, Figure 3.16, right), 1:1 diasteroisomeric mixture, showed an affinity (K_{inst}= 1.2) for the protein comparable to the one of FK506 (to which was assigned K_{inst}= 1.0, as standard). (*R*)-Elte421 (**2**) and (*S*)-Elte421 (**3**), synthesized as enantiopure compounds, turned out to have similar binding affinity to Elte421 (K_{inst}= 1.6 and K_{inst}= 1.1, respectively). Regarding amide derivatives, ElteN420 (**4**, blue triangles) resulted to be the less potent inhibitor of Eltex family with a K_{inst}= 5. As above discussed, propyl moiety on the side of PKA, pointed in both epimers *outward*, in the same direction of the pipecolic clamp, possibly interfering, FKBP12 binding. Starting from this disappointing result, we decided not to assign *R*-ElteN420 and *S*-ElteN420 to the organic synthesis. On the other hand, ElteN378 (**5**, green circles) showed a binding affinity higher (K_{inst}= 0.5) than FK506 and comparable to the one of Rapamycin (K_{inst}= 0.5), showing it to bethe most powerful synthetic inhibitor of FKBP12 protein, ever described in literature before. The affinity of Eltex family's members for FKPB12 protein in summarized in figure 3.17.
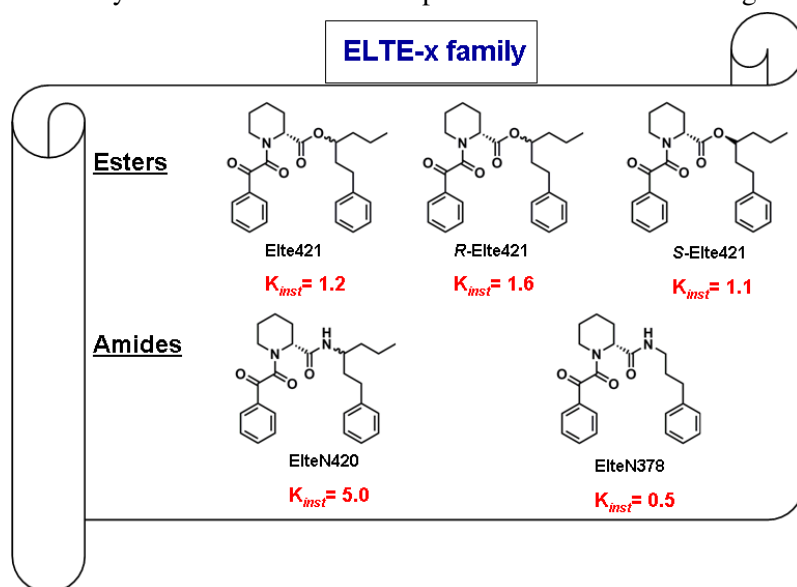
Figure 3.17. Eltex family with k_{inst} values

3.3 Conclusions and future perspective

In the present study, we have demonstrated, using an interdisciplinary approach based on computational, synthetic, and chemico-physical techniques, that the best potential FKBP binders bearing the pipecolyl α-keto amide subunit (and very likely the best PPI inhibitors) are characterized in water solution by the abundance of quasi-cyclic structures stabilized by intraligand hydrophobic interactions. The conformational entropy in such ligands, as occurs in the rigid natural macrolides FK506 and Rapamycin, is low. At the same time such ligands optimally expose, again as in FK506 and Rapamycin, the two contiguous carbonyl oxygen in the peptidomimetic chain for FKBP docking. These peculiar structural and chemico-physical features define at the same time an Eltex compound and the minimal pharmacore in the FKBP family. On the basis of the above hypothesis, we have successfully designed and synthesized ElteN378, a new low atomic weight FKBP ligand with affinity comparable to that of the macrolide Rapamycin.

Furthermore, we believe that our computationally driven design of new potent FKBP12 inhibitors, based on preliminary and costless simulations of the ligand in water bulk solution to monitor its conformational behavior, may provide also a valuable mean to identify the optimal position for inserting a so-called 'effector domain' for the allosteric interactions with a third partner protein. An effective immunosuppresant ligand must bind FKBP via the PKA driven mechanism as well as the partner protein with the effector domain on the opposite (convex) side of the PKA unit. Therefore, due care must be taken to ensure that structural modifications or group insertion in compounds such as ElteN378 do not abrogate the potency of the ligand by interfering with or altering the mean conformational structure of the PKA binding domain in a water environment, e.g., by severely perturbing the ω, ψ free energy surface and/or obstructing the solvent-exposed carbonyl group in the PKA unit. This computational/synthetic procedure, for example, could assist the design of a sensors for FKBP12, a possible biomarker for early diagnosis in Alzheimer's or Parkinson's desease.
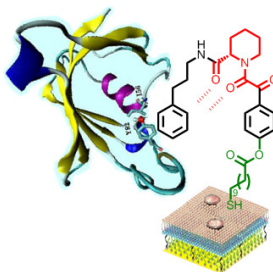
Figure 3.18. Schematic representation of a possible sensor, based on a modified ElteN378 derivative.

An FKBP sensor device can be envisaged by judiciously attaching to ElteN378 a long polymeric chain ending with an anchoring group for biochemical sensing in Self-assembled monolayers or supported lipid bilayers deposited on gold surfaces (Figure 3.18).

3.4 Experimental Section

General synthetic procedures

All the reactions are monitored by TLC on commercially available precoated plates (silica gel 60 F 254) and the products were visualized with acidic vanillin solution.

Silica gel 60, 230–400 mesh, is used for column chromatography, unless otherwise stated. EtP refers to light petroleum, bp 40–60 °C and AcOEt to ethylacetate. ^{1}H and^{13}C NMR spectra were recorded at 400,300, 200 and 100, 50 MHz, respectively. FTIR spectra are recorded in CDCl$_3$ solutions. ESI-mass spectra are measured with a LCQ-FLEET, Thermo Scientific instrument. THF was distilled from sodium in the presence of the blue colour of benzophenone kethyl, DCM was distilled from CaH$_2$. Commercial available reagents, catalysts and ligands are used as obtained, unless otherwise stated, from freshly opened container without further purifications.

Synthesis of (3R/S)-1-phenylhexan-3-ol (7)

7
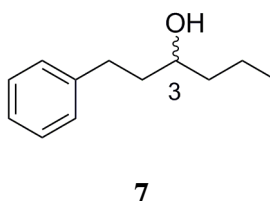
To a solution of 3-phenylpropionaldheyde (**6**) (3.00g, 22.36mmol) in 15 mL of dry THF was added drop wise a solution of propylmagnesium chloride 2M in ether at -78°C, under a N$_2$ atmosphere. The reaction mixture was stirred at -50°C. After 4 h the TLC analysis still showed the spot of the starting material so 20% of propylmagnesium chloride 2M in ether was added at -78°C. The reaction was stirred at -10°C for 17 hours, then poured onto 20 mL of saturated solution of NH$_4$Cl and warmed at r.t. The solution was extracted with diethyl ether (3x50 mL), the recollected organic layer was dried over Na$_2$SO$_4$, filtered and evaporated to obtain a light yellow oil (3.55 g). The crude was purified by flash chromatography with EtP : AcOEt 10 : 1 as eluent to obtain a colourless oil (1.56 g) as pure product in 40% yield.[44]

Synthesis of (3*R/S*)-*tert*-butyl 1-phenylhexan-3-yl piperidine-1,2-dicarboxylate (8)

8
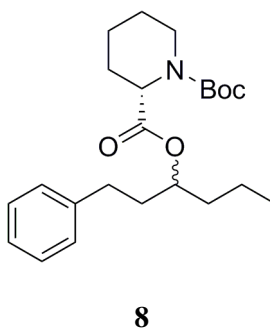
To a solution of (3*R/S*)-1-phenylhexan-3-ol (**7**) (0.70g, 3.89mmol) in 7 mL of dry DCM N-Boc pipecolic acid (1.78 g, 7.76 mmol), DMAP (0.05 g, 0.39 mmol) and diisopropylcarbodiimide (1.21 mL, 7.76 mmol) were added at 0°C, under a N_2 atmosphere. A white precipitate was observed. The reaction mixture was stirred for 3 h at r.t. then poured onto 30 mL of diethyl ether and washed with a saturated solution of NH_4Cl (3x50 mL), followed by a saturated solution of $NaHCO_3$ (2x70 mL). The recollected organic layer was dried over Na_2SO_4, filtered and evaporated to obtain a colorless oil (1.60 g). The ^1H NMR spectrum still showed the presence of diisopropylurea, removed washing the crude, dissolved in 20 mL of ether, with a saturated solution of NH_4Cl (4x30 mL). The organic layer was dried over Na_2SO_4, filtered and evaporated to obtain a colourless oil (0.90 g) as pure product in 60% yield. ^1H NMR, 400 MHz, CDCl$_3$, δ: 0.91 (t, 3H, J =7.90 Hz, CH$_3$); 1.24-1.39 (m, 2H); 1.45 (s, 9H); 1.46-1.63 (m, 6H); 1.78-1.93 (m, 4H); 2.54-2.71 (m, 2H); 2.87-3.08 (m, 1H); 3.88-4.12 (m, 1H); 4.72-4.83 (m, 1H); 4.87-5.05 (m, 1H); 7.14-7.31 (m, 5H). In the ^{13}C NMR spectrum the total number of signals is due the partial superimposition of the carbon chemical shifts of the two rotamers for each diastereoisomer. ^{13}C NMR, 100MHz, CDCl$_3$, δ: 13.89; 18.55; 20.76; 24.67; 26.23; 28.33; 31.77; 36.06; 41.10; 42.08; 53.89; 54.87; 74.41; 79.74; 80.31; 125.93; 128.28; 128.40; 141.68; 155.84; 171.78. IR (CDCl$_3$), cm^{-1}: 1726.88 (m, C=O$_{ester}$ stretch.); 1683.87 (s, C=O$_{carb}$ stretch.); 13.65.59 (m, C-O stretch.); 1275.26 (m, N-CO-O stretch. as); 1043.01 (w, N-CO-O stretch. sy).

Synthesis of (3*R/S*)-1-phenylhexan-3-yl piperidine-2-carboxylate (9)
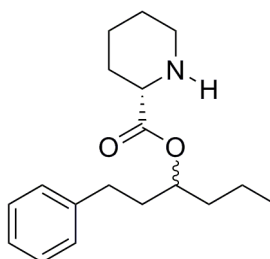
9

To a solution of (3*R/S*)-(*tert*-butyl 1-phenylhexan-3-yl piperidine-1,2-dicarboxylate (**8**) (0.12 g, 0.31 mmol) in 3 ml of dry DCM, TFA 99% (0.3 mL) was added drop wise at 0°C. The reaction mixture turned to yellow. The solution was stirred at r.t. for 1 h then poured onto 20 mL of a saturated solution of NaHCO$_3$ and extracted with DCM (3x40 mL). The organic layer was washed with a saturated solution of NaHCO$_3$, dried over Na$_2$SO$_4$, filtered and evaporated to obtain a yellowish oil (0.80 g) as pure product in 92% yield. ^1H NMR, 400MHz, CDCl$_3$, δ: 0.90 (t, 3H, J = 7.52 Hz); 1.24-1.39 (m, 2H); 1.42-1.63 (m, 6H); 1.78-1.93 (m, 5H); 2.54-2.71 (m, 3H); 3.01-3.13 (m, 1H); 3.29-3.36 (m, 1H); 4.97-5.05 (m, 1H); 7.14-7.30 (m, 5H). ^{13}C NMR, 100MHz, CDCl$_3$, δ : 13.94; 18.48, 24.14, 25.88, 29.39, 31.74, 35.83, 36.30, 45.68; 58.72; 74.01; 125.86, 128,28, 128.36, 141.61; 173.33. IR (CDCl$_3$), cm-1: 1722.58 (vs, C=O stretch.); 1602.15 (m, N-H bend.); 1197.84, 1124.73 (s, 2 C-O stretch.). IR (CDCl$_3$), cm^{-1}: 1722.58 (vs, C=O stretch.); 1602.15 (m, N-H bend.); 1197.84, 1124.73 (s, 2 C-O stretch.).

Synthesis of phenylglyoxyl chloride (10)
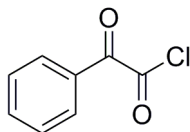
10

To a solution of phenylglyoxylic acid (0.3 g, 2 mmol) in 1 mL of dry thionyl chloride, 0.1 eq. of DMF (0.015 g, 0.2 mmol) were added, under N_2 atmosphere. The reaction mixture was heated at 35°C and stirred at this temperature overnight. The solution was finally evaporated under vacuum at a maximum temperature of 40 degrees to obtain a yellow oil containing an amount of powdery deposit as pure product in 93% yield. ^{1}H NMR, 400MHz, CDCl$_3$, δ:7.58 (m, 2H, H$_{meta}$), 7.77 (m, 1H, H$_{para}$), 8.01 (m, 2H, H$_{orto}$). IR (CDCl$_3$), cm^{-1}: 3064.65 (w, CH$_2$ $_{arom}$ stretch.), 1774.19 (s, ClC=O stretch.), 1696.77 (s, C=O stretch.), 1593.54, 1451.61 (m, C$_{ar}$=C$_{ar}$ stretch.), 1253.76 (s, C-Cl stretch.).

Synthesis of (3*R/S*)-1-phenylhexan-3-yl 1-(2-oxo-2-phenylacetyl)piperidine-2-carboxylate (1) Elte421
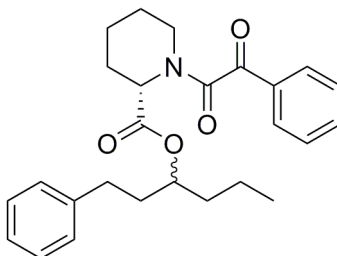
4

To a solution of amine (**9**) (0.085 g, 0.3 mmol) in 1 mL of dry DCM, TEA was added (85 µL, 0.6 mmol) and the solution was cooled at -10 °C, under a N_2 atmosphere. A solution of phenylglyoxyl chloride (**10**) (0.05 g, 0.3 mmol) was slowly added, dropwise at -10°C, then the reaction mixture was allowed to warm at r.t. and stirred for 4 h. The solution was poured onto 20 mL of DCM and washed with Brine (3 x 30 mL). The recollected organic phase was dried over Na$_2$SO$_4$, filtered and evaporated to obtain a yellowish oil (0.109 g). The crude was purified with flash chromatography with EtP:AcOEt=4:1 as eluent to obtain a colorless oil (0.085 g) as pure product in 68% yield. In the ^{1}H NMR spectra certain signals indicate the presence of two diatereoisomers (d1 and d2 in 1:1 ratio) and two rotamers (r1 and r2 in 3:1 ratio) respectively. ^{1}H NMR, 400MHz, DMSO-*d6*, δ: 0.76 (t, 3H, *J* = 8.5Hz, d1 r2); 0.79 (t, 3H, *J* = 8.5Hz, d2 r2); 0.869 (t, 3H, *J* = 7.5Hz, d1 r1); 0.874 (t, 3H, *J* = 7.5Hz, d2 r1); 0.99-1.17 (m, 2H); 1.21-1.40 (m, 2H); 1.39-1.49 (m, 2H); 1.55-1.64 (m, 2H); 1.68-1.80 (m,

3H); 1.84-1.92 (m, 2H); 2.16-2.29 (m, 1H); 2.38-2.45 (m, 2H); 2.51-2.86 (m, 2H); 2.86-2.96 (m, 1H); 3.07-3.17 (m, 1H); 3.33-3.40 (m, 1H); 4.32-4.37 (m, 1H); 4.38-4.44 (m, 1H, d1+d2 r2); 4.78-4.86 (m, 1H, d1+d2 r2); 4.93-5.02 (m, 1H, d1+d2 r1); 5.23 (at, J = 6.25 Hz, d1+d2 r1); 7.05-7.28 (m, 5H); 7.54-7.58 (m, 3H); 7.61-7.80 (m, 3H); 7.89-7.85 (m, 2H, d1+d2 r2); 7.94 (ad, 2H, J = 8.0 Hz, d1+d2 r1). In the ^{13}C NMR spectrum the total number of signals is due the partial superimposition of the carbon chemical shifts of the two rotamers for each diastereoisomer. ^{13}C NMR, 100MHz, CDCl$_3$, δ: 13.71;13.97; 18.43; 18.61; 21.21; 22.42; 24.45; 24.91; 26.37; 27.36; 31.75; 35.85; 36.28; 44.27; 51.72; 56.60; 75.39; 125.99; 128.21; 128.37; 129.03; 129.75; 133.19; 134.74; 141.16; 166.77; 167.35; 169.84; 170.10; 191.53; 191.73. IR (CDCl3), cm^{-1}: 1726.88 (s, OC=O stretch.); 1679.56 (m, NC=O stretch.); 1640.86 (m, PhC=O stretch.). ESI-MS: m/z = 865 [2M+Na]$^+$; 444 [M+Na]$^+$.

R-ESTER

Synthesis of (3*S*)-1-phenylhex-5-en-3-ol ((*S*)-11)

(*S*)-11
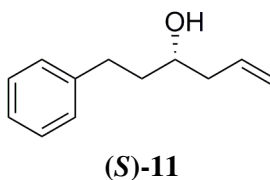
To a solution of (+)-β-allyldiisopinocamphenylborane 1M in dioxane (5.00 mL, 5.00 mmol) in freshly distilled diethyl ether (2.6 mL), 3-phenylpropionaldehyde (**6**) (0.66 mL, 5.00 mmol) was added at -100 °C under a N$_2$ atmosphere and then allowed to reach 0 °C. The reaction was stirred under a N$_2$ atmosphere at 0 °C for 1 h and then allowed to reach r.t. NaOH 3M (3.50 mL) and H$_2$O$_2$ 30 % (1 mL) were added and the mixture was stirred at reflux at for 1 hour. A white precipitate was observed. Distilled water (20 mL) was added and the aqueous layer was extracted with diethyl ether (3x50 mL). The organic layer was washed with brine (3x60 mL), dried over MgSO$_4$, filtered and evaporated under vacuum to obtain 1.91 g of a pale yellow oil. The crude was purified by flash chromatography using Tol : AcOEt 5:1 as eluent to obtain the final product (0,48 g) as colourless oil in 55 % yield. ^{1}H NMR, 400MHz, CDCl$_3$, δ : 1.73 (br, 1H, OH), 1.72-1.82 (m, 2H, CH$_2$, H-2), 2.20 (dtt, J_1 = 14.0 Hz, J_2 = 8.0 Hz, J_3 = 0.8 Hz, 1H, H-4), 2.33 (dtt, J_1 = 14.0 Hz, J_2 = 5.2 Hz, J_3 = 1.2 Hz, 1H, H-4), 2.66 (dt, J_1 = 13.6 Hz, J_2 = 8.4 Hz, 1H, H-1), 2.83 (dt, J_1 = 13.6 Hz, J_2 = 7.6 Hz, 1H, H-1), 3.71-3.65 (m, 1H, H-3), 5.13-5.18 (m, 2H, CH$_2$-6), 5.83 (dddd, J_1 = 16.0 Hz, J_2 = 10.0 Hz, J_3 = 7.6 Hz, J_4 = 6.0 Hz, 1H, H-5), 7.18-7.32 (m, 5H, H$_{arom}$). ^{13}C NMR, 100MHz, CDCl$_3$, δ : 32.00 (1C, C-2); 38.40 (1C, C-1); 42.00 (1C, C-4); 69.80 (1C, C-3); 118.30 (1C, C-6); 125.80 (1C, C$_{para}$); 128.30 (2C, C$_{orto}$); 128.40 (2C, C$_{meta}$); 134.00 (1C, C-5); 144.00 (1C, C$_{quat}$). IR (CDCl$_3$), cm^{-1}: 3390 (s, OH stretch. free), 3062, 3026 (s, CH$_{arom}$ stretch.), 2860 (m, CH$_{aliph.}$ stretch.), 1640 (m, C=C stretch.), 1494 (s, C=C stretch.), 1454 (s, CH bend.), 1047 (s, C-OH strech.).[45]

Synthesis of (3*R*)-1-phenylhexan-3-ol ((*R*)-7)

(*R*)-7
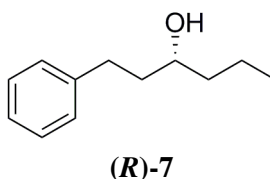
Pd/C 5% (0.032 g) was added in a double neck rounded bottom flask. Separately a solution of (3S)-1-phenylhex-5-en-3-ol (**(S)-11**)(0.33 g, 1.88 mmol) was dissolved in dry MeOH (26 mL) and added into the flask. After two nitrogen-vacuum cycles two hydrogen-vacuum cycles were performed. The reaction mixture was stirred in a hydrogen atmosphere at ordinary pressure and at r.t. for 2.5 h. The reaction mixture was filtered, the solid fraction was washed with 10 mL of DCM and the collected liquid layer was evaporated under vacuum to obtain 0.26 g of a colourless oil. The crude was purified by flash chromatography using EtP : AcOEt 5 : 1 as eluent to obtain 0.24 g of a colourless oil as final product in 71 % yield. ^{1}H NMR, 400MHz, CDCl$_3$, δ : 0.95 (t, *J*= 7.1 Hz, 3H, CH$_3$), 1.33-1.51 (m, 5H, 2CH$_2$ + OH), 1.70- 1.86 (m, 2H, CH$_2$), 2.19-2.72 (m, 1H, H-1), 2.73-2.86 (m, 1H, H-1), 3.66-3.67 (m, 1H, H-3), 7.19-7.23 (m, 3H, H$_{ortho-para)}$, 7.27-7.32 (m, 2H, H$_{meta}$). ^{13}C NMR, 100MHz, CDCl$_3$, δ : 14.33; 19.02; 32.23; 39.33; 39.98 (5C, C$_{aliph}$); 71.34 (1C, C-3); 126.00 (1C, C$_{para}$); 128.61(2C, C$_{orto}$); 128.62 (1C, C$_{meta}$); 142.43 (1C, C$_{quat}$). [α]$_D^{23}$: -11.24, (c = 1.69, EtOH), (Lit: -4.05 (c = 1.85, EtOH).[37,38]

Synthesis of tert-butyl (15R,2S)-1-phenylhexan-3-yl piperidine-1,2-dicarboxylate ((R)-8)

(R)-8
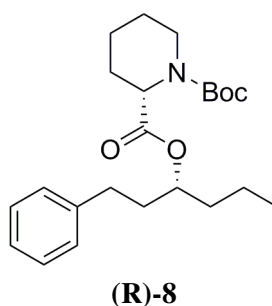
To a solution of (3R)-1-phenylhexan-3-ol (**(R)-7**) (0.28 g, 1.53 mmol) in 10 mL of dry DCM, N-Boc pipecolic acid (0.42 g, 1.84 mmol), DMAP (0.018 g, 0.15 mmol) and diisopropylcarbodiimide (0.29 mL, 1.84 mmol) were added at 0°C, under a N$_2$ atmosphere. A white precipitate indicated the formation of DCU. The reaction was stirred under a N$_2$ atmosphere at r.t for 5 h, then poured onto 20 mL of diethyl ether. The organic layer was filtered and alternately washed several times with saturated solutions of NH$_4$Cl and NaHCO$_3$,dried over Na$_2$SO$_4$, filtered and evaporated under vacuum to obtain 0.28 g of a yellow oil as pure product in 47 % yield. ^{1}H NMR, 400MHz, CDCl$_3$, δ : 0.91 (t, *J*= 7.90 Hz, 3H, CH$_3$), 1.24-1.39 (m, 2H, 2H-38), 1.45 (s, 9H, C(CH$_3$)$_3$), 1.46-1.63 (m, 6H, 3CH$_2$), 1.78-1.93 (m, 4H, 2CH$_2$), 2.54-2.71 (m, 2H, CH$_2$-4), 2.87-3.08 (m, 1H, H-5), 3.88-4.12 (m, 1H, H-5), 4.72-4.83 (m, 1H, H-2), 4.87-5.05 (m, 1H, H-15), 7.14-7.31 (m, 5H, H$_{arom}$). ^{13}C NMR, 100MHz, CDCl$_3$, δ : 13.89; 18.52; 20.76; 22.47; 24.34; 24.67; 24.86; 26.86 (5C, C$_{aliph.}$); 28.33 (3C, C$_{t–butyl}$); 31.86; 36.25; 36.40; 41.08; 42.16; 53.89; 54.87 (4C, C$_{aliph}$ + rotamer); 74.44 (1C, C-15); 79.85; 80.33 (1C, C$_{t–butyl}$- 9 + rotamer); 125.97; 128.32; 128.41; 141.45 (6C, C$_{arom}$); 155.40; 155.93 (1C, C=O$_{carb}$); 171.81 (1C, C=O$_{ester}$). IR (CDCl$_3$), cm^{-1}: 1726.88 (m, C=O$_{ester}$ stretch.), 1683.87 (s, C=O$_{carbamate}$ stretch.), 1365.59 (m, C-O stretch.), 1275.26 (m, N-CO-O stretch. as), 1043.01 (w, N-CO-O stretch. sy). [α]$_D^{23}$ (CHCl$_3$): -0.47 (c = 1.80 mg/mL).

Synthesis of (15*R*,2*S*)-1-phenylhexan-3-yl piperidine-2-carboxylate ((*R*)-9)

(*R*)-9
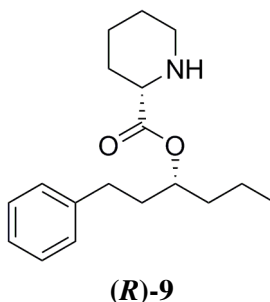
To a solution of *tert*-butyl (15*R*,2*S*)-1-phenylhexan-3-yl piperidine-1,2-dicarboxylate ((*R*)-8) (0.19 g, 0.48 mmol) in DCM (2 mL) 1 mL of a solution of TFA 99% (0.20 mL, 2.58 mmol) in 2 mL of DCM was added drop wise at 0°C. The reaction mixture turned yellow. The reaction mixture was stirred at r.t. for 4 h during which 1.5 mL of the acid solution were added at 0°C because the TLC analysis showed spot corresponding to the starting material. A saturated solution of $NaHCO_3$ (20 mL) was added drop wise and the aqueous layer was extracted with DCM (3x25 mL). The organic layer was washed with a saturated solution of $NaHCO_3$ (4 x 80 mL), dried over Na_2SO_4, filtered and evaporated under vacuum to obtain 0.12 g of a pale yellow oil as pure product in 86 % yield. ^{1}H NMR, 400MHz, $CDCl_3$, δ : 0.82 (t, *J*=7.2 Hz, 3H, CH_3-1), 0.83 (t, *J*= 7.2 Hz, 3H, CH_3), 1.24-1.39 (m, 2H, 2H-38), 1.42-1.63 (m, 6H, $2CH_2$), 1.78-1.93 (m, 5H, CH_2-17 + CH_2-37 + NH), 2.54-2.71 (m, 3H, H-5 + CH_2-4), 3.01-3.13 (m, 1H, H-5), 3.29-3.36 (m, 1H, H-2), 4.97-5.05 (m, 1H, H-15),6.50 (d, *J*= 9.5 Hz, 1H, NH1), 6.63 (d, *J*= 9.01 Hz, 1H, NH), 7.14-7.30 (m, 5H, H_{arom}). ^{13}C NMR, 100MHz, $CDCl_3$, δ : 13.94 (1C, CH3); 18.48; 24.14; 25.88; 29.39; 31.74; 35.83; 36.30; 45.68 (8C, $C_{aliph.}$); 58.72 (1C, C-2); 74.01 (1C, C-15); 125.86; 128.28; 128.36; 141.61 (6C, C_{arom}); 173.33 (1C, C=O_{ester}). IR ($CDCl_3$), cm^{-1}: 1722.58 (vs, C=O stretch.), 1602.15 (m, N-H bend.), 1197.84, 1124.73 (s, 2 C-O stretch.). $[α]_D^{23}$ ($CHCl_3$): -1.53, (c = 1.50 mg/mL). $[α]_D^{26}$ (EtOH): -6.43, (c = 1.85 mg/mL).

Synthesis of (15*R*,2*S*)-1-phenylhexan-3-yl 1-(2-oxo-2-phenylacetyl)piperidine-2-carboxylate *R*-Elte420

2
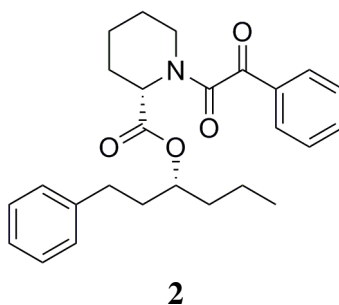
To a solution of (15*R*,2*S*)-1-phenylhexan-3-yl piperidine-2-carboxylate ((*R*)-9) (0.12 g, 0.41 mmol) in freshly distilled dichloromethane (4 mL), TEA (0.11 mL, 0.82 mmol) was added under a N_2 atmosphere. The reaction mixture was cooled to 0 °C and a solution of 2-oxo-2-phenylacetyl chloride (0.070 g in 0.39 mL of freshly distilled DCM, 0.41 mmol) was added drop wise. The solution turned pale yellow. The reaction mixture was kept stirred under a N_2 atmosphere at r.t. for 4 h. DCM (35 mL) was added and the reaction mixture was washed with brine (3x30 mL), dried over Na_2SO_4, filtered and evaporated under vacuum to obtain 0.14 g of an orange oil. The crude was purified by flash column

chromatography using EtP : AcOEt 7:1 as eluent to obtain 0.060 g of a colourless oil as pure product in 34 % yield. In the ^{1}H NMR spectrum when the attribution of signals to different rotamers is possible (∗) refers to the minor rotamer. ^{1}H NMR, 400MHz, C$_6$D$_6$, δ : 0.76 (t, J= 7.03 Hz, 3H, CH$_3$); 0.84 (t, J= 7.12 Hz, 3H, CH-3*); 0.9-1.82 (m, 10H, CH$_2$-37 + CH$_2$-38 + CH$_2$-3 + CH$_2$-4 + CH$_2$- 5); 2.06-2.12 (m, 2H, CH$_2$-16); 2.25-2.43 (m, 2H, CH$_2$-17); 2.44- 2.70 (m, 2H, CH$_2$-17);3.01-3.12 (m, 1H, H-6); 3.31-3.45 (m, 1H, H-6); 4.52-4.54 (m, 2H, CH$_2$- 16); 4.80-4.87 (m, 1H, H-21); 4.93-5.00 (m, 1H, H- 15); 5.09-5.17 (m, 1H, H-2); 5.54-5.58 (m, 1H, H-15); 6.94-7.15 (m, 8H, H$_{arom}$); 8.18-8.21 (m, 2H, H$_{orto}$*); 8.30-8.34 (m, 2H, H$_{orto}$). ^{13}C NMR, 100MHz, C$_6$D$_6$, δ : 13.66; 18.40; 20.97; 24.45; 25.81; 31.70; 35.91; 36.25; 43.72; 51.60 (10C, $_{Caliph.);}$ 74.62 (1C, C-15); 125.99; 128.21; 128.37; 129.03; 129.75; 133.19; 134.74; 141.16 (10C, C$_{arom}$); 167.75 (1C, C=O$_{carb}$); 170.23 (1C, C=O$_{ester}$); 191.68 (1C, C=O$_{ketone}$). IR (CDCl$_3$), cm^{-1}:1726.88 (s, OC=O stretch.); 1679.56 (m, NC=O stretch.); 1640.86 (s, PhC=Ostretch.), 1447.31 (m, Car=Car stretch.). [α]$_D^{25}$: -31.42, (c = 1.85, EtOH). ESI-MS: m/z 865 [2M+Na]$^+$, 444 [M+Na]$^+$.

S-ESTER

Synthesis of (3R)-1-phenylhex-5-en-3-ol (R)-11
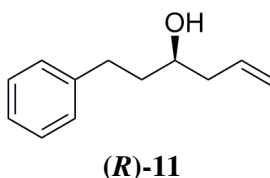
(R)-11

For the synthesis of this compound, we exploited the procedure described above for the synthesis of (3S)-1-phenylhex-5-en-3-ol (S)-11, excepted from using the (-)-β-allyldiisopinocamphenylborane instead of the (+)-β -allyldiisopinocamphenylborane. We obtained the final product as a colourless oil in 65 % yield. ^{1}H NMR , ^{13}C NMR and IR spectra have been recorded and were comparable to the ones of (3S)-1-phenylhex-5-en-3-ol described above.

Synthesis of (S)-1-phenylhexan-3-ol (S)-7
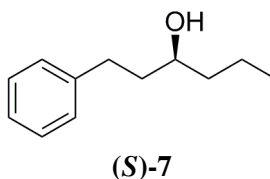
(S)-7

For the synthesis of this compound, we exploited the procedure described above for the synthesis of (3R)-1-phenylhexan-3-ol (R)-7 excepted from using the (3R)-1-phenylhex-5-en-3-ol (R)-11 instead of the (S)-1-phenylhex-5-en-3-ol (S)-11. We obtained the final product as a colourless oil in 55 % yield. ^{1}H NMR and ^{13}C NMR have been made and are the same as the one of (R)-1-phenylhexan-3-ol written above. [α]$_D^{24}$ (EtOH): +11.02, (c = 1.85 mg/mL).

Synthesis of (15S,2S)-1-phenylhexan-3-yl 1-(2-oxo-2-phenylacetyl)piperidine-2-carboxylate (*S*)-8

(*S*)-8
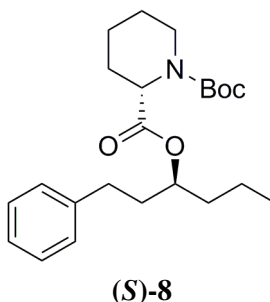
a) *Initial amidation:* For the synthesis of this compound, we exploited the procedure described above for the synthesis of (15R,2S)-*tert*-butyl-1-phenylhexan-3-yl piperidine-1,2-dicarboxylate (***R*)-8** except that we used the (*S*)-1-phenylhexan-3-ol (*S*)-7 instead of the (*R*)-1-phenylhexan- 3-ol (*R*)-7. We obtained the final product as a colourless oil in 42% yield. $[\alpha]_D^{25}$: -11,50, (c =1.85, EtOH).

(*S*)-9
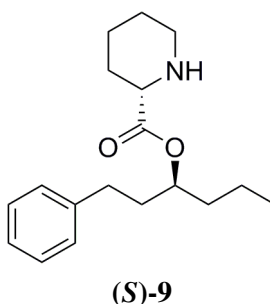
b) *Deprotection.* To a solution of tert-butyl (*S*)-1-phenylhexan-3-yl piperidine-1,2-dicarboxylate **(S)-8** (0.20 g, 0.52 mmol) in DCM (3 mL) 1 mL of a solution of TFA 99% (0.20 mL in 2 mL of dichloromethane, 2.58 mmol) was added drop wise at 0°C. The reaction mixture turned yellow and was stirred at r.t. for 4 h during which 0.5 mL of TFA in 1.5 mL of DCM are added at 0 °C. The mixture was poured onto 20 mL of NaHCO$_3$ sat.sol. and extracted with DCM (3 x 25 mL). The recollected organic layer was washed with a saturated solution of NaHCO$_3$ (4x80 mL), dried over Na$_2$SO$_4$, filtered and evaporated under vacuum to obtain 0.128 g of a pale yellow oil as pure product in 86 % yield. ^{1}H NMR, 400MHz, CDCl$_3$, δ: 0.88 (t, *J*= 7.42 Hz, 3H, CH$_3$), 1.24-1.39 (m, 2H, CH$_2$), 1.42-1.61 (m, 6H, 3 CH$_2$), 1.78-1.92 (m, 5H, 2 CH$_2$ + NH), 2.54-2.70 (m, 3H, H +CH$_2$), 3.00-3.11 (m, 1H), 3.29-3.34 (m, 1H), 4.97-5.03 (m, 1H, H-15), 7.12- 7.29 (m, 5H, H$_{arom}$). ^{13}C NMR, 100MHz, CDCl$_3$, δ: 13.94 (1C, CH$_3$), 18.44, 24.12, 25.82, 29.37, 31.72, 35.84, 36.28, 45.65 (8C, C$_{aliph.}$), 58.72 (1C, C-2), 74.03 (1C, C-15), 125.87, 128.27, 128.28, 128.35, 128.38, 141.61 (6C, C$_{arom}$), 173.30 (1C, C=O$_{ester}$).$[\alpha]_D^{25}$ (EtOH): -8,91, (c =1.85 mg/mL).

4
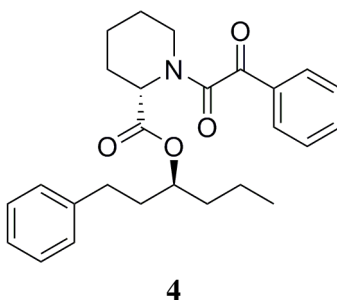
c) *Final amidation*. To a solution of (*S*)-1-phenylhexan-3-yl piperidine-2-carboxylate (**S**)-9 (0.09 g,

0.32 mmol) in freshly distilled DCM (3 mL), TEA (89 µL, 0.64 mmol) was added under a N_2 atmosphere. The reaction mixture was cooled to 0 °C and a solution of 2-oxo-2-phenylacetyl chloride (0.054 g, 0.32 mmol) in 2 mL of dry DCM was added drop wise. The solution turned pale yellow. The reaction mixture was stirred under a N_2 atmosphere at r. t for 4 h. DCM (35 mL) was added and the reaction mixture was washed with brine (3x30 mL), dried over Na_2SO_4, filtered and evaporated under vacuum to obtain 0.14 g of an orange oil. The crude was purified by flash column chromatography using EtP : AcOEt 7 : 1 as eluent to obtain 0.060 g of a colourless oil as pure product in 34 % yield. In the ^{1}H NMR spectrum when the attribution of signals to different rotamers is possible (∗) refers to the minor rotamer. ^{1}H NMR, 400MHz, C_6D_6, δ: 0.63 (t, J= 7.2 Hz, 3H, CH_3); 0.67 (t, J= 7.2 Hz, 3H, CH_3*); 0.74 (t, J= 7.2 Hz, 3H, CH_3*); 0.79 (t, J= 7.2 Hz, 3H, CH_3*); 0.9-1.82 (m, 10H, CH_2-37 + CH_2-38 + CH_2-3 + CH_2-4 + CH_2-5); 2.06-2.12 (m, 2H, CH_2-16); 2.25-2.43 (m, 2H, CH_2-17); 2.44-2.70 (m, 2H, CH_2-17);3.01-3.12 (m, 1H, H-6); 3.31-3.45 (m, 1H, H-6); 4.40-4.45 (m, 2H, CH_2-16); 4.71-4.79 (m, 1H, H-21); 4.82-4.91 (m, 1H, H-15); 5.05-5.08 (m, 1H, H-2); 5.49-5.51 (m, 1H, H-15); 6.94-7.15 (m, 8H, H_{arom}); 8.08-8.09 (m, 2H, H_{orto}*); 8.20-8.22 (m, 2H, H_{orto}). ^{13}C NMR, 100MHz, C_6D_6, δ: 13.65; 18.54; 21.07; 24.48; 25.86; 31.69; 36.23; 43.77; 51.59; 56.35 (10C, $C_{aliphatic}$); 74.80 (1C, C-15); 125.65; 125.93; 125.99 (3C, C_{arom}); 129.69; 129.96; 133.87; 134.04; 141.44 (5C, C_{arom}); 167.64 (1C, C=O_{carb}); 170.13 (1C, C=O_{est}); 191.67 (1C, C=O_{ketone}).

AMIDE

Synthesis of (3R/S)-1-phenylhexan-3-yl 4-methylbenzenesulfonate (12)
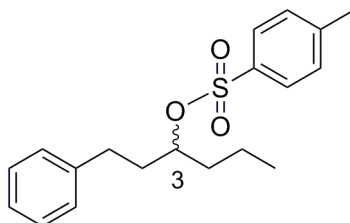
12

To a solution of (3R/S)-1-phenylhexan-3-ol (**7**) (0.43 g, 2.44 mmol) in 2 mL of dry pyridine, p-tosyl chloride (0.93 g, 4.88 mmol) was added, under a N_2 atmosphere. The suspension was stirred at rt for 15 h, then poured onto 15 mL of DCM. The reaction mixture was washed with HCl 10% (3x20 mL), $NaHCO_3$ sat. sol. (3x20 mL) and Brine (2x50 mL), then dried over Na_2SO_4, filtered and evaporated to obtain a yellowish oil (0.64 g).The ^{1}H-NMR spectrum of the crude showed the presence of p-tosyl chloride as impurity, not removable by flash chromatography at this stage. The impurity was easily removed in the next step of the procedure. ^{1}H NMR, 400MHz, CDCl$_3$, δ : 0.84 (t, 3H, J=7.13 Hz, CH_3); 0.91 (t, 3H, J=7.61 Hz, $CH_{3tosyl\ chloride}$); 1.19-1.38 (m, 4H, 2CH_2); 1.52-1.76 (m, 2H, CH_2);1.85-1.94 (m, 2H, CH_2); 2.45 (s, 3H, CH_{3tosyl}); 2.45 (s, 3H, $CH_{3tosyl\ chloride}$); 2.49-2.64 (m, 2H, CH_2); 4.60-4.66 (m, 1H, H-3); 7.16-7.35 (m, 5H, H_{arom}); 7.33 (d, 2H, J=8.10, H_{tosyl}); 7.80 (d, 2H, J= 7.13 Hz, H_{tosyl}). ^{13}C NMR, 100MHz, CDCl$_3$, δ : 13.63; 17.88 (2C); 21.69 (1C, CH_3); 31.06; 35.76; 36.20 (3C); 83.35 (1C, C-3); 125.96; 128.23; 126.56; 128.39; 129.68 (5C, C_{arom}); 134.65; 141.02; 144.41 (3C).

Synthesis of (3*R/S*)-1-(3-azidohexyl)benzene (13)
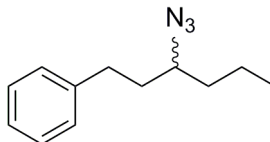
13

To a solution of (3*R/S*)-1-phenylhexan-3-yl 4-methylbenzenesulfonate (**12**) (0.51 g, 1.55mmol) in 3 mL of dry DMF, NaN$_3$ (0.8 g, 12.4 mmol) was added and the light pink suspension is stirred, under a N$_2$ atmosphere, for 15 h, then poured onto 20 mL of AcOEt. The reaction mixture was washed with Brine (4 x 25 mL), the recollected organic layer was then dried over Na$_2$SO$_4$, filtered and evaporated to obtain a yellowish oil (0.32 g). The crude was purified with flash chromatography with EtP : AcOEt 10 : 1 as eluent to obtain a colourless oil (0.15 g) as pure product in 98% yield. ^{1}H NMR, 400MHz, CDCl$_3$, δ : 0.93 (t, 3H, *J*=7.13Hz, CH$_3$); 1.35-1.57 (m, 4H, 2CH$_2$); 1.78-1.84 (m, 2H, CH$_2$); 2.63-2.84 (m, 2H); 3.22-3.30 (m, 1H, H-3); 7.18-7.32 (m, 5H, H$_{arom}$). ^{13}C NMR, 100MHz, CDCl$_3$, δ : 13.86 (1C, CH$_3$); 19.30; 32.40; 36.17; 36.59 (4C, C$_{aliph}$); 62.03 (1C, C-3); 126.01 (1C, C$_{para}$); 128.47 (4C, C$_{orto-meta}$); 141.30 (1C, C$_{quat}$). IR (CDCl$_3$), cm^{-1}: 3090.51; 3030.17 (m,CH$_{arom}$ stretc.); 2099.13 (vs, N$_3$ stretch.).

Synthesis of (3*R/S*)-1-phenylhexan-3-amine (14)
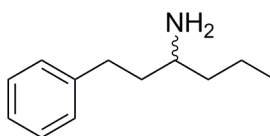
14

Pd/C 5% (0.06g, 0.031 mmol)was added in a double neck rounded bottom flask, then a solution of (3*R/S*)-1-(3-azidohexyl)benzene (**13**) (0.09g, 0.44mmol) in 3 mL of MeOH was added. The suspension was stirred at r.t. in a H$_2$ atmosphere at ordinary pressure for 3 h, then filtered to obtain a the final pure product as colourless oil in 38% yield. ^{1}H NMR, 300 MHz, CDCl$_3$, δ : 0.92 (t, 3H, *J*=6.93Hz, CH$_3$); 1.22-1.35 (m, 2H, CH$_2$); 1.39-1.48 (m, 2H, CH$_2$); 1.52-1.63 (m, 1H, H-8); 1.70-1.80 (m, 1H, H-8); 2.58-2.67 (m, 1H, H-9); 2.70-2.79 (m, 2H, CH$_2$), 7.15-7.30 (m, 5H, H$_{arom}$). ^{13}C NMR, 100 MHz, CDCl$_3$, δ: 14.20 (1C, CH$_3$); 19.22, 32.59; 39.91; 40,42 (4C, C$_{aliph}$); 50.56 (1C, C-9); 125.65 (1C, C$_{para}$); 128.31 (4C, C$_{orto-meta}$); 142.47 (1C, C$_{quat}$).

Synthesis of (15*R/S*,2*S*)-*tert*-butyl 2-(1-phenylhexan-3-ylcarbamoyl)piperidine-1-carboxylate (15)
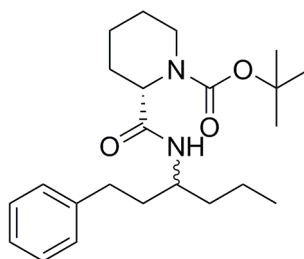
15

A solution of N-Boc pipecolic acid, enantiopure L (0.36 g, 1.58 mmol) was dissolved into freshly distilled DCM (5 mL) under a nitrogen atmosphere. Then, DIC (0.25 mL, 1.58 mmol), a solution of (3*R/S*)-1-phenylhexan-3-amine (**14**) (0.14 g, 0.79 mmol)in DCM and DMAP (0.0097 g, 0.079 mmol, 0.1 eq.) were added at 0°C, under a N_2 atmosphere. A white precipitate was observed corresponding to the formation of DCU. The reaction was stirred at room temperature for 18 hours, then poured onto diethyl ether (20 mL). The organic layer was alternately washed several times with saturated solutions of NH_4Cl and $NaHCO_3$, dried over Na_2SO_4, filtered, evaporated and dried under vacuum to obtain 0.21 g of orange oil. The crude product was purified by flash chromatography using 10:1 followed by 8 : 1 DCM : AcOEt as eluent to obtain 0.14 g of colourless oil as pure product in 46 % yield. ^{1}H NMR, 400MHz, $CDCl_3$, δ: 0.90 (t, *J*= 7.22 Hz, 3H, CH_3), 1.25-1.85 (m, 21H, H_{aliph}), 2.24-2.44 (bs, 1H, H-6), 2.55-2.68 (m, 2H, CH_2 H-5), 2.70-2.83 (bs, 1H, H-6), 3.93-4.06 (bs, 1H, H-15), 4.69-4.77 (bs, 1H, H-2), 5.60-6.13 (bs, 1H, NH), 7.15-7.29 (m, 5H, H_{arom}). ^{13}C NMR, 100MHz, $CDCl_3$, δ: 13.91; 13.94; 19.05; 19.21; 20.56; 24.93; 28.34; 28.37; 32.37; 32.59; 37.39; 37.58 (12C, C_{aliph}); 53.40 (1C, C-15); 54.94 (1C, C-2); 80.62 (1C, C-9); 125.83 (1C, C-4); 125.90; 128.29; 128.30; 128.37; 128.43; 141.81 (6C, C_{arom}); 170.74 (1C, C=O_{Boc}); 182.68 (1C, C=O_{amide}). IR ($CDCl_3$), cm^{-1}: 3422.41 (m, NH stretch.), 3353.44 (m, NH stretch.), 1673.11 (C=O stretch.).

(15*R/S*,2*S*)-1-(2-oxo-2-phenylacetyl)-N-(1-phenylhexan-3-yl)piperidine-2-carboxamide   Elte420 (4)
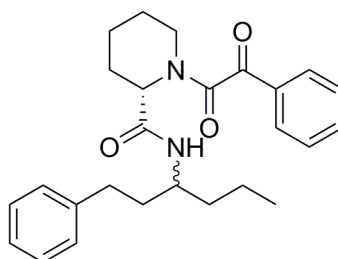
4

a) *Deprotection of N-Boc piperidine*: To a solution of (15*R/S*,2*S*)-*tert*-butyl 2-(1-phenylhexan- 3-ylcarbamoyl)piperidine-1-carboxylate (0.12 g, 0.31 mmol) in 2 mL of DCM, 1 mL of a solution of

TFA 99 % (0.4 mL, 5.22 mmol) in 2 mL of DCM was added drop wise at 0 ∘C. The reaction mixture turned yellow. The solution was stirred at room temperature for 1 h and 2 mL of the acid solution are added at 0°C since residual starting material was monitored by TLC. Then, a saturated solution of $NaHCO_3$ (25 mL) was added drop wise and the reaction mixture was extracted with DCM (3 x 30 mL). The recollected organic layer was washed with a saturated solution of $NaHCO_3$ (2x35 mL), dried over Na_2SO_4, filtered, evaporated and dried under vacuum to obtain the NH-piperidine ring as a yellow oil (0.075 g, 76% yield).

b) *Final amidation:* To a solution of the previous crude (0.065 g, 0.23 mmol) in freshly distilled DCM (4 mL), phenylglyoxylic acid (0.44 g, 0.29 mmol), DMAP (0.0055 g, 0.045 mmol) and DIC (0.045 mL, 0.29 mmol) were added at 0°C under a N_2 atmosphere. A white precipitate was observed. The reaction mixture was stirred under a N_2 atmosphere at r.t. for 18 h. Diethyl ether (20 mL) was added and the organic layer was alternately washed several times with saturated solutions of NH_4Cl and $NaHCO_3$, dried over Na_2SO_4, filtered and evaporated under vacuum to obtain 0.080 g of a yellow oil. The crude was purified by chromatography (eluent EtP : AcOEt/ 5:1) to obtain a mixture containing three different types of urea as by-products. To get rid of them, the mixture was again purified by flash chromatography using (eluent toluene:Et_2O/ 10:1) to obtain ElteN420 (**4**) as a colourless oil (0.011 g) in 11 % yield. The 1H-NMR spectrum of ElteN420 appeared quite complex due to the presence of two rotamers (1:1.3 ratio), each as 1:1 mixture of diastereoisomers.[46] When the attribution of signals to different rotamers is possible (r1) refers to the minor rotamer. ^{1}H NMR, 400MHz, CDCl$_3$, δ: 0.81 (m, 3H, CH$_3$); 1.1-1.83 (m, 10CH$_2$, CH$_2$-16+ CH$_2$-37 + CH$_2$-38 + CH$_2$-3 + CH$_2$-4); 2.23-2.35 (m, 2H, CH$_2$-17); 2.50-2.73 (m, 3H, CH$_2$-5, H-6); 3.15-3.24 (m, 1H, H-2); 3.37-3.44 (m, 1H, H-21); 3.87- 4.08 (m, 2H, H-15 + H-151); 4.58-4.66 (m, 1H, H-61); 5.10-5.16 (m, 1H, H-6); 5.72-5.80 (m, 1H, NH); 6.27-6.37 (m, 1H, NH1); 7.06-7.24 (m, 5H, H$_{arom}$); 7.39-7.50 (m, 2H, H$_{meta}$); 7.54- 7.63 (m, 1H, H$_{para}$), 7.88-7.93 (m, 2H, H$_{orto}$). IR (CDCl$_3$), cm^{-1}: 3418.10 (w, NH stretch.), 3021.55 (w, CH$_{arom}$ stretch.), 2926.72 (m, CH$_{aliph.}$ stretch.), 1679.56 (s, NC=O stretch.), 1640.86 (s, PhC=O stretch.). ESI-MS: *m/z* 862.77 [2M+Na]+, 443.31 [M+Na]+.

Synthesis of (2S)-1-(2-oxo-2-phenylacetyl)-N-(3-phenylpropyl)piperidine-2-carboxamide ElteN378

17
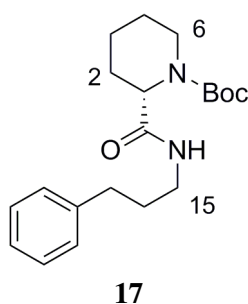
a) *Initial amidation.* To a solution of 3-phenylpropan-1-amine (0.16 g, 1.2 mmol) in 6 mL of dry DMF, N-Boc pipecolic acid (0.425 g, 1.85 mmol, 1.6 equiv.), DIPEA (1.0 mL, 1.85 mmol) and HATU (1.70 mL, 10.90 mmol, 6 equiv.) were added at 0°C, under a N_2 atmosphere. The reaction was stirred under a N atmosphere at r.t. overnight, then poured onto 30 mL of diethyl ether. The organic layer was filtered and alternately washed several times with saturated solutions of NH_4Cl and $NaHCO_3$,dried over Na_2SO_4, filtered and evaporated under vacuum to obtain a yellowish oil (0.33 g). The crude was purified by flash column chromatography using DCM : AcOEt 8 : 1 as eluent to obtain 0.50 g of a

colourless oil as pure product in 80 % yield. The ^{1}H-NMR showed the presence of a mixture of rotamers. When the attribution of signals to different rotamers is possible (∗) refers to the minor rotamer. ^{1}H NMR, 400MHz, CDCl$_3$, δ: 1.31-1.70 (m, 15H, CH$_2$-5 + CH$_2$-16 + CH$_2$-3* + 3CH$_3$); 1.78-1.87 (m, 2H, CH$_2$-3); 2.25-2.35 (m, 2H, CH$_2$-4); 2.64 (at, J=7.71 Hz, 2H, CH$_2$-15); 2.69-2.79 (m, 2H, CH$_2$-15*); 3.23-3.29 (m, 2H, CH$_2$-17); 3.29-3.39 (m, 2H, CH-6); 3.99-4.10 (m, 1H, H-2*); 4.68-4.74 (m, 1H, H-2); 6.12 (bs, 1H, NH); 7.15-7.21 (m, 3H, H$_{arom}$); 7.25-7.30 (m, 2H, H$_{arom}$). ^{13}C NMR, 100MHz, CDCl$_3$, δ: 20.54; 24.90; 25.40; 28.37; 31.38; 33.18 (11C, C$_{aliph}$); 80.57 (1C, C9); 128.48; 128.31; 125.98; 141.27 (6C, C$_{arom}$); 170.89 (2C, C=O$_{amide}$ + C=O$_{Boc}$).
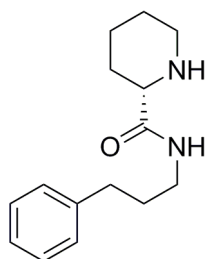
18

b) *Deprotection*. To a solution of (2S)-*tert*-butyl 2-(3-phenylpropylcarbamoyl)piperidine-1-carboxylate (0.36 g, 1.04 mmol) in DCM (6 mL) 1 mL of a solution of TFA 99% (0.70 mL in 2 mL of DCM, 9.03 mmol) was added drop wise at 0°C. The reaction mixture turned yellow and was stirred at r. t for 4 h during which 1.22 mL of TFA in 3.0 mL of DCM (5 equiv.) were added at 0 °C. The mixture was poured onto 30 mL of NaHCO$_3$ sat.sol. and extracted with DCM (3 x 55 mL). The recollected organic layer was washed with a saturated solution of NaHCO$_3$ (4x80 mL), dried over Na$_2$SO$_4$, filtered and evaporated under vacuum to obtain 0.184 g of a pale yellow powder in 72 % yield. The crude was directly used for the next step, without any purification. ^{13}C NMR, 100MHz, CDCl$_3$, δ: 24.03; 25.86; 30.08; 31.10; 33.36; 38.62; 45.77; 60.29 (8C, C$_{aliph}$); 125.89; 128.34; 128.40; 141.54 (6C, C$_{arom}$); 173.93 (1C, C=O$_{amide}$).
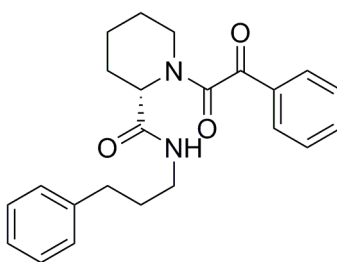
5

c) *Final amidation*. To a solution of phenylglyoxylic acid (0.06 g, 0.406 mmol, 1 equiv.) in DMF dry (3 mL), HATU (0.31 g, 0.81 mmol, 2 equiv.) was added. The reaction mixture was stirred for 10 min. at r.t., then a solution of N-(3-phenylpropyl)piperidine-2-carboxamide (0.1 g, 0.406 mmol) in 3 mL of DMF dry, followed by DIPEA (0.211 μL, 1.34 mmol, 3.3 equiv.) were added. The solution turned yellow. After 18 h of magnetic stirring the mixture was poured onto a saturated solution of NH$_4$Cl and extracted with DCM (3 x 50 mL),the organic layer was washed with a saturated solution of NaHCO$_3$ (1 x 50 mL) and water (4 x 50 mL), then dried over Na$_2$SO$_4$, filtered and evaporated under vacuum to obtain a yellowish oil (0.105 g). The crude was purified by flash chromatography using AcoEt : EtP

10 : 1 as eluent to obtain the final pure product as colourless oil (0.91 g) in 78% yield. The ^{1}H-NMR showed the presence of a 1.6:2.4 mixture of rotamers. When the attribution of signals to different rotamers is possible (∗) refers to the minor rotamer. ^{1}H NMR, 400MHz, CDCl$_3$, δ : 1.27- 1.84 (m, 8H, 3 CH$_2$+ CH$_2$*); 2.19- 2.30 (m, 2H, CH$_2$); 2.60 (at, J=7.38 Hz, 2H, CH$_2$); 2.62-2.70 (m, 2H, CH$_2$*); 3.15-3.33 (m, 4H, CH$_2$ + CH$_2$*); 3.35-3.41 (m, 1H); 4.00-4.03 (m, 1H, H*); 4.53-4.60 (m, 1H, H*); 5.11-5.15 (m, 1H); 6.16 (bt, 1H, J=6.12 Hz, 1H, NH); 6.68 (bt, 1H, J=6.28 Hz, NH*); 7.10-7.23 (m, 5H, H$_{arom}$); 7.41-7.48 (m, 2H, H$_{meta}$); 7.55-7.62 (m, 1H, H$_{para}$), 7.89-7.91 (m, 2H, H$_{orto}$). ^{13}C NMR, 100MHz, CDCl$_3$, δ : 20.41; 20.70; 25.05; 25.20; 25.83; 26.61; 31.14; 31.28; 33.14; 33.19 (5C, C$_{aliph}$); 39.25 (1C); 39.41 (1C); 39.52 (1C, C*); 44.55 (1C, C*); 51.79 (1C,); 57.06 (1C, C*); 125.99; 126.01; 128.38; 128.41; 128.46; 128.48; 129.18; 129.22; 129.63; 129.87; 132.71; 132.93; 135.03; 135.40; 141.28; 141.33(20 C, 10C$_{arom}$ + 10C*$_{arom}$); 166.29; 167.58; 168.33; 169.50 (4C, 2C=O$_{amide}$ + 2C=O*$_{amide}$); 191.58; 192.43 (2C, C=O$_{ketone}$ + C=O$_{ketone}$*). ESI-MS: m/z 778.92 [2M+Na]$^+$, 401.33 [M+Na]$^+$, 377.17 [M-H]$^-$. IR (CDCl$_3$), cm^{-1}: 3435.34 (w, NH free stretch.), 3366.37 (w, NH free stretch.), 3030.17 (w, CH $_{arom}$ stretch.), 2943.96 (m, CH$_{aliphatic}$ stretch.), 1679.56 (s, NC=O stretch.), 1640.86 (s, PhC=O stretch.). [α]$_D^{24}$ (EtOH): -23.28, (c = 1.80 mg/mL).

3.5 References

1. Marks, A.R., *Physiological Review*, **1996**, *76*, 631-649.

2. Snyder, S.H., Sabatini, D.M., Lai, M.M., Steiner, J.P., Hamilton, G.S. and Suzdak, P.D., *Trends Pharmacol Sci.*, **1998**,*19*(1), 21-25.

3. Blackburn, E. A.; Walkinshaw, M. D., *Curr. Opin. Pharmacol.*, **2011**, *11*, 365-371.

4. Chattopadhaya, S.; Harikishore, A.; Yoon, H. S., *Curr. Med. Chem.*, **2011**, *18*, 5380-5397.

5. Galat, A., *J. Chem. Inf. Model.*, **2008**, *48*, 1118-1130.

6. Gerard, M., Deleersnijder, A., Demeulemeester, J., Debyser, Z., Baekelandt, V., *Mol. Neurobiol.*, **2011**, *44*, 13-27.

7. Ivery, M, *Med. Res. Rev.*, **2000**, *20*, 452-484.

8. Galat, A., *Curr Top Med Chem*, **2003**, *3*, 1315-1347.

9. Kang, C.B., Ye, H., Dhe-Paganon S., Yoon, S., *Neurosignals*, **2008**, *16*, 318-325.

10. Rosen, M.K., Standaert, R.F., Galat, M., Schreiberen, S. L., *Science Wash. DC*, **1990**, *248*, 863-866.

11. Rosen, M. K.; Schreiber, S. L., *Angew. Chem.*, Int. Ed.Engl., **1992**, *31*, 384-400.

12. Kissinger, C. R.; et al., *Nature*, **1995**, *378*, 641-644.

13. Waickman, A. T.; Powell, J. D., *J. Immunol.*, **2012**, *188*, 4721-4729.

14. Sugata, H. et al., *Neuroscience Letters*, **2009**, *459*, 96-99.

15. Gerard, M., Deleersnijder, A., *The Journal of Neuroscience*, **2010**, *30*(7),2454-2463.

16. Lisi, L., Navarra, P., Cirocchi, R., Sharp, A., Stigliano, E., Feinstein, D. L., Dello Russo, C., *J. Neuroimmunol,*. **2012**, *243*, 43-51.

17. Manabe, Y., Warita, H., Murakami, T., Shiote, M., Hayashi, T., Omori, N., Nagano, I., Shoji, M., Abe, K., *Brain Res.*, **2002**, *935*, 124-128.

18. Benjamin, D., Colombi, M., Moroni, C., Hall, M. N., *Nature*, **2011**, *10*, 868-880.

19. Esposito, M., Ruffini, F., Bellone, M., Gagliani, N., Battaglia, M., Martino, G., Furlan, R., *J. Neuroimmunol.,* **2010**, *220*, 52-63.

20. Lyons, W., Steiner, J. P., Snyder, S. H., Dawson, T. M., *J. Neurosci.*, **1995**, *15*, 2985-2994.

21. Edlich, F., Weiwad, M., Wildemann, D., Jarczowski, F., Kilka, S. et al., *J. Biol. Chem.*, **2006**, *281*, 14961-14970.

22. Wang, X., Etzkorn, F., *Biopolymers*, **2006**, *84*, 125-146.

23. Mo, S. J., Ban, Y. H., Park, J. W., Yoo, Y. J., Yoon, Y. J.,*J. Ind. Microbiol. Biotechnol.*, **2009**, *36*, 1473-1482.

24. Dubowchik, G. M., Ditta, J. L., Herbst, J. J., Bollini, S., Vinitsky, A., *Biol Med Chem Lett*, **2000**, *10*.

25. Choi, C., et all., *Biol Med Chem Lett*, **2002**, *12*, 1421-1428.

26. Burkhard, P., Hommel, U., Sanner, M., Walkinshaw, M. D., *J Mol Biol*, **1999**, *287*, 853-858.

27. Furber, M., *J Am Chem Soc*, **1995**, *117*, 7267-7268.

28. Roehrig, C. H., Loch, C., Guan, J.-Y., Siegal, G., Overhand, M., *ChemMedChem*, **2007**, *2*, 1054-1070.

29. Bizzarri, M., Tenori, E., Martina, M.R., Marsili, S., Caminati, G., Menichetti, S. and Procacci, P. *J. Phys. Chem. Lett.*, **2011**, *2*, 2834-2839.

30. Bizzarri, M., Marsili, S., Procacci, P., *J. Phys. Chem. B*, **2011**, *115*, 6193-6201.

31. Hummer, G., *Nat. Chem.*, **2010**, *2*, 906-906.

32. Liu, P., Kim, B., Friesner, R. A., Berne, B. J., *Proc. Natl. Acad. Sci.*, U.S.A., **2005**, *102*, 13749-13754.

33. Marsili, S., Signorini, G. F., Chelli, R., Marchi, M., Procacci, P., *J. Comput. Chem.*, **2010**, *31*, 1106-1161.

34. Martina, M.R., Tenori, E., Bizzarri, M., Menichetti, S., Caminati, G., Procacci, P., *J. Med. Chem.*, **2013**, *56*, 1041-1051.

35. Williams, T., Kelley, C. **2011**; http://sourceforge.net/projects/gnuplot

36. Esaki, H., Ohtaki, R., Maegawa, T., Monguchi, Y., Sajiki, H., *J. Org. Chem.,* **2007**, *72*, 2143-2150.

37. Denmark, S. E., Wynn, T. Lewis, *J. Am. Chem. Soc.,* **2001**, *123*, 6199-6200.

38. Esaki, H., Ohtaki, R., Maegawa, T., Monguchi, Y., Sajiki, H., *J. Org. Chem,.* **2007**, *72*, 2143-2150.

39. Patent WO 2004/099214 A1, 13-19.

40. Kozany, C., Maerz, A., Kress, C., Hausch, F. *ChemBioChem*, **2009**, *10*, 1402-1410.

41. Roehrig, C. H., Loch, C., Guan, J.-Y., Siegal, G., Overhand, M. *ChemMedChem*, **2007**, *2*, 1054-1070.

42. Holt, D. A. et all. *J. Am. Chem. Soc.*, **1993**, *115*, 9925-9938.

43. Lakowicz, J. R. *Principles of Fluorescence Spectroscopy*, Springer, New York, **2006**.

44. Shi, L. et all., *J. Am. Chem. Soc.*, **2005**, *127*, 10836-10837.

45. Reddy, M. R.; Brown, H. C.; Ramachandran, P., *J. Organometallic Chem.*, **2001**, *624*, 239-243.

46. For this reason any reasonable ^{13}C NMR spectrum can be recorded despite very long acquisition times and/or delays.

4. A tartrate model compound for TACE inhibition

4.1 Introduction

The protein Tumor Necrosis factor-a Converting Enzyme (**TACE**), also called, ADAM17, is a 70-kDa enzyme that belongs to the ADAM (A Disintegrin And Metalloprotease) protein family of disintegrins and metalloproteases.[1] TACE is a membrane-anchored proteinase that releases, from its membrane-bound precursor (pro-TNF-α), the soluble form of the cytokine Tumor necrosis factor-a (s-TNFα),a soluble 17kDa extracellular domain (ectodomain). This process is known as 'shedding' and is of known physiological importance (Figure 4.1).
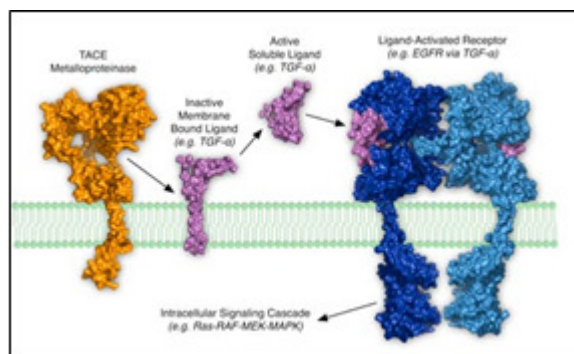
Figure 4.1. Shedding process of s-TNFα involving TACE.

TNFα, when produced in excess, is known to play a pivotal role in inflammatory processes as in rheumatoid artritis (RA) and septic shock. In RA, for example, the s-TNFa, released by activated macrophages, interacts with the TNFR1 receptor constitutively expressed on chondrocytes of the joints triggering a signaling pathway that culminates in the expression and secretion of Matrix Metalloproteinases MMP-1 and MMP-13. The latter proteins hydrolyze the collagen of the joint cartilage severely impairing its function.[2] The pro-inflammatory response induced by the circulating s-TNFa has also been related to Multiple Sclerosis relapsing.[3] It was shown, in particular, that the absence of s-TNFa in transgenic mice suppresses experimental autoimmune encephalomyelitis disease onset and progression.[4,5] The implication of TACE in multiple diseases via TNFα release makes this sheddase an ideal therapeutic target, promoting an enduring effort[6] in the design of small molecules aimed at selectively inhibiting its cleavage capabilities.

The catalytic domain of TACE is characterized by a long binding groove delimited by β-strand IV and helix C.[7] The latter provides the consensus sequence HEXXHXXGXXH including three critical histidines (His405, His409, His415) that coordinate a zinc ion located at the center of the groove (Figure 4.2, left).
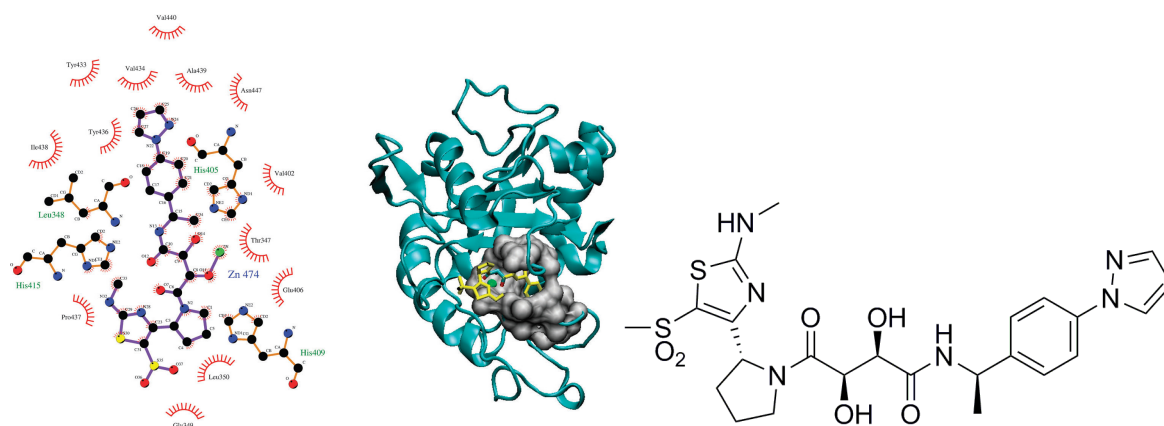
Figure 4.2. Left: Ligplot diagram of the TACE binding pocket with the Dai inhibitor Drug-38.Center: Representation of the active site of TACE using the Drug-38-TACE co-crystal PDB structure reported by Dai. Right: Dai inhibitor Drug-38

In the absence of any ligand, the zinc ion is also coordinated by a water molecule kept in place by the interaction with Glu406 also located in the consensus sequence. Effective inhibitors must displace the catalytic water molecule to bind the zinc ion and they must comprise a group capable of fitting into the so called *primed pocket*, a deep well with hydrophobic walls drilled at the center of the major catalytic groove (Figure 4.2, right). As a consequence, TACE and MMP inhibitors are comprised of two main units:[8]

> ➤ a peptidomimetic backbone designed to recognize the primed pocket,

> ➤ a zinc binding group (ZBG).

Hydroxamate is a very effective ZBG but has a low 'drugability', because its affinity for zinc is so high to cause unspecific interactions with MMPs and other metal containing enzymes.[9] Hence, developing selective TACE inhibitors is indeed desirable. This is why a number of ZBGs with affinity lower than that of hydroxamate are currently being tested.[10] A novel promising family of TACE nanomolar inhibitors is represented by bis-amides of L-tartaric acid first developed by *Rosner et all*.[11] These compounds have been recently patented[12] and feature a tartrate core linking a left hand side (LHS) and right hand side (RHS) substituent through amide bonds. The tartrate core acts as a tridentate zinc chelator in the resolved co-crystals while the RHS (R)-1-(4-(1H-pyrazol-1-yl)phenyl)-ethanamine group fits into the primed narrow pocket. In 2011, *Dai et al*. turned their attention to optimizing the LHS amine building blocks in the hope of improving their oral pharmacokinetic profiles while maintaining or further improving its biochemical potencies.[13] In a recent computational study,[14] it has been shown that the Dai compounds all share a common conformational pattern in bulk water solution, characterized by an equilibrium between bent structures (stabilized by hydrophobic interactions of the LHS and RHS moieties) and extended structures. Such structures solvent-expose the tartrate core hydroxy and oxo groups such that zinc coordination can occur with two, rather than three, oxygen atoms. These findings suggested the hypothesis of a two-step TACE docking mechanism of the Dai compounds and raise a series of questions about the protonation state of the inhibitors under physiological conditions, of how the protonation states influences the conformational landscape and how strongly these ligands bind the zinc cation in water solution. To confirm these hypotheses, we have synthesized and thoroughly characterized using extensive photo-physical measurements and *ab initio* and molecular mechanics/dynamics calculations, a novel substance, called

MBET306 (**23**), featuring pyrrolydine LHS and ethyl–phenyl RHS moieties that are common to all Dai powerful inhibitors (Figure 4.3).
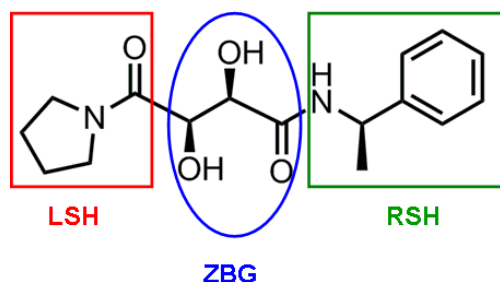
Figure 4.3. MBET306 (**23**): 2,3-dihydroxy-4-oxo-N-((R)-1-phenylethyl)-4-(pyrrolidin-1-yl)-butanamide.

The moderate affinity for zinc shown by MBET306 is important from a pharmaceutical standpoint, as one can use an appropriate combination of the LHS and the RHS moiety to build selective drugs for TACE with little or no affinity for other zinc MMPs. This design, by preserving all the chemical determinants that impart to the Dai compounds their peculiar conformational behavior in bulk solution, can act as a versatile synthetic precursor to be extended to other tartrate-based leads by building upon its minimal LHS and RHS moieties. For this aim, we exploited a combined synthetic, computational and experimental approach, below reported.[15]

4.2 Results and Discussion

4.2.1 Computational and Zn binding

MBET306 (**23**) was built using the crystallographic structure of its synthetic sequel drug-38 designed by *Dai et al.*[13] removing the thiazole and pyrazole rings. We simulated the most likely species of MBET306 at physiological pH, i.e. the neutral species (hereafter termed N) and the two possible anions, i.e. O2, with the proton lacking on the hydroxy flanking the LHS pyrrolidine ring, and O3, with the deprotonated hydroxy flanking the RHS phenyl–ethyl moiety. As discussed above, MBET306 is characterized by various rotameric conformers separated by high free energy barriers, making problematic an effective conformational sampling
using conventional molecular dynamics simulations. Therefore a Hamiltonian Replica Exchange (HREM) generalized ensemble approach was used.[16] HREM analysis basically showed that all the conformations could be lumped into two main macrostates characterized by a *compact* and *extended* arrangement (Figure 4.4).
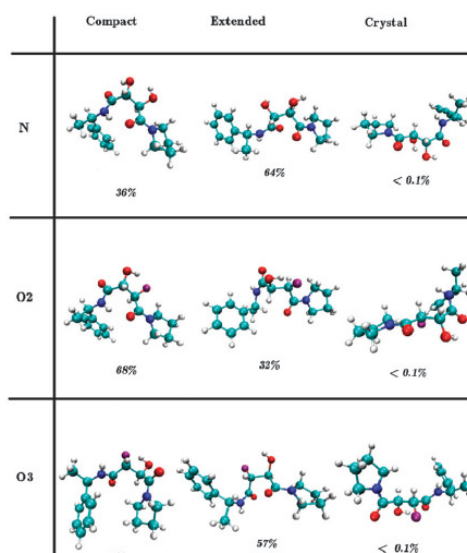
Figure 4.4. Compact/extended conformations for the neutral and anionic species for MBET306; percentages have been calculated from the HREM simulations at P = 1 atm and T = 300 K.

The former structures were stabilized by the hydrophobic interactions of the RHS phenyl moiety with the LHS pyrrolydine-ring and systematically exhibited the amide bond flanking the ethyl–phenyl RHS in the *trans* conformation.[15] Correspondingly, the extended structures showed the *cis* isomerism of the same amide bond. The correlation between *cis–trans* isomerism of the RHS amide bond and extended/compact structures was observed in all three species N, O2 and O3. Such a correlation could be quantitatively assessed by computing the Free Energy Surface (FES) with respect to the two collective variables represented by the ω angle of the RHS amide bond and by the phenyl ring-pyrrolidine ring distance. In all three cases (MBET306 in N, O2 and O3 forms) the FES exhibited two deep minima corresponding to the macrostates extended *cis*-RHS-amide-bond and the compact *trans*-RHS-amide-bond (Figure 4.5).
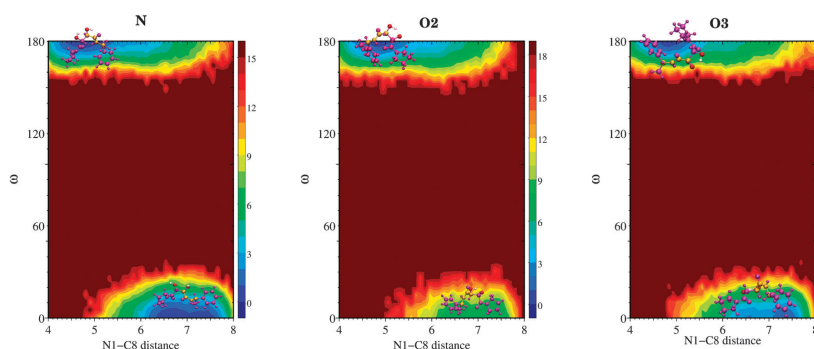
Figure 4.5 Free energy surface (FES) of MBET306 neutral, and monoanionic O2, O3 species.

Remarkably, the fraction of crystal-like conformations (i.e. with the two hydroxy groups and the LHS carboxy group pointing in the same direction,Figure 4.6) was negligibly small for both the neutral and the anionic species, amounting at most to a few hundred configurations. While for non crystal-like conformations of MBET306 (and of the parent Dai compounds) the entropic and enthalpic contributions both played an important role in the balance between extended and compact structures, H-REM data and ab initio calculations consistently showed that the limited incidence of crystal conformations in bulk solution for MBET306 and derivatives have certainly an enthalpic origin. The

small population of the crystal-like conformations in bulk solution (that also systematically adopt the *trans*-RHS amide state) implies that an inhibitor based on the MBET306 design should reasonably dock the binding groove in the compact *trans*-RHS-amide states to fit its RHS in the primed pocket, as *cis* states must undergo a costly isomerization on the protein surface to be able to enter the pocket. For all conformations and species at physiological pH, the ligand reorganization energy was consistently found strongly positive. Therefore, in order to evolve in the final binding extended conformation, the compact ligand in the *trans* RHS-amide state must hence undergo a rotation, a conformational transition that is strongly discouraged for electrostatic reasons in bulk solution, but that could be possibly favored upon binding to the TACE catalytic zinc. This hypothesis was confirmed from Zn binding assays and CD data.
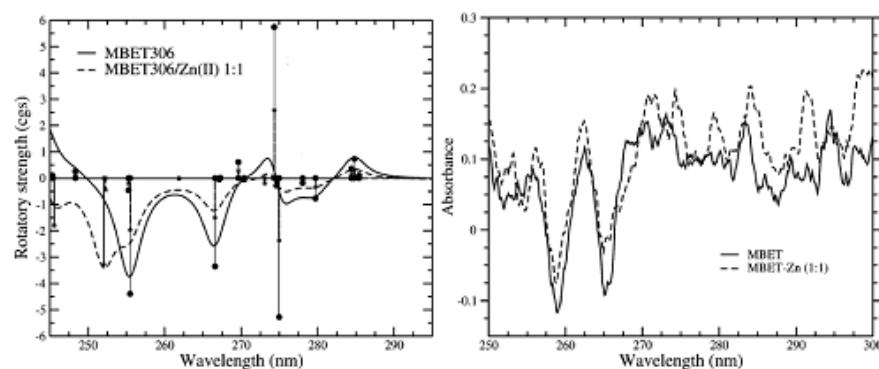
Figure 4.6 Right: Experimental absorption spectra as a function of the MBET306 concentration at fixed $ZnCl_2$ concentration of 35 mM at T = 25 1C and pH = 8. Left: Simulated absorption spectrum of Zn(MBET306)+ complexes as a function of concentration of MBET306

$ZnCl_2$ addition to MBET306 solution had no significant effect on absorption or emission spectra when pH is below 7, implying that cationic and neutral species (that prevail for pH < 7) were unable to bind the Zn(II). Thus, zinc binding studies were performed at pH=8 where we assumed that ground-state aggregates were negligible and that the most abundant species was the monomeric anionic form of MBET306. Furthermore, molecular dynamics and ab initio calculations have shown that these ZBG oxygen atoms tend to be disposed, in the unbound monoanionic ligand, at the vertices of a quadrilateral so as to minimize electrostatic repulsion, while in the known co-crystals three ZBG oxygen atoms were found at the vertices of octahedron face for tridentate zinc chelation. Since the absorption data for the free ligand (Figure 4.6) were interpreted in terms of a potentially *bidentate* (non crystallike) arrangement of the ZBG in the various species (N, O2 and O3), zinc complexation must induce conformational changes in the MBET306 central tartrate core, promoting a rotation around the sp3 bonds C1–C2 and C2–C3 energetically favoring the typical ZBG *tridentate* arrangement of the LHS oxo and hydroxy oxygen atoms observed in the TACE co-crystals of the Dai compounds. All these date confirmed the two step TACE docking of MBET306 mechanism.

4.2.2. Organic synthesis

Encouraged by promising results from in-depth theoretical calculations we decide to assign MBET306 (**23**) to organic synthesis. The synthetical procedure allowed to realize a new TACE inhibitor, featuring pyrrolydine LHS and ethyl–phenyl RHS moieties (Scheme 4.1).
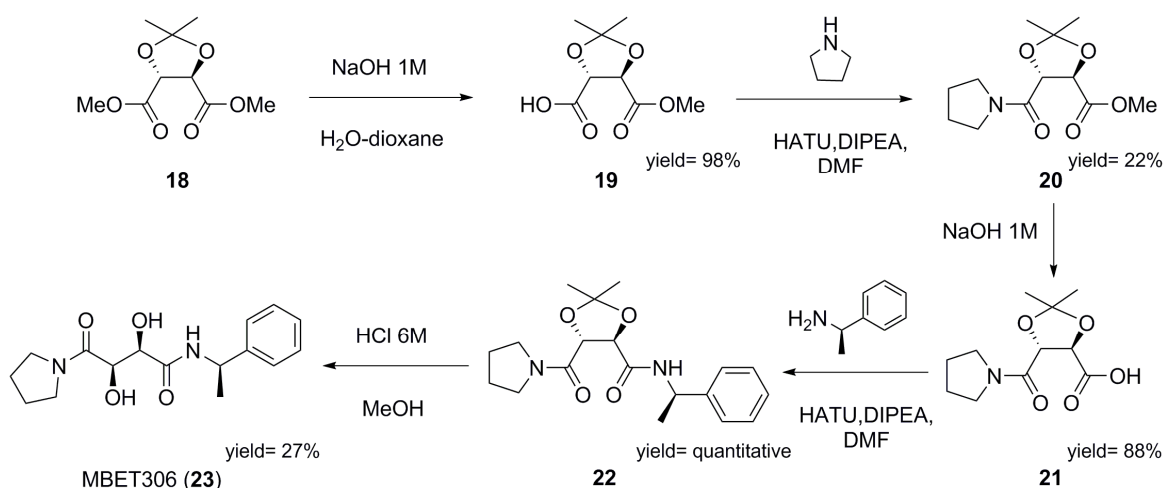
Scheme 4.1 Synthesis of MBET306 (**23**)

Commercially available (4R,5R)-dimethyl 2,2-dimethyl-1,3-dioxolane-4,5-dicarboxylate (**18**) is an analogue of the dimethyl ester of L-(+)-tartaric acid, protected as isopropylidene ketal. One of its ester moiety could be selectively hydrolyzed, carefully controlling the stoichiometry and the temperature. The reaction was achieved in a fairly good yield, using a1 equiv. of 1M solution of NaOH in a 1 : 1 water : dioxane mixture, at 0°C. The free obtain carboxylic acid (**19**) was activated with HATU and readily reacted with an excess of pyrrolidine in a DIPEA solution of dry DMF. After flash cromathography purification, the residual ester moiety of (**20**) was removed and R-(+)-α-Methylbenzylamine was insert on RHS using the same HATU-DIPEA in DMF protocol, above described. The final step of the procedure involved the deprotection of hydroxyl groups with a 6 M solution of HCl in MeOH. HCl solution had to be slowly added, over a period of two days, since a 'one pot' adding led to the degradation of (**22**). In conclusion, TACE inhibitor MBET306 (**23**) was thus obtain with a straightforward procedure without challenging synthetical efforts.

4.3 Conclusion

In this study we have synthesized and characterized a new compound, named MBET306 (**23**), based on the bis-amides of L-tartaric acid, recently identified by Dai et al. as potent TACE inhibitors. Overall, the collected experimental and theoretical data indicate that zinc complexation induces a strong stabilization of the crystal-like ZBG arrangement in the monoanion, lending support for a *two step* TACE docking mechanism via a zinc-bound intermediate stable enough to allow the reorganization of the drug inside the TACE binding pockets in its final bound state. Finally, the mild affinity of the tartrate core in MBET306 for Zn(II) is indeed important from a pharmaceutical standpoint, as drugs based on the MBET306 design, while binding strongly the protein e.g. by attaching on the RHS the highly TACE specific quinoline moiety should be less aggressive versus other zinc matrix metalloprotainases, reducing the risk of unspecific interactions.

4.4 Experimental Section

General synthetic procedures

All the starting materials for the ligand synthesis were obtained commercially and used as received. ^{1}H and ^{13}C NMR spectra were recorded at 400 and 100 MHz on a Varian Mercury-400 instrument. FTIR spectra were recorded in CDCl3 solutions. ESI-mass spectra are measured using a LCQ-FLEET, Thermo Scientific instrument. DMSO, methanol and chloroform for the spectroscopic characterization of the ligand solutions were from Sigma Aldrich, Italy.

Synthesis of 5-(methoxycarbonyl)-2,2-dimethyl-1,3-dioxolane-4-carboxylic acid (19)
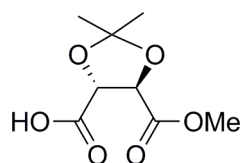
19

To a solution of (4R,5R)-dimethyl 2,2-dimethyl-1,3-dioxolane-4,5-dicarboxylate (**18**) (2.02 g, 9.24 mmol) in 1 : 1 water : dioxane (47 mL) NaOH 1 M (9.24 mL) was added drop wise, at 0°C. The reaction mixture was stirred for 2 hours at 0°C, then poured onto water (50 mL) and extracted with DCM (2 x 100 mL) and AcOEt (2 x 100 mL). The recollected organic phase was dried over Na_2SO_4, filtered and evaporated under vacuum to obtain a colourless oil as final product (1.86 g) in 98% yield. NMR spectra are described in literature.[17] ESI-MS: *m/z* = 204.92 [M+H]$^+$; 227.17 [M+Na]$^+$; 242.42 [M+K]$^+$, 203.09 [M-H]$^-$; 406.67 [2M-H]$^-$.

Synthesis of methyl 2,2-dimethyl-5-(pyrrolidine-1-carbonyl)-1,3-dioxolane-4-carboxylate (20)
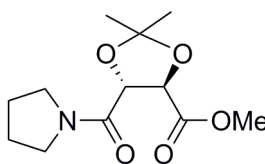
20

To a solution of 5-(methoxycarbonyl)-2,2-dimethyl-1,3-dioxolane-4-carboxylic acid (**19**) (0.73 g, 3.60 mmol) in dry DMF (7 mL) HATU (2.74 g, 7.20 mmol) was added. The reaction mixture was stirred for 10 min. at r.t. Pyrrolidine (595 µL, 7.20 mmol) was added dropwise, followed by DIPEA (1,88 mL, 10.8 mmol), the solution turned yellow. After 22 hours of magnetic stirring the mixture was poured onto a saturated solution of NH_4Cl and extracted with DCM (3 x 50 mL),the organic layer was washed with water (4 x 50 mL), then dried over Na_2SO_4, filtered and evaporated under vacuum to

obtain a yellowish oil (0.58 g). The crude was purified by flash chromatography using AcoEt : EtP 2 : 1 as eluent to obtain a colourless oil (0.2 g) as final pure product in 22 % yield. ^{1}H NMR, 400MHz, , CDCl$_3$, δ: 1.46 (d, 6H, J= 11,2 Hz, 2CH$_3$); 1.84-1.92 (m, 2H, CH$_{2pyr}$); 1.92-2.20 (m, 2H, CH$_{2pyr}$); 3.36-3.61 (m, 3H, CH$_{2pyr}$ + CH$_{pyr}$); 3.69-3.75 (m 1H, CH$_{pyr}$); 3.79 (s, 3H, CH$_3$); 4.79 (d, 1H, J= 5,5 Hz, CH); 5.23 (d, 1H, J= 5,5 Hz, CH). ^{13}C NMR, 100MHz,CDCl$_3$, δ: 23.89; 26.04; 26.13; 26.18; 46.45; 46.52; 52.53; 76.07 (9C, C$_{aliph}$); 112.88 (1C); 166.30 (1C, C=O$_{ester}$); 179.99 (1C, C=O$_{amide}$). IR (CDCl$_3$), cm^{-1}: 2978, 2952, 2833 (w, CH$_{aliph.}$ stretch.); 1752 (m, C=O$_{ester}$ stretch.); 1645 (s, C=O$_{amide}$ stretch.).

Synthesis of 2,2-dimethyl-5-(pyrrolidine-1-carbonyl)-1,3-dioxolane-4-carboxylic acid (21)
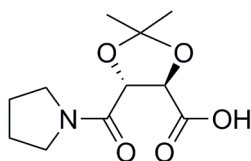
21

To a solution of methyl 2,2-dimethyl-5-(pyrrolidine-1-carbonyl)-1,3-dioxolane-4-carboxylate (**20**) (0.19 g, 0.75 mmol) in 1 : 1 water : dioxane (5 mL) NaOH 1 M (0.75 mL) was added dropwise, at 0°C. The reaction mixture was stirred for 2 hours at 0°C, then poured onto water (50 mL) and extracted with AcOEt (2 x 20 mL). The aqueous layer was acidified up to pH=2 with HCl 1M, then extracted with AcOEt (3 x 20 mL). The recollected organic phase was dried over Na$_2$SO$_4$, filtered and evaporated under vacuum to obtain a colourless oil as final product (0.16 g) in 88% yield. ^{1}H NMR, 400MHz, , CDCl$_3$, δ: 1.48 (d, 6H, J= 12,8 Hz, 2CH$_3$); 1.81-2.60 (m, 4H, 2CH$_{2pyr}$); 3.51-3.60 (m, 2H, CH$_{2pyr}$); 3.64-3.76 (m, 2H, CH$_{2pyr}$); 4.70 (d, 1H, J= 7,6 Hz, CH); 4.88 (d, 1H, J= 7,6 Hz, CH); 8.20 (bs, 1H, COOH). ^{13}C NMR, 100MHz,CDCl$_3$, δ: 23.48; 26.01; 26.08; 26.10; 47.21; 47.56; 76.03 (8C, C$_{aliph}$); 112.49 (1C); 167.80 (1C, C=O$_{amide}$); 170.07 (1C, C=O$_{acid}$). IR (CDCl$_3$), cm^{-1}: 2978, 2952, 2833 (w, CH$_{aliph.}$ stretch.); 3300-2200 (broad, OH$_{acid}$ stretch.); 1769 (s, C=O$_{acid}$ stretch.); 1645 (vs, C=O$_{amide}$ stretch.). ESI-MS: m/z = 242.33 [M-H]$^-$; 266.33 [M+Na]$^+$.

Synthesis of 2,2-dimethyl-N-((S)-1-phenylethyl)-5-(pyrrolidine-1-carbonyl)-1,3-dioxolane-4 carboxamide (22)
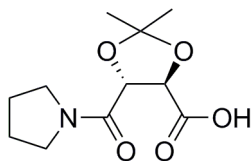
22

To a solution of 2,2-dimethyl-5-(pyrrolidine-1-carbonyl)-1,3-dioxolane-4-carboxylic acid (**21**) (0.14 g, 0.55 mmol) in dry DMF (5 mL) HATU (0.42 g, 1.11 mmol) was added. The reaction mixture was stirred for 10 min. at r.t. R-(+)-α-Methylbenzylamine (141 µL, 1.11 mmol) was added drop wise, followed by DIPEA (290 µL, 1.67 mmol), the solution turned yellow. After 18 hours of magnetic stirring the mixture was poured onto a saturated solution of NH$_4$Cl and extracted with AcOEt (3 x 50 mL),the organic layer was washed with water (4 x 50 mL), then dried over Na$_2$SO$_4$, filtered and evaporated under vacuum to obtain a colourless oil (0.19 g) as final pure product in quantitative yield. ^{1}H NMR, 400MHz, , CDCl$_3$, δ: 1.50 (s, 3H, CH$_3$); 1.51 (d, 6H, J= 10,0 Hz, 2CH$_3$); 1.81-1.97 (m, 4H, 2CH$_{2pyr}$); 3.49 (td, J$_1$= 6.8 Hz, J$_2$= 1.2 Hz, 2H, CH$_{2pyr}$); 3.65 (td, J$_1$= 6.8 Hz, J$_2$= 1.2 Hz, 2H, CH$_{2pyr}$); 4.82 (d, 1H, J= 5,4 Hz, CH); 5.00 (d, 1H, J= 5,4 Hz, CH); 5.09-5.16 (m, 1H, CH); 6.88 (d, J= 8.0 Hz, 1H, NH); 7.24-7.36 (m, 5H, H$_{arom}$). ^{13}C NMR, 100MHz,CDCl$_3$, δ: 21.80; 23.90; 26.06; 26.34; 26.63; 46.43; 46.46; 48.35; 77.45 (9C, C$_{aliph}$); 112.80 (1C); 126.02; 127.42; 128.66; 142.56 (6C, C$_{arom}$);166.89 (1C, C=O$_{amidePyr}$); 169.61 (1C, C=O$_{amide}$). IR (CDCl$_3$), cm^{-1}: 3409 (m, NH stretch.); 3090, 3064, 3030 (w, CH$_{arom}$ stretch.); 2978, 2935, 2833 (w, CH$_{aliph.}$ stretch.); 1666 (s, NHC=O$_{amide}$ stretch.); 1645 (vs, NC=O$_{amide}$ stretch.). ESI-MS: *m/z* = 715.40 [2M+Na]$^+$.

Synthesis of 2,3-dihydroxy-4-oxo-N-((S)-1-phenylethyl)-4-(pyrrolidin-1-yl)butanamide (23)
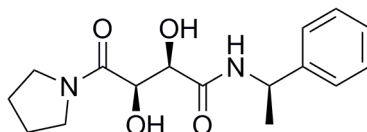
23

To a solution of 2,2-dimethyl-N-((S)-1-phenylethyl)-5-(pyrrolidine-1-carbonyl)-1,3-dioxolane-4 carboxamide (**22**) (0.065 g, 1,18 mmol) in MeOH, HCl 6M (1.6 mL, 9 eq.) were added at 0°C over a period of two days. The reaction mixture was evaporated and the crude was purified by flash chromatography using AcOEt as eluent to obtain (**23**) a colourless oil (0.015 g) as final pure product in 27 % yield. ^{1}H NMR, 300MHz, , CDCl$_3$, δ: 1.46 (d, 3H, J= 7.0 Hz, CH$_3$); 1.76-1.92 (m, 4H, 2CH$_{2pyr}$); 3.33-3.68 (m, 4H, 2CH$_{2pyr}$); 4.14-4.17 (m, 1H, CH); 4.63-4.67 (m, 1H, CH); 4.99-5.11 (m, 1H, CH); 7.10 (d, J= 7.0 Hz, 1H, NH); 7.25-7.30 (m, 5H, H$_{arom}$).^{13}C NMR, 100MHz,CDCl$_3$, δ: 21.97; 23.79; 26.05; 46.50; 48.81; 69.98; 71.54 (7C, C$_{aliph}$); 126.14; 127.41; 128.67; 142.87 (6C, C$_{arom}$);170.60 (1C, C=O$_{amidePyr}$); 170.88 (1C, C=O$_{amide}$). IR (CDCl$_3$), cm^{-1}: 3495 (broad, OH$_{bonded}$ stretch.); 3409 (m, NH stretch.); 3090, 3064, 3030 (w, CH$_{arom}$ stretch.); 2978, 2926, 2833 (w, CH$_{aliph.}$ stretch.); 1666 (s, NHC=O$_{amide}$ stretch.); 1636 (vs, NC=O$_{amide}$ stretch.). ESI-MS: *m/z* = 329.33 [M+Na]$^+$; 635.00 [2M+Na]$^+$; 403.42 [M+HPO$_4$]$^-$.

4.5 References

1. Black, R.A., *The International Journal of Biochemistry & Cell Biology*, **2002**, *34*, 1-5.

2. Vincenti, M., Brinckerhoff, C., *Arthritis Res.*, **2002**, *4*, 157-164.

3. Gijbels, K., Masure, S., Carton, H., Opdenakker, G. *J. Neuroimmunol.*, **1992**, *44*, 29-34.

4. Kassiotis, G., Kollias, G. *J. Exp. Med.*, **2001**, *193*, 427-434.

5. Pereira, J., Lebrun-Julien, F., Suter, U., *Trends Neurosci.*, **2012**, *35*, 123-134.

6. Li, N.G., Shi, S.H., Tang, Y.P., Li, W., Yin, L., Duan, J.A. *Curr. Med. Chem.*, **2012**, *19*, 2924-2956.

7. Maskos, K., Fernandez-Catalan, C., Huber, R., Bourenkov, G., Bartunik, H. et al., *Proc. Natl. Acad. Sci.* USA, **1998**, *95*, 3408-3412.

8. Dasgupta, S., Murumkar, P., Giridhar, R., Yadav, M., *Bioorg. Med. Chem.*, **2009**, *17*, 444-459.

9. Sheppeck, J.E., Tebben, A., Gilmore, J.L., Yang, A., C, Decicco, C.P., Duan, J.W., *Bioorg. Med. Chem. Lett.*, **2007**, *17*, 1408-1412.

10. Tu, G., Xu, W., Huang, H., Li, S., *Curr. Med. Chem.*, **2008**, *15*, 1388-1395.

11. Rosner, K., Guo, Z., Orth, P., Shipps, G.J., Belanger, D. *Bioorg. Med. Chem. Lett.*, **2010**, *20*, 1189-1193.

12. Chaoyang, D. *US Pat.*, 8,039,4672011.

13. Dai, C., *Bioorg. Med. Chem. Lett.*, **2011**, *21*(10), 3172-3176.

14. Guardiani, C., Procacci, P., *Phys. Chem. Chem. Phys.*, **2013**,*15*, 9186-9196.

15. Banchelli, M., Guardiani, C., Tenori, E., Menichetti, S., Caminati, G., Procacci, P. *Phys. Chem. Chem. Phys*, **2013**, *15*, 18881-18893.

16. Liu, P., Kim., B., Friesner, R. A., Berne, B. J., *Proc. Natl. Acad. Sci.*, U.S.A., **2005**, *102*, 13749-13754.

17. G. Song, Li., Guochao, L., Junhai, X., Aihua, N. Lili, W., Wu, Z., Zhibing, Z. *Patent* US2010/331345, A1, **2010**.

Abbreviations

aq.	aqueous
DCM	dichloromethane
DIC	diisopropylcarbodiimide
DMAP	*N,N*-dimethylamino-4-pyridine
equiv.	equivalent
Et$_2$O	diethyl ether
IR	infrared
mmol	millimole
NMR	nuclear magnetic resonance
NPs	nanoparticles

capaci di rivivere i nostri 15 anni ma allo stesso tempo la sua maturità nell'ascoltarmi e la sua affidabilità la rendono per me una confidente perfetta. Un grazie anche a Stefano (il Prof. Zanobetti), un'importante e costante presenza in questi anni, per tutti i consigli chimici e non.

Un ringraziamento particolare va alla mia famiglia. Un grazie a mio babbo Mauro, tessera numero uno del mio 'fanclub' per avermi spronato con grinta a combattere per raggiungere i miei obbiettivi e avermi sostenuto con pazienza nei momenti di crisi. Il suo costante interesse per il mio lavoro mi ha fornito la giusta determinazione per non arrendermi davanti alle difficoltà incontrate. Un grazie a mia mamma Anna per tutto l'amore che non smette mai di dimostarmi, per l'orgoglio che vedo nei suoi occhi quando mi guarda e mi gratifica più di ogni altra cosa, per avermi cresciuto come una donna forte e consapevole di me stessa, proprio come lo è lei, capace di affontare qualsiasi tipo di difficoltà senza lasciarsi scoraggiare. Senza il loro supporto i risultati ottenuti sarebbero stati impensabili. Un affettuoso ringraziamento va ai miei nonni che mi hanno cresciuto e con orgoglio hanno seguito ogni passo della mia vita anche se probabilmente non hanno mai capito cosa facessi tutti il giorno in laboratorio. E che sicuramente ora che hanno letto questa frase stanno sorridendo da qualche parte lassù.

Un ringraziamento particolare va al mio tato Lorenzo, la persona che due anni fa è entrata nella mia vita, mi ha preso per mano e ogni giorno cammina al mio fianco nel vortice delle vita, senza mai farmi mancare un sorriso. Lo ringrazio per aver capito quanto fosse importante per me il mio dottorato, il mio progetto, la mia ricerca e per avermi sempre supportato nel portarla avanti anche quando questo ha comportato sacrifici da parte di entrambi. Aver anteposto la mia felicità alla sua è stata la più grande dimostrazione d'amore mai ricevuta.

Infine, ringrazio tutte le persone che mi sono state vicine e che hanno creduto in me, ma anche quelle che non lo hanno fatto, perché proprio queste ultime mi hanno stimolato a dare il meglio di me per dimostare che si sbagliavano.